NAVAL POSTGRADUATE SCHOOL
Monterey, California

THESIS

566553

AN EXPERIMENTAL INVESTIGATION OF
SUPPORT STRUT INTERFERENCE ON
A THREE-PERCENT FIGHTER MODEL
AT HIGH ANGLES OF ATTACK

by

John Douglas Sommers

September 1989

Thesis Advisor: S. K. Hebbar

REPORT DOCUMENTATION PAGE

Form Approved
OMB No 0704-0188

1a REPORT SECURITY CLASSIFICATION	1b RESTRICTIVE MARKINGS
UNCLASSIFIED	

2a SECURITY CLASSIFICATION AUTHORITY	3 DISTRIBUTION / AVAILABILITY OF REPORT
2b DECLASSIFICATION / DOWNGRADING SCHEDULE	Approved for public release; distribution is unlimited

4 PERFORMING ORGANIZATION REPORT NUMBER(S)	5 MONITORING ORGANIZATION REPORT NUMBER(S)

6a NAME OF PERFORMING ORGANIZATION	6b OFFICE SYMBOL (If applicable)	7a. NAME OF MONITORING ORGANIZATION
Naval Postgraduate School	67	Naval Postgraduate School

6c. ADDRESS (City, State, and ZIP Code)	7b ADDRESS (City, State, and ZIP Code)
Monterey, CA 93943-5000	Monterey, CA 93943-5000

8a NAME OF FUNDING / SPONSORING ORGANIZATION	8b OFFICE SYMBOL (If applicable)	9 PROCUREMENT INSTRUMENT IDENTIFICATION NUMBER

8c. ADDRESS (City, State, and ZIP Code)	10 SOURCE OF FUNDING NUMBERS			
	PROGRAM ELEMENT NO	PROJECT NO	TASK NO	WORK UNIT ACCESSION NO

11 TITLE (Include Security Classification)
AN EXPERIMENTAL INVESTIGATION OF SUPPORT STRUT INTERFERENCE ON A THREE-PERCENT FIGHTER MODEL AT HIGH ANGLES OF ATTACK

12 PERSONAL AUTHOR(S)
Sommers, John D.

13a TYPE OF REPORT	13b TIME COVERED	14 DATE OF REPORT (Year, Month, Day)	15 PAGE COUNT
Master's Thesis	FROM _____ TO _____	September 1989	147

16 SUPPLEMENTARY NOTATION
The views expressed in this thesis are those of the author and do not reflect the official policy or position of the Department of Defense or the U.S. Government.

17 COSATI CODES			18 SUBJECT TERMS (Continue on reverse if necessary and identify by block number)
FIELD	GROUP	SUB-GROUP	High Angle of Attack Aerodynamics
			Strut Interference
			Flow Visualization, Laser Sheet
			Balance Measurements

19 ABSTRACT (Continue on reverse if necessary and identify by block number)
A low-speed wind-tunnel investigation was conducted to examine the aerodynamic interference caused by support struts on a three-percent scale model of the YF-17 lightweight fighter prototype. The study was undertaken at the request of the NASA-Ames Research Center to obtain background data in support of an upcoming investigation in which a full-scale F/A-18 will be mounted in the 80x120 foot wind tunnel. Force and moment measurements were made for various strut configurations using a precision six-component strain gage balance. Flow visualization studies were also conducted using smoke injected upstream of the model and illuminated by a laser sheet to highlight flow phenomenon around the model. Results of the investigation indicate that only minor aerodynamic interference was caused by the strut configurations tested. Of the configurations tested, it was determined by a subjective analysis that a slight reduction in interference could be realized by attaching the forward struts to the wing tips and the aft strut to the tail hook pivot point.

20 DISTRIBUTION / AVAILABILITY OF ABSTRACT	21 ABSTRACT SECURITY CLASSIFICATION
☒ UNCLASSIFIED/UNLIMITED ☐ SAME AS RPT ☐ DTIC USERS	UNCLASSIFIED

22a NAME OF RESPONSIBLE INDIVIDUAL	22b TELEPHONE (Include Area Code)	22c OFFICE SYMBOL
S. K. Hebbar	(408) 646-2997	67Hb

DD Form 1473, JUN 86

Previous editions are obsolete

S/N 0102-LF-014-6603

i

T245497

An Experimental Investigation of
Support Strut Interference on a Three-Percent Fighter Model
at High Angles of Attack

by

John D. Sommers
Lieutenant, United States Navy
B.S., San Diego State University, 1982

Submitted in partial fulfillment
of the requirements for the degree of

MASTER OF SCIENCE IN AERONAUTICAL ENGINEERING

from the

NAVAL POSTGRADUATE SCHOOL
September 1989

E. Roberts Wood, Chairman,
Department of Aeronautics and Astronautics

ABSTRACT

A low-speed wind-tunnel investigation was conducted to examine the aerodynamic interference caused by support struts on a three-percent scale model of the YF-17 lightweight fighter prototype. The study was undertaken at the request of the NASA-Ames Research Center to obtain background data in support of an upcoming investigation in which a full-scale F/A-18 will be mounted in the 80x120 foot wind tunnel. Force and moment measurements were made for various strut configurations using a precision six-component strain gage balance. Flow visualization studies were also conducted using smoke injected upstream of the model and illuminated by a laser sheet to highlight flow phenomenon around the model. Results of the investigation indicate that only minor aerodynamic interference was caused by the strut configurations tested. Of the configurations tested, it was determined by a subjective analysis that a slight reduction in interference could be realized by attaching the forward struts to the wing tips and the aft strut to the tail hook pivot point.

THESIS DISCLAIMER

The reader is cautioned that computer programs developed in this research may not have been exercised for all cases of interest. While every effort has been made, within the time available, to ensure that the programs are free of computational and logic errors, they cannot be considered validated. Any application is at the risk of the user.

TABLE OF CONTENTS

ACKNOWLEDGEMENT

I. INTRODUCTION

A. BACKGROUND

Any advancement in the field of high angle-of-attack (AOA) aerodynamics research, known variously as high alpha aerodynamics, supermaneuverability and post-stall (PST) capability, has the potential for increasing the tactical effectiveness and safety of future fighter aircraft. In an effort to gain or maintain airborne tactical superiority for their fighter aircraft, several countries are currently placing a high priority on research in this field.

The 1989 Paris air show showcased recent developments in Soviet high AOA capability [Ref. 1]. Of particular note was the demonstration of a maneuver known as "Pougachev's Cobra". The maneuver is named after the Soviet test pilot who performed it, Viktor Pougachev, and was demonstrated with the Sukhoi Su-27 long-range interceptor. A sequence of photographs [Ref. 1] depicting the execution of the maneuver is shown in Figures 1-4 and is described below.

1. Approaching from right to left, the Su-27 is estimated to have an airspeed of 240 knots in level flight [Fig. 1].

2. The pilot initiates the maneuver by pitching nose up. Figure 2 depicts the aircraft with a pitch attitude of approximately 45°.

3. Within 2.5 seconds, the pitch attitude has increased to 110°-120° above the horizontal. The Su-27 is still traveling in the same direction and decelerating rapidly [Fig. 3].

4. After an additional 3 seconds, the Su-27 recovers with the nose on the horizon and accelerates from its minimum airspeed of approximately 60 knots [Fig. 4].

Throughout the maneuver, there is no appreciable gain or loss of altitude, peak aerodynamic loads have not exceeded 3.5-4 g's, and, according to a Soviet spokesman, the pilot is capable of employing any of the Su-27's weapons systems.

Western observers were surprised that the Su-27 could perform the Cobra maneuver consistently. They also speculated that the Su-27's demonstrated agility in such extreme

1

Figure 1. Sukhoi Su-27 Approaching at 240 Knots, Level Flight
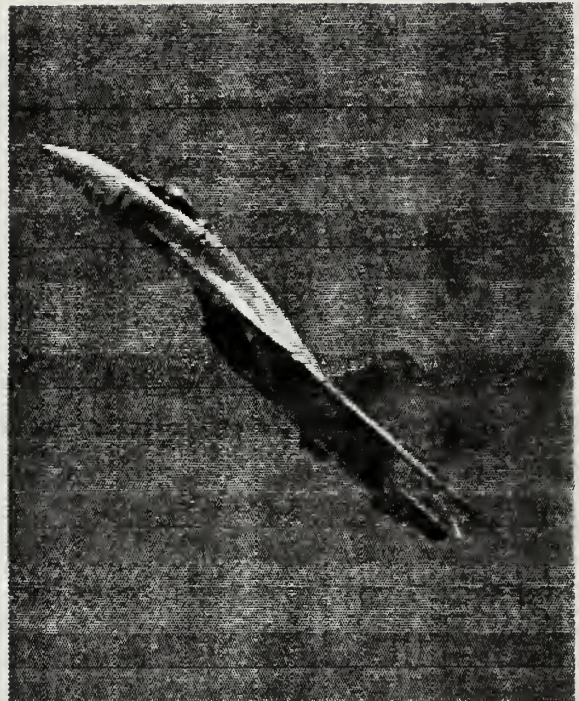
Figure 2. Su-27 Pitching Nose Up at Initiation of "Cobra" Maneuver

Figure 3. Maximum Pitch Attitude of 110°-120° Above the Horizon
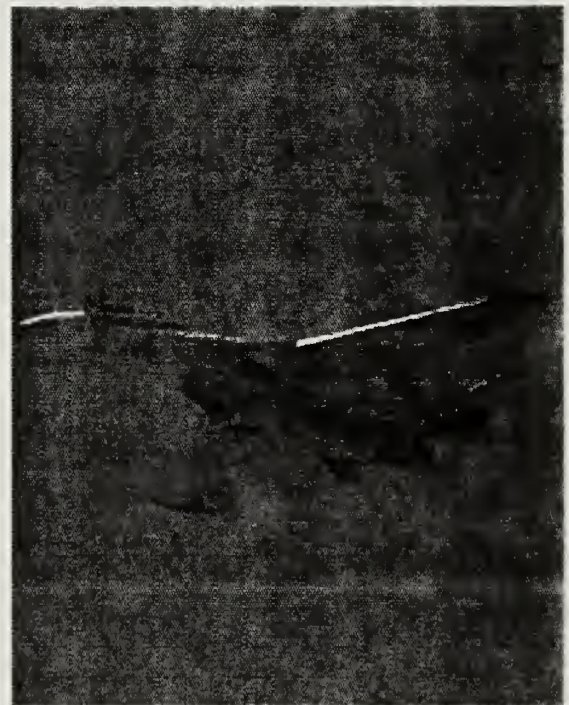
Figure 4. Recovery with Nose Level, 60 Knots Airspeed

flight conditions could translate into enhanced safety and tactical performance while in less severe flight conditions. While the Su-27's high AOA capability is impressive in its own right, it is underscored by the fact that no current U.S. fighter can match it [Ref. 2].

The current high AOA technology program being conducted by NASA may serve to close the apparent gap in performance capabilities between U.S. and potential adversary fighter aircraft. The high angle-of-attack research program (HARP), is an intercenter NASA program with close cooperation between Ames-Dryden, Ames-Moffett, Langley, and Lewis Research Centers [Ref. 3]. The program objectives are to provide flight validated design methods that will enable future tactical aircraft to utilize, rather than avoid, the high AOA flight regime, to develop and demonstrate control concepts that will improve high AOA maneuverability and agility, and to enhance flight safety [Ref. 4].

The program approach includes flight testing [Fig. 5], computational methods [Fig. 6] and ground based experiments. One of the scheduled ground based experiments is the testing of a full-scale McDonnell Douglas F/A-18 in the 80x120 foot wind tunnel at the NASA-Ames Research Center [Fig. 7]. The tunnel can develop air velocities that closely approximate flight conditions. An ex-Navy Blue Angels F/A-18 will be used to develop high AOA instrumentation and structural devices such as forebody strakes and vortex blowing/suction systems and flow visualization techniques. In addition, tail buffet, forebody flows, vortical flows and inlet performance will be studied at AOA's up to 60°.

Before testing can begin several modifications must be incorporated into the wind tunnel to accommodate the aircraft over the range of AOA's to be investigated. Of particular interest is the design and configuration of the struts that will support and pitch the aircraft. Two factors that will influence the final design are the structural feasibility and the aerodynamic interference of the flow over the aircraft caused by the struts. The structural feasibility will hinge on the ability of the struts to pitch the aircraft through the range of interest and the necessary factor of safety associated with both the location and the method of attachment of the struts to the aircraft. Aerodynamic interference caused by the support struts should be minimized to the maximum extent practical, consistent with the requirements imposed by the structural feasibility, and the remaining interference should be documented so their contribution may be isolated from the phenomena of interest during data reduction. When combined with other required experimental corrections this

3
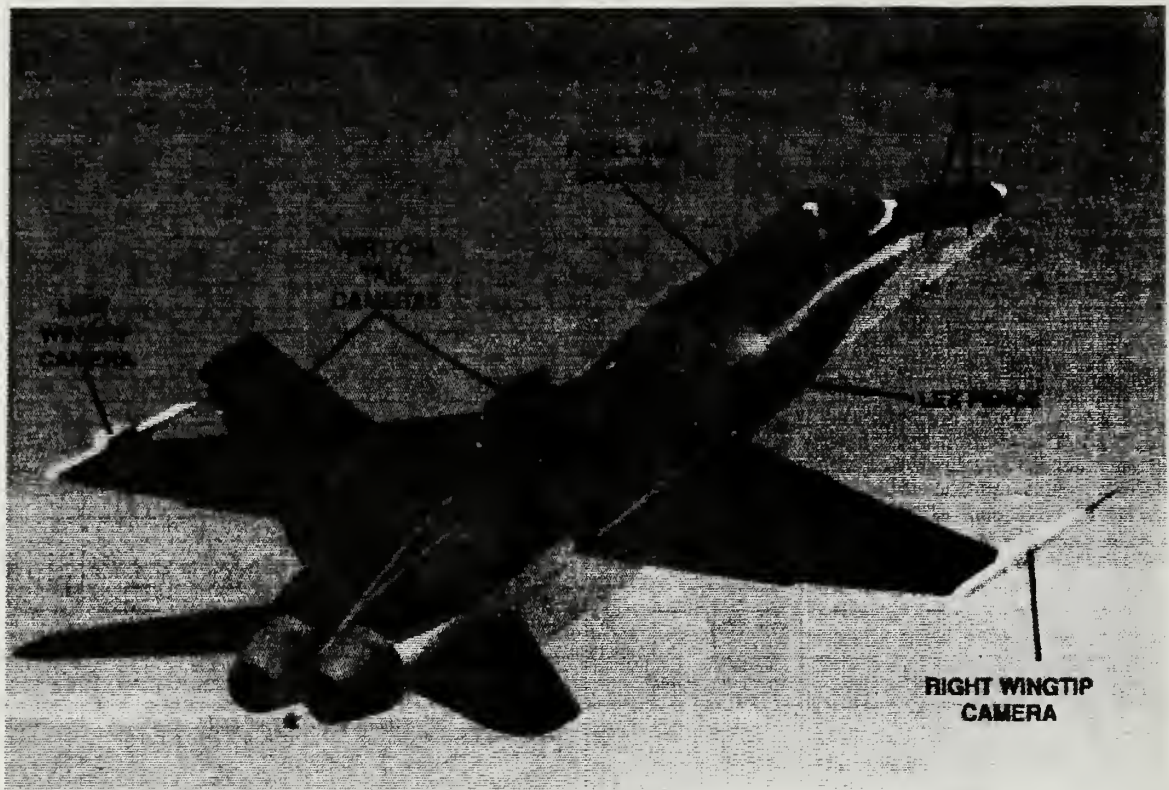
Figure 5. NASA's High AOA Research Vehicle (HARV) Conducting Flight Tests with Smoke for Flow Visualization [Ref. 4]

Figure 6. Computer-Generated Computational Fluid Dynamics (CFD) Prediction of Surface Flow at 30° AOA [Ref. 4]

4

methodology will allow for the results of the wind tunnel study to be more readily applied to the prediction of aircraft performance in free flight.
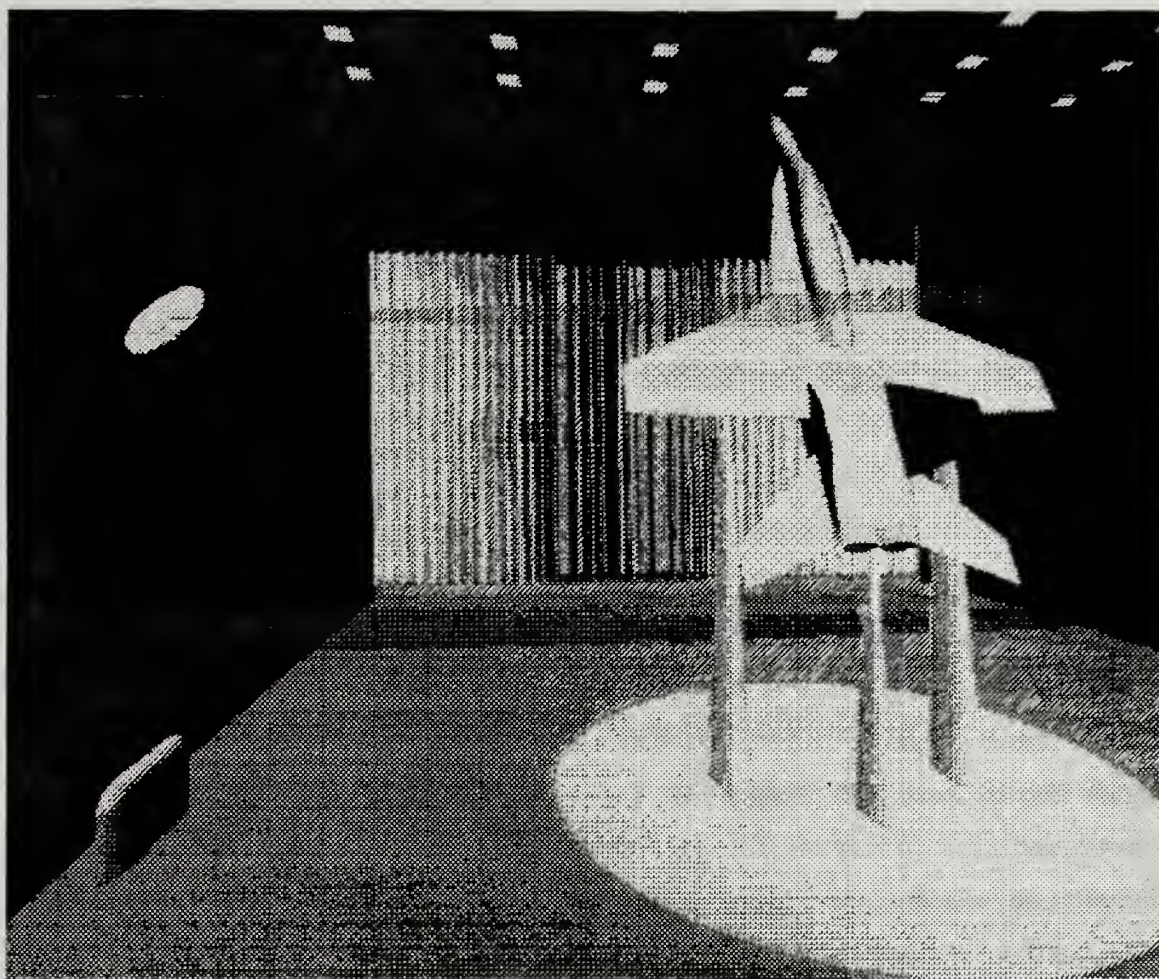
Figure 7. Computer-Generated Depiction of an F/A-18 Mounted on Struts in the NASA-Ames 80x120 Foot Wind Tunnel with a Laser Sheet for Flow Visualization [Ref. 3]

This study was undertaken at the request of NASA-Ames Research Center, to experimentally investigate the interference effects of the support struts, and arrive at an aerodynamically optimum support strut configuration. The study was conducted on a small scale (3%), utilizing the Naval Postgraduate School's 32x45 inch, low-speed wind tunnel. A model of the Northrop YF-17, the lightweight fighter prototype from which the F/A-18 evolved, served as the test model. In addition, a strut assembly on a scale compatible with the YF-17 model allowed for the evaluation of various strut configurations.

B.   STRUT INTERFERENCE

The ideal method of simulating free flight in a wind tunnel environment would be one in which no mechanical means of supporting the aircraft model were required. Suspending a wind tunnel model in a test section without mechanical strings or supports eliminates primary error in the measurement of pressure at the attachment point of the supports, as well as secondary error due to distortion of the wake as the flow passes over the supports. Intrusion into the flow field by the support system can cause gross errors in the data. For example, data for a missile at high angles of attack can vary as much as 40% depending on support location [Ref. 5]. Some elaborate schemes have been devised that avoid such undesirable effects. Advanced magnetic suspension and balance systems (MSBS) avoid the problem by using strong magnetic fields to suspend the model and to provide dynamic force and moment data. MSBS. while appropriate for some relatively small-scale applications, does not provide a practical solution to the problem of mounting a full-scale aircraft in a large wind tunnel. In order to provide the necessary factor of safety, and to keep the operation of the wind tunnel both physically and economically feasible, a more conventional method of mounting the F/A-18 in the 80x120 foot wind tunnel will be used. The proposed support system consists of a tripod arrangement of struts extending up through the tunnel floor. The aft strut is attached to the tail of the aircraft and provides pitch control by variation of the strut length. The two forward struts will be attached under the wings or at a position near the main landing gear. Each of the three struts is enclosed by an airfoil-shaped shroud whose length is adjustable independently from that of the strut itself. The entire assembly is mounted on a turntable that provides yaw control. As the turntable rotates, the shrouds automatically swivel in the opposite direction to remain aligned with the oncoming airstream.

As stated earlier, such an arrangement will induce some interference on the flow over the aircraft. The focus of this investigation is to determine the interference caused by the support struts. The general procedure followed here to determine the interference effects consists of mounting a 3% scale model of the YF-17 on a six-component strain gage balance and sting support and then introducing scale models of the support struts in various configurations. The most desirable strut configuration, from an interference point of view, will yield the least amount of deviation in force and moment data when compared to that

6

obtained when no struts are installed. Even though there is some additional interference introduced by the sting, vertical support arm, splitter plate and other apparatus associated with the mounting of the (dummy) support struts (see Chapter II), these effects are common to all the configurations including the no-strut configuration. Therefore, when making comparisons, these effects will contribute equally to each configuration and the effects due to the dummy support struts will be isolated.

Recognizing that the optimum aerodynamic strut configuration may not be the most practical with regard to the structural constraints stated earlier, data for all of the configurations tested will be presented. It is hoped that this data will assist in the evaluation of the strut interference associated with the final configuration.

In addition to the force and moment data, flow visualization studies were carried out using smoke illuminated by laser sheet to highlight the flow phenomena about the aircraft and models, thus assisting in the qualitative understanding of the flow patterns induced by the strut interference.

C.   METHODOLOGY

1.   Force and Moment Measurements

The forces and moments acting on a wind tunnel model can be determined indirectly by measuring the pressures acting on the surface of the model. Such a procedure requires that a large number of instrumented ports be located on a specially constructed model. A more accurate and reliable method consists of the direct measurement of forces and moments by means of a balance assembly. The balance may be mounted either internally or externally. In addition, the balance may be either mechanical or electrical. Most large wind tunnels utilize external balances that are connected to the model via struts. The struts also serve as the sole means of support for the model. Such is the case for the 80x120 foot wind tunnel at NASA-Ames. Smaller models can satisfy the support requirements by using a sting mount. The sting mount utilizes an internal balance which is electrically operated. The YF-17 model utilized in this investigation was fitted with a six-component, precision strain gage balance. The strain gages inside the balance change their resistance when subjected to small deflections which are in turn proportional to the forces and moments imposed on the model. The gages are appropriately arranged within the

7

balance such that forces and moments may be resolved. Each strain gage is in a Wheatstone bridge circuit. As the voltage across the strain gage varies, an imbalance is sensed and the resulting voltage is recorded by the data acquisition circuitry. After amplification and processing of these voltages, the aerodynamic forces and moments are determined by combining the readings from each strain gage channel via equations appropriate for the physical orientation of the gages within the balance.

2. Flow Visualization

A deeper insight into the flow phenomena can be obtained from actual visualization of the flow patterns around wind tunnel models. A more intuitive understanding of the flow is often obtained when the flow patterns are made visible. Many methods have been used to visualize the flow of air over a wind tunnel model including the use of tufts, oil or dye films applied to the surface of the model and smoke. Tufts and oil/dye films are useful for visualization of flows near the surface of the model. To visualize the flow of air above the surface, smoke has proved to be extremely useful. The smoke may be produced on board the model itself or by injection upstream. To produce smoke on board the model, either smoke ports or substances such as titanium tetrachloride applied to the surface have proved successful [Ref. 6]. Various systems have been used to inject smoke ahead of the model. Smoke rakes and smoke wires are useful in visualizing two-dimensional flows, while smoke tubes are appropriate for three-dimensional flows.

When utilizing a smoke tube, much of the flow detail within the column of smoke can be obscured by smoke itself. To overcome this problem a sheet of laser light is used to illuminate a thin "slice" of the smoke. The illuminated smoke is visible through the surrounding smoke and thus flow phenomenon can be directly observed or recorded. Such a system has been installed in the NPS 32x45 inch wind tunnel [Ref. 7], and was utilized during the course of this investigation for visualization of the flowfield around the aircraft and strut models.

II. EXPERIMENTAL APPARATUS

A. WIND TUNNEL

The investigations were carried out in the 32x45 inch, closed-circuit, single return, horizontal flow wind tunnel located in the basement of Halligan Hall at the Naval Postgraduate School. The wind tunnel was designed by the Aerolab Development Company of Pasadena, California, and installed at NPS in the mid 1950's. Figure 8 depicts the layout of the wind tunnel.

Figure 8. NPS Low Speed Wind Tunnel
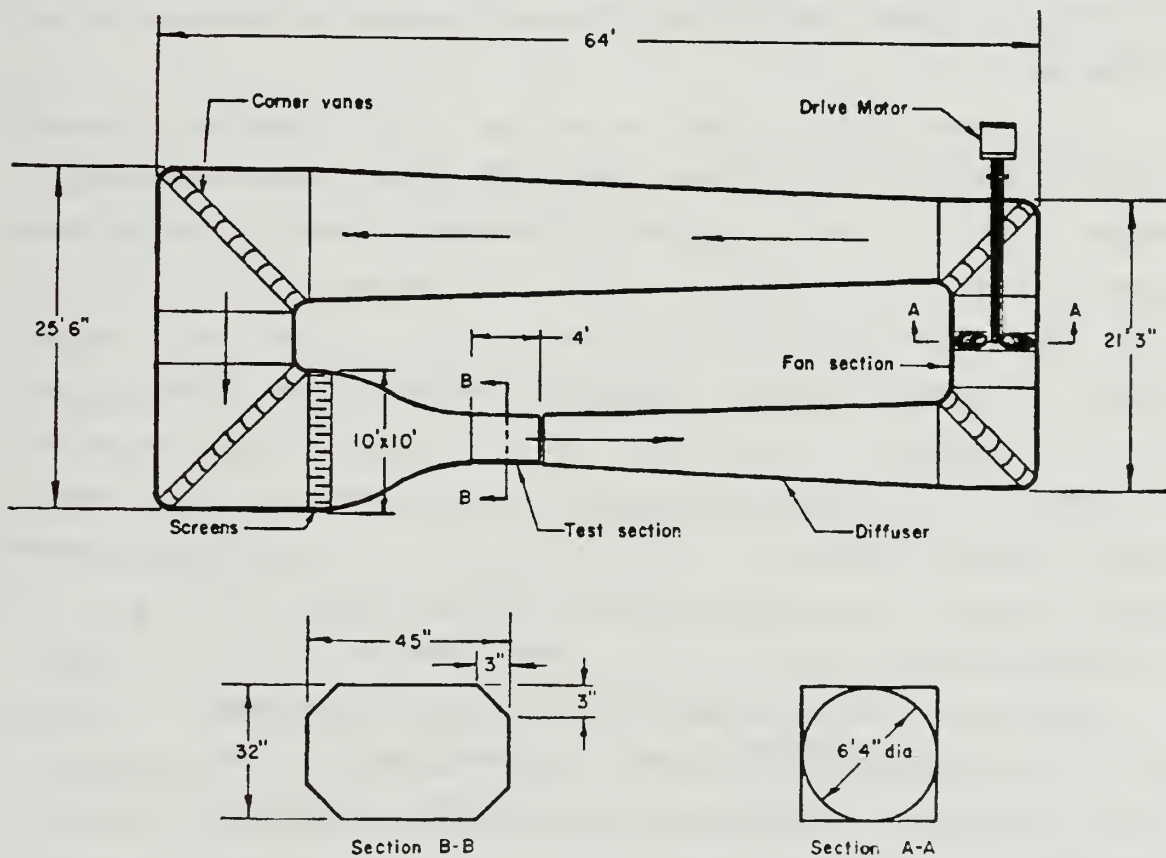
Power is supplied by a one-hundred horsepower electric motor driving a variable pitch, three-bladed fan via a four-speed truck transmission. This power section arrangement allows for efficient operation over various speed regimes up to approximately 180 miles per hour. The fan section has a diameter of six feet four inches. A set of eight stator blades immediately following the fan assist in removing the swirl imparted by the fan. The flow is turned ninety degrees at each of the four corners. Each corner encloses a set of curved turning vanes to assist the flow in negotiating the turn.

The tunnel gradually diverges upon exiting the fan section until it reaches the settling chamber which has the largest cross sectional area. At the exit of the settling chamber the relatively low-speed flow passes through two fine-mesh wire screens. These anti-turbulence screens are separated by approximately six inches and serve to smooth the flow before entering the contraction section. The contraction section has an area ratio of approximately 10:1 and serves to further reduce fluctuations and accelerate the flow prior to entering the test section.

The test section has the smallest cross sectional area; 9.88 square feet. The cross section is basically rectangular with corner fillets which obviate or alleviate the synergetic boundary layer effects at the wall intersections. This design is characteristic of the entire tunnel except the fan section, where the cross section is circular. The fillets in the test section contain fluorescent lights to illuminate the model. The test section is slightly divergent to compensate for the contracting effect due to boundary layer growth along the walls. Major dimensions of the test section are 32 inches high, 45 inches wide and 48 inches long. A reflection plane positioned three inches above the floor of the test section houses a remotely driven/operated turntable to which the lower horizontal arm of the model support is attached. The turntable allows for adjustment of model attitude about the vertical axis during tunnel operation, and has a digital readout accurate to +/- 0.1 degree.

Optical access to the test section is provided by hinged glass windows on each side and a 3/4 inch plexiglass window in the ceiling. The outboard side window was replaced by the strut assembly during this investigation but optical access was preserved by the use of clear plexiglass. The upper window provides the attachment and pivot point for the upper horizontal arm of the model support.

To ensure that the test section remains at atmospheric pressure, a breather slot extending completely around the exit of the test section allows for air exchange. The tunnel then slightly diverges until it completes the circuit at the fan section.

Flow measurement is provided by several components integral to the tunnel. Temperature is sensed by a dial thermometer extending into the settling chamber. Four pressure taps are flush mounted in the walls of the settling chamber and connected to a common manifold. A similar arrangement exists at the entrance to the test section. The two manifolds are connected to a water-filled manometer which displays the pressure difference in centimeters of water giving the test section dynamic pressure. A digital readout of the test section pressure difference is provided by a pressure transducer circuit connected to the manometer. Atmospheric pressure is indicated on a barometer mounted on the exterior of the tunnel. A pitot tube located at the entrance to the test section and connected to an airspeed indicator provides approximate velocity readings. These readings are useful only as a rough estimate of the velocity in the test section and are totally unreliable below 40 knots.

Actual test section velocity is determined by substitution of the appropriate wind tunnel conditions into the following equation [Ref. 8]:

$$U_{\text{r}} = \{[(2)(2.046)(\Delta p)]/[(0.93)(\rho)]\}^{1/2}$$

where:

U_{r} = Test section velocity (ft/sec)

2.046 = Conversion factor

Δp = manometer reading (cm H_2O)

0.93 = Settling chamber total pressure correction

ρ = air density (lbm/ft^3)

11

B. YF-17 MODEL

A three percent scale model of the Northrop YF-17 lightweight fighter prototype was used to simulate the McDonnell Douglas F/A-18 that will be used in full scale testing at NASA-Ames. The YF-17 model was chosen due to its close similarity to the F/A-18 and its availability. The model was on loan to NPS from the Northrop Corporation.

The model had been previously utilized at NPS for investigating high AOA phenomenon [Ref. 9]. The investigation was conducted in the low-speed wind tunnel and included both force/moment measurements and flow visualization. Thus, the model was part of a proven system. Even though some dissimilarities exist between the YF-17 and the F/A-18, they were minor enough to justify the use of the model to investigate aerodynamic trends (rather than obtain exact values), as stated in the goals for this investigation.

Some of the more obvious dissimilarities are listed below and depicted in Figures 9 and 10.

1. The YF-17 Leading Edge Extensions (LEX's) have a simple planform while the F/A-18 LEX's have a compound planform. The F/A-18 LEX's extend further forward. There are two slots in each LEX on the YF-17 while only a smaller aft slot exists on each of the F/A-18 LEX's.

2. The fuselage extending aft of the canopy on the top of the YF-17 has a significant taper resulting in a low ridge at the tail. The F/A-18 "turtleback" does not taper as much and maintains a more rounded cross section.

3. The YF-17 horizontal tail has a sharp, angular trailing edge tip while the F/A-18 has a rounded one.

4. The YF-17 model's nozzles blend together in order to accommodate the sting. The F/A-18 has two distinct conical nozzles.

5. The YF-17's wings and fuselage are aerodynamically very clean with no protrusions. The F/A-18 has several protrusions on the underside of the wing which house flap and aileron actuators and the fuselage has several antenna and other protrusions including the tail hook.

6. The YF-17 model is configured with wing tip missiles. It is anticipated that the F/A-18 to be used in full scale testing will only have the launch rails without the missiles attached.
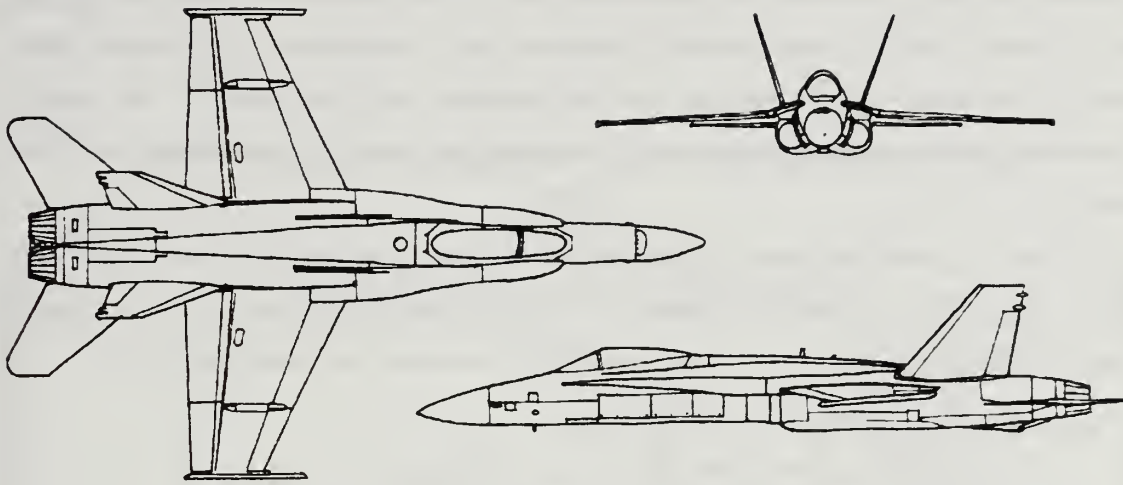
Figure 9. McDonnell Douglas F/A-18
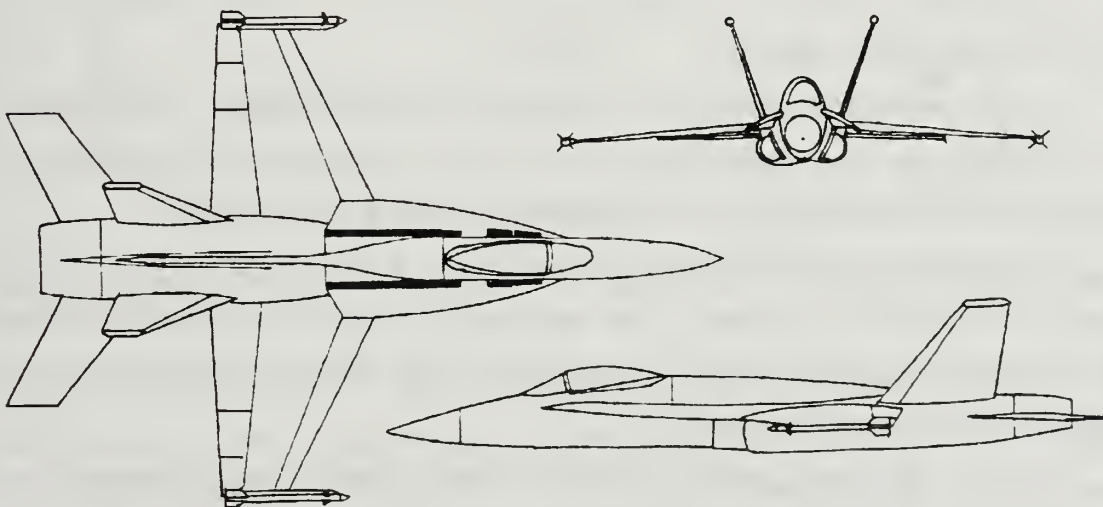
Figure 10. Northrop YF-17 (3% Scale Model Configuration)

13

The YF-17 model was fabricated by the Northrop Corporation's Aero Sciences branch in the early 1970's using stainless steel, aluminum and brass. The design allows for air to flow through the inlets and exit through the nozzles. Variable flap and aileron settings can be attained by replacement of the components with control surfaces of preset deflections. Neutral control settings were utilized throughout this investigation. The balance block section of the model accommodates a one-inch diameter precision balance. The balance is positioned and secured by the use of a locating pin under the removable turtleback section.

To ensure good flow characteristics over the surface of the model all screw holes were filled in with clay. Clay was also used to fill in the forward LEX slots in order to more accurately simulate an F/A-18. Key dimensions of the model are listed below:

1. Total Length = 19.125 in.
2. Wing Span = 12.60 in.
3. Wing Area = 45.36 in².
4. Wing MAC = 3.88 in.
5. Frontal Area = 2.88 in².
6. Planform Area = 89.28 in².
7. Side Area = 53.42 in².

C. SUPPORT STRUT MODEL

The strut model was fabricated by NASA-Ames Research Center. It was designed to accommodate the strut configurations that are under consideration for mounting the full scale F/A-18 in the 80x120 foot low speed wind tunnel at NASA-Ames.

The components were fabricated and assembled on a scale compatible with the YF-17 model and the NPS wind tunnel. This requirement necessitated the use of a splitter plate to simulate the proper separation between the ground plane of the 80x120 foot wind tunnel and the strut supported aircraft.

In order to utilize the turntable in the NPS tunnel for angle of attack variation, it was necessary to mount the YF-17 in a vertical plane (90° right wing down orientation). To accommodate this orientation, the strut assembly replaced the outboard side observation window in the test section. The overall effect was a three percent scale model of a strut

mounted aircraft in the 80x120 foot wind tunnel, rotated ninety degrees on its right side. Figure 11 depicts the installation of the support strut assembly in the test section with the aircraft model pitched to approximately 30° nose up as viewed from the contraction section upstream.
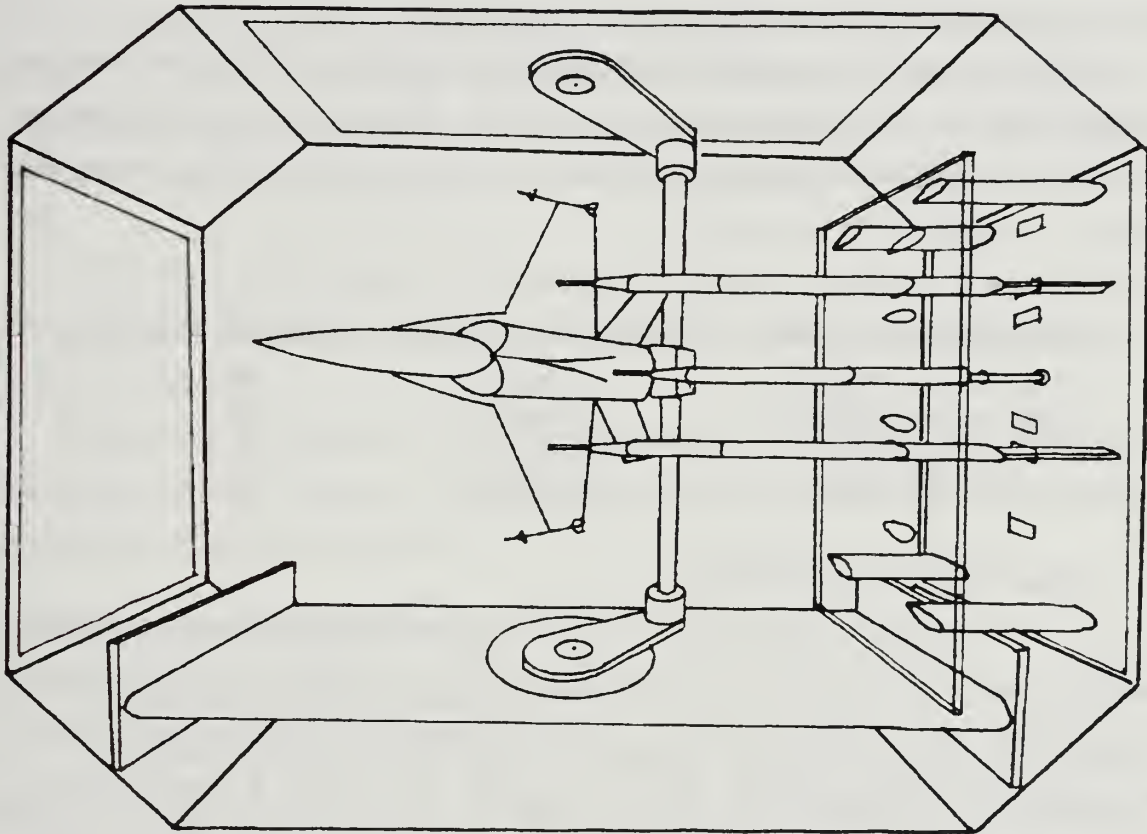
Figure 11. Installation of Aircraft and Strut Models in the Test Section of the NPS 32x45 Inch Wind Tunnel

To retain optical access to the test section, transparent plexiglass was utilized to the maximum extent possible. However, due to structural considerations the stand-off supports for the splitter plate were fabricated from steel. The aft strut was fabricated from aluminum and the two forward struts were fabricated from wood with steel cores.

The struts are threaded at the tips to allow for extensions to be attached. Three extension lengths were provided: 1.5, 0.5, and 0.4 inches. The extensions on the forward

struts are aligned with the lateral axis passing through the aircraft's moment center. The forward struts may assume three positions; 1.875, 4.531, or 6.188 inches outboard of the aircraft's centerline. These positions roughly correspond to the wing root, midspan and wingtip respectively. Since the tips of the strut extensions are very nearly aligned with the axis of rotation the forward struts' length requires only minor adjustment as the aircraft is pitched. The aft strut is aligned with the centerline of the aircraft and is able to pivot about a point just below the simulated ground plane (splitter plate).

The tips of the strut extensions are kept adjacent to the underside of the model as angle of attack is varied by sliding the struts in or out. Certain limits exist at high angles of attack, depending on the length of the aft strut extension and the simulated attachment point on the model as outlined below:

AFT STRUT LOCATION	EXTENSION LENGTH	MAXIMUM AOA
TAIL HOOK PIVOT	0.4 INCH	60°
TAIL HOOK PIVOT	1.5 INCH	60°
NOZZLE LIP	0.4 INCH	55°
NOZZLE LIP	1.5 INCH	40°

D.   MODEL/BALANCE SUPPORT

The YF-17 model accommodates a one inch diameter precision balance or a blank made from solid stainless steel of the same dimensions. The balance or blank slides into the model from the rear and is secured by a single pin located just aft of the canopy under the removable turtleback assembly. The aft end of the balance/blank is tapered and slips into the forward end of the hollow sting adapter. Four equally spaced sets of screws, aligned at 45 degrees off axis, serve to compress the hollow sting against the balance/blank. The sting attaches to the vertical support arm. The vertical support arm is connected at both ends to horizontal support arms. The upper support arm pivots about a one-inch steel pin passing through the 3/4 inch thick plexiglass overhead observation window. The lower support arm is attached to the turntable in the reflection plane. Heavy construction, and close tolerances between the components keep vibrations to a minimum.

E. FORCE AND MOMENT BALANCE

A precision balance on loan to NPS from the NASA-Ames Research Center was utilized for force and moment measurements.

The balance was a Task Corporation model XIV B, one-inch diameter, six-component, precision strain gage balance. It requires an excitation voltage of 5.00 D.C. volts for each of its six channels. The output consists of two normal (N1,N2), two side (S1,S2), one axial (A), and one roll (R) channels. A 21-foot wire bundle connects the balance to the signal conditioner in the data acquisition system. The wire bundle is comprised of several very fine gage teflon coated wires. In an effort to protect the fragile wires, plastic spiral wrap and woven nylon sheathing were utilized along the length of the cable.

The cable threads through the hollow sting and a hole in the vertical support arm. The cable then passes to the outside of the tunnel via the breather slot and connects to the signal conditioner.

The balance was calibrated at NASA-Ames Research Center [Ref. 10]. Calibration data, conversion values, maximum channel loads and percent accuracies (based on maximum load values) are listed in Appendix A.

F. DATA ACQUISITION SYSTEM

1. Data Acquisition Hardware

As the YF-17 model is subjected to various forces and moments, the balance responds by sending voltage signals through its six channels. In order for the balance to operate, each channel requires an excitation voltage. The function of the data acquisition hardware is to supply the balance with the required excitation voltage and to convert the output voltage signals from the balance into a format useable by the data acquisition software.

The hardware components are assembled in an equipment cabinet and computer operator's station adjacent to the wind tunnel. The functional arrangement of the system is depicted in figure 12, and each component is described in detail below.
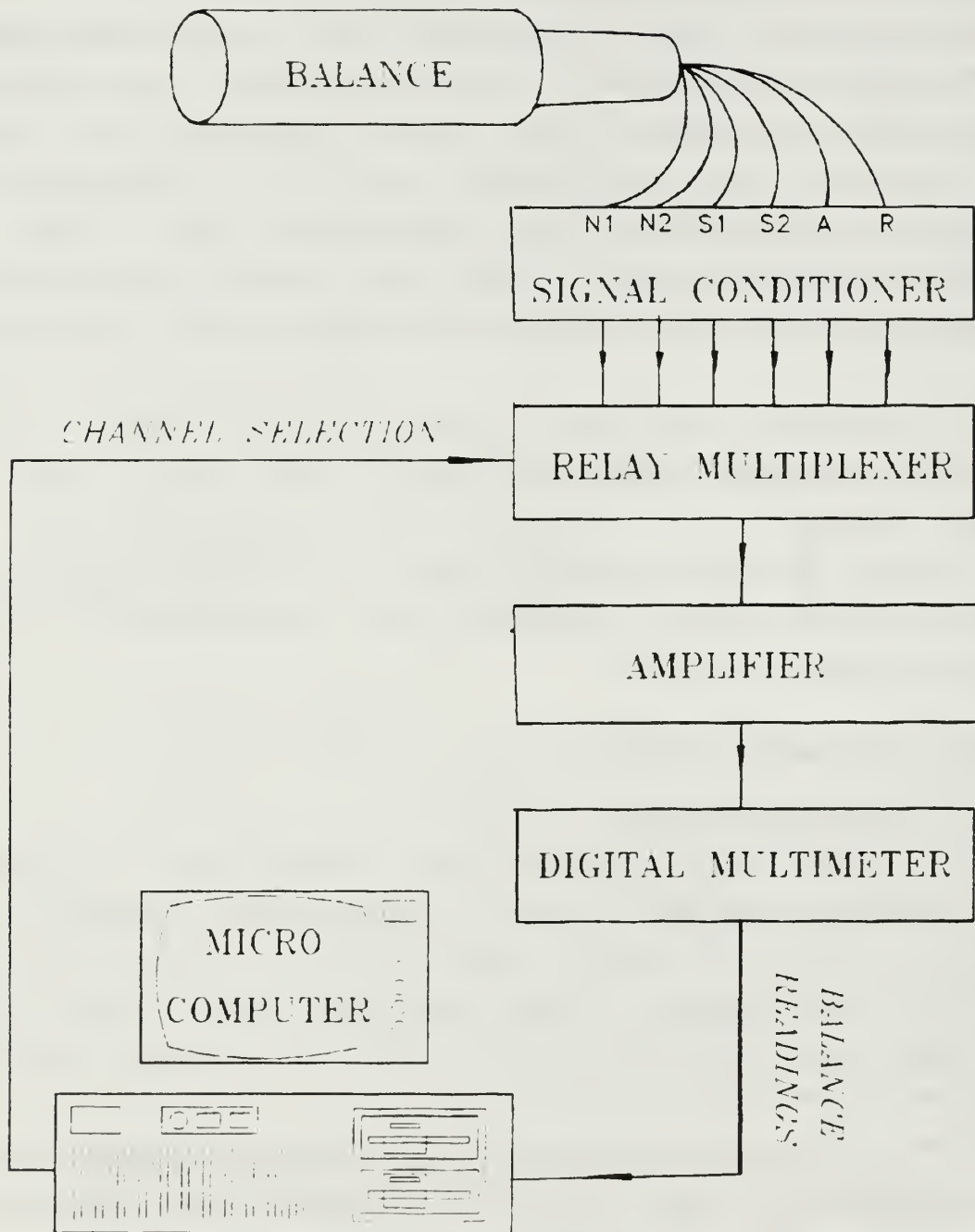
Figure 12. Data Acquisition System

a. Signal Conditioner

The six balance channels are directly connected to the rear of the signal conditioner with cannon plugs. Each channel's required excitation voltage of 5.00 D.C. volts is separately adjusted by potentiometers located on the front panel. Monitoring of the excitation voltages is accomplished by connecting a digital multimeter to the input jacks on the front panel. Separate output potentiometers are used to zero the Wheatstone bridge circuitry associated with each channel in the balance during calibration. Monitoring of the output voltages is also available on the front panel of the signal conditioner, but is usually accomplished after the signal is amplified/digitized and passed to the microcomputer.

b. Relay Multiplexer

The signal conditioner outputs voltage signals from all six balance channels simultaneously via six pairs of wires. The amplifier is capable of handling only one channel at a time. The Hewlett Packard PC Instruments 61011A Relay Multiplexer sequentially samples each of the six channel's signals and routes them to the amplifier. The relay multiplexer's channel selection is automatically controlled by the PC Instruments software in the microcomputer.

c. Amplifier

The sequentially sampled balance channel output voltages are amplified before measurement to improve resolution. The Pacific Amplifier model #8256 is a low noise amplifier with selectable gains up to 1000. Two screws on the front panel may be used to zero and calibrate the amplifier, with one screw used at low gain and the other at high gain.

d. Digital Multimeter

The Hewlett Packard PC Instruments G1013A Digital Multimeter (DMM) measures the amplified D.C. voltage signals from the amplifier. It performs these measurements under the control of the Hewlett Packard PC Instruments software in the microcomputer. The DMM automatically selects the optimum voltage range for the signal being measured. To make these measurements the DMM uses a 4 1/2 digit A/D (analog-to-digital) converter. Measurements can be taken continuously (2.5 or 12.5 readings/second)

19

or triggered one at a time. The readings taken at 2.5 per second exhibit the greatest accuracy. The amplifier outputs are connected to the HI and LO input jacks on the DMM's front panel. Calibration constants are stored in a non-volatile memory device inside the DMM.

e. *Microcomputer*

An IBM-AT microcomputer controls the functions of the Hewlett Packard PC Instruments and receives the digitized balance readings. A Hewlett Packard Interface Card installed in the microcomputer provides the connection to the DMM and Relay Multiplexer via a ribbon-cable bus. The data collected can be stored on the hard disk drive or transferred to 5 1/4 inch floppy disks. Hard copy of the reduced data is available from a Hewlett Packard LaserJet printer.

2. Data Acquisition Software

Two computer programs are used for calibration and data acquisition. These programs are in addition to the shell program that controls the operation of the Hewlett Packard PC Instruments in the data acquisition system.

a. *PANELS Program*

The Soft Front Panel and instrument control program (PANELS) allows for computer generated video readout of the amplified/digitized output from each of the six balance channels and a channel that monitors the calibration/balance of the amplifier. Each channel is monitored separately to assist in the balancing of the bridge circuitry associated with that channel. The PANELS program also issues the enable command that activates the DMM.

b. *BREAD.BAS Program*

The Balance READ (BREAD) program , written in BASIC, is imbedded within the shell program that also controls the Hewlett Packard PC Instruments DMM and relay multiplexer. BREAD.BAS sequentially samples the six amplified/digitized channel output voltages ten times each through the action of the relay multiplexer. The readings are averaged and combined with the appropriate calibration constants and conversion factors listed in Appendix A. After manipulation within the program the N1, N2, S1, S2, A and

20

R channels are combined to yield normal, side and axial forces in pounds and the pitching, rolling and yawing moments in foot-pounds. Tare readings are subtracted to separate airloads from static forces and moments not zeroed out during balance calibration. A listing of the program is provided in Appendix B.

G. FLOW VISUALIZATION SYSTEM

During the course of previous investigations at the Naval Postgraduate School [Refs. 7,9], a flow visualization system utilizing smoke and a laser sheet for illumination has been developed and refined. Although the laser and optics set up has remained unchanged, during the course of this investigation the smoke injection apparatus and operating techniques were modified to avoid the adverse effects associated with the placement of the smoke generator inside the tunnel and to simplify operation. The general layout of the system is depicted in figure 13 and each component is described in detail below.

1. Laser

The source of illumination is a Spectra-Physics model 164, five-Watt Argon-ion laser. The laser requires a Spectra-Physics model 625 power supply for operation. In addition, it requires 2.2 gpm of cooling water delivered at a pressure of at least 25 psig.

The laser emits a 1.25 mm blue-green beam with a divergence of 0.69 mrad. The laser itself is classified as a class IV laser product, and as such several safety precautions and interlocks have been incorporated to protect the operator. Safety interlocks internal to the laser power supply monitor water pressure, voltage and circuit continuity. An external interlock switch mounted on the access door leading to the wind tunnel's internal work space trips the circuit breakers on the power supply when the door is open. Rotating safety lights and warning signs alert personnel to laser radiation exposure hazards.

2. Optics

Transportation and beam-to-sheet conversion of the laser light was performed by the optics between the laser and the wind tunnel.

A Newport Corporation F-LFI laser fiber illuminator provides a safe and simple way to transport visible laser light to remote or difficult-to-access locations. It consists of a ten meter long armor-cabled fiber, a quick-connect laser coupling head and a convenient
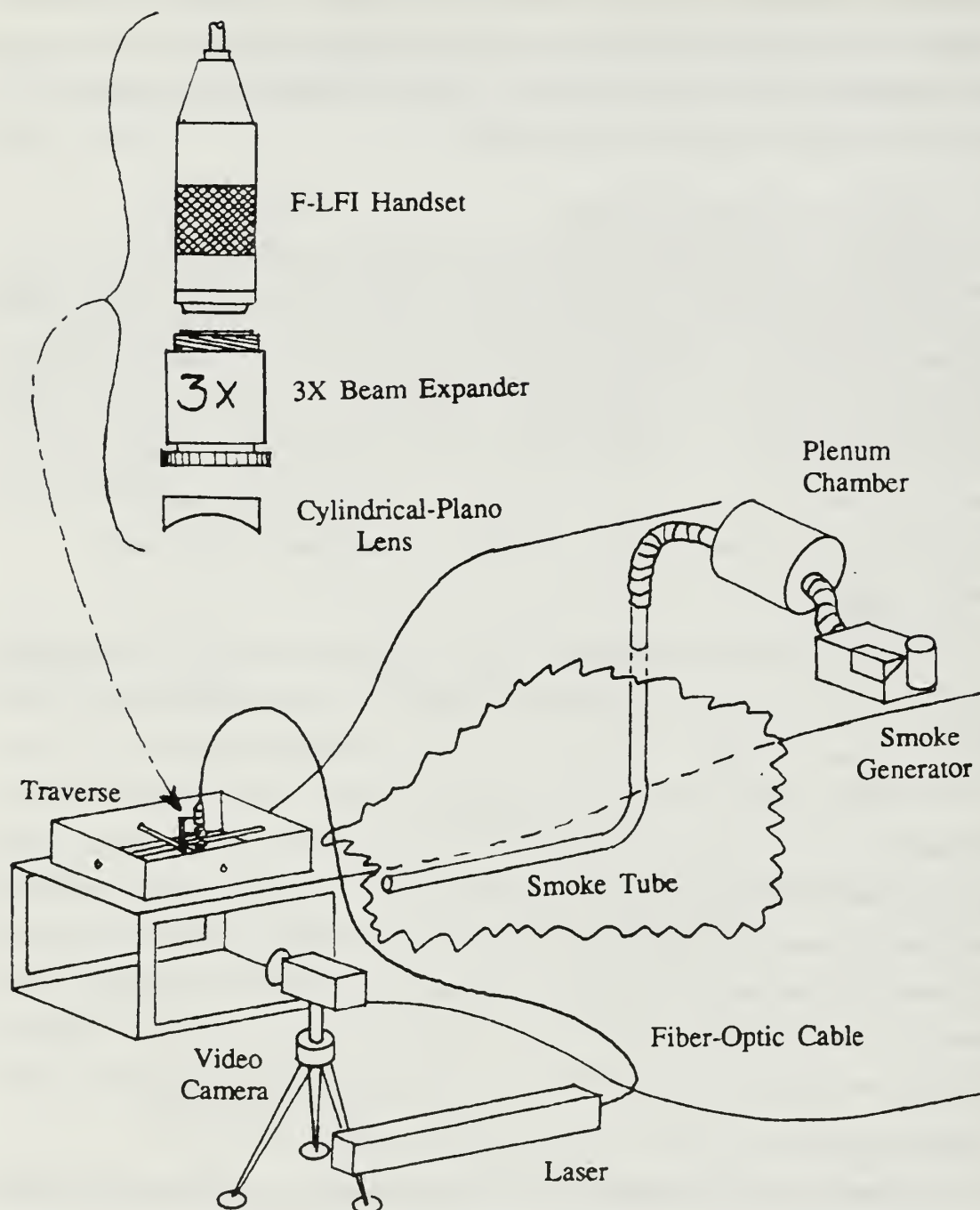
Figure 13. Flow Visualization System

output handpiece. The cable holds a 200 micron diameter silica fiber (Newport Corporation model FA-2UV-10) which is held in the coupler by crimp connectors. The fiber has a throughput efficiency of approximately 80%. A mounting collet screws directly into the

threaded output bezel of the laser. The coupler's lens focuses the beam on the fiber endface. Fine horizontal and vertical adjustments center the focused beam on the fiber core, while the outer barrel rotates to position the endface of the fiber in the focal plane of the lens. A three-position sliding bar on the coupler can be set to block the beam, attenuate it, or pass it unattenuated. The handpiece emits a six-millimeter collimated beam with less than 10 mrad divergence.

The six-millimeter beam enters a Newport Corporation model T81-3X beam expander. The term "expander" is a misnomer in this application because as the beam passes through the component it is contracted. The 3X in the model number corresponds to the magnification factor of the "expander". Thus, as it exits, the collimated beam has a diameter of approximately two millimeters. A plano-cylindrical lens then fans the beam out in one plane to form a thin sheet of laser light with a width of approximately three millimeters at the center of the wind tunnel test section.

The fiber optic handset, 3X beam expander and plano-cylindrical lens are all mounted on a six-inch rail which is attached to a traverse mechanism. The traverse allows the optics to be positioned over any area of interest in the test section by rotating the two worm-gears passing through the optics mounting block. The traverse mechanism can be mounted on any of the three test section windows, but for the purposes of this application was mounted above the upper window.

3. Smoke Generation and Injection

Although many methods exist for injection of smoke, the most appropriate method for studying the flow over a three dimensional body in the present set-up appears to be the injection of smoke from a tube. This produces a column of smoke which, when it passes over the body, clearly highlights the formation and bursting of vortices as well as other flow phenomena. Smoke rakes and wires, while useful for two dimensional bodies, do not cover sufficient area to illustrate three-dimensional flow. With their inherent traits in mind, and heeding the lessons learned in previous investigations, a system utilizing a smoke tube was chosen for this investigation.

Previous investigations in the low speed wind tunnel had utilized a smoke tube but the entire system was internal to the wind tunnel, with the major components installed

in the settling chamber and contraction section. Even though the tunnel was operated at low speed (10 m/s) during flow visualization, and the apparatus was installed in the lowest velocity region of the tunnel, it seems reasonable to expect some flow disturbances in the test section caused by the apparatus. In an effort to reduce these undesirable effects, several modifications to the existing smoke injection apparatus were incorporated and are described below.

a. Smoke Generator

A Rosco model 1500 fog/smoke machine was chosen due to its portability, ease of use, safety features and proven performance in previous investigations. The model 1500 produces smoke by forcing Rosco Fog Fluid under pressure into a heat exchanger where it is heated to a temperature near its vaporization point. The heated and pressurized liquid is then discharged through the nozzle into a flexible, two-inch diameter hose where it vaporizes and upon further cooling forms an aerosol consisting of millions of fine, reflective particles ranging from 0.5 to 60 microns. The machine is capable of producing 1500 cubic feet of smoke per minute. The smoke produced is relatively dry and leaves residue on surfaces only after prolonged exposure.

The smoke generator may be operated by controls located on the machine or by the use of a remote control with a 25 foot cable. Controls consist of an on/off switch for continuous or momentary operation and a fog output volume dial. The smoke generator was installed outside of the tunnel directly above the entrance to the contraction section.

b. Smoke Injection

The smoke is routed to a ten-gallon cylindrical plenum chamber via a two-inch diameter insulated hose. The plenum chamber serves to dampen any surges of pressure caused by surging of the smoke machine, and it also helps to cool the smoke slightly to avoid buoyancy effects when injected in the tunnel. The smoke exits the plenum chamber and travels through successively smaller diameter hoses until it reaches the one-inch diameter smoke tube protruding through the ceiling of the contraction section. The smoke tube was fabricated from one inch diameter copper tubing. The tube extends vertically into the entrance of the contraction section three feet downstream of the anti-

24

turbulence screens. The lowest velocity occurs in this portion of the tunnel, and thus the presence of the tubing has a minimum impact on flow quality in the test section. The tube is bent 90 degrees with a radius of curvature of seven inches. The horizontal portion of the tube extends seven feet toward the entrance of the test section. The end of the tube is highly polished and sharpened to a razor edge and is positioned three feet ahead of the model. This end treatment is intended to alleviate any separation, and help smooth the flow as the smoke and air intercept at the exit of the tube. After the smoke exits the tube, it begins to form a slightly divergent column with a diameter of approximately three inches in the test section.

4. Image Recording and Processing Equipment

In an effort to reduce the amount of wind tunnel time required, the flow visualization sessions were video taped. This allowed for the runs to be reviewed on a monitor rather than repeating runs in the wind tunnel.

The video equipment consisted of a Sony DXC-3000AK, three-chip CCD, color video camera, a Sony VO-5850 3/4 inch editing VCR, and a Sony color television monitor. The image processing from video to hard copy format was performed at NASA-Ames Research Center. A "frame-grabber" converted the images to computer format which was then processed and printed out on a laser printer. This process was selected due to the ability of the computer to enhance the images and to avoid the delays and expense associated with photo processing.

III. EXPERIMENTAL CONDITIONS AND PROCEDURES

A. EXPERIMENTAL CONDITIONS

As previously stated, the goal of this investigation was to study the interference effects of support struts on the model flowfield and to arrive at an optimum configuration for the struts. In order to simplify the comparison of data resulting from different strut configurations, the following parameters were held constant during the two phases of the investigation:

1. Test section dynamic pressure (Δp).

2. Aircraft configuration (see YF-17 model description).

3. Aircraft roll and yaw angle ($0°$).

1. Conditions During Force and Moment Measurements

The balance used in this investigation was rated up to 400 pounds for normal force measurement and up to 21 foot-pounds for rolling moment measurement (see Appendix A). Unfortunately the expected forces and moments in this investigation were considerably lower than the capacity of the balance. In order to increase the signal from the balance, the test section velocity was established at 50 m/sec. This value was high enough to make the balance sensitive to the resulting forces and moments but low enough to be attainable in the test section even at blockage ratios as high as those associated with the model pitched to $60°$ AOA.

2. Conditions During Flow Visualization

While it would have been desirable to conduct this phase of the investigation at the same velocity as the force/moment measurement phase, certain limitations existed that forced the velocity to be greatly reduced. The Rosco smoke machine was not capable of producing the volume of smoke required at 50 m/s. At high velocities the column of smoke was very unsteady, due in part to the unsteady flow in the tunnel and in part due to the

oscillations of the smoke tube. The previous investigations established that the optimum velocity for flow visualization in this wind tunnel is 10-15 m/s. Although this value seems low, no discernable difference was observed in the flow pattern as the velocity was varied except for the fact that the flow quality at 10 m/s was somewhat improved.

B. EXPERIMENTAL PROCEDURE

The investigation was conducted in two phases; determination of forces/moments and flow visualization. Procedures regarding the operation of the wind tunnel were common to both phases and the reader is directed to Reference 8 for a detailed discussion.

1. Force and Moment Determination

In an effort to obtain force/moment data suitable for comparing the effects of different support strut configurations, a methodical procedure was devised to minimize data variations due to inconsistencies in technique or hardware configuration during model assembly or runs on different days.

a. *Equipment Assembly*

The balance wire bundle was laid out and inspected for kinks, broken wires and security of the end connectors. The wire bundle was threaded through the hollow sting/balance adaptor assembly one channel at a time. The balance and sting were secured by tightening the four tap screws until the two components were securely compressed together with no free play.

The tail section was removed from the YF-17 model and the wire bundle was threaded through. The turtleback was removed and the balance was inserted into the model's fuselage until it was aligned with the hole located at the moment center. Care was taken to align the "normal" and "side" axes of the balance with those of the model. The balance was secured by inserting the locating pin until it was just flush with the body of the model. If inserted too tightly the locating pin would preload the balance with a normal force and if too loose it would allow excessive vibration. The tail section and turtleback were then reinstalled.

The assembled model/balance/sting was mounted on the vertical support after threading the wire bundle through the hole in the mounting block. Two set screws

allowed for the model to be secured at any roll angle. The wire bundle was secured to the vertical support by wire ties and then threaded to the exterior of the tunnel through the breather slot.

Each balance channel was connected to the rear of the signal conditioner via a cannon plug. The order of wire connection for each channel, starting at the slot on the top of the cannon plug and proceeding clockwise, was as follows:

1. Black
2. Channel color
3. Green
4. Red

The outer test section observation window was removed and the support strut assembly was mounted in its place. After alignment of the struts with the aircraft model's lateral and longitudinal axes, the assembly was secured by the four mounting bolts on the frame of the assembly.

The equipment was assembled at the initiation of the investigation and not altered or disassembled until the completion of data acquisition.

b. Static Calibration of Balance

With the aircraft model assembled and installed in the wind tunnel, the data acquisition system was energized and allowed to warm up for at least one hour.

Each channel's excitation voltage was set at +5.00 D.C. volts. The PANELS program on the microcomputer was started and the digital multimeter was enabled via the program's menu. The program displays an array of nine boxes representing available channels. Assignment of the channels during this investigation was as follows:

0. Not assigned
1. Not assigned
2. N1 (Normal Force)
3. N2 (Normal Force)
4. S1 (Side Force)
5. S2 (Side Force)
6. A (Axial Force)

7.   R (Rolling Moment)

8.   Calibration (Zero Set)

As each channel was selected the voltage was displayed on the screen. Each of the channels was zeroed starting with channel eight.

Channel eight was selected and the amplifier gain set to unity. Using the bottom screw on the amplifier, the voltage was set to zero +/- 200 microvolts. The gain was then increased to 1000 and the voltage reading was set to zero +/-200 microvolts using the upper screw on the amplifier. This voltage was checked periodically to ensure that no drift had occurred.

The model roll was set at 0° (wings level) and channels 4, 5, 6, and 7 were zeroed (+/-200 microvolts) using the potentiometers on the signal conditioner. This orientation was chosen to zero these channels because no rolling moment, side or axial forces should exist at 0° AOA, with wings level.

The model was then rolled 90° (right wing down). In this orientation no normal or axial forces should exist. Channel 6 was rechecked for zero and the potentiometers for channels 2 and 3 were adjusted to yield 0 +/- 200 microvolts. The PANELS program was then exited.

The program BREAD.BAS was accessed in the missile directory on the C drive of the microcomputer. The aircraft was subjected to various static forces and moments by either stacking or suspending calibrated weights at various locations on the model. All forces and moments were calibrated except the axial force. The resulting data are presented in Appendix C. Figure 14 illustrates the convention used for forces and moments during this investigation.

c.   Determination of the Zero-Lift and Trim AOA's

The struts were removed from the strut assembly and the holes were covered with blanks. The tunnel was then started and the velocity adjusted to 50 m/s. The aircraft was pitched between -5° and +5° (indicated or geometric) AOA. The forces and moments were obtained by use of the program BREAD.BAS at approximately one degree increments. The zero-lift AOA was determined by examination of the normal force plot. The trim AOA was determined by examination of the pitching moment plot. As shown
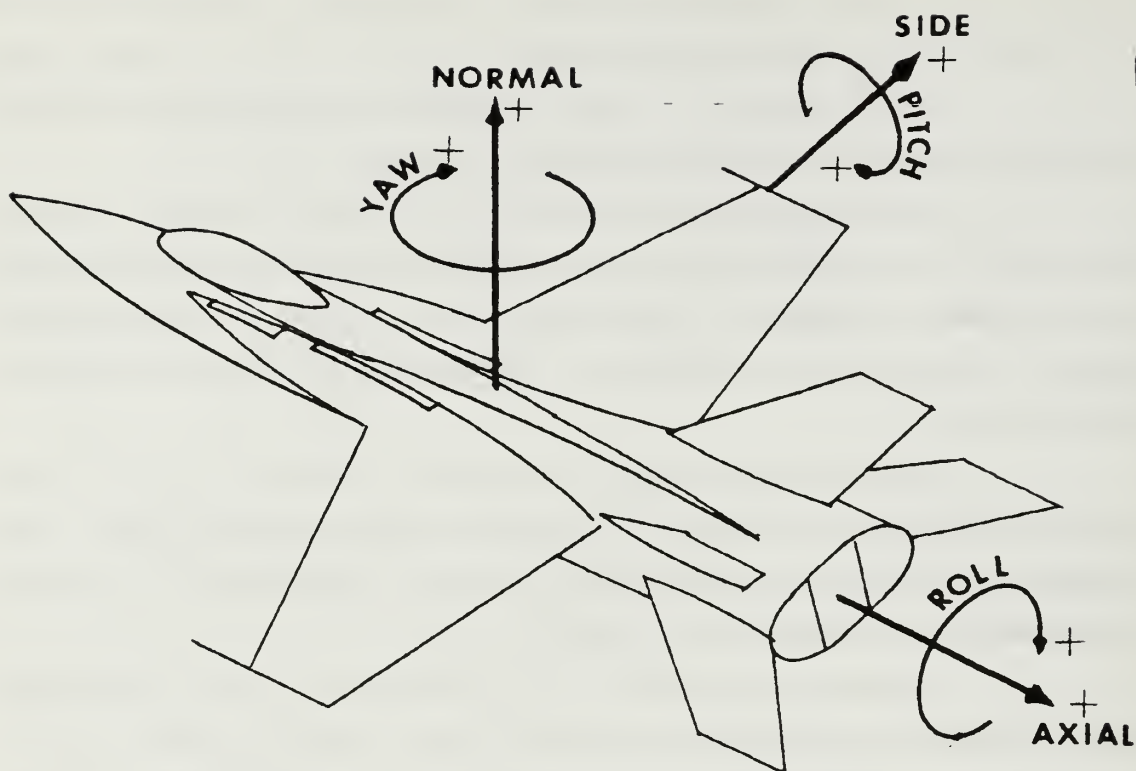
Figure 14. Force and Moment Conventions

in Appendix D, the normal force and pitching moment both pass through zero at an indicated AOA of zero degrees. Thus, the zero-lift AOA and the trim AOA were practically coincident with the 0° indicated AOA.

d. *Data Collection for Various Strut Configurations*

After installing the struts in one of the configurations of interest, they were adjusted such that the extensions were approximately 1/16" from the model. The balance zero was checked and adjusted as necessary by use of the PANELS program, the amplifier zero-set screws, and the channel potentiometers on the signal conditioner as described earlier. The tunnel was then run with a dynamic head of 14.37 cm H_2O which, under standard conditions, yields a test section velocity of 50 m/s. BREAD.BAS was accessed and the aircraft model was pitched from 0° to 60° (or maximum attainable) AOA. Data were taken at approximately 5° increments with the struts repositioned to maintain the

1/16" clearance. The tunnel's dynamic head was also readjusted to maintain the starting value. Following the end of a run the program BREAD.BAS was exited and the data file (WINTUN.DAT) renamed so that the next run would not overwrite it. Two runs were made for each strut configuration to access data repeatability. If it was necessary to roll the aircraft or remove the aircraft/sting from the vertical support arm to reconfigure the struts between runs, the balance was re-zeroed using the PANELS program. Raw force and moment data for the various strut configurations are plotted in Appendix E.

2. Flow Visualization

a. *Operation*

Detailed procedures describing the safety precautions and operation of the laser are given in operator's manual [Ref. 11]. With the laser operating at low power, the optics were "tuned" to yield a three-millimeter thick laser sheet. The laser sheet was then rotated such that it formed a plane perpendicular to the longitudinal axis of the model. The smoke machine was turned on and allowed to come to operating temperature.

With the struts and aircraft set in the desired configuration/orientation, the tunnel was started and the test section velocity adjusted to approximately 10 m/s. The laser power was set to maximum. While viewing the test section through the upper window, the smoke machine was operated via the remote control. The column of smoke was adjusted by slightly rotating the smoke tube protruding through the ceiling of the wind tunnel. Once the smoke passed over the region of interest, the laser sheet was moved via the traverse to illuminate the region. It was found that a denser column of smoke could be obtained by opening one of the air exchange doors in the settling chamber. This not only created a more favorable pressure gradient to assist flow of smoke from the generator to the test section, but also served to exhaust some of the smoke from the otherwise closed-circuit tunnel. Thus, longer run times were attainable before purging the tunnel of excess smoke.

b. Recording Technique

The video camera was positioned near the inboard observation window and the zoom and focus were adjusted to frame the region of interest. The video signal was fed to the VCR and displayed on the television monitor. A placard labeled with the current AOA was taped to the outboard observation window so that the images could be identified during playback. The tunnel was started and the smoke and laser sheet were positioned on the aircraft model. The VCR was then set to record while the smoke and laser sheet were translated along the longitudinal axis of the aircraft model. During recording, the lighting conditions within the test section and the video gain on the camera were adjusted to achieve an optimum image.

c. Image Processing

The video tape was played back and representative images were selected for conversion to hard copy. The "frame-grabber" then converted the video images to digitized computer files that were displayed on a Macintosh computer. The image processing program was capable of enhancing the image through the use of several software routines. Once satisfied with the quality of the image, it was printed on a laser printer. A representative selection of the images obtained are presented in Appendix G.

IV. DATA REDUCTION

A. RAW DATA AVERAGING

Although every effort was made to establish constant conditions for the tare determination at the beginning of each run, some factors beyond experimental control such as slight voltage fluctuations in the power supply and the inability to establish exact pitch attitudes consistently led to some variation in the data from run to run for the same strut configuration. The data did, however, exhibit very similar trends for like configurations. Examination of the raw data established that a constant offset was often observed between runs for the same strut configuration, otherwise the data exhibited excellent repeatability. To reduce the data, a simple procedure of averaging the data for different runs with the same strut configuration was used. As stated above, it was extremely difficult to establish exact pitch attitudes, even though the readout of the AOA was assumed to be accurate to within +/- 0.1 degree. The desired AOA's were multiples of 5.0 degrees, but the actual AOA's established varied by as much as +/- 0.5 degree from the target AOA's. This necessitated that the AOA's be averaged as well as the forces and moments associated with them to yield a single data set for each configuration. The raw force and moment data for each run, as well as the averaged data set were plotted as a function of AOA and are presented in Appendix E.

B. PERCENT INTERFERENCE DETERMINATION

During the force and moment runs the ambient pressure varied from 29.93 in. Hg to 30.11 in. Hg, and the ambient temperature varied between 67° F to 70° F. This variation in ambient pressure and temperature corresponds to a maximum density spread of 0.00232 slugs/ft³ to 0.00235 slugs/ft³. The test section dynamic pressure was held constant at 14.37 cm H_2O. This constant dynamic pressure, when coupled with the variation in density, yields a test section velocity variation of 50.0 m/s to 50.3 m/s. This variation was considered to be well within experimental accuracy, and therefore the test section velocity was assumed to be nominally constant for all of the force and moment runs.

33

Another variable associated with the different configurations was the amount of blockage associated with the struts within the test section. The percent increase in blockage was small enough to ignore due to the relatively small frontal area associated with the struts. The remaining blockage effects due to the presence of the aircraft model, vertical support arm, splitter plate and the reflection plane were common to all of the configurations, and therefore did not present variables to be accounted for when comparing the interference due to the struts.

With the above assumptions in mind, and recognizing the only remaining variable at a given AOA was the configuration of the struts, the following procedure was utilized to evaluate the aerodynamic interference effects of the struts.

The averaged force and moment data obtained with no struts present was considered to be the base configuration. The percent difference in the force and moment data was then taken between each strut configuration and the base configuration. The results were then compiled and plotted as a function of AOA. The graphs obtained for all of the configurations tested are presented in Appendix F.

V. RESULTS AND DISCUSSION

A. FORCE AND MOMENT DATA

1. Balance Static Calibration

Examination of the calibration data presented in Appendix C [Figs. 15-19] indicates that a one-to-one relationship exists between the indicated and applied static loads and moments over the range of values tested. No axial force data was obtained during this portion of the investigation due to the difficulty involved in constructing an apparatus capable of applying a purely axial load while the model was mounted on the sting. The range of values tested for the static moments more than adequately covered the range of values expected for runs where the test section velocity was established at 50 m/s. The statically applied normal and side forces, however, did not completely encompass the anticipated range of values. While this may have presented a problem if the graphs for the static forces were solely intended for the calibration of the balance and data acquisition system, the underlying intent was to verify the proper operation of the system over a reasonable range and to ensure that the software was free of errors. Therefore, the tests were determined to be adequate, and the proper operation of the system was confirmed.

2. Determination of the Zero-Lift and Trim AOA's

Examination of Figures 20 and 21 in Appendix D indicate that at an indicated (geometric) AOA of 0°, the normal force and pitching moment are both nearly zero, implying that the zero-lift AOA and the trim AOA each correspond to almost zero angle of attack. Therefore, the absolute AOA is essentially the same as the indicated (geometric) AOA. Henceforth, no distinction is made and the indicated AOA is used directly for all further calculations and observations without applying corrections to account for any possible but small misalignment between the X-axes of the balance and the aircraft model.

3. Force and Moment Data for Various Strut Configurations

Appendix E contains the raw data and averaged values obtained for the various strut configurations. The plots for each configuration consist of the normal, side and axial forces, as well as the pitching, rolling and yawing moments as a function of AOA. The first group of graphs [Figures 22-27], correspond to the no-strut (base) configuration. These figures are described in detail below to establish the base trends for comparison purposes, and to comment on the data repeatability.

1. Normal force [Figure 22].
   - 0°-20° : Constant positive slope of 0.8 lbs/deg.
   - 20°-30° : Constant positive slope of 0.4 lbs/deg.
   - 30°-40° : Constant positive slope of 0.5 lbs/deg.
   - 40°-55° : Decreasing positive slope of 0.5 to 0.0 lbs/deg.
   - 55°-60° : Constant positive slope of 0.2 up to a maximum normal force of 28.7 lbs.

   Data repeatability was excellent with a maximum variation in the order of 0.3 lbs observed near 35°-40° AOA.

2. Side force [Figure 23].
   - 0°-25° : Approximately constant negative slope of -0.044 lbs/deg.
   - 25°-35° : Approximately constant positive slope of 0.05 lbs/deg.
   - 35°-40° : Level slope.
   - 40°-55° : Negative slope averaging -0.1 lbs/deg.
   - 55°-60° : Constant positive slope of 0.05 lbs/deg.

   The general trends for both data sets are very similar, but a nearly constant offset exists between the curves. This offset is attributed to different tare values obtained at the initiation of data acquisition. Maximum deviation between data sets was on the order of 0.5 lbs.

3. Axial force [Figure 24].
   - 0°-20° : Negative slope of approximately -0.016 lbs/deg.
   - 20°-30° : Decreasing positive slope leveling off at a local maximum of 0.23 lbs.
   - 30°-60° : Negative slope of approximately -0.012 lbs/deg.

   The axial force is the only force/moment that was expected to have a non-zero value at 0° AOA. The data repeatability was generally good and the curves for the data sets actually crossed at 30°.

4. Pitching moment [Figure 25].
   - 0°-15° : Constant positive slope of 0.019 ft lbs/deg.
   - 15°-35° : Constant negative slope of -0.029 ft lbs/deg.
   - 35°-45° : Constant positive slope of 0.05 ft lbs/deg.
   - 45°-60° : Constant negative slope of -0.043 ft lbs/deg.

   Data repeatability was excellent with a maximum variation of 0.1 ft-lbs observed at 30° AOA.

36

5. Rolling moment [Figure 26].
   0°-20° : Negative slope of approximately -0.003 ft lbs/deg.
   20°-25° : Constant positive slope of 0.008 ft lbs/deg.
   25°-35° : Negative slope of approximately -0.009 ft lbs/deg.
   35°-60° : Generally positive slope.
   Data repeatability was very good up to 35° AOA, after which relatively erratic behavior was observed.

6. Yawing moment [Figure 27].
   0°-40° : Relatively shallow negative slope of -0.005 ft lbs/deg.
   40°-50° : Steep negative slope of approximately -0.06 ft lbs/deg.
   50°-55° : Level slope.
   55°-60° : Positive slope of 0.06 ft lbs/deg.
   Data repeatability was generally good with a constant offset similar to that observed for the side force.

The averaged raw data [Figs. 28-111], in combination with the percent interference data in Appendix F [Figs. 112-135], was used to evaluate each of the strut configurations. The criterion for evaluation was subjectively based on the similarity of the force and moment data for each strut configuration to that obtained for the no-strut case. Care should be taken when examining the percent interference plots; the very large excursions are usually associated with very small force or moment values for the no-strut configuration. Because the formula for percent interference contains the value for the no-strut configuration in the denominator, very small force or moment values can yield very large values for percent interference. Thus, cross reference between the raw data and percent interference plots is necessary to gain a more accurate assessment of the interference associated with any of the strut configurations.

Each set of force and moment plots were evaluated separately with particular attention given to identify the configurations yielding the maximum and minimum amount of interference. Additionally, significant trends not manifested in the base configuration, or large shifts in the overall curve were noted. The results of the subjective analysis for each set of force and moment plots are presented below.

1. Normal force.
   All of the strut configurations tested exhibited very similar trends and values over the entire range of AOA's. The only noted exception was a decrease in the normal force when the forward struts were either at the inboard or gear positions and the aft strut was located at the hook pivot point [Figs. 28, 64, 100]. A general trend

37

associated with all of the configurations was an increased normal force at AOA's below 20°. No one configuration could be identified as superior, but the configurations with the forward struts located either inboard or at the gear positions and with the aft strut located at the hook pivot point were considered to exhibit the greatest interference, particularly at the higher AOA's.

2. Side force.
    The general shape of the curve was maintained for all of the strut configurations. There were upward and downward shifts for certain configurations, but due to the small (<3 lbs) values associated with the side force and the uncertainty in the data caused by variations in voltage and tare readings, little weight was given to their significance. As such, no configuration could be identified as either the best or the worst.

3. Axial force.
    The base configuration has a local minimum at 20° AOA. While all of the other configurations also have local minima at or near 20° AOA, none of them are as low as that for the base configuration. Configurations with the forward strut located either inboard or at the gear positions and the aft strut located at the hook pivot point [Figs. 30, 102] showed a positive slope between 55° and 60° AOA, while the no strut configuration maintained a negative slope. The configurations exhibiting the minimum amount of interference had the forward struts located at the outboard positions [Figs. 54, 60, 91], while the maximum interference was associated with the forward struts both at the inboard and gear positions [Figs. 30, 102]. No conclusive decision regarding the best or the worst location for the aft strut position could be reached on the basis of the axial force data. It is interesting to note that at AOA's between 55° and 60° a negative axial force was present for nearly all configurations including the no strut configuration.

4. Pitching moment.
    All of the curves were shifted upward at the lower AOA's (0°-30°) when compared to the base configuration. The largest shift was associated with configurations with the aft strut located at the hook pivot point. The no strut configuration exhibited a local minimum at 35° AOA [Fig. 25]. The value of the minima was closer to that obtained for the base configuration when the aft strut was located at the nozzle lip. When the forward struts were located at the outboard position the dip in the curve more closely approximated that observed for the base configuration. Thus, the best configuration was judged to be one with the forward struts located outboard and the aft strut located at the nozzle lip [Fig. 61]. The configuration exhibiting the most interference had the forward struts located inboard and the aft strut located at the hook pivot point [Figs. 31, 67].

5. Rolling moment.
    Although the base configuration exhibited a local minimum at 35° AOA, it was accentuated when struts were present. The greatest amount of interference was observed when the forward struts were located inboard and the aft strut was at the

nozzle lip [Figs. 38, 74]. The least amount of interference was associated with the forward struts located outboard and the aft strut at the hook pivot point [Figs. 56, 92]. All of the configurations, including the base configuration, exhibited greater variation at AOA's greater than 35°.

6. Yawing moment.
The curve was offset downward at low AOA's for all configurations when compared to the base configuration. The least amount of offset was noted when the aft strut was located at the hook pivot point. The minimum associated with the no strut configuration between 50°-55° AOA was also shifted downward with the forward struts located at the inboard, gear, middle and outboard locations exhibiting progressively larger offsets. Thus, the configuration with the forward struts located inboard and the aft strut at the hook pivot point [Figs. 33, 69] showed the least amount of interference while the greatest interference occurred with the forward struts located outboard and the aft strut at the nozzle lip [Fig. 63].

As an overall evaluation, the configuration judged best, from an interference point of view, had the forward struts located outboard (at the wing tips) and the aft strut at the hook pivot point. It is emphasized that this was a subjective analysis based on both the raw/averaged data and the percent interference plots. It is also important to note that no one configuration exhibited interference of such magnitude as to make it unsuitable from an aerodynamic point of view. In fact, it is not unlikely that if the data were subjectively analyzed by another investigator a different configuration may have been judged best overall.

The fact that all of the configurations tested exhibited only slight interference effects, with no one configuration overwhelmingly superior to others (based on the force and moment data) gives the NASA-Ames investigators the freedom to consider the structural constraints associated with mounting a full scale F/A-18 without having to be unduly concerned with strut interference.

B. FLOW VISUALIZATION IMAGES

Flow visualization, whether by direct viewing of the smoke/laser sheet, video taping, or subsequent conversion to hard copy of the images, revealed that no discernable strut interference effects could be observed, regardless of the configuration. The visual cues of motion and color greatly enhance the understanding of the flow behavior. These cues, along with a certain amount of clarity and definition, were lost when the video was

converted to hard copy. The images do, however, illustrate that any interference effects due to the struts were negligible.

Appendix G contains flow visualization sequences for 30°, 40°, 50°, and 60° AOA [Figs. 136-155]. Each AOA sequence contains images with and without struts present. The images with struts present depict the forward struts located at the middle position with 0.5" extensions and the aft strut at the hook pivot point with a 1.5" extension.

The sequences depict the general trend of vortical flow development with both increasing AOA and the streamwise distance along the model. It was noted that two distinct sets of vortices were present. One set resulted from the flow over the forebody ahead of the canopy, and the other set was produced by the LEX's. The relative intensity, subsequent burst point, and symmetry (or asymmetry) of these vortices was strongly dependent upon AOA, but appeared unaffected by strut configuration. It was not possible to document the flow along the underside of the aircraft and around the struts due to the restricted optical access and the shadows cast by the upper horizontal support arm and the struts themselves.

For a thorough discussion of the flow phenomenon observed, and for additional photographic documentation of the flow field for various combinations of pitch, roll and yaw, the reader is directed to Reference 9.

C. CORRELATION BETWEEN FORCE AND MOMENT DATA AND FLOW VISUALIZATION IMAGES

Since only minor excursions were noted in the force and moment data for the various strut configuration tested, it was not surprising that the flow visualization system was unable to document any significant change in the flow patterns around the model. The fact that only the flow over the upper surfaces could be recorded due to the restrictions imposed by the limited optical access, and the hypothesis that the majority of strut interference would be manifested locally on the lower surface of the model and in the wake behind the struts, make it unlikely that the flow visualization data could be used to correlate the minor interference effects documented in the force and moment data. The flow visualization images do, however, correlate with the results of Reference 9, with regard to the general trends at varying AOA's.

VI. CONCLUSIONS AND RECOMMENDATIONS

A. CONCLUSIONS

At the request of the NASA-Ames Research Center, an experimental investigation of support strut interference on a three-percent fighter model at high angles of attack was conducted using balance measurements and flow visualization studies. The purpose of the investigation was to document the interference effects associated with various support strut configurations so that an aerodynamically optimum configuration could be identified. In addition, the interference trends associated with all of the strut configurations tested were documented to assist in trade-off studies where aerodynamic and structural considerations are conducted.

It was found, through a subjective analysis of the force and moment data, that the strut configuration exhibiting the least amount of interference had the forward struts located at wing tips and the aft strut located at the tail hook pivot point. This configuration, however, was not overwhelmingly superior to the other configurations tested. In fact, the interference detected by the force and moment balance was very slight even for the configuration judged to be the least desireable. The interference effects were so slight that they were not able to be documented by the flow visualization system.

The evaluation was somewhat complicated by the limitations of the data acquisition system, flow visualization system and the wind tunnel. These limitations are outlined below.

1. The balance used in this investigation was rated to measure forces and moments considerably larger than those encountered.

2. The data acquisition system was subject to small variations in voltage, which, in turn, caused drift and variation in the measurement of the forces and moments.

3. Restricted visual access to the test sections and optical obstruction caused by the mounting apparatus, aircraft model and support struts limited the acquisition of flow visualization data.

4. The force and moment data and the flow visualization images were both somewhat influenced by the flow quality in the test section.

41

B.   RECOMMENDATIONS

In addition to the recommendations listed in Reference 9, the following recommendations are based on the results of this investigation:

1. Acquire a balance more appropriately rated for the range of forces and moments expected during investigations in the NPS low-speed wind tunnel.

2. Extensive modification to the data acquisition system to include the elimination of amplifiers and the HP instruments. These components could be replaced by a high-speed data acquisition board installed directly in the computer, and supported by appropriate software.

3. Evaluate the feasibility of different smoke generation techniques that would eliminate the need to intrude on the flow upstream of the test section. The use of titanium tetrachloride applied directly to the surface of the model or specially constructed models with smoke ports are two possible alternatives.

4. Refine the conversion process of flow visualization images from video to hard copy such that the clarity and details are not lost. This could be accomplished by photography of the video image on a high quality monitor while in freeze frame.

5. Measure the turbulence in the wake downstream of the model and struts at high angle of attack using either hot films or laser Doppler velocimetry (LDV).

APPENDIX A

BALANCE CALIBRATION CONSTANTS

BALANCE CALIBRATION   CAL DATE: 7247   COMP DATE: 7287

INV. #: 440517   KIND: FORCE

PIN NO.: 3   SIZE: 1.00

MAKE: TASK 14B   RIG NO.: 2

GA	CAPACITY	MAX LOAD	JHMS	X GAGE	CAL SHUNT	CAL ROG
N1	400.00	400.00	350.	0.1667	100.K	4625
N2	400.00	400.00	350.	0.1667	100.K	4626
A	100.00	100.00	175.		50.K	4618
S1	200.00	200.00	350.	0.1375	100.K	4623
S2	200.00	200.00	350.	0.1375	100.K	4597
RM	21.00	20.83	175.		50.K	4623

	K POS(1)	K POS(2)	K NEG(1)	K NEG(2)	MAX DEV	%ACC
N1	5.0861E-02	-5.4826E-09	5.1591E-02	1.7157E-08	0.224	0.056
N2	4.7211E-02	-1.7015E-08	4.7763E-02	8.9153E-09	0.196	0.049
A	1.4309E-02	-7.1962E-10	1.4290E-02	-1.3322E-09	0.115	0.115
S1	3.1309E-02	-3.8153E-08	3.2073E-02	-8.9316E-09	-0.263	0.132
S2	3.0366E-02	-3.8607E-08	3.1167E-02	-7.2517E-09	0.315	0.153
RM	3.0885E-03	2.5672E-09	3.0908E-03	-2.4769E-09	0.042	0.204

DEG OF FIT = 2   ACCURACY = 15   INT DEG OF FIT = 2

N1/N2+	=	-5.8036E-03	N1/N2-	=	-1.0257E-02
N1/A +	=	0.0000E+00	N1/A -	=	0.0000E+00
N1/S1+	=	-4.1655E-03	N1/S1-	=	4.5396E-03
N1/S2+	=	0.0000E+00	N1/S2-	=	0.0000E+00
N1/RM+	=	-5.8079E-02	N1/RM-	=	4.4940E-02
N2/N1+	=	-4.6218E-02	N2/N1-	=	-5.1778E-02
N2/A +	=	2.8393E-03	N2/A -	=	4.4056E-03
N2/S1+	=	8.1694E-03	N2/S1-	=	9.0385E-03
N2/S2+	=	-4.1463E-03	N2/S2-	=	0.0000E+00
N2/RM+	=	-7.7279E-02	N2/RM-	=	6.1125E-02
A /N1+	=	-8.6893E-04	A /N1-	=	2.1217E-03
A /N2+	=	0.0000E+00	A /N2-	=	-9.1524E-04
A /S1+	=	-6.0359E-04	A /S1-	=	0.0000E+00
A /S2+	=	-7.7722E-05	A /S2-	=	0.0000E+00

```
A /RM+      =   1.1115E-01          A /RM-      =   9.7148E-02
S1/N1+      =   6.3459E-04          S1/N1-      =   7.1275E-03
S1/N2+      =   0.0000E+00          S1/N2-      =   0.0000E+00
S1/A +      =   0.0000E+00          S1/A -      =   8.9235E-03
S1/S2+      =   0.0000E+00          S1/S2-      =   0.0000E+00
S1/RM+      =   1.1148E-01          S1/RM-      =   5.2630E-02
S2/N1+      =   2.4237E-03          S2/N1-      =   3.7176E-03
S2/N2+      =   0.0000E-00          S2/N2-      =   5.2619E-03
S2/A +      =  -2.2455E-03          S2/A -      =  -7.2915E-03
S2/S1+      =  -6.6785E-03          S2/S1-      =  -6.3560E-03
S2/RM+      =   2.6377E-01          S2/RM-      =   6.2581E-02
RM/N1+      =   0.0000E+00          RM/N1-      =  -3.5945E-04
RM/N2+      =   1.9928E-04          RM/N2-      =   0.0000E+00
RM/A +      =   0.0000E+00          RM/A -      =   0.0000E+00
RM/S1+      =   0.0000E+00          RM/S1-      =   0.0000E+00
RM/S2+      =   2.5893E-04          RM/S2-      =   0.0000E+00
N1/N2*N2+   =   7.1926E-07          N1/N2*N2-   =  -7.9499E-07
N1/A *A +   =   0.0000E+00          N1/A *A -   =   0.0000E+00
N1/S1*S1+   =  -4.0352E-06          N1/S1*S1-   =   1.9670E-06
N1/S2*S2+   =   0.0000E+00          N1/S2*S2-   =   0.0000E+00
N1/RM*RM+   =   6.7860E-04          N1/RM*RM-   =   3.2320E-04
N2/N1*N1+   =   6.8577E-07          N2/N1*N1-   =  -5.2897E-06
N2/A *A +   =   1.7755E-05          N2/A *A -   =  -1.0467E-05
N2/S1*S1+   =  -2.1719E-06          N2/S1*S1-   =   4.8493E-07
N2/S2*S2+   =  -1.8582E-06          N2/S2*S2-   =   0.0000E+00
N2/RM*RM+   =   1.9294E-03          N2/RM*RM-   =   1.1773E-03
A /N1*N1+   =  -4.4537E-07          A /N1*N1-   =   4.2547E-06
A /N2*N2+   =   0.0000E+00          A /N2*N2-   =  -4.5946E-06
A /S1*S1+   =  -4.7936E-06          A /S1*S1-   =   0.0000E+00
A /S2*S2+   =   4.1033E-06          A /S2*S2-   =   0.0000E+00
A /RM*RM+   =  -2.0697E-04          A /RM*RM-   =   7.5001E-04
S1/N1*N1+   =  -5.5350E-06          S1/N1*N1-   =   1.2923E-05
S1/N2*N2+   =   0.0000E+00          S1/N2*N2-   =   0.0000E+00
S1/A *A +   =   0.0000E+00          S1/A *A -   =   4.0345E-05
S1/S2*S2+   =   0.0000E+00          S1/S2*S2-   =   0.0000E+00
S1/RM*RM+   =  -2.4592E-03          S1/RM*RM-   =   9.3969E-04
S2/N1*N1+   =  -1.7099E-06          S2/N1*N1-   =   5.2110E-07
S2/N2*N2+   =   0.0000E+00          S2/N2*N2-   =   8.6265E-06
S2/A *A +   =  -1.2072E-05          S2/A *A -   =  -3.7054E-05
S2/S1*S1+   =   2.7825E-06          S2/S1*S1-   =  -9.9830E-06
S2/RM*RM+   =  -6.2217E-03          S2/RM*RM-   =  -8.0007E-04
RM/N1*N1+   =   0.0000E+00          RM/N1*N1-   =  -1.5497E-07
RM/N2*N2+   =  -1.1512E-07          RM/N2*N2-   =   0.0000E+00
RM/A *A +   =   0.0000E+00          RM/A *A -   =   0.0000E+00
RM/S1*S1+   =   0.0000E+00          RM/S1*S1-   =   0.0000E+00
RM/S2*S2+   =   5.1560E-08          RM/S2*S2-   =   0.0000E+00
```

BREAD.BAS PROGRAM

```
1000 DEF SEG: CLEAR ,&HFE00: GOTO 1030    'Begin  PCIB Program
     Shell
1010 GOTO 2900              'User program
1020 GOTO 2670              'Error handling
1030 I=&HFE00               'Copyright Hewlett-Packard 1984,1985
1040 PCIB.DIR$=ENVIRON$("PCIB")
1050 I$=PCIB.DIR$+"\PCIBILC.BLD"
1060 BLOAD I$,I
1070 CALL I(PCIB.DIR$,I%,J%): PCIB.SEG=I%
1080 IF J%=0 THEN GOTO 1120
1090 PRINT "Unable to load.";
1100 PRINT "   (Error #";J%;")"
1110 END
1120 '
1130 DEF SEG=PCIB.SEG: O.S=5: C.S=10: I.V=15
1140 I.C=20: L.P=25: LD.FILE=30
1150 GET.MEM=35: L.S=40: PANELS=45: DEF.ERR=50
1160 PCIB.ERR$=STRING$(64,32): PCIB.NAME$=STRING$(16,32)
1170 CALL DEF.ERR(PCIB.ERR,PCIB.ERR$,PCIB.NAME$,PCIB.GLBERR):
     PCIB.BASERR=255
1180 ON ERROR GOTO 1020
1190 J=-1
1200 I$=PCIB.DIR$+"\PCIB.SYN"
1210 CALL O.S(I$)
1220 IF PCIB.ERR<>0 THEN ERROR PCIB.BASERR
1230 I=0
1240 CALL
    I.V(I,READ.REGISTER,READ.SELFID,DEFINE,INITIALIZE.SYSTEM)
1250 IF PCIB.ERR<>0 THEN ERROR PCIB.BASERR
1260 CALL
    I.V(I,ENABLE.SYSTEM,DISABLE.SYSTEM,INITIALIZE,POWER.ON)
1270 IF PCIB.ERR<>0 THEN ERROR PCIB.BASERR
1280 CALL I.V(I,MEASURE,OUTPUT,START,HALT)
1290 IF PCIB.ERR<>0 THEN ERROR PCIB.BASERR
1300 CALL
    I.V(I,ENABLE.INT.TRIGGER,DISABLE.INT.TRIGGER,
    ENABLE.OUTPUT,DISABLE.OUTPUT)
1310 IF PCIB.ERR<>0 THEN ERROR PCIB.BASERR
1320 CALL I.V(I,CHECK.DONE,GET.STATUS,SET.FUNCTION,SET.RANGE)
1330 IF PCIB.ERR<>0 THEN ERROR PCIB.BASERR
1340 CALL I.V(I,SET.MODE,WRITE.CAL,READ.CAL,STORE.CAL)
1350 IF PCIB.ERR<>0 THEN ERROR PCIB.BASERR
```

```
1360 CALL I.V(I,DELAY,SAVE.SYSTEM,J,J)
1370 IF PCIB.ERR<>0 THEN ERROR PCIB.BASERR
1380 I=1
1390 CALL I.V(I,SET.GATETIME,SET.SAMPLES,SET.SLOPE,SET.SOURCE)
1400 IF PCIB.ERR<>0 THEN ERROR PCIB.BASERR
1410 CALL I.C(I,FREQUENCY,AUTO.FREQ,PERIOD,AUTO.PER)
1420 IF PCIB.ERR<>0 THEN ERROR PCIB.BASERR
1430 CALL I.C(I,INTERVAL,RATIO,TOTALIZE,R100MILLI)
1440 IF PCIB.ERR<>0 THEN ERROR PCIB.BASERR
1450 CALL I.C(I,R1,R10,R100,R1KILO)
1460 IF PCIB.ERR<>0 THEN ERROR PCIB.BASERR
1470 CALL I.C(I,R10MEGA,R100MEGA,CHAN.A,CHAN.B)
1480 IF PCIB.ERR<>0 THEN ERROR PCIB.BASERR
1490 CALL I.C(I,POSITIVE,NEGATIVE,COMN,SEPARATE)
1500 IF PCIB.ERR<>0 THEN ERROR PCIB.BASERR
1510 I=2
1520 I=3
1530 CALL I.V(I,ZERO.OHMS,SET.SPEED,J,J)
1540 IF PCIB.ERR<>0 THEN ERROR PCIB.BASERR
1550 CALL I.C(I,DCVOLTS,ACVOLTS,OHMS,R200MILLI)
1560 IF PCIB.ERR<>0 THEN ERROR PCIB.BASERR
1570 CALL I.C(I,R2,R20,R200,R2KILO)
1580 IF PCIB.ERR<>0 THEN ERROR PCIB.BASERR
1590 CALL I.C(I,R20KILO,R200KILO,R2MEGA,R20MEGA)
1600 IF PCIB.ERR<>0 THEN ERROR PCIB.BASERR
1610 CALL I.C(I,AUTOM,R2.5,R12.5,J)
1620 IF PCIB.ERR<>0 THEN ERROR PCIB.BASERR
1630 I=4
1640 CALL
     I.V(I,SET.COMPLEMENT,SET.DRIVER,OUTPUT.NO.WAIT,
     ENABLE.HANDSHAKE)
1650 IF PCIB.ERR<>0 THEN ERROR PCIB.BASERR
1660 CALL
     I.V(I,DISABLE.HANDSHAKE,SET.THRESHOLD,SET.START.BIT,
     SET.NUM.BITS)
1670 IF PCIB.ERR<>0 THEN ERROR PCIB.BASERR
1680 CALL I.V(I,SET.LOGIC.SENSE,J,J,J)
1690 IF PCIB.ERR<>0 THEN ERROR PCIB.BASERR
1700 CALL I.C(I,POSITIVE,NEGATIVE,TWOS,UNSIGNED)
1710 IF PCIB.ERR<>0 THEN ERROR PCIB.BASERR
1720 CALL I.C(I,OC,TTL,R0,R1)
1730 IF PCIB.ERR<>0 THEN ERROR PCIB.BASERR
1740 CALL I.C(I,R2,R3,R4,R5)
1750 IF PCIB.ERR<>0 THEN ERROR PCIB.BASERR
1760 CALL I.C(I,R6,R7,R8,R9)
1770 IF PCIB.ERR<>0 THEN ERROR PCIB.BASERR
1780 CALL I.C(I,R10,R11,R12,R13)
1790 IF PCIB.ERR<>0 THEN ERROR PCIB.BASERR
1800 CALL I.C(I,R14,R15,R16,J)
1810 IF PCIB.ERR<>0 THEN ERROR PCIB.BASERR
```

```
1820 I=6
1830 CALL
     I.V(I,SET.FREQUENCY,SET.AMPLITUDE,SET.OFFSET,SET.SYMMETRY)
1840 IF PCIB.ERR<>0 THEN ERROR PCIB.BASERR
1850 CALL I.V(I,SET.BURST.COUNT,J,J,J)
1860 IF PCIB.ERR<>0 THEN ERROR PCIB.BASERR
1870 CALL I.C(I,SINE,SQUARE,TRIANGLE,CONTINUOUS)
1880 IF PCIB.ERR<>0 THEN ERROR PCIB.BASERR
1890 CALL I.C(I,GATED,BURST,J,J)
1900 IF PCIB.ERR<>0 THEN ERROR PCIB.BASERR
1910 I=7
1920 CALL
     I.V(I,AUTOSCALE,CALIBRATE,SET.SENSITIVITY,SET.VERT.OFFSET)
1930 IF PCIB.ERR<>0 THEN ERROR PCIB.BASERR
1940 CALL
     I.V(I,SET.COUPLING,SET.POLARITY,SET.SWEEPSPEED,SET.DELAY)
1950 IF PCIB.ERR<>0 THEN ERROR PCIB.BASERR
1960 CALL
     I.V(I,SET.TRIG.SOURCE,SET.TRIG.SLOPE,SET.TRIG.LEVEL,
     SET.TRIG.MODE)
1970 IF PCIB.ERR<>0 THEN ERROR PCIB.BASERR
1980 CALL
     I.V(I,GET.SINGLE.WF,GET.TWO.WF,GET.VERT.INFO,
     GET.TIMEBASE.INFO)
1990 IF PCIB.ERR<>0 THEN ERROR PCIB.BASERR
2000 CALL
     I.V(I,GET.TRIG.INFO,CALC.WFVOLT,CALC.WFTIME,CALC.WF.STATS)
2010 IF PCIB.ERR<>0 THEN ERROR PCIB.BASERR
2020 CALL
     I.V(I,CALC.RISETIME,CALC.FALLTIME,CALC.PERIOD,
     CALC.FREQUENCY)
2030 IF PCIB.ERR<>0 THEN ERROR PCIB.BASERR
2040 CALL
     I.V(I,CALC.PLUSWIDTH,CALC.MINUSWIDTH,CALC.OVERSHOOT,
     CALC.PRESHOOT)
2050 IF PCIB.ERR<>0 THEN ERROR PCIB.BASERR
2060 CALL
     I.V(I,CALC.PK.TO.PK,SET.TIMEOUT,SCOPE.START,
     MEASURE.SINGLE.WF)
2070 IF PCIB.ERR<>0 THEN ERROR PCIB.BASERR
2080 CALL I.V(I,MEASURE.TWO.WF,J,J,J)
2090 IF PCIB.ERR<>0 THEN ERROR PCIB.BASERR
2100 CALL I.C(I,R10NANO,R100NANO,R1MICRO,R10MICRO)
2110 IF PCIB.ERR<>0 THEN ERROR PCIB.BASERR
2120 CALL I.C(I,R100MICRO,R1MILLI,R10MILLI,R100MILLI)
2130 IF PCIB.ERR<>0 THEN ERROR PCIB.BASERR
2140 CALL I.C(I,R1,R10,R20NANO,R200NANO)
2150 IF PCIB.ERR<>0 THEN ERROR PCIB.BASERR
2160 CALL I.C(I,R2MICRO,R20MICRO,R200MICRO,R2MILLI)
2170 IF PCIB.ERR<>0 THEN ERROR PCIB.BASERR
```

```
2180 CALL I.C(I,R20MILLI,R200MILLI,R2,R20)
2190 IF PCIB.ERR<>0 THEN ERROR PCIB.BASERR
2200 CALL I.C(I,R50NANO,R500NANO,R5MICRO,R50MICRO)
2210 IF PCIB.ERR<>0 THEN ERROR PCIB.BASERR
2220 CALL I.C(I,R500MICRO,R5MILLI,R50MILLI,R500MILLI)
2230 IF PCIB.ERR<>0 THEN ERROR PCIB.BASERR
2240 CALL I.C(I,R5,R50,CHAN.A,CHAN.B)
2250 IF PCIB.ERR<>0 THEN ERROR PCIB.BASERR
2260 CALL I.C(I,EXTERNAL,POSITIVE,NEGATIVE,AC)
2270 IF PCIB.ERR<>0 THEN ERROR PCIB.BASERR
2280 CALL I.C(I,DC,TRIGGERED,AUTO.TRIG,AUTO.LEVEL)
2290 IF PCIB.ERR<>0 THEN ERROR PCIB.BASERR
2300 CALL I.C(I,X1,X10,STANDARD,AVERAGE)
2310 IF PCIB.ERR<>0 THEN ERROR PCIB.BASERR
2320 I=8
2330 CALL I.V(I,OPEN.CHANNEL,CLOSE.CHANNEL,J,J)
2340 IF PCIB.ERR<>0 THEN ERROR PCIB.BASERR
2350 CALL C.S
2360 IF PCIB.ERR<>0 THEN ERROR PCIB.BASERR
2370 I$=PCIB.DIR$+"\PCIB.PLD"
2380 CALL L.P(I$)
2390 IF PCIB.ERR<>0 THEN ERROR PCIB.BASERR
2400 I$="DMM.01": I=3: J=0: K=0: L=1
2410 CALL DEFINE(DMM.01,I$,I,J,K,L)
2420 IF PCIB.ERR<>0 THEN ERROR PCIB.BASERR
2430 I$="Func.Gen.01": I=6: J=0: K=1: L=1
2440 CALL DEFINE(FUNC.GEN.01,I$,I,J,K,L)
2450 IF PCIB.ERR<>0 THEN ERROR PCIB.BASERR
2460 I$="Scope.01": I=7: J=0: K=2: L=1
2470 CALL DEFINE(SCOPE.01,I$,I,J,K,L)
2480 IF PCIB.ERR<>0 THEN ERROR PCIB.BASERR
2490 I$="Counter.01": I=1: J=0: K=3: L=1
2500 CALL DEFINE(COUNTER.01,I$,I,J,K,L)
2510 IF PCIB.ERR<>0 THEN ERROR PCIB.BASERR
2520 I$="Dig.In.01": I=4: J=0: K=4: L=1
2530 CALL DEFINE(DIG.IN.01,I$,I,J,K,L)
2540 IF PCIB.ERR<>0 THEN ERROR PCIB.BASERR
2550 I$="Dig.Out.01": I=4: J=1: K=4: L=1
2560 CALL DEFINE(DIG.OUT.01,I$,I,J,K,L)
2570 IF PCIB.ERR<>0 THEN ERROR PCIB.BASERR
2580 I$="Relay.Act.01": I=8: J=0: K=5: L=1
2590 CALL DEFINE(RELAY.ACT.01,I$,I,J,K,L)
2600 IF PCIB.ERR<>0 THEN ERROR PCIB.BASERR
2610 I$="Relay.Mux.01": I=2: J=0: K=6: L=1
2620 CALL DEFINE(RELAY.MUX.01,I$,I,J,K,L)
2630 IF PCIB.ERR<>0 THEN ERROR PCIB.BASERR
2640 I$=ENVIRON$("PANELS")+"\PANELS.EXE"
2650 CALL L.S(I$)
2660 GOTO 1010
2670 IF ERR=PCIB.BASERR THEN GOTO 2700
```

```
2680 PRINT "BASIC error #";ERR;" occurred in line ";ERL
2690 STOP
2700 TMPERR=PCIB.ERR: IF TMPERR=0 THEN TMPERR=PCIB.GLBERR
2710 PRINT
     "PC Instrument error #";TMPERR;" detected at line ";ERL
2720 PRINT "Error: ";PCIB.ERR$
2730 IF LEFT$(PCIB.NAME$,1)<>CHR$(32) THEN PRINT
     "Instrument: ";PCIB.NAME$
2740 STOP
2750 COMMON PCIB.DIR$,PCIB.SEG
2760 COMMON LD.FILE,GET.MEM,PANELS,DEF.ERR
2770 COMMON
     PCIB.BASERR,PCIB.ERR,PCIB.ERR$,PCIB.NAME$,PCIB.GLBERR
2780 COMMON
     READ.REGISTER,READ.SELFID,DEFINE,INITIALIZE.SYSTEM,
     ENABLE.SYSTEM,DISABLE.SYSTEM,INITIALIZE,POWER.ON,
     MEASURE,OUTPUT,START,HALT,ENABLE.INT.TRIGGER,
     DISABLE.INT.TRIGGER,ENABLE.OUTPUT,DISABLE.OUTPUT,
     CHECK.DONE,GET.STATUS
2790 COMMON
     SET.FUNCTION,SET.RANGE,SET.MODE,WRITE.CAL,READ.CAL,
     STORE.CAL,DELAY,SAVE.SYSTEM,SET.GATETIME,SET.SAMPLES,
     SET.SLOPE,SET.SOURCE,ZERO.OHMS,SET.SPEED,SET.COMPLEMENT,
     SET.DRIVER,OUTPUT.NO.WAIT,ENABLE.HANDSHAKE,
     DISABLE.HANDSHAKE
2800 COMMON
     SET.THRESHOLD,SET.START.BIT,SET.NUM.BITS,
     SET.LOGIC.SENSE,SET.FREQUENCY,SET.AMPLITUDE,SET.OFFSET,
     SET.SYMMETRY,SET.BURST.COUNT,AUTOSCALE,CALIBRATE,
     SET.SENSITIVITY,SET.VERT.OFFSET,SET.COUPLING,
     SET.POLARITY,SET.SWEEPSPEED
2810 COMMON
     SET.DELAY,SET.TRIG.SOURCE,SET.TRIG.SLOPE,SET.TRIG.LEVEL,
     SET.TRIG.MODE,GET.SINGLE.WF,GET.TWO.WF,GET.VERT.INFO,
     GET.TIMEBASE.INFO,GET.TRIG.INFO,CALC.WFVOLT,CALC.WFTIME,
     CALC.WF.STATS,CALC.RISETIME,CALC.FALLTIME,CALC.PERIOD
2820 COMMON
     CALC.FREQUENCY,CALC.PLUSWIDTH,CALC.MINUSWIDTH,
     CALC.OVERSHOOT,CALC.PRESHOOT,CALC.PK.TO.PK,SET.TIMEOUT,
     SCOPE.START,MEASURE.SINGLE.WF,MEASURE.TWO.WF,
     OPEN.CHANNEL,CLOSE.CHANNEL
2830 COMMON
     FREQUENCY,AUTO.FREQ,PERIOD,AUTO.PER,INTERVAL,RATIO,
     TOTALIZE,R100MILLI,R1,R10,R100,R1KILO,R10MEGA,R100MEGA,
     CHAN.A,CHAN.B,POSITIVE,NEGATIVE,COMN,SEPARATE,DCVOLTS,
     ACVOLTS,OHMS,R200MILLI,R2,R20,R200,R2KILO,R20KILO,R200KILO
2840 COMMON
     R2MEGA,R20MEGA,AUTOM,R2.5,R12.5,POSITIVE,NEGATIVE,TWOS,
     UNSIGNED,OC,TTL,R0,R1,R2,R3,R4,R5,R6,R7,R8,R9,R10,R11,
     R12,R13,R14,R15,R16,SINE,SQUARE,TRIANGLE,CONTINUOUS,
```

```
          GATED,BURST,R10NANO,R100NANO,R1MICRO,R10MICRO,R100MICRO
2850 COMMON
     R1MILLI,R10MILLI,R100MILLI,R1,R10,R20NANO,R200NANO,
     R2MICRO,R20MICRO,R200MICRO,R2MILLI,R20MILLI,R200MILLI,
     R2,R20,R50NANO,R500NANO,R5MICRO,R50MICRO,R500MICRO,
     R5MILLI,R50MILLI,R500MILLI,R5,R50,CHAN.A,CHAN.B,
     EXTERNAL,POSITIVE
2860 COMMON
     NEGATIVE,AC,DC,TRIGGERED,AUTO.TRIG,AUTO.LEVEL,X1,X10,
     STANDARD,AVERAGE
2870 COMMON
     DMM.01,FUNC.GEN.01,SCOPE.01,COUNTER.01,DIG.IN.01,
     DIG.OUT.01,RELAY.ACT.01,RELAY.MUX.01
2880 'End PCIB Program Shell
2890 '
2900 'Program to scan with the DMM and RELAY.MUX.01
2910 'This program was written by T.SESTAK and modified by
2920 'P. ROANE ,P. RABANG, and J.SOMMERS for use with the TASK
     6 component
2925 'balance. The TASK  balance used with this program is the
     1.00",
2926 'MK. XIV internal balance with NASA inventory #440517.
2930 '
2940 'This section after the SHELL program directs reading
2950 'the voltages from the balance, computes forces measured
2960 'by the strain gages, then stores the values in two
     arrays,
2970 'one for the TARE one for FORCE.  This data file can then
2980 'be used for graphs or other displays.  Each test run
2990 'will generate a windtun.dat file which should be copied
3000 'under another name before the next test run so that it
3010 'will not be overwritten.
3020 '
3030     'dimension arrays
3040 DIM READING[7],FORCE[140,8],TARE[8],TREAD[7,10]
3050 COLOR 14,1,1
3060 CLS
3070 '
3080 AOA=0
3090 VALUE=5
3100 LOCATE 12,28
3110 PRINT"SETTING UP DATA FILES"
3120 '
3130     'The program will write the data to several files.
3140 STATEFILE$ = "C:\PCIB\WIND.HPC"
     'stored in PCIB subdirectory
3150 DATAFILE$ = "C:WINDTUN.DAT"          'stored on disc C
3160 DISKFILE$ = "A:WINDTUN.DAT"          'stored on disc A
3170 BALANFILE$ = "C:\MISSILE\BALANCE.DAT
     'stored on disc C
```

```
3180 '
3190 RELAY.SETTLING.TIME = .8              '800 ms
3200 LOCATE 16,35:PRINT"D O N E"
3210 CALL DELAY(VALUE)
3220 '
3230 CLS:LOCATE 12,28:PRINT"INITIALIZING INSTRUMENTS"
3240 CALL INITIALIZE.SYSTEM(STATEFILE$)
3250 IF PCIB.ERR <> 0 THEN ERROR PCIB.BASERR
3260 CALL ENABLE.SYSTEM
3270 IF PCIB.ERR <> 0 THEN ERROR PCIB.BASERR
3280 LOCATE 16,35:PRINT"D O N E"
3290 CALL DELAY(VALUE)
3300 '
3310 'This part of the program is to preserve the data if
3320 'if the program is aborted in mid run.  Parity errors
3330 'in the Hewlett Packard PC Instruments setup caused by
3340 'electrical noise and undervoltage at NPS requires
3350 'this.  A voltage regulated, uninteruptible power source
3360 'would ameliorate this problem. Just in case- this little
3370 'sequence allows reentry into the program and the data
3380 'arrays with minimal inconvenience.
3390 '
3400 CLS:LOCATE 12,20:INPUT"WERE YOU INTERRUPTED (Y OR N)";A$
3410 IF A$="Y" GOTO 3570
3420 '
3430 'The next three variables are counters in the arrays
3440 'FORCE and TARE
3450 '
3460 TRIAL = 0
3470 TRY = 0
3480 '
3490 'open the datafile so each scan can be recorded
3500 '
3510 OPEN DATAFILE$ FOR OUTPUT AS #1
3520 CLOSE #1
3530 OPEN BALANFILE$ FOR OUTPUT AS #3
3540 CLOSE #3
3550 GOTO 3700
3560 '
3570 OPEN DATAFILE$ FOR INPUT AS #1
3580 INPUT #1,
    TARE(1),TARE(2),TARE(3),TARE(4),TARE(5),TARE(6),TARE(7),
    TARE(8)
3590 FOR X = 1 TO 140
3600    INPUT #1,
    FORCE(X,1),FORCE(X,2),FORCE(X,3),FORCE(X,4),FORCE(X,5),
    FORCE(X,6),FORCE(X,7),FORCE(X,8)
3610 NEXT X
3620 CLOSE #1
3630 '
```

```
3640 GOTO 3700
3650 'A$ is used as a marker for interrupted run sequences
3660 'in the program, it is set to <>"Y" so the
3670 'uninterrupted sequences are used unless otherwise
     directed
3680 '
3690 A$="N"
3700 KEY OFF
3710 '
3720 'prompt to begin each scan or quit program if desired
3730 '
3740 CLS:LOCATE 12,10
3750 INPUT "TO START SCAN ENTER ANY KEY EXCEPT Q,
     Q TO QUIT";ANSWER$
3760 IF ANSWER$ = "Q" THEN GOTO 6630
3770 '
3780 'THIS ENTERS THE AOA FOR EACH TRIAL AND DISPLAYS IT IN
     THE PRINTOUT
3790 '
3800 CLS:LOCATE 12,10
3810 PRINT "THE CURRENT ANGLE OF ATTACK IS ";AOA
3820 '
3830 '
3840 LOCATE 15,10:PRINT
     "INPUT THE ANGLE OF ATTACK (AOA) FOR THE NEXT TRIAL"
3850 INPUT AOA         'READING(1)
3860 GOTO 3870
3870 '
3880 READING(1)=AOA
3890 '
3900 'This variable is a marker in the iteration loop
3910 'interaction equations for convergence.
3920 '
3930 CYCLE = 0
3940 '
3950 'This loop scans the pitch angle and 6 balance channels
3960 'and stores the values in the array READING
3970 'Each channel is read ten times and averaged.
3980 'The user may reject the current readings and input a new
set.
3990 '
4000 CLS
4010 PRINT"******************** DIRECT BALANCE READINGS
     **********************
4020 PRINT"                          CHECK OF SYSTEM OPERATION
4030 PRINT
                    " IN VOLTS       N1          N2          S1
     S2         A         R "
4040 PRINT
                    " ********     ******     ******     ******
```

```
          ******      ******      ******"
4050 '
4060 'This file is for storing the direct voltage readings and
     averages.
4070 'The data file is continually appended.
4080 'The data is for further analysis of the direct voltage
     readings.
4090 OPEN BALANFILE$ FOR APPEND AS #3
4100 '
4110 FOR CNT = 1 TO 10
4120 FOR CHANNEL = 2 TO 7
4130    CALL OUTPUT(RELAY.MUX.01, CHANNEL)
4140            IF PCIB.ERR <> 0 THEN ERROR PCIB.BASERR
4150    CALL DELAY(RELAY.SETTLING.TIME)
4160            IF PCIB.ERR <> 0 THEN ERROR PCIB.BASERR
4170    CALL MEASURE(DMM.01, READING[CHANNEL])
4180            IF PCIB.ERR <> 0 THEN ERROR PCIB.BASERR
4190 TREAD(CHANNEL,CNT) = READING(CHANNEL)
4200 NEXT CHANNEL
4210 PRINT USING
                   "         +.######  +.######  +.######
     +.######   +.######
     +.######";READING(2),READING(3),READING(4),READING(5),
     READING(6),READING(7)
4220 PRINT #3, USING
                   "   +###.#   +.######   +.######
     +.######   +.######   +.######
     +.######";READING(1),READING(2),READING(3),READING(4),
     READING(5),READING(6),READING(7)
4230 NEXT CNT
4240 '
4250 '   CALL SUBROUTINE TO AVERAGE READINGS
4260 GOSUB 6690
4270 '
4280 PRINT"- - - - - - - - - - - - - - - - - - - - - - - - - - -
     - - - - - - - - - - -"
4290 PRINT USING
                   "MEAN VALUE +.######  +.######   +.######
     +.######   +.######
     +.######";READING(2),READING(3),READING(4),READING(5),
     READING(6),READING(7)
4300 PRINT #3, USING
                   "   +###.#   +.######   +.######
     +.######   +.######   +.######
     +.######";READING(1),READING(2),READING(3),READING(4),
     READING(5),READING(6),READING(7)
4310 CLOSE #3
4320 PRINT" ":BEEP
4330 PRINT"<CR> TO CONTINUE, "1" TO GET NEW READINGS"
4340 INPUT XYZ
```

```
4350 IF XYZ=1 GOTO 3940
4360 '
4370 'These equations take voltage readings from the balance,
4380 'converts them to counts, then applies the primary force
4390 'equations to the results.  These values are applied to
4400 'the balance interaction equations. Each channel has
4410 'separate equations for positive and negative readings
     and
4420 'may have a "+" or "-" reading on any test run so the
4430 'rather involved logic path below is my solution to the
4440 'problem.  For more information consult Calibration
     laboratory
4450 'guidelines at NASA Ames Research Facility for TASK
     balances
4460 '
4470 '************** CONVERT SIGNAL TO FORCES **************
4480 '****************************************************
4490 '
4500 'Direct balance readings are multiplied by a scale factor
4510 '5000000 then divided by the balance excitation voltage
     to
4520 'get a reading in COUNTS. The program will send each
     reading
4530 'to the appropriate equation and convert to force or
     moment
4540 'then return to send the next reading for calculation
4550 'The data acquisition system for using this program used
     an
4560 'amplifier with 1000 gain. The scale factor is divided
     by 1000.
4570 '
4580 VEX=5                           'Excitation Voltage
4590 N1=READING(2)*5000!/VEX
4600 N2=READING(3)*5000!/VEX
4610 S1=READING(4)*5000!/VEX
4620 S2=READING(5)*5000!/VEX
4630 A=READING(6)*5000!/VEX
4640 R=READING(7)*416.67#/VEX
4650 '
4660 'send each reading to the appropriate equation
4670 '
4680 IF READING(2)>0 THEN GOTO 4770 ELSE GOTO 4920
4690 IF READING(3)>0 THEN GOTO 4790 ELSE GOTO 4940
4700 IF READING(4)>0 THEN GOTO 4830 ELSE GOTO 4980
4710 IF READING(5)>0 THEN GOTO 4850 ELSE GOTO 5000
4720 IF READING(6)>0 THEN GOTO 4810 ELSE GOTO 4960
4730 IF READING(7)>0 THEN GOTO 4870 ELSE GOTO 5020
4740 '
4750 '************** POSITIVE FORMULAS **************
4760 '
```

```
4770 EN1 = .050861*N1 - 5.4826E-09*(N1*N1)
4780 GOTO 4690
4790 EN2 = .047211*N2 - 1.7015E-08*(N2*N2)
4800 GOTO 4700
4810 EA = .014309*A - 7.1962E-10*(A*A)
4820 GOTO 4730
4830 ES1 = .031309*S1 - 3.8153E-08*(S1*S1)
4840 GOTO 4710
4850 ES2 = .030366*S2 - 3.8607E-08*(S2*S2)
4860 GOTO 4720
4870 ER = .0030885*R + 2.5672E-09*(R*R)
4880 GOTO 5030
4890 '
4900 '************** NEGATIVE FORMULAS *************
4910 '
4920 EN1 = .051591*N1 + 1.7157E-08*(N1*N1)
4930 GOTO 4690
4940 EN2=.047763*N2+8.915299E-09*(N2*N2)
4950 GOTO 4700
4960 EA = .01429*A - 1.3322E-09*(A*A)
4970 GOTO 4730
4980 ES1 = .032073*S1 - 8.931601E-09*(S1*S1)
4990 GOTO 4710
5000 ES2 = .031167*S2 - 7.2517E-09*(S2*S2)
5010 GOTO 4720
5020 ER = .0030908*R - 2.4769E-09*(R*R)
5030 '
5040 '
5050 'a heading for the iteration values
5060 '
5070 PRINT"                                                      "
5080 PRINT"******************** FORCE INTERACTION ITERATIONS
     ******************
5090 PRINT"                          CHECK FOR CONVERGENCE
5100 PRINT
                    " CYCLE   AOA      N1       N2       S1
     S2       A        R "
5110 PRINT
                    "   #     DEG   POUNDS   POUNDS   POUNDS
     POUNDS   POUNDS   FT-LBS"
5120 PRINT
                    "  *****   ***   ******   ******   ******
     ******   ******   ******"
5130 '
5140 'The loop that controls the balance interaction
5150 'equations and allows a visual convergence check
5160 '
5170 FOR I = 1 TO 10
5180 IF READING(2)>0 THEN GOTO 5270 ELSE GOTO 5470
5190 IF READING(3)>0 THEN GOTO 5300 ELSE GOTO 5500
```

```
5200 IF READING(4)>0 THEN GOTO 5360 ELSE GOTO 5560
5210 IF READING(5)>0 THEN GOTO 5390 ELSE GOTO 5590
5220 IF READING(6)>0 THEN GOTO 5330 ELSE GOTO 5530
5230 IF READING(7)>0 THEN GOTO 5420 ELSE GOTO 5620
5240 '
5250 '***************POSITIVE FORMULAS**************
5260 '
5270 XN1=
     EN1+.0058036*N2+.0041655*S1+.058079*R-7.1926E-07*(N2*N2)
     +4.0352E-06*(S1*S1)-.0006786*(R*R)
5280 GOTO 5190
5290 '
5300 XN2=
     EN2+.046218*N1-.0028393*A-.0081694*S1+.0041463*S2
     +.077279*R-6.8577E-07*(N1*N1)-1.7755E-05*(A*A)
     +2.1719E-06*(S1*S1)+1.8582E-06*(S2*S2)-.0019294*(R*R)
5310 GOTO 5200
5320 '
5330 XA=
     EA+8.6893E-04*N1+6.0359E-04*S1+7.7722E-05*S2-.11115*R
     +4.4537E-07*(N1*N1)+4.7936E-06*(S1*S1)-4.1033E-06
     *(S2*S2)+2.0697E-04*(R*R)
5340 GOTO 5230
5350 '
5360 XS1 =
     ES1-6.3459E-04*N1-.11148*R+5.535E-06*(N1*N1)+.0024592
     *(R*R)
5370 GOTO 5210
5380 '
5390 XS2=
     ES2-.0024237*N1+.0022455*A+.0066785*S1-.26377*R
     +1.7099E-06*(N1*N1)+1.2072E-05*(A*A)-2.7825E-06*(S1*S1)
     +.0062217*(R*R)
5400 GOTO 5220
5410 '
5420 XR=
     ER-1.9928E-04*N2-2.5893E-04*S2+1.1512E-07*(N2*N2)
     -5.156E-08*(S2*S2)
5430 GOTO 5630
5440 '
5450 '*************** NEGATIVE FORMULAS ************
5460 '
5470 XN1=
     EN1+.010257*N2-.0045396*S1-.04494*R+7.9499E-07*(N2*N2)
     -1.967E-06*(S1*S1)-.0003232*(R*R)
5480 GOTO 5190
5490 '
5500 XN2=
     EN2+.051778*N1-.0044056*A-9.038499E-03*S1-.061125*R
     +5.2897E-06*(N1*N1)+1.0467E-05*(A*A)-4.8493E-07*(S1*S1)
```

```
            -.0011773*(R*R)
5510 GOTO 5200
5520 '
5530 XA=
     EA-.0021217*N1+9.1524E-04*N2-.097148*R-4.2547E-06
     *(N1*N1)+4.5846E-06*(N2*N2)-7.5001E-04*(R*R)
5540 GOTO 5230
5550 '
5560 XS1=
     ES1-.0071275*N1-.0089235*A-.05268*R-1.2923E-05*(N1*N1)
     -4.0345E-05*(A*A)-9.3969E-04*(R*R)
5570 GOTO 5210
5580 '
5590 XS2=
     ES2-.0037176*N1-.0052619*N2+.0072915*A+.006856*S1
     -.062581*R-5.211E-07*(N1*N1)-8.6265E-06*(N2*N2)
     +3.7054E-05*(A*A)+9.983001E-06*(S1*S1)+8.0007E-04*(R*R)
5600 GOTO 5220
5610 '
5620 XR= ER+3.5945E-04*N1+1.5497E-07*(N1*N1)
5630 '
5640 'Shift all the new variables back to the old name
5650 'for the next iteration
5660 N1=XN1
5670 N2=XN2
5680 A=XA
5690 S1=XS1
5700 S2=XS2
5710 R=XR
5720 '
5730 'A marker for the iterations
5740 CYCLE = CYCLE + 1
5750 'print the iterations to watch for convergence
5760 '
5770 PRINT USING
                    "  ##   +##.#  +###.##  +###.##  +###.##
     +###.##  +###.##  +###.##";CYCLE,AOA,N1,N2,S1,S2,A,R
5780 NEXT I
5790 '
5800 INPUT "IF CONVERGENCE IS ADEQUATE ENTER Y, IF ANOTHER RUN
     IS DESIRED ENTER N";ANSWR$
5810 IF ANSWR$ = "N" THEN GOTO 5060
5820 '
5830 NORMAL = N1 + N2
5840 SIDE = S1 + S2
5850 AXIAL = A
5860 PITCH = (N1-N2) * .1667
5870 YAW = (S1-S2) * .1375
5880 ROLL = R*12.0
5890 '
```

```
5900 TRIAL = TRIAL + 1
5910 INPUT;"IS THIS A TARE READING, Y OR N";ANS$
5920 IF AN$ <> "Y" GOTO 6190
5930 COLOR 10,4,1
5940 TRIAL = 0
5950 TRY = TRY + 1
5960 IF A$<>"Y" GOTO 6000
5970 CLS: LOCATE 12,10
5980 INPUT"ENTER THE VALUE OF THE LAST TRY BEFORE
     INTERRUPT";ITRY
5990 TRY = ITRY + 1
6000 TARE(1) = TRY
6010 TARE(2) = AOA
6020 TARE(3) = NORMAL
6030 TARE(4) = SIDE
6040 TARE(5) = AXIAL
6050 TARE(6) = PITCH
6060 TARE(7) = ROLL
6070 TARE(8) = YAW
6080 '
6090 PRINT"
          "
6100 PRINT"* * * * * * * * * * * TARE CALCULATIONS * * * *
     * * * * * * * * *
6110 PRINT
                    " TRIAL     AOA     NORMAL     SIDE
     AXIAL     PITCH     ROLL     YAW"
6120 PRINT
                    "   #       DEG     POUNDS     POUNDS
     POUNDS    FT-LBS    FT-LBS    FT-LBS"
6130 PRINT
                    " *****     *****    ******     ******
     ******    ******    ******    ******"
6140      'A loop to list all values so far
6150 FOR J = 1 TO TRY
6160 PRINT USING"   ##    +##.##    ###.##    ###.##    ###.##
     ###.##    ###.##
     ###.##";TARE(1),TARE(2),TARE(3),TARE(4),TARE(5),TARE(6),
     TARE(7),TARE(8)
6170 NEXT J
6180 GOTO 6450
6190 '
6200 IF A$<>"Y" GOTO 6240
6210 CLS: LOCATE 12,10
6220 INPUT"ENTER THE VALUE OF THE LAST TRIAL BEFORE
     INTERRUPT";ITRIAL
6230 TRIAL = ITRIAL + 1
6240 FORCE(TRIAL,1) = TRIAL
6250 FORCE(TRIAL,2) = AOA
6260 FORCE(TRIAL,3) = NORMAL - TARE(3)
```

58

```
6270 FORCE(TRIAL,4) = SIDE - TARE(4)
6280 FORCE(TRIAL,5) = AXIAL - TARE(5)
6290 FORCE(TRIAL,6) = PITCH - TARE(6)
6300 FORCE(TRIAL,7) = ROLL - TARE(7)
6310 FORCE(TRIAL,8) = YAW - TARE(8)
6320 '
6330 'print the values and store in file
6340 '
6350 PRINT"
          "
6360 PRINT"* * * * * * * * * * * FORCE CALCULATIONS * * *
    * * * * * * * * * *
6370 PRINT
              " TRIAL   AOA   NORMAL   SIDE   AXIAL
      PITCH    ROLL     YAW"
6380 PRINT
              "   #     DEG   POUNDS   POUNDS   POUNDS
      FT-LBS   FT-LBS   FT-LBS"
6390 PRINT
              " *****  *****  ******  ******  ******
    ******  ******  ******"
6400 'a loop to list all values so far
6410 '
6420 FOR J = 1 TO TRIAL
6430 PRINT USING"   ##    +###.#  +###.##  +###.##  +###.##
    +###.##  +###.##
    +###.##";FORCE(J,1),FORCE(J,2),FORCE(J,3),FORCE(J,4),
    FORCE(J,5),FORCE(J,6),FORCE(J,7),FORCE(J,8)
6440 NEXT J
6450 '
6460 'Write the data to the output data files
6470 COLOR 14,1,1
6480 OPEN DATAFILE$ FOR OUTPUT AS #1
6490 WRITE #1,
    TARE(1),TARE(2),TARE(3),TARE(4),TARE(5),TARE(6),TARE(7),
    TARE(8)
6500 FOR X = 1 TO 140
6510 WRITE #1,
    FORCE(X,1),FORCE(X,2),FORCE(X,3),FORCE(X,4),FORCE(X,5),
    FORCE(X,6),FORCE(X,7),FORCE(X,8)
6520 NEXT X
6530 CLOSE #1
6540 '
6550 OPEN DISKFILE$ FOR OUTPUT AS #2
6560  WRITE #2,
    TARE(1),TARE(2),TARE(3),TARE(4),TARE(5),TARE(6),TARE(7),
    TARE(8)
6570 FOR X = 1 TO 140
```

```
6580     WRITE #2,
    FORCE(X,1),FORCE(X,2),FORCE(X,3),FORCE(X,4),FORCE(X,5),
    FORCE(X,6),FORCE(X,7),FORCE(X,8)
6590 NEXT X
6600 CLOSE #2
6610 '
6620     'Prompt for next scan
6630 '
6640 INPUT "DO YOU WANT ANOTHER SCAN (Y OR N)";ANSW$
6650 IF ANSW$ <>"N" THEN GOTO 3690
6660 '
6670 END
6680 '
6690     'This subroutine averages the balance voltage readings
6700     'by computing the mean and standard deviation.
6710     'Any readings less or greater than one standard
    deviation
6720     'are thrown out and a new mean is computed
6730 '
6740 FOR CHANNEL = 2 TO 7
6750 N=10
6760 SREAD=0
6770 SSDEV=0
6780 '
6790     'Mean of balance voltage readings
6800 FOR CNT = 1 TO 10
6810 SREAD = SREAD + TREAD(CHANNEL,CNT)
6820 NEXT CNT
6830 MEAN = SREAD/N
6840 READING(CHANNEL) = MEAN
6850 IF(N < 10) THEN GOTO 7020
6860 '
6870     'Standard deviation routine
6880 FOR CNT = 1 TO 10
6890 DIF = TREAD(CHANNEL,CNT) - MEAN
6900 SDEV = DIF * DIF
6910 SSDEV = SSDEV + SDEV
6920 NEXT CNT
6930 DEV = SQR(SSDEV/N)
6940 HI = MEAN + DEV
6950 LO = MEAN - DEV
6960 FOR CNT = 1 TO 10
6970 ARG = TREAD(CHANNEL,CNT)
6980 IF (ARG < HI) AND (ARG > LO) THEN GOTO 7010
6990 TREAD(CHANNEL,CNT) = 0!
7000 N = N - 1
7010 NEXT CNT
7020 NEXT CHANNEL
7030 RETURN
7040 END
```

APPENDIX C

BALANCE STATIC CALIBRATION DATA
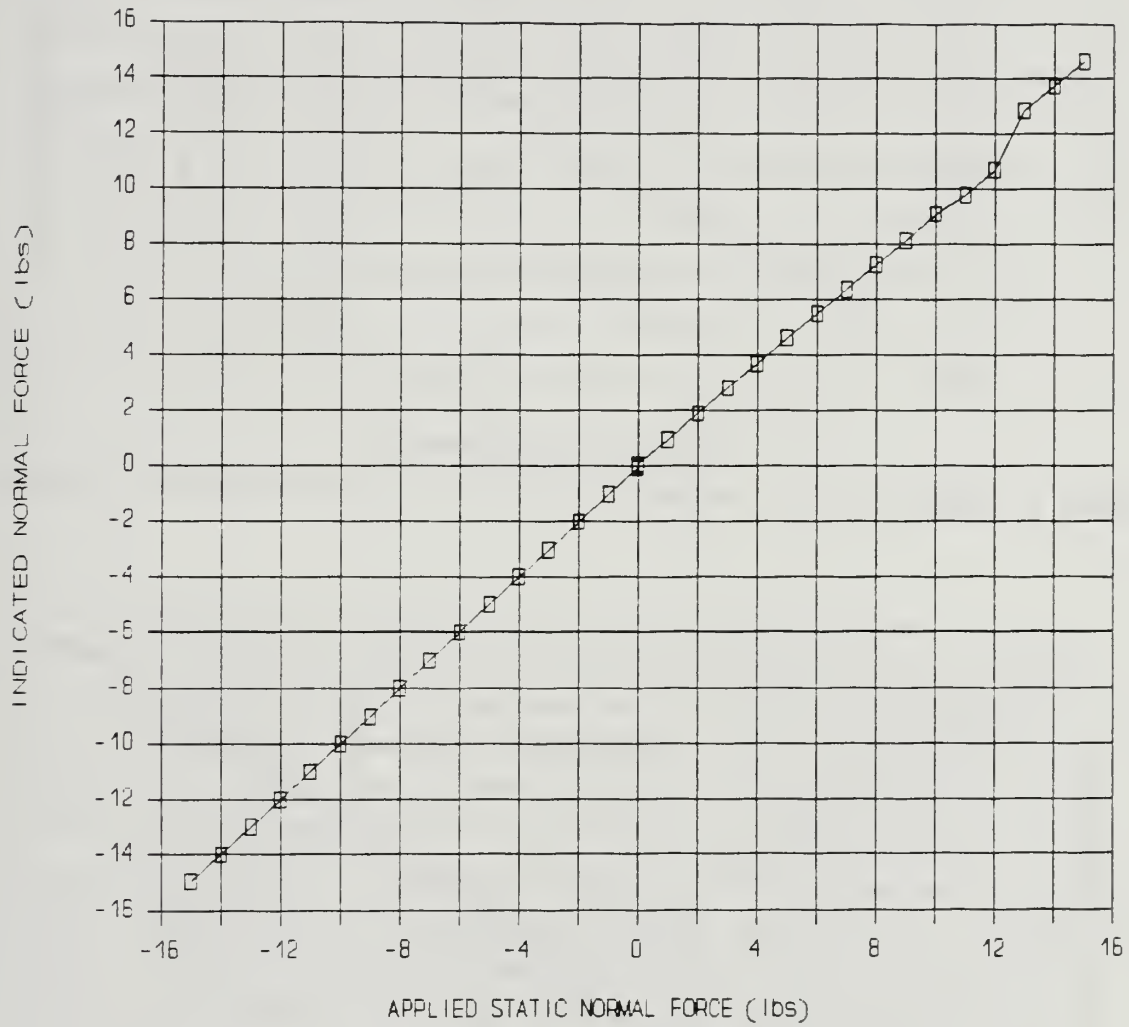
Figure 15. Normal Force Static Calibration
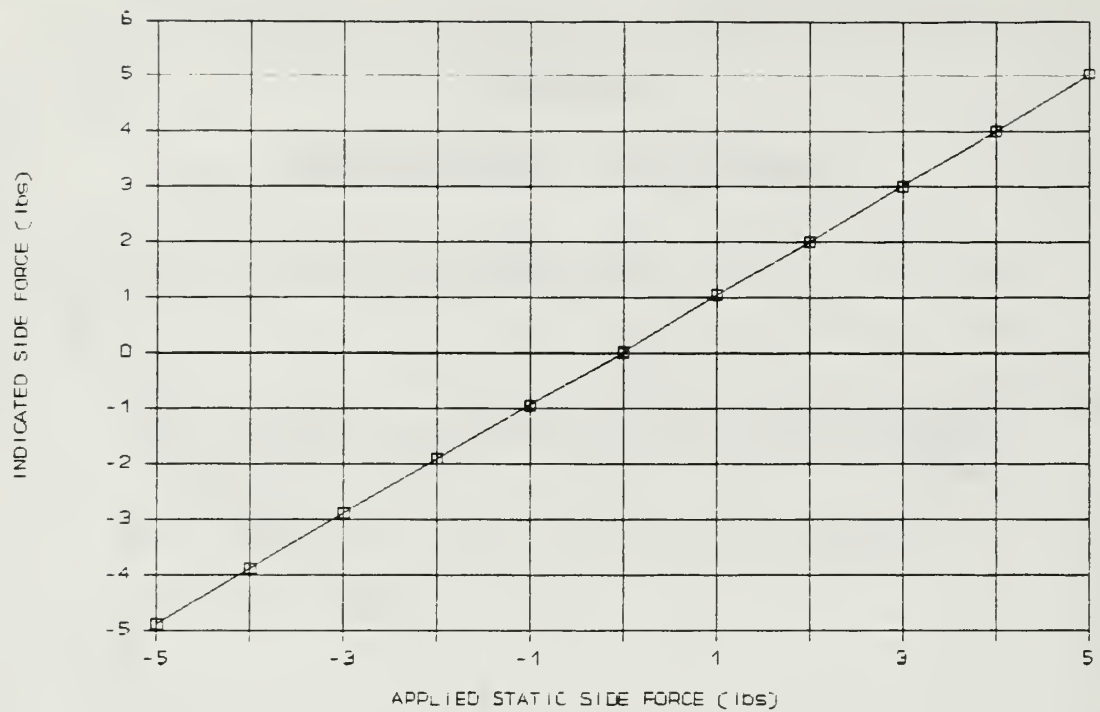
Figure 16. Side Force Static Calibration
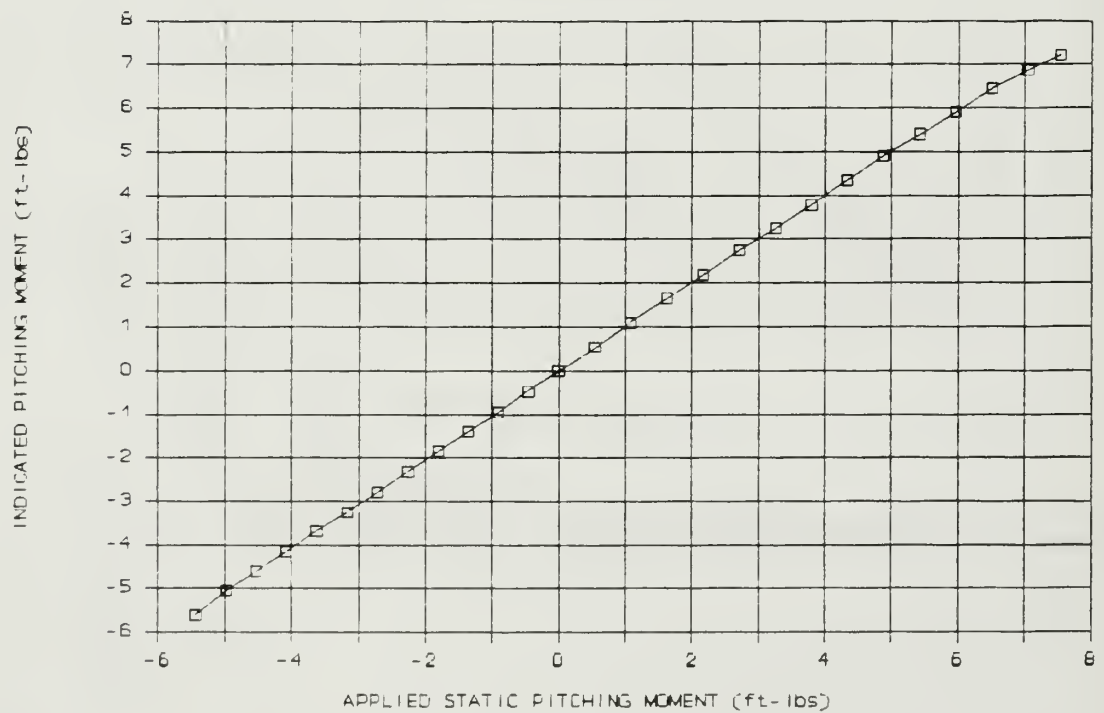
Figure 17. Pitching Moment Static Calibration
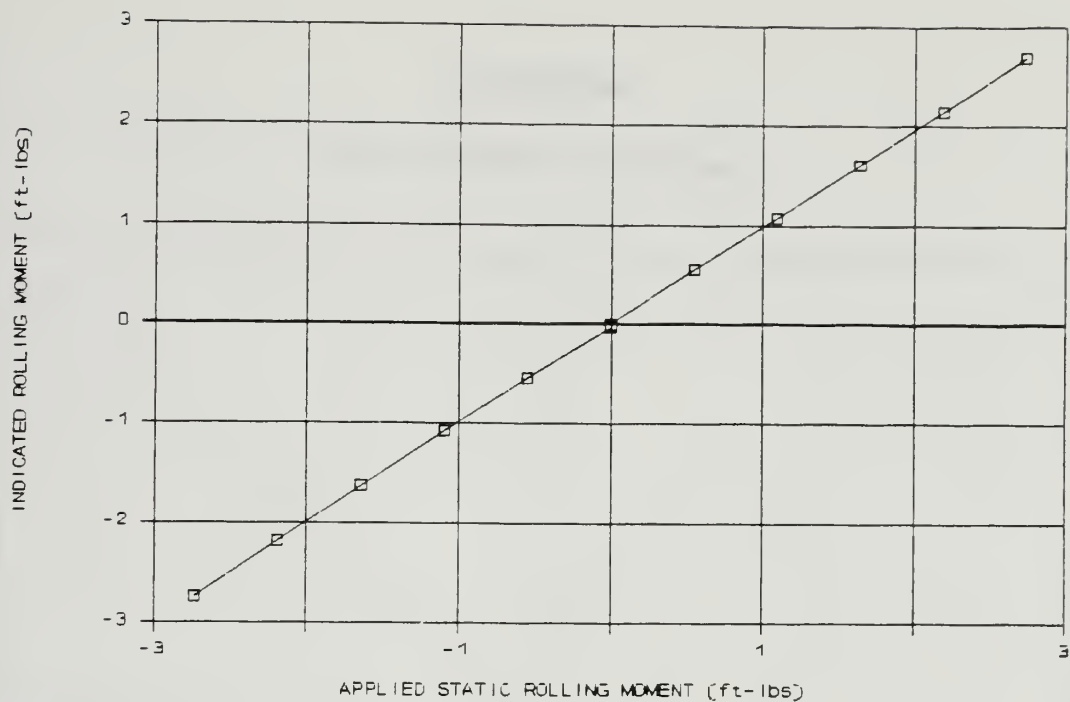
Figure 18. Rolling Moment Static Calibration
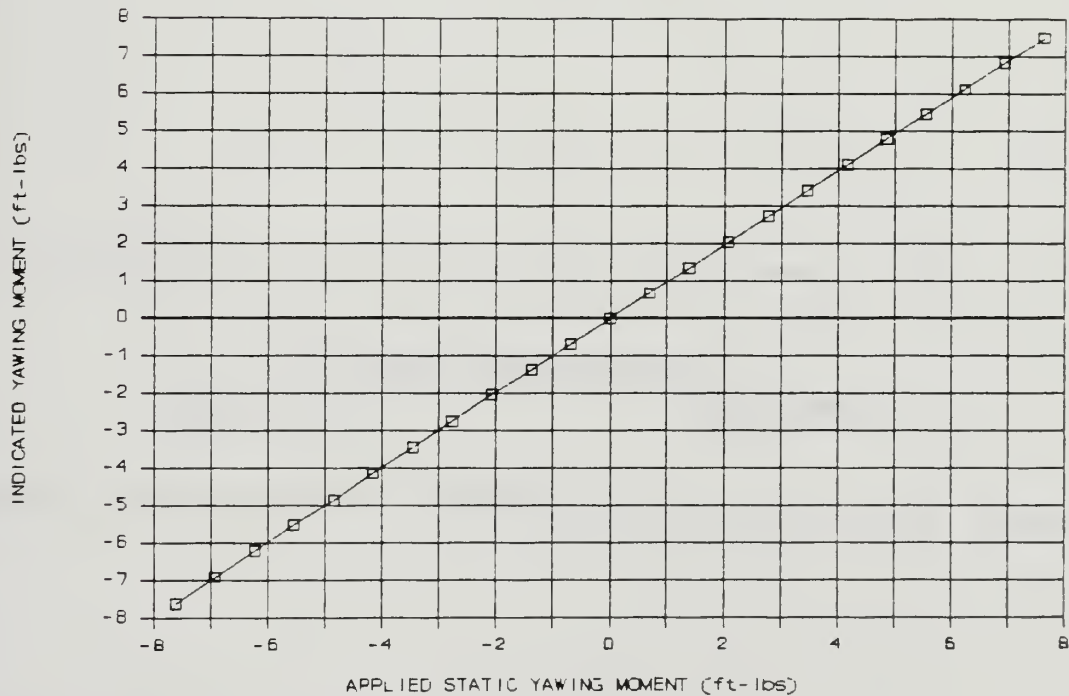
Figure 19. Yawing Moment Static Calibration

APPENDIX D

ZERO-LIFT & TRIM AOA DATA
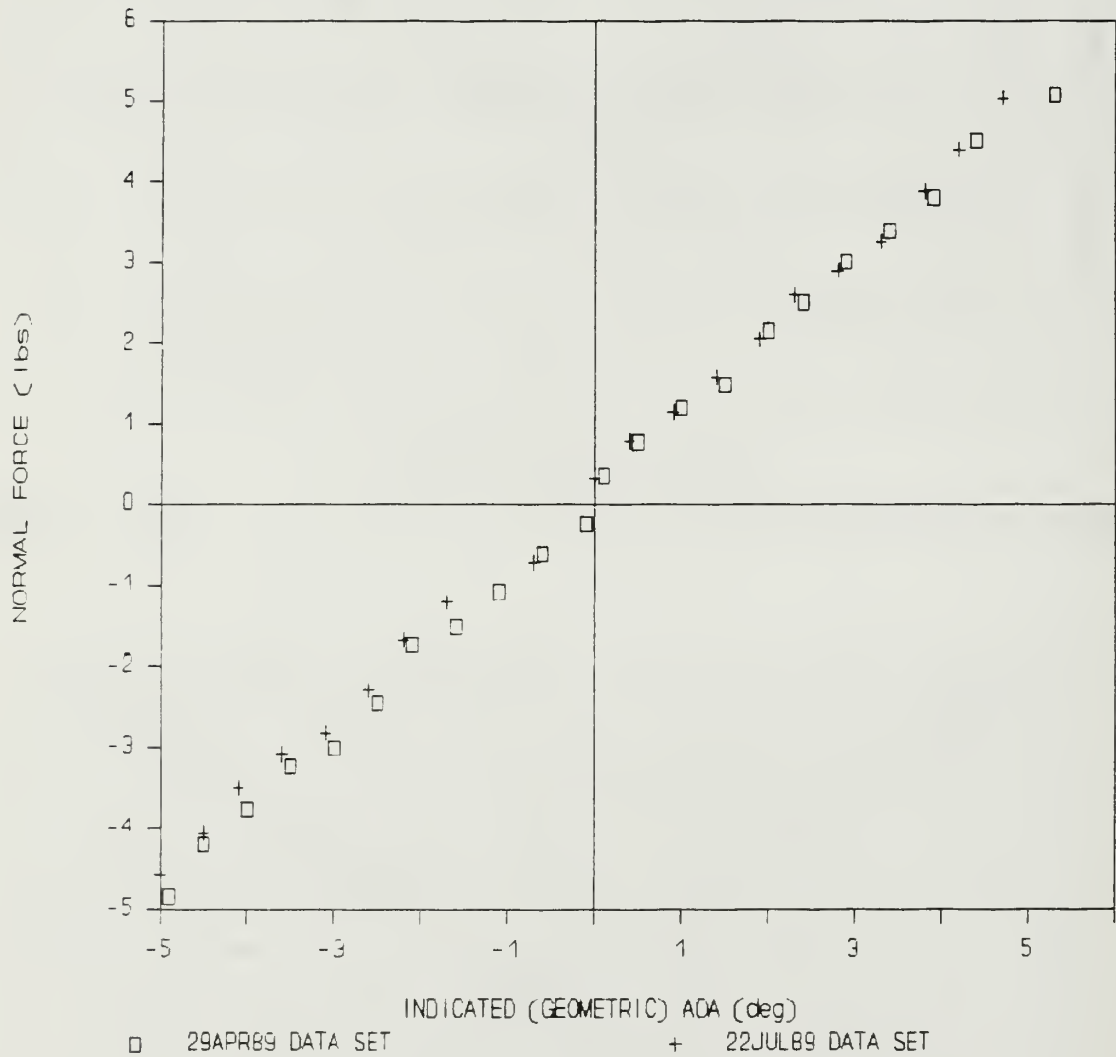
Figure 20. Determination of the Zero-Lift AOA
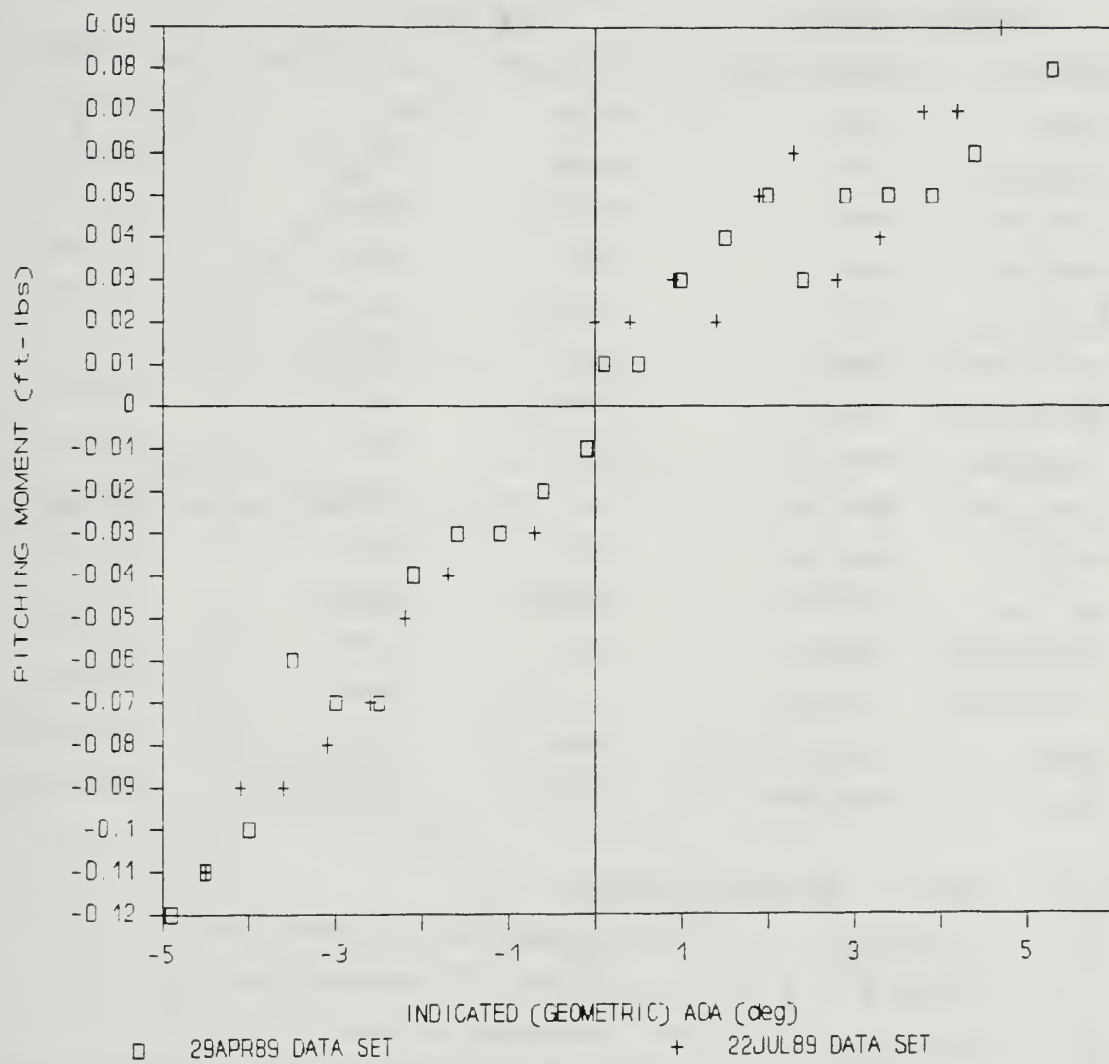
Figure 21. Determination of the Trim AOA

APPENDIX E

RAW FORCE/MOMENT DATA FOR VARIOUS STRUT CONFIGURATIONS

FORWARD STRUTS		AFT STRUTS		
LOCATION	EXTENSION	LOCATION	EXTENSION	FIGURES
None	N/A	None	N/A	22-27
Inboard	Long	Hook	Short	28-33
Inboard	Long	Nozzle	Short	34-39
Middle	Long	Hook	Short	40-45
Middle	Long	Nozzle	Short	46-51
Outboard	Long	Hook	Short	52-57
Outboard	Long	Nozzle	Short	58-63
Inboard	Medium	Hook	Long	64-69
Inboard	Medium	Nozzle	Long	70-75
Middle	Medium	Hook	Long	76-81
Middle	Medium	Nozzle	Long	82-87
Outboard	Medium	Hook	Long	88-93
Outboard	Medium	Nozzle	Long	94-99
Gear	Medium	Hook	Long	100-105
Gear	Medium	Nozzle	Long	106-111

Note: None = Struts removed

Inboard = 1.875" outboard of centerline

Middle = 4.531" outboard of centerline

Outboard = 6.188" outboard of centerline

Gear = 1.875" outboard of centerline, 2" below wing

Hook = 4.375" aft of moment center

Nozzle = Nozzle lip

Short = 0.4"

Medium = 0.5"

Long = 1.5"
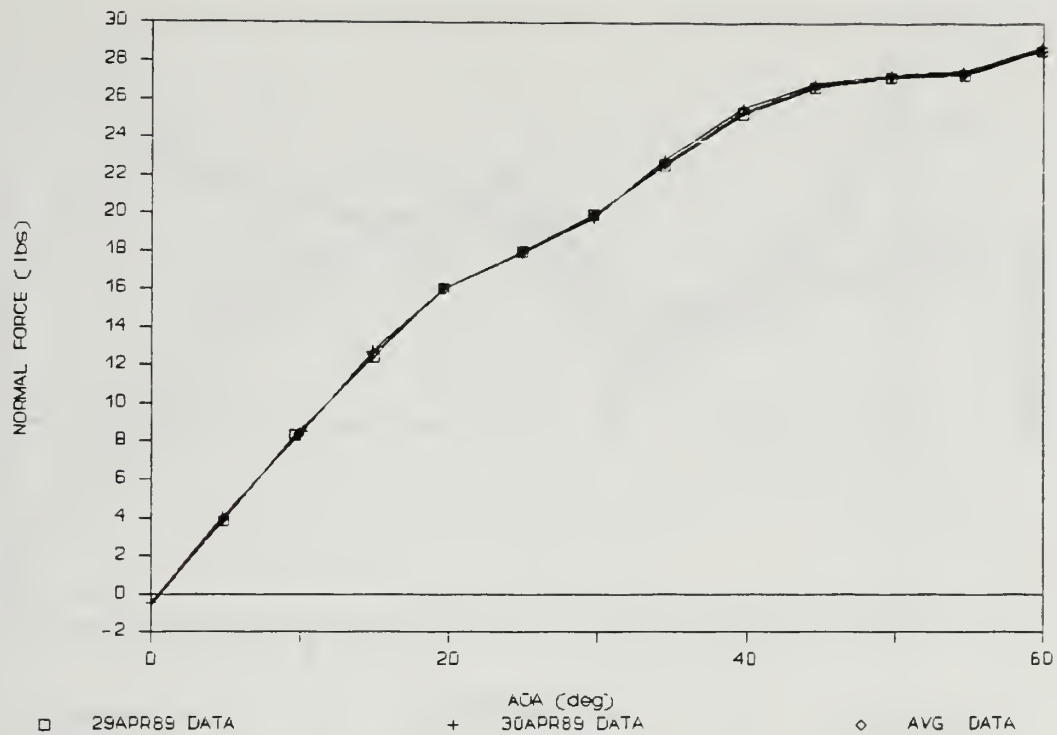
Figure 22. Normal Force (No Struts)
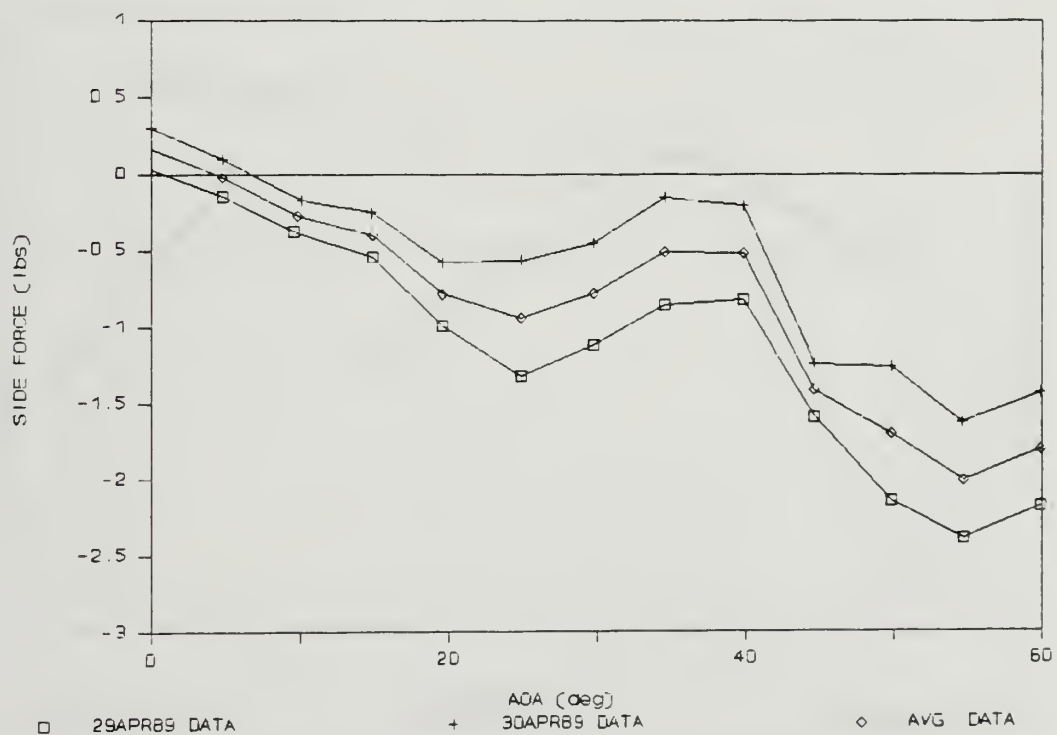
Figure 23. Side Force (No Struts)
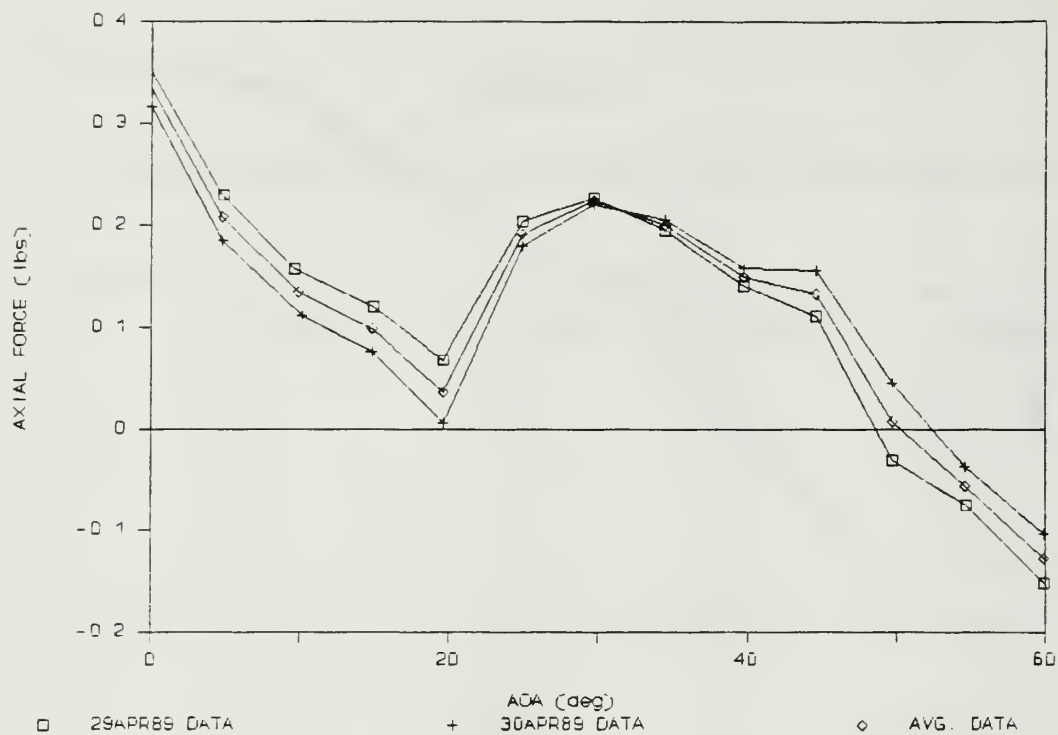
Figure 24. Axial Force (No Struts)
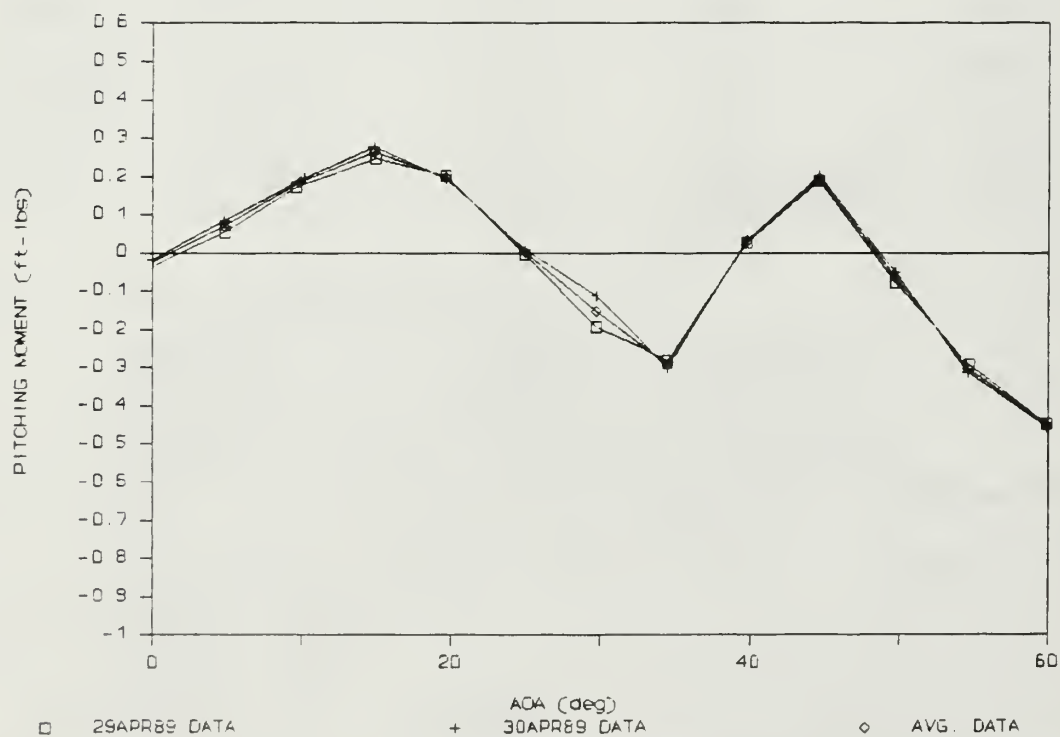
Figure 25. Pitching Moment (No Struts)

68
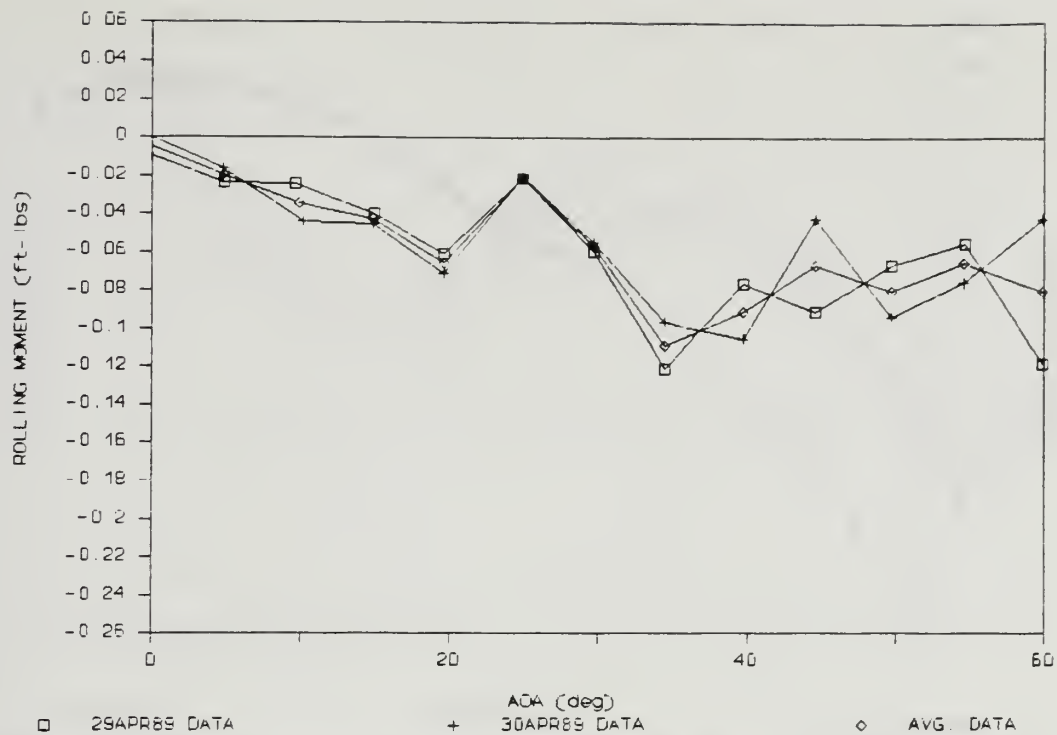
Figure 26. Rolling Moment (No Struts)
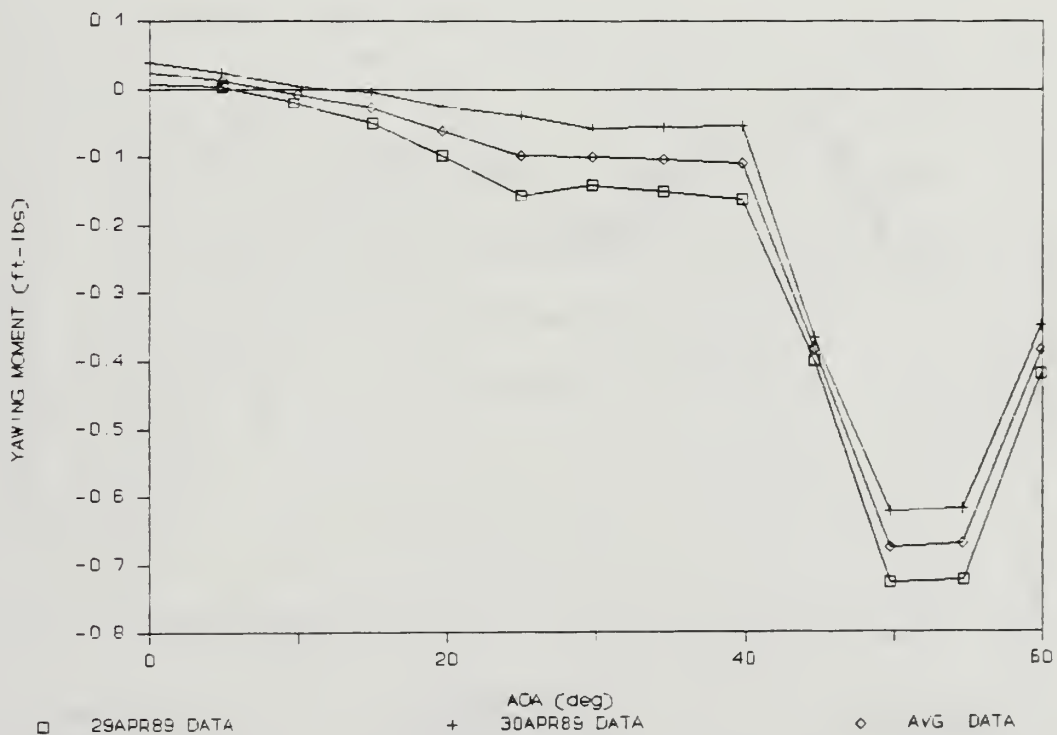
Figure 27. Yawing Moment (No Struts)
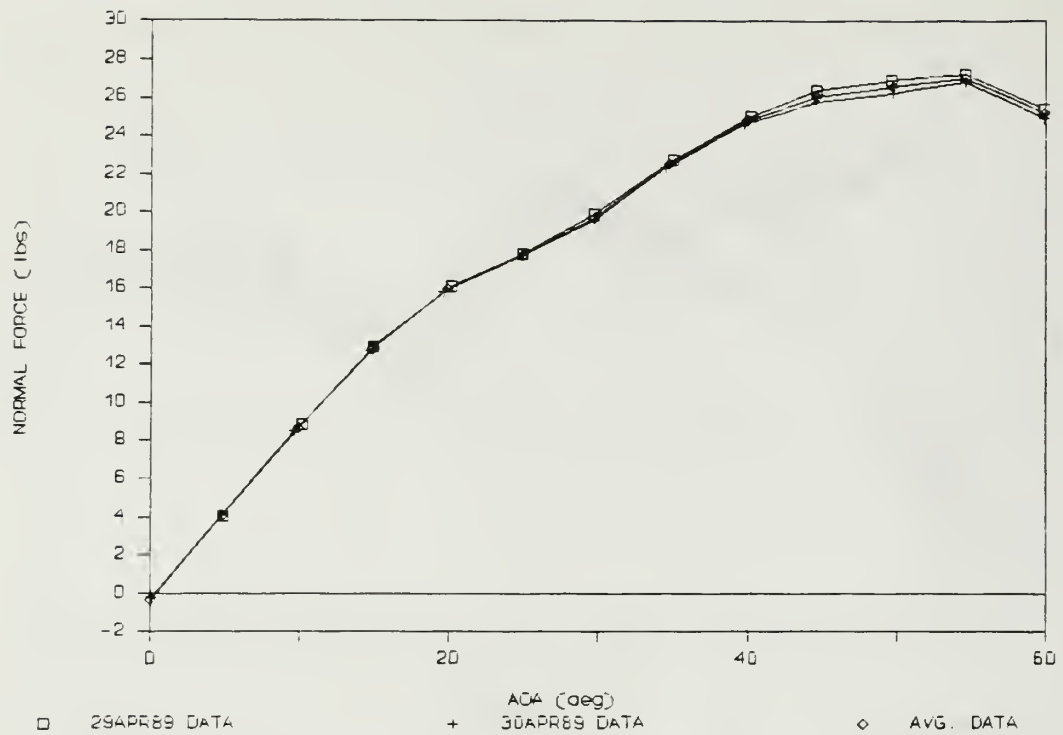
Figure 28. Normal Force (Fwd: Inboard/Long. Aft: Hook/Short)
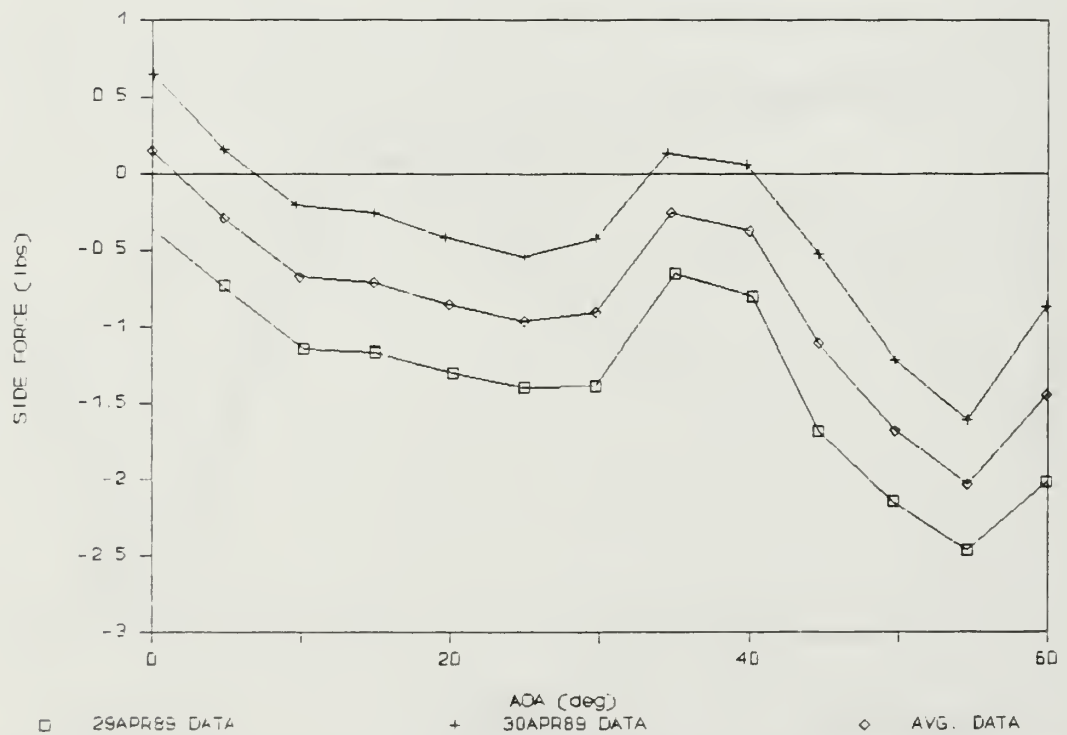
Figure 29. Side Force (Fwd: Inboard/Long. Aft: Hook/Short)
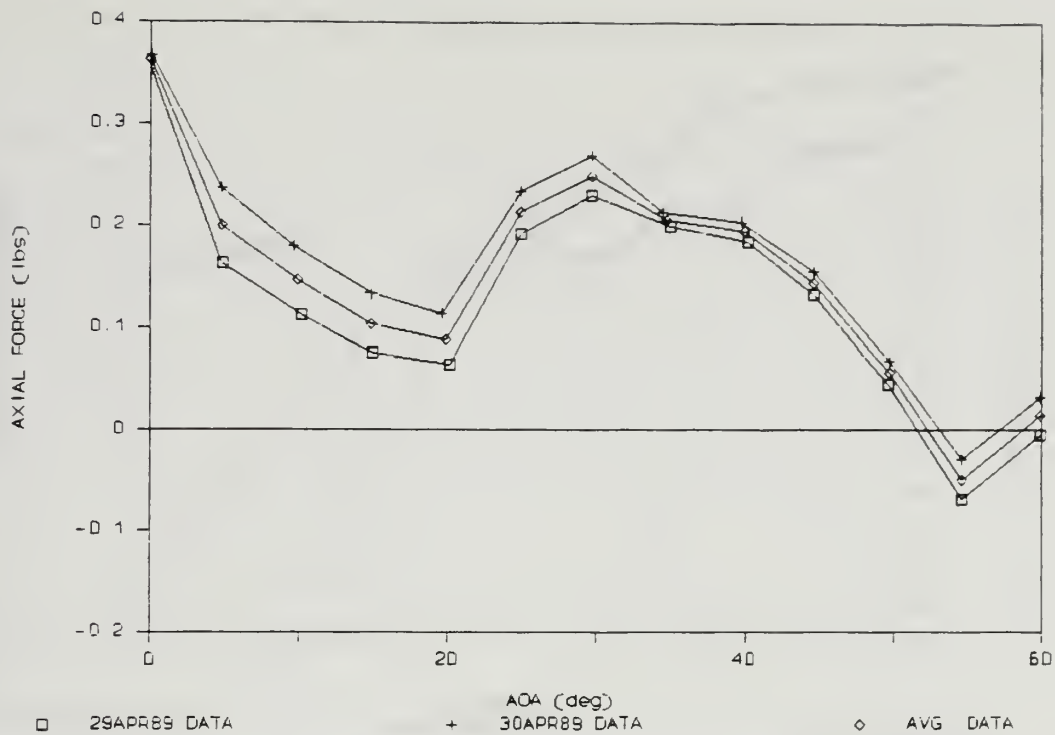
Figure 30. Axial Force (Fwd: Inboard/Long, Aft: Hook/Short)
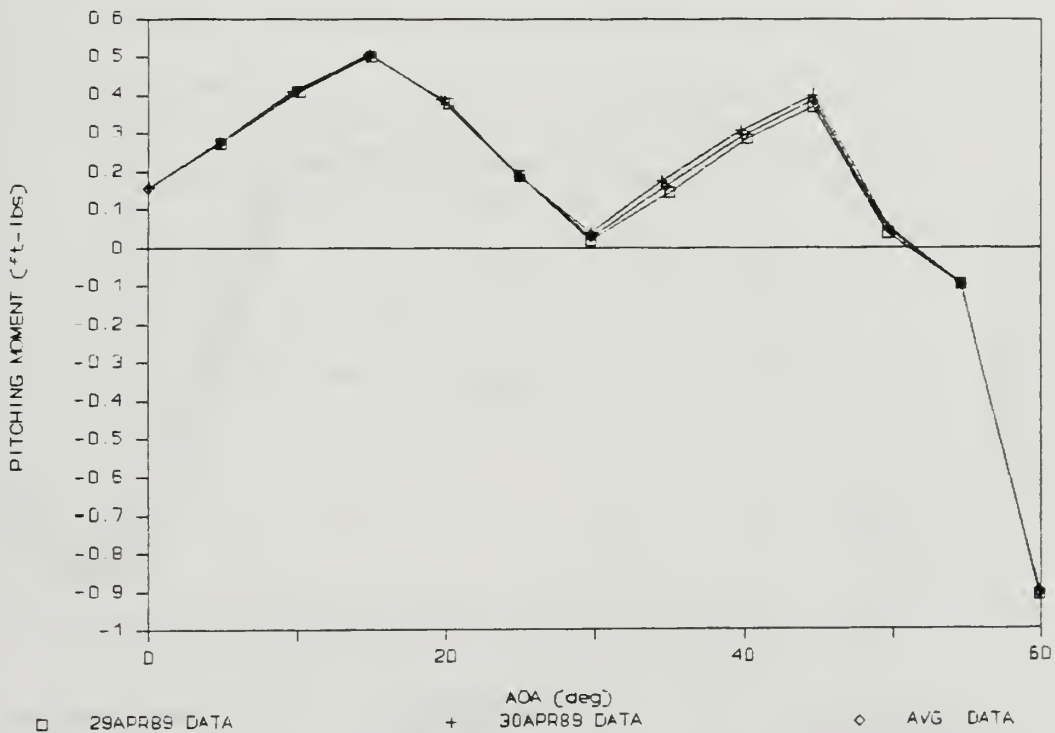
Figure 31. Pitching Moment (Fwd: Inboard/Long, Aft: Hook/Short)

71
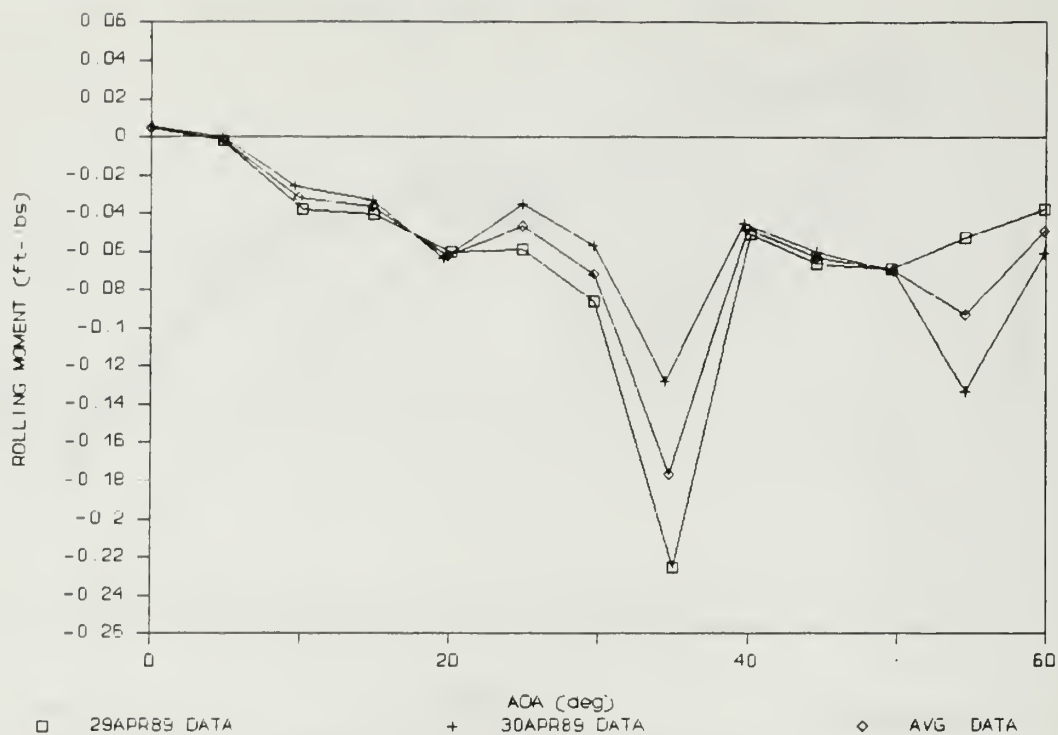
Figure 32. Rolling Moment (Fwd: Inboard/long, Aft: Hook/Short)
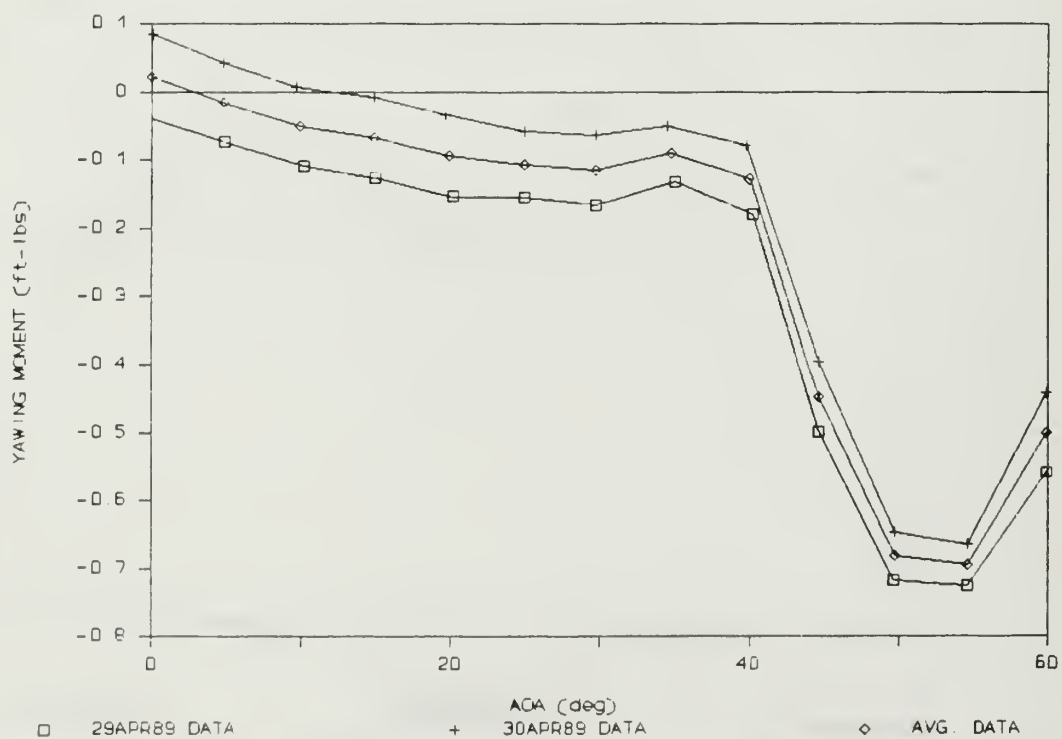
Figure 33. Yawing Moment (Fwd: Inboard/Long, Aft: Hook/Short)

72
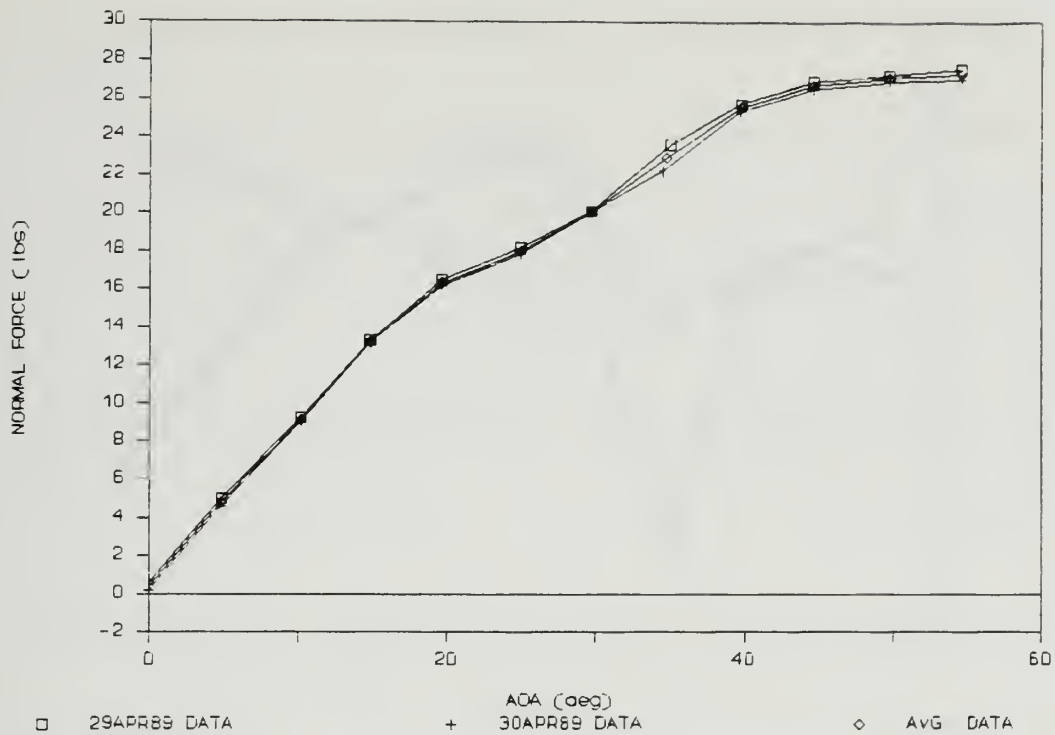
Figure 34. Normal Force (Fwd: Inboard/Long, Aft: Nozzle/Short)
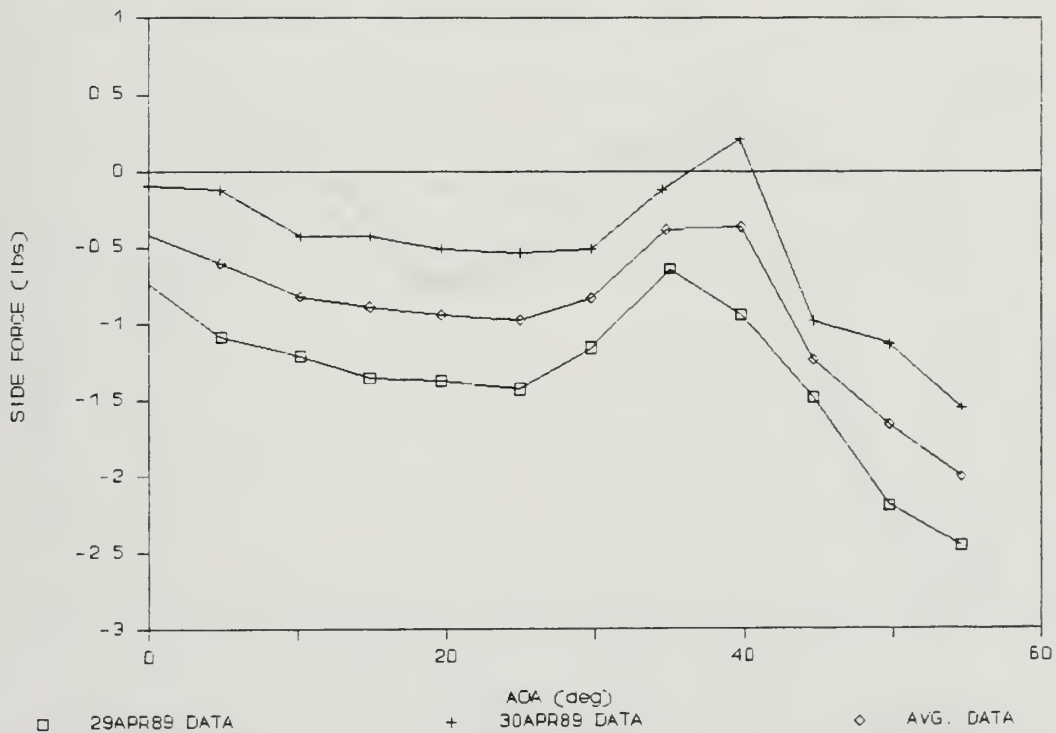
Figure 35. Side Force (Fwd: Inboard/Long, Aft: Nozzle/Short)
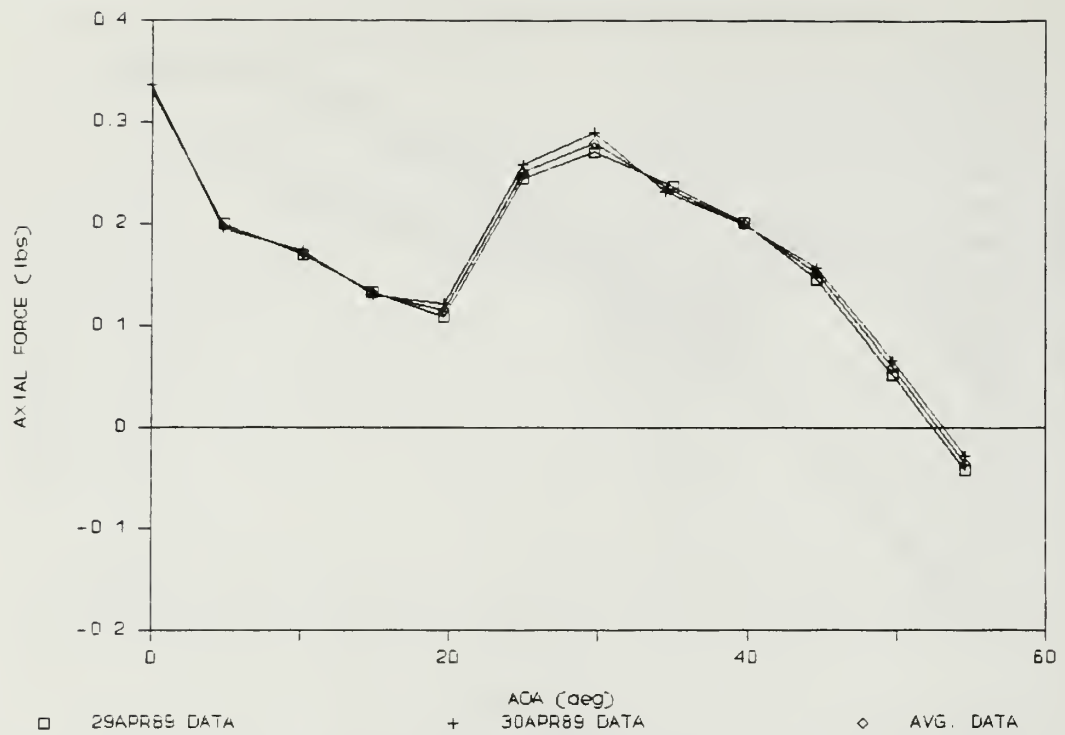
Figure 36. Axial Force (Fwd: Inboard/Long, Aft: Nozzle/Short)
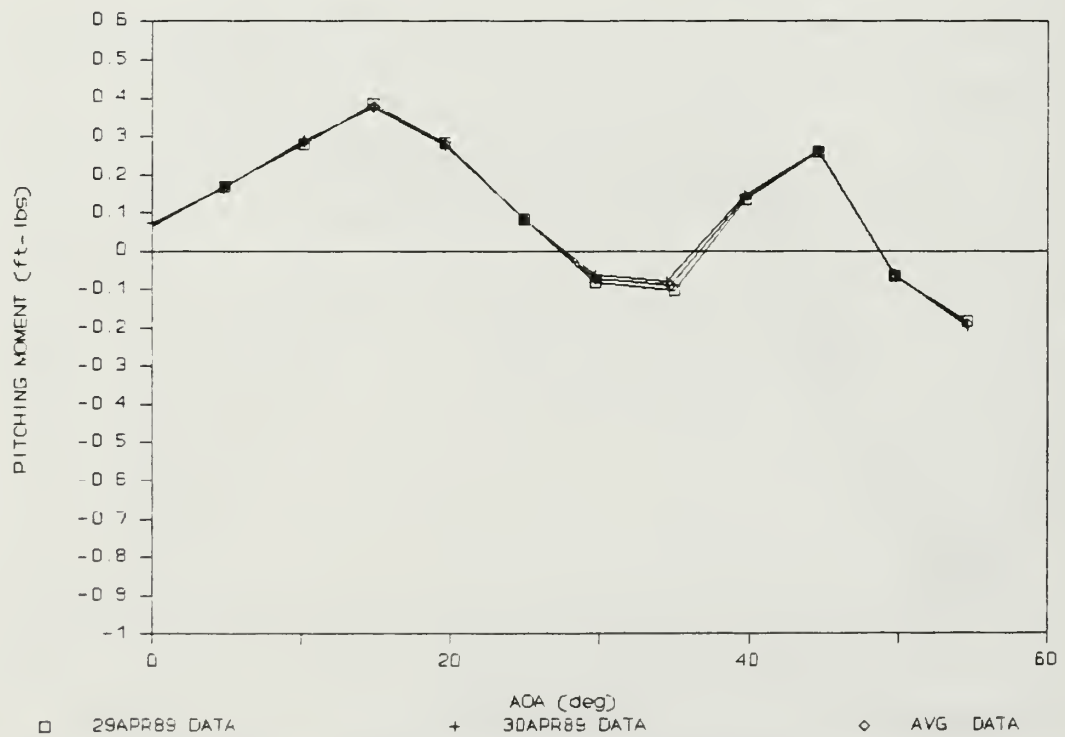
Figure 37. Pitching Moment (Fwd: Inboard/Long, Aft: Nozzle/Short)

74
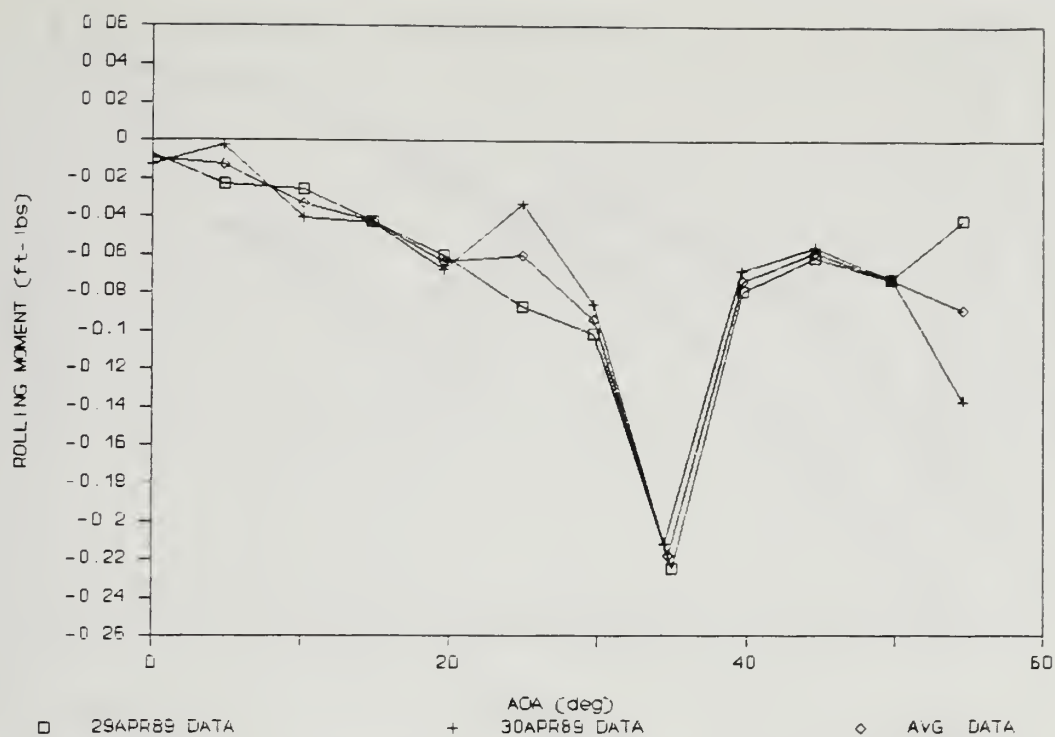
Figure 38. Rolling Moment (Fwd: Inboard/Long, Aft: Nozzle/Short)
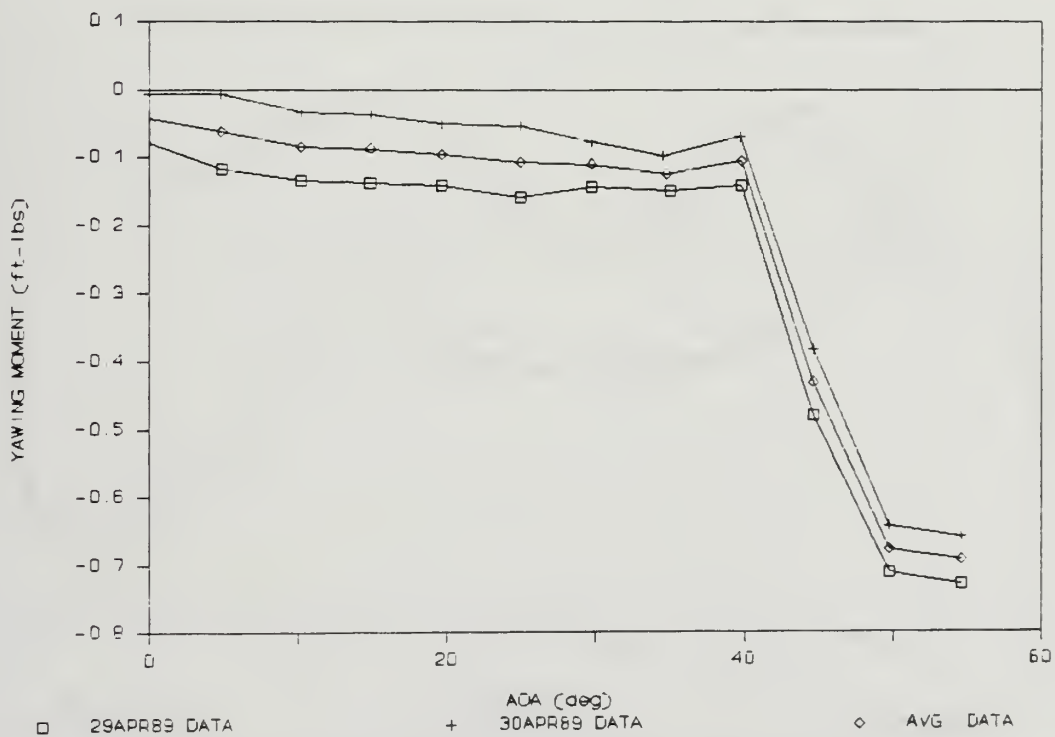
Figure 39. Yawing Moment (Fwd: Inboard/Long, Aft: Nozzle/Short)
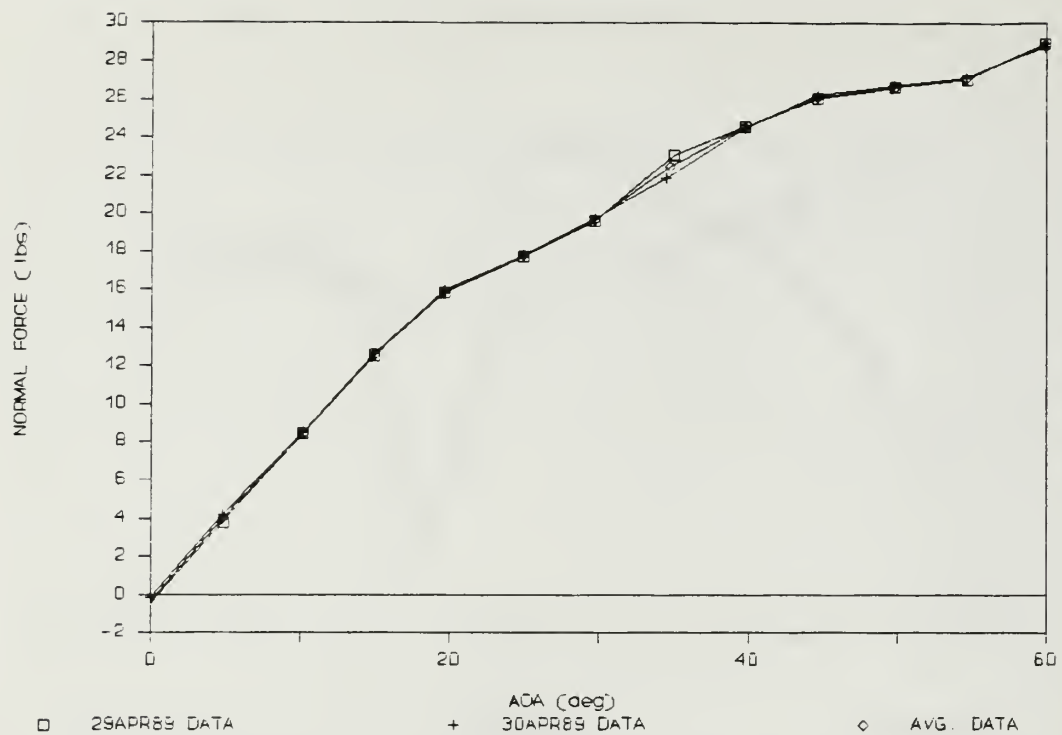
Figure 40. Normal Force (Fwd: Middle/Long, Aft: Hook/Short)
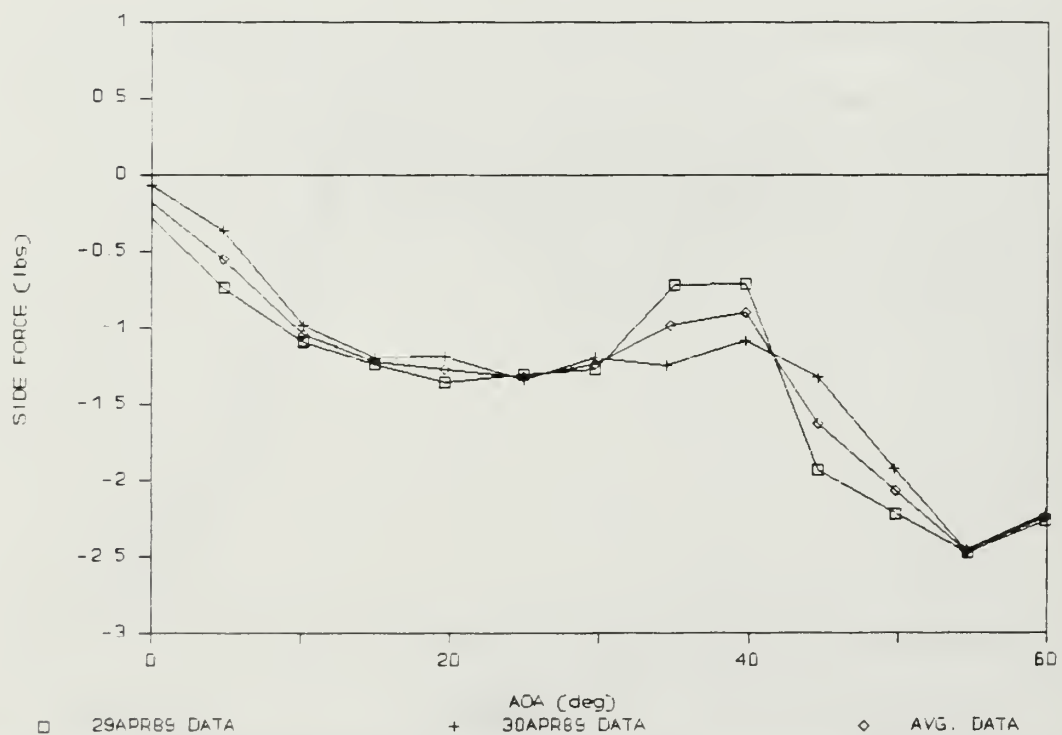
Figure 41. Side Force (Fwd: Middle/Long, Aft: Hook/Short)
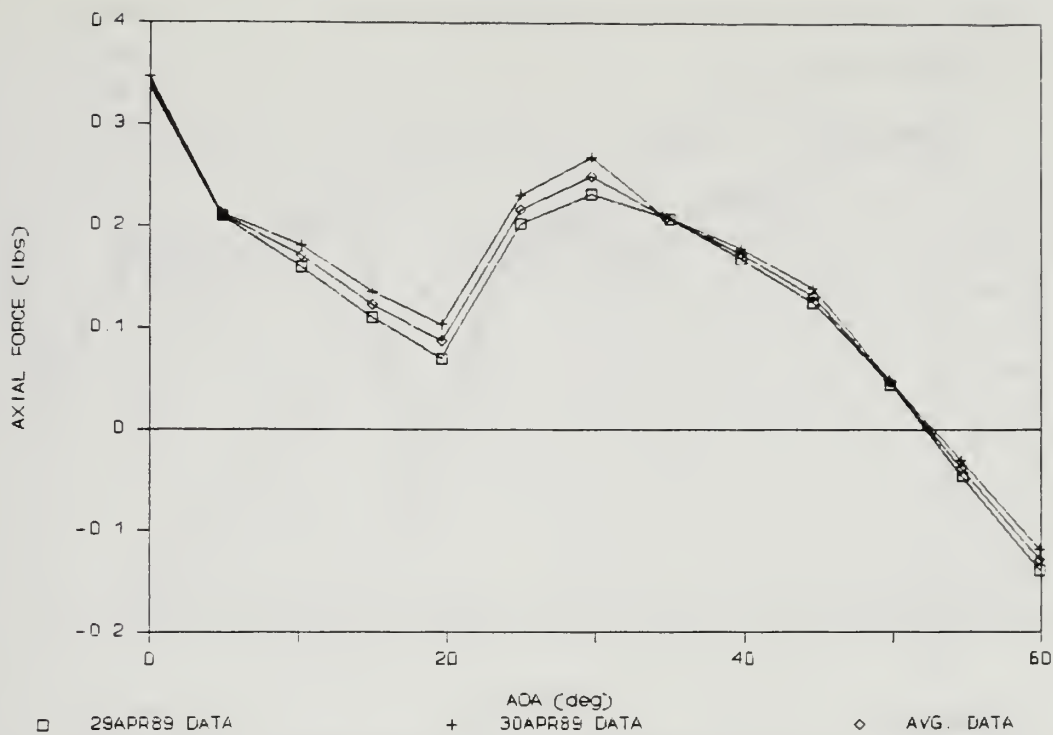
Figure 42. Axial Force (Fwd: Middle/Long, Aft: Hook/Short)
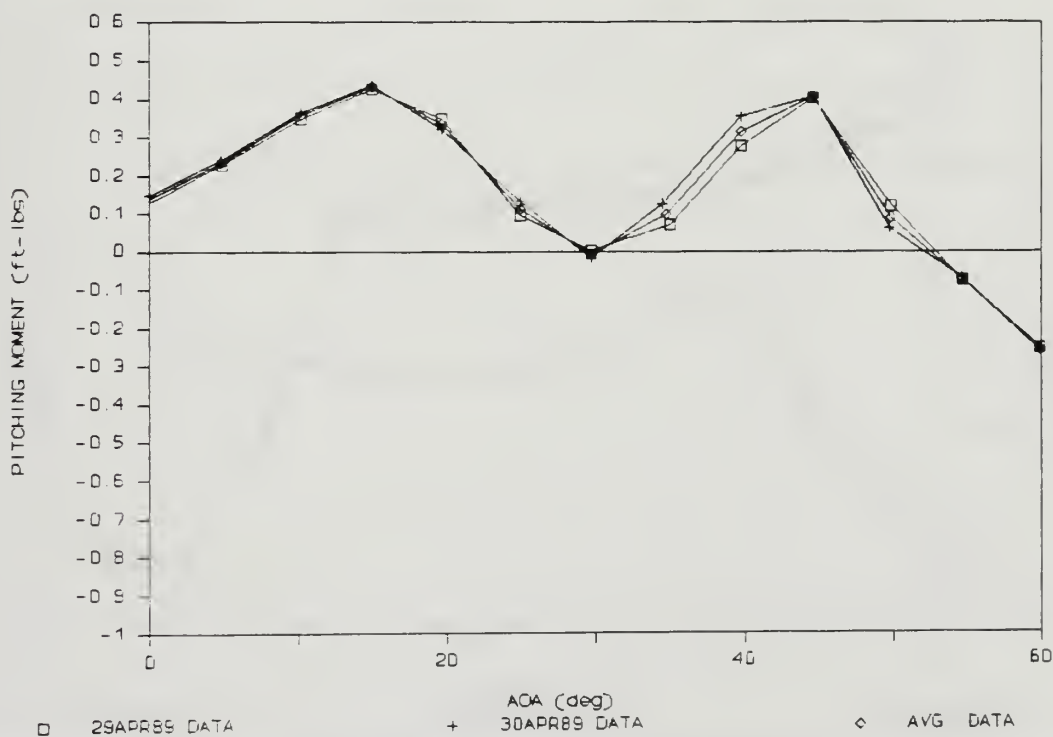
Figure 43. Pitching Moment (Fwd: Middle/Long, Aft: Hook/short)

77
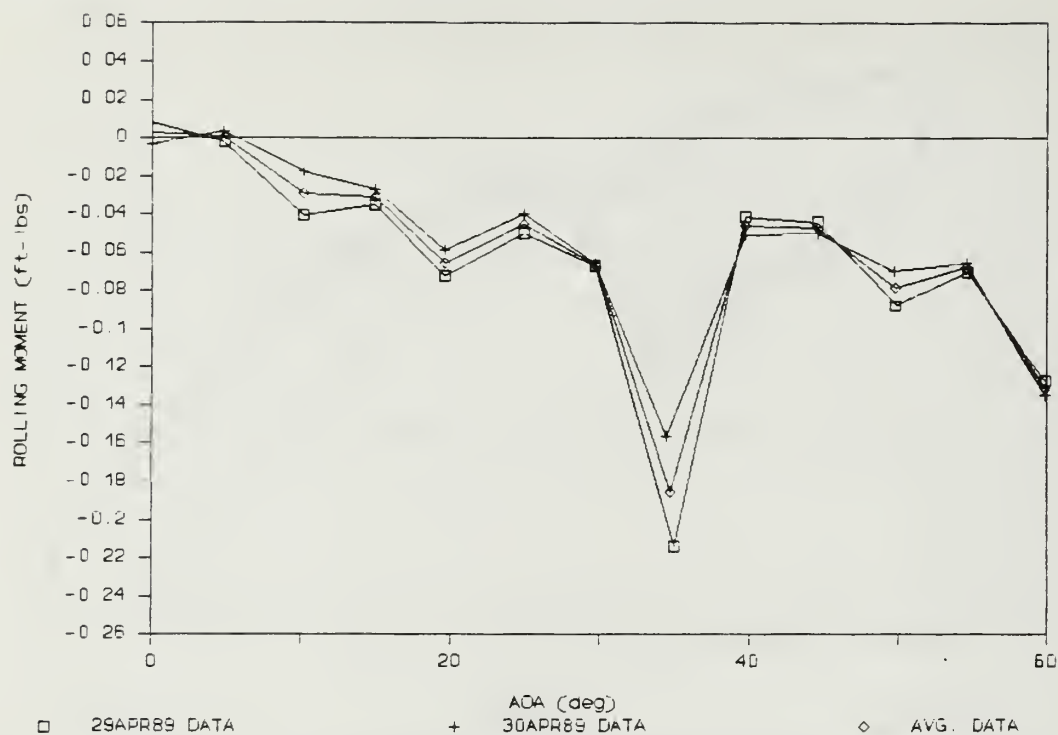
Figure 44. Rolling Moment (Fwd: Middle/Long, Aft: Hook/Short)
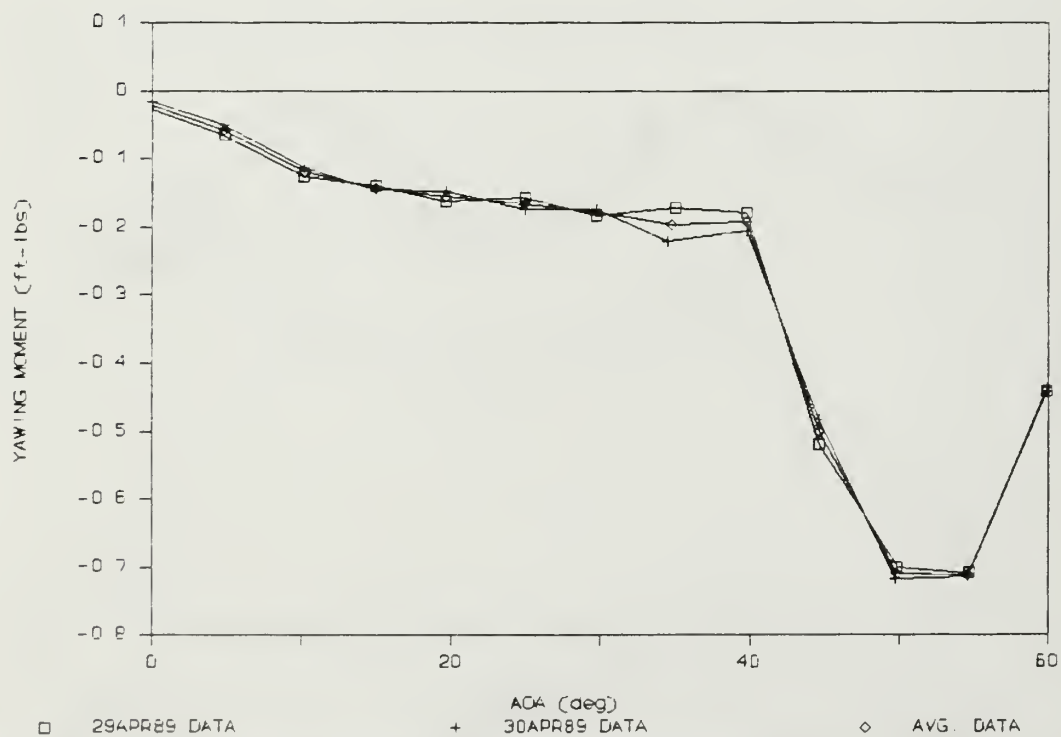
Figure 45. Yawing Moment (Fwd: Middle/Long, Aft: Hook/Short)
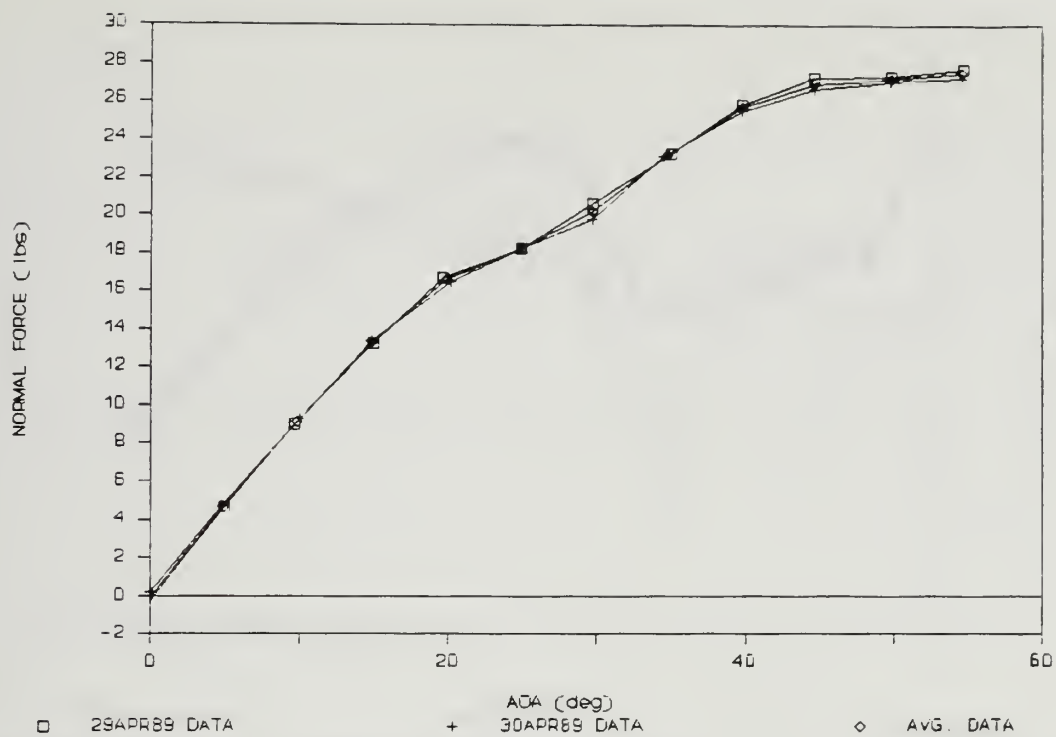
Figure 46. Normal Force (Fwd: Middle/Long, Aft: Nozzle/short)
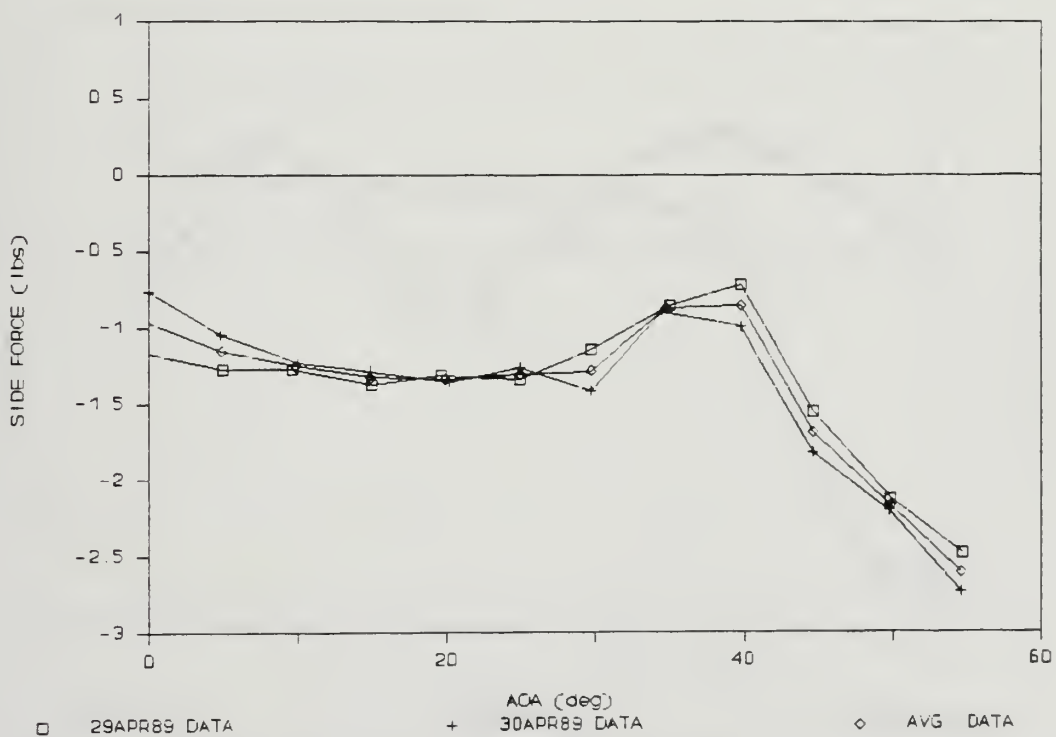
Figure 47. Side Force (Fwd: Middle/Long, Aft: Nozzle/Short)
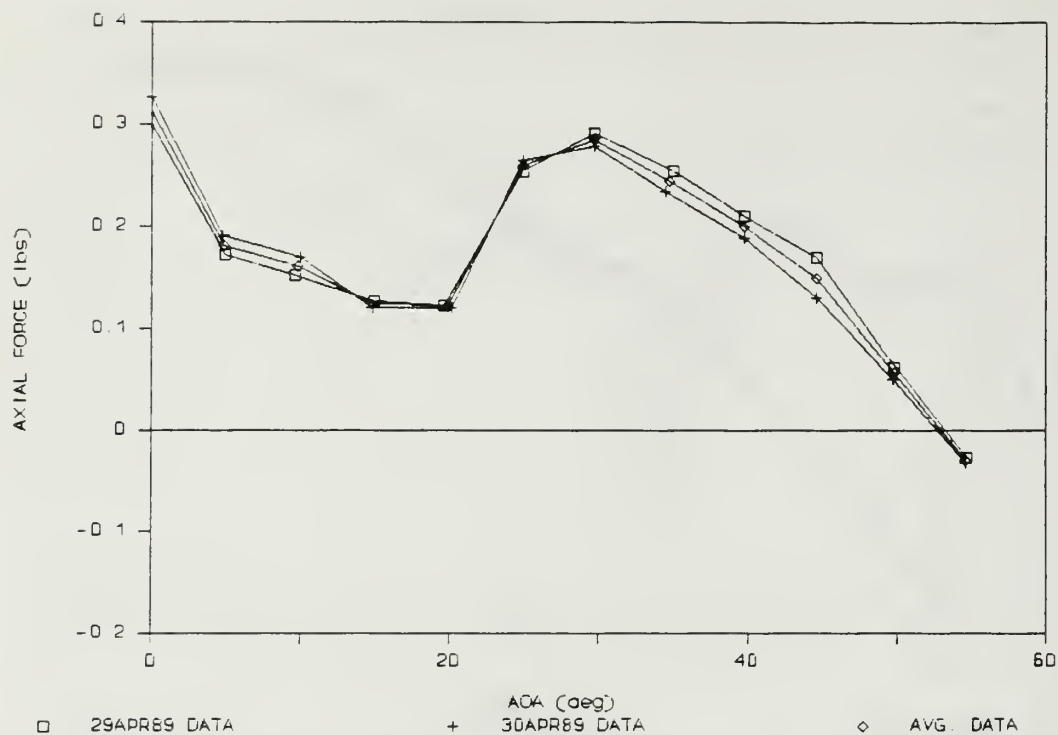
Figure 48. Axial Force (Fwd: Middle/Long, Aft: Nozzle/Short)
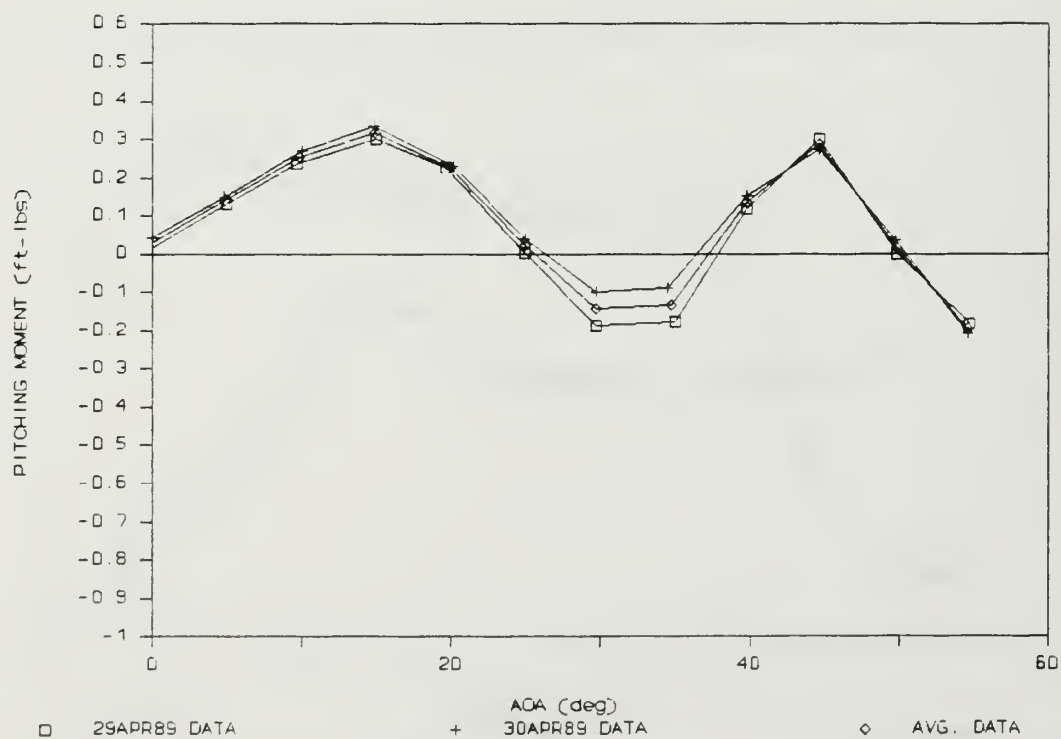
Figure 49. Pitching Moment (Fwd: Middle/Long, Aft: Nozzle/Short)

80
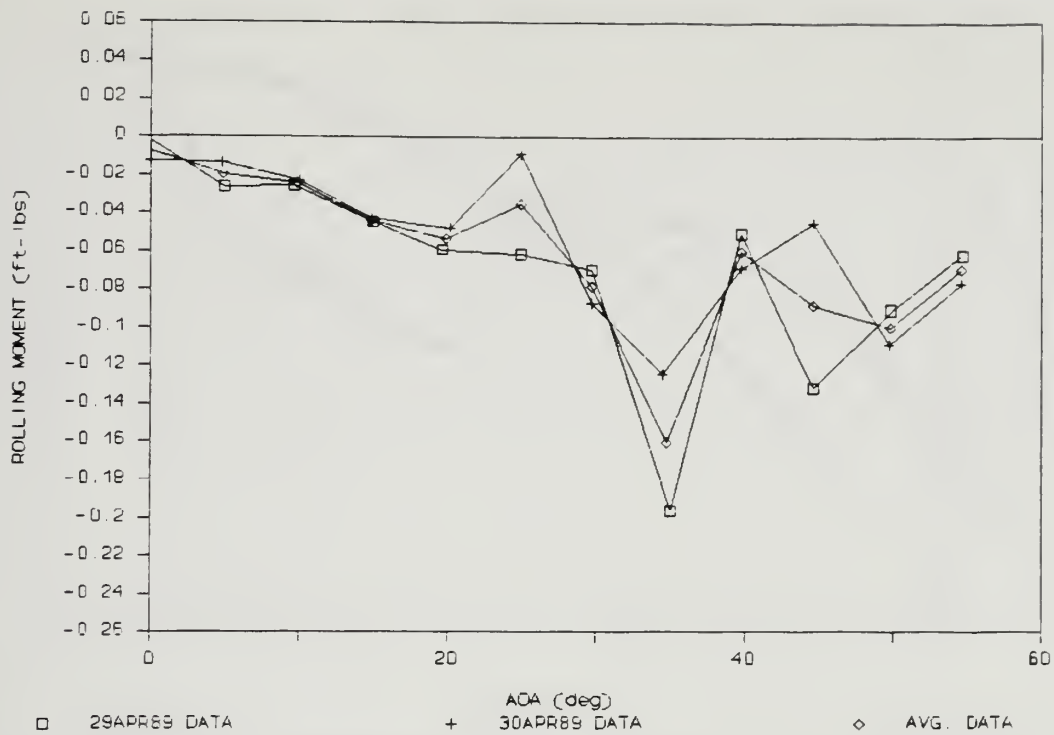
Figure 50. Rolling Moment (Fwd: Middle/Long, Aft: Nozzle/Short)
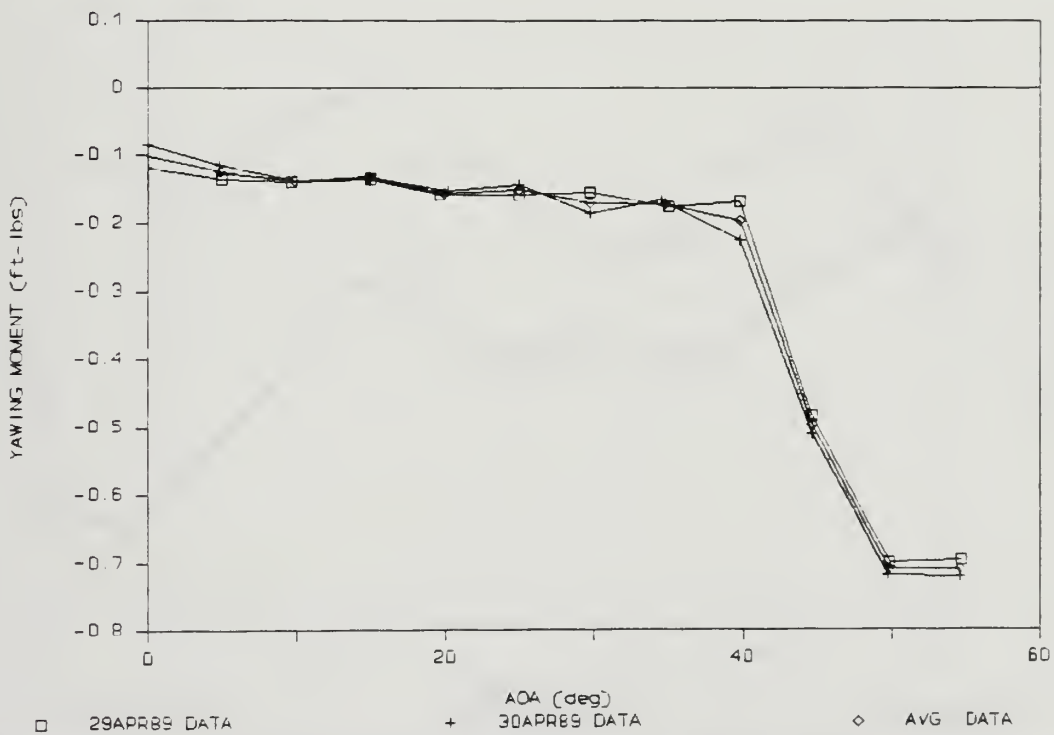
Figure 51. Yawing Moment (Fwd: Middle/Long, Aft: Nozzle/Short)
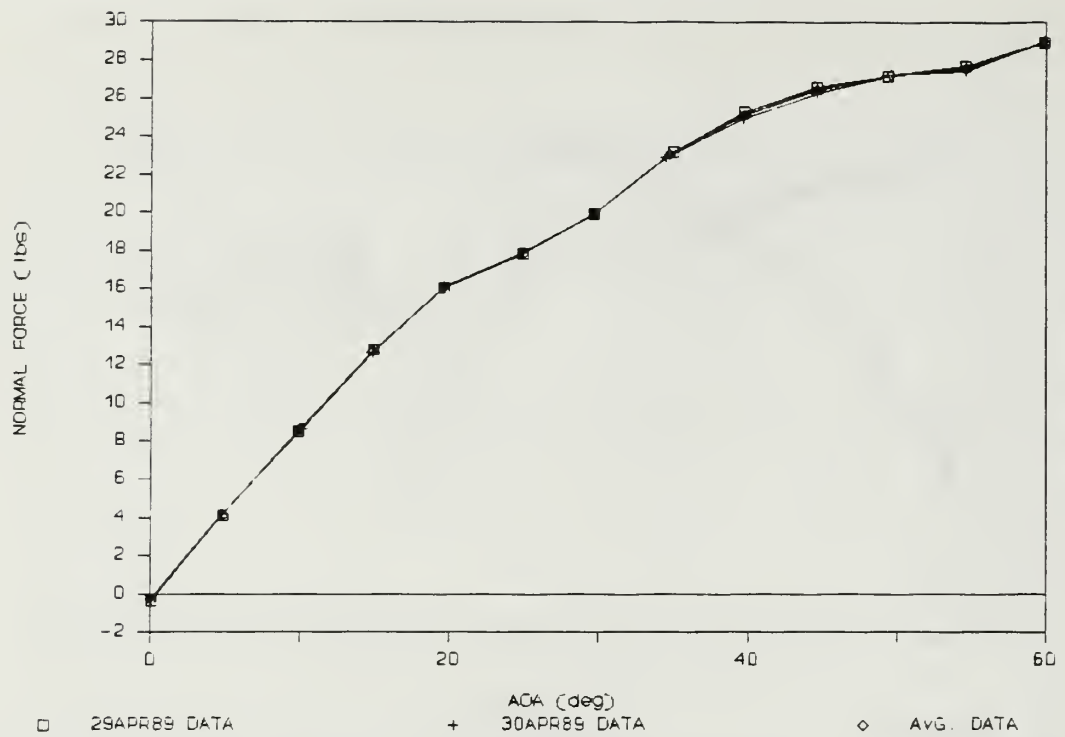
Figure 52. Normal Force (Fwd: Outboard/Long, Aft: Hook/Short)
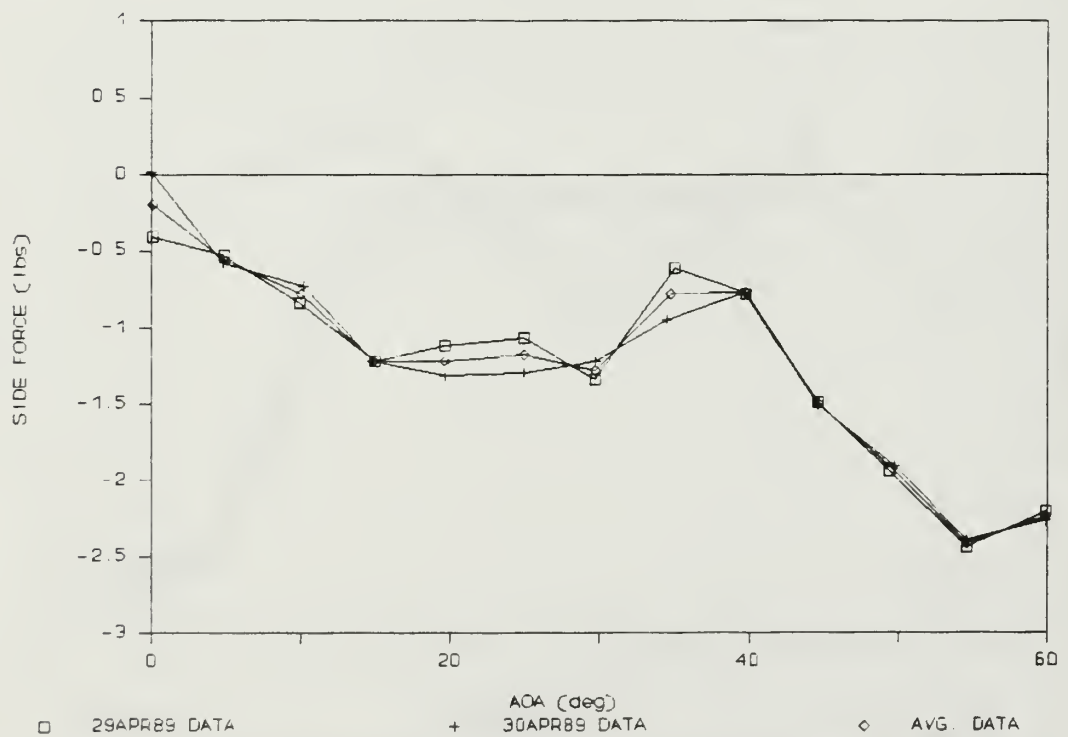
Figure 53. Side Force (Fwd: Outboard/Long, Aft: Hook/Short)

82
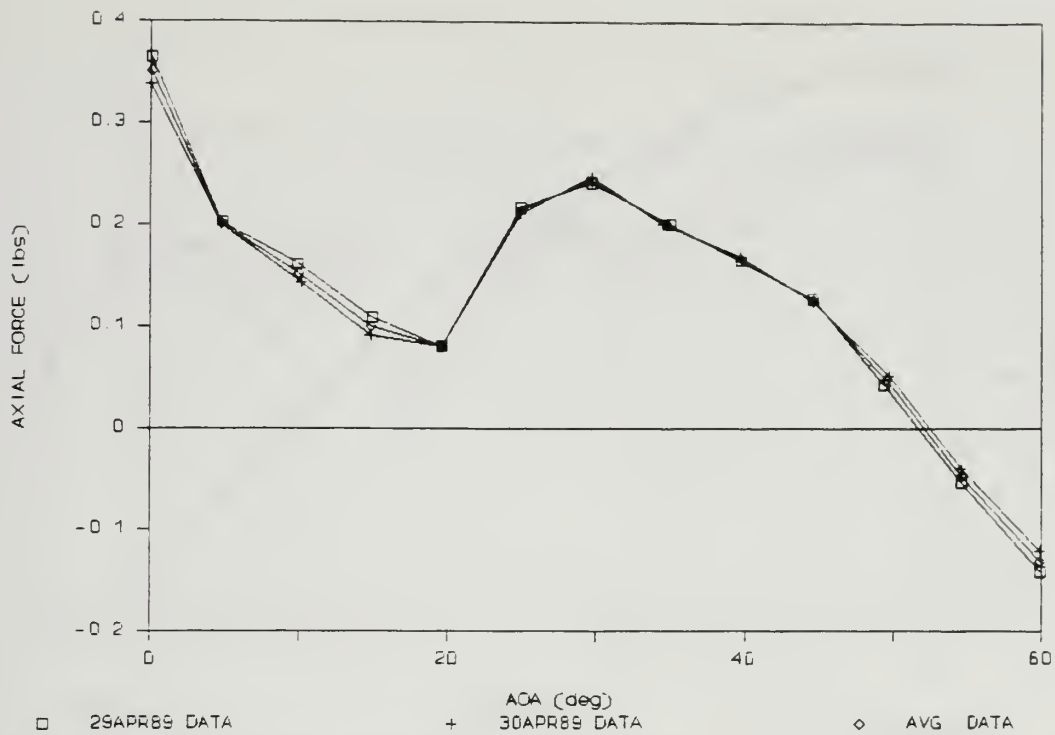
Figure 54. Axial Force (Fwd: Outboard/Long. Aft: Hook/Short)
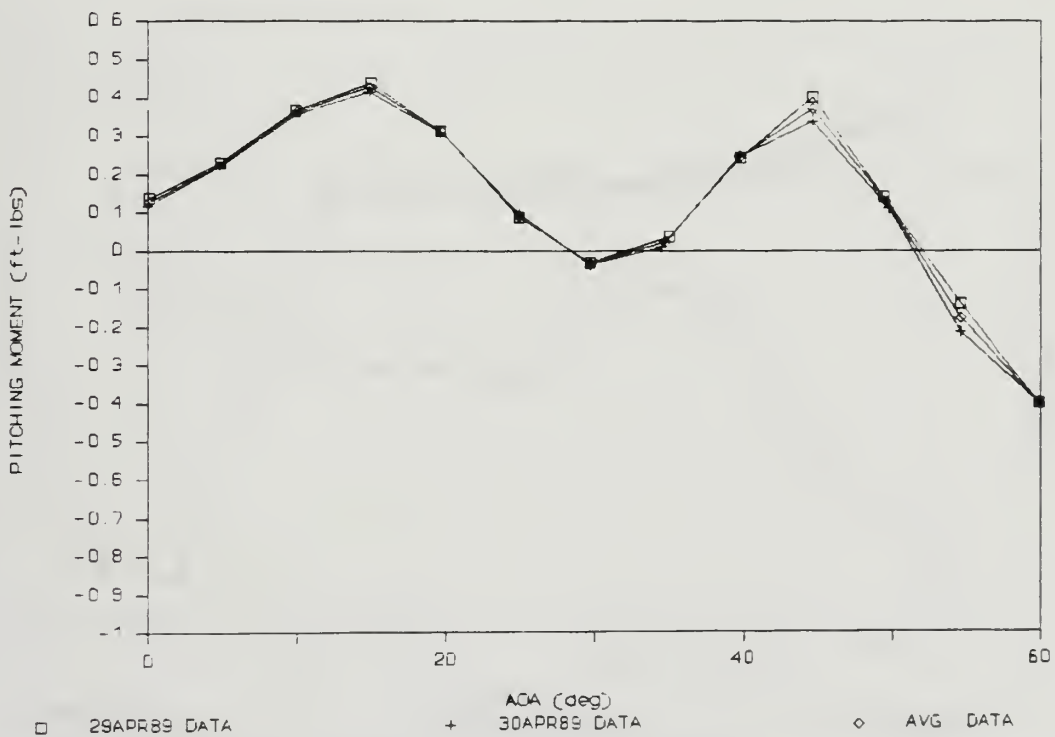
Figure 55. Pitching Moment (Fwd: Outboard/Long. Aft: Hook/Short)
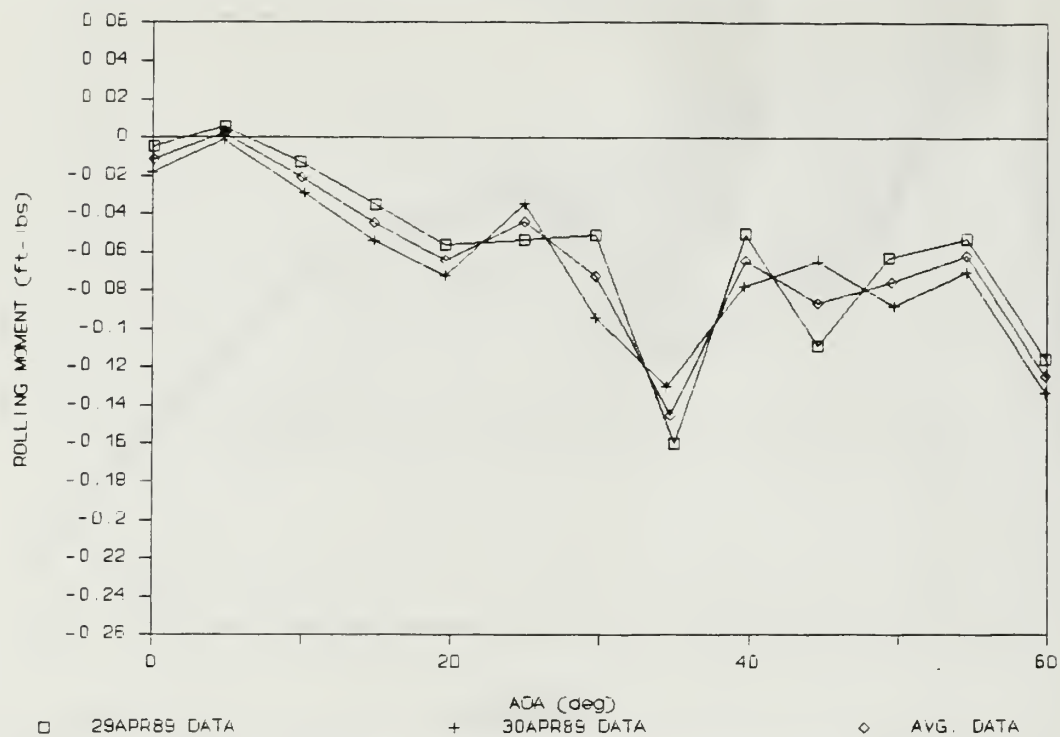
Figure 56. Rolling Moment (Fwd: Outboard/Long, Aft: Hook/Short)
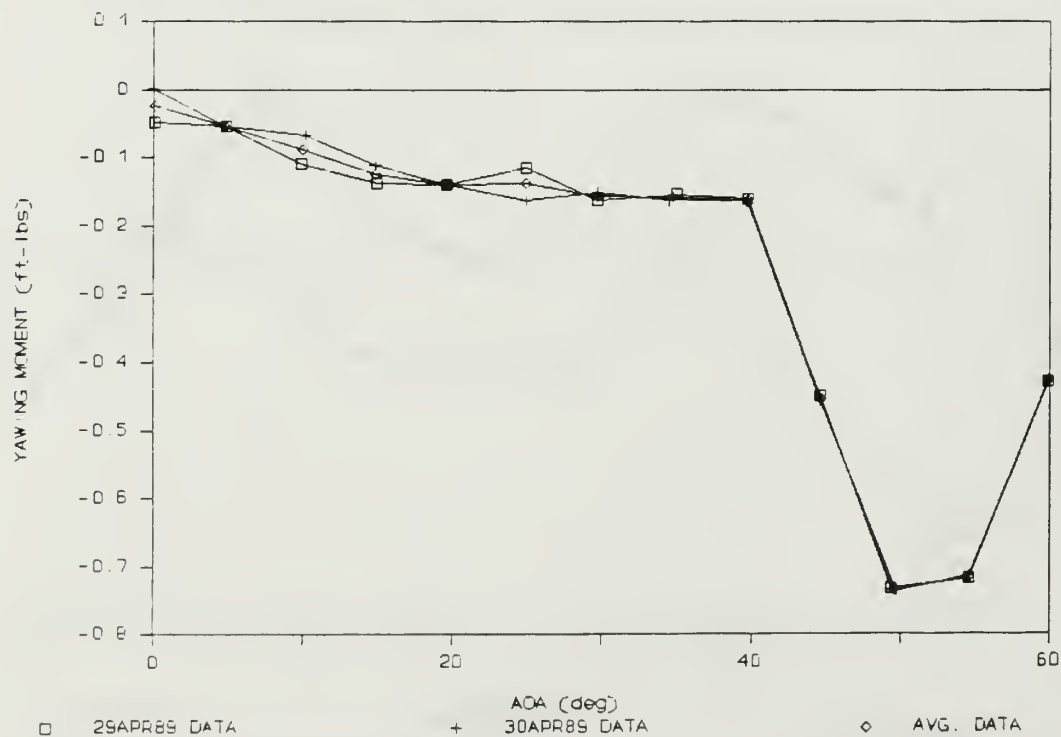
Figure 57. Yawing Moment (Fwd: Outboard/Long, Aft: Hook/Short)

84
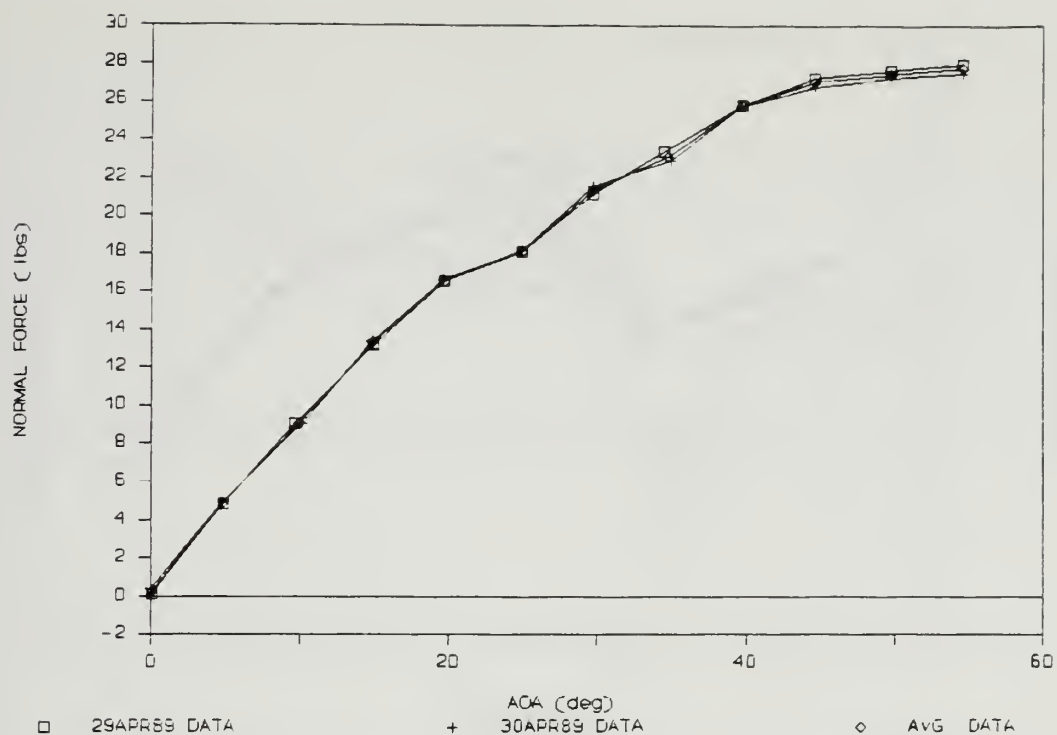
Figure 58. Normal Force (Fwd: Outboard/Long, Aft: Nozzle/Short)
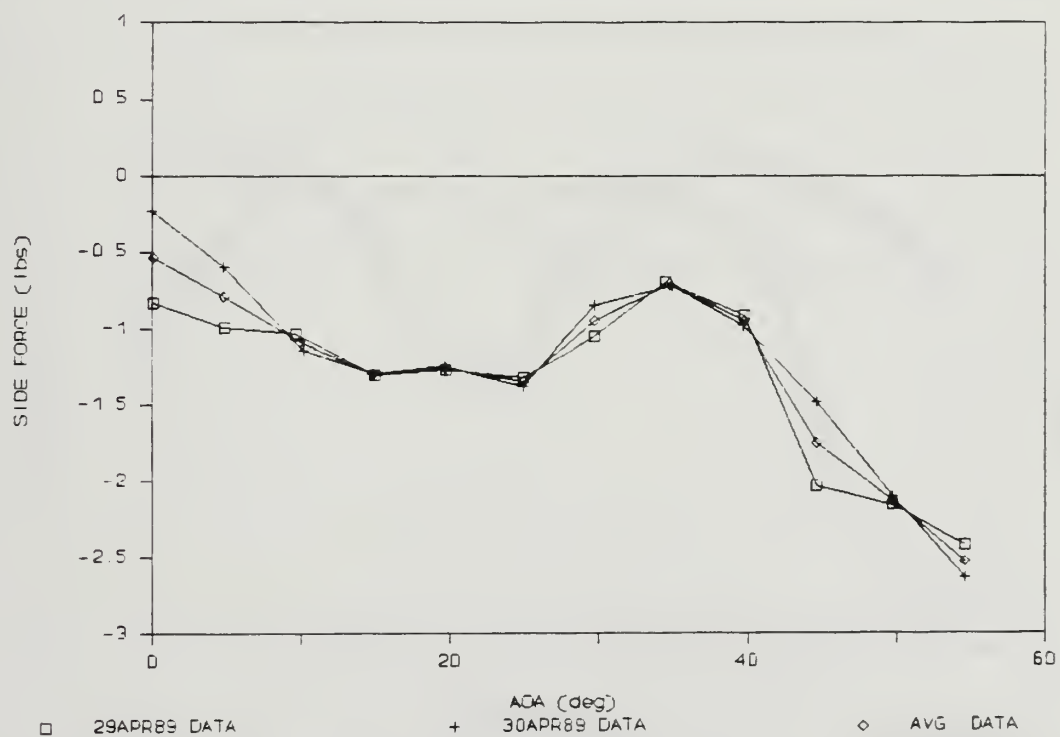
Figure 59. Side Force (Fwd: Outboard/Long, Aft Nozzle/Short)
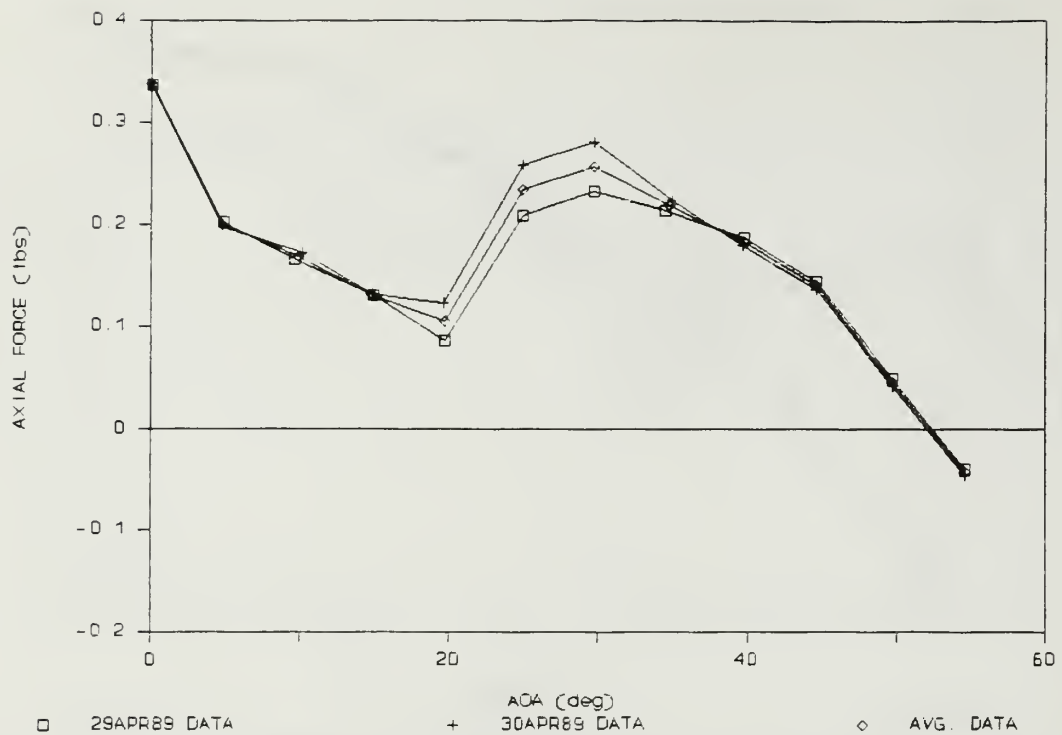
Figure 60. Axial Force (Fwd: Outboard/Long, Aft: Nozzle/Short)
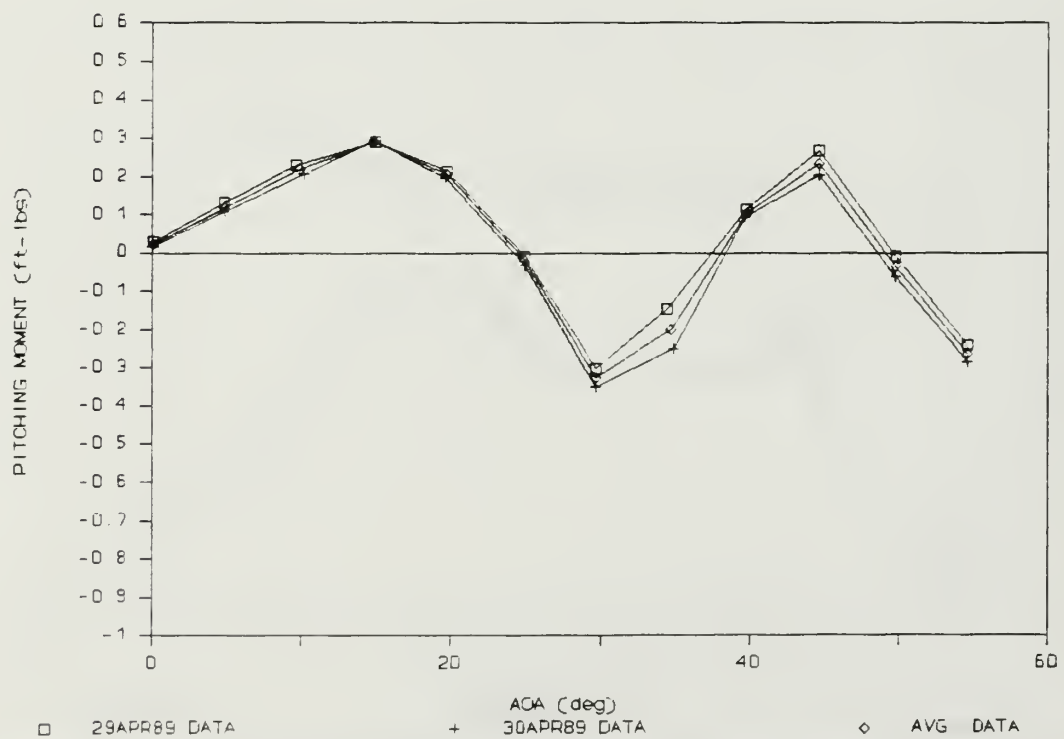
Figure 61. Pitching Moment (Fwd: Outboard/Long, Aft: Nozzle/Short)
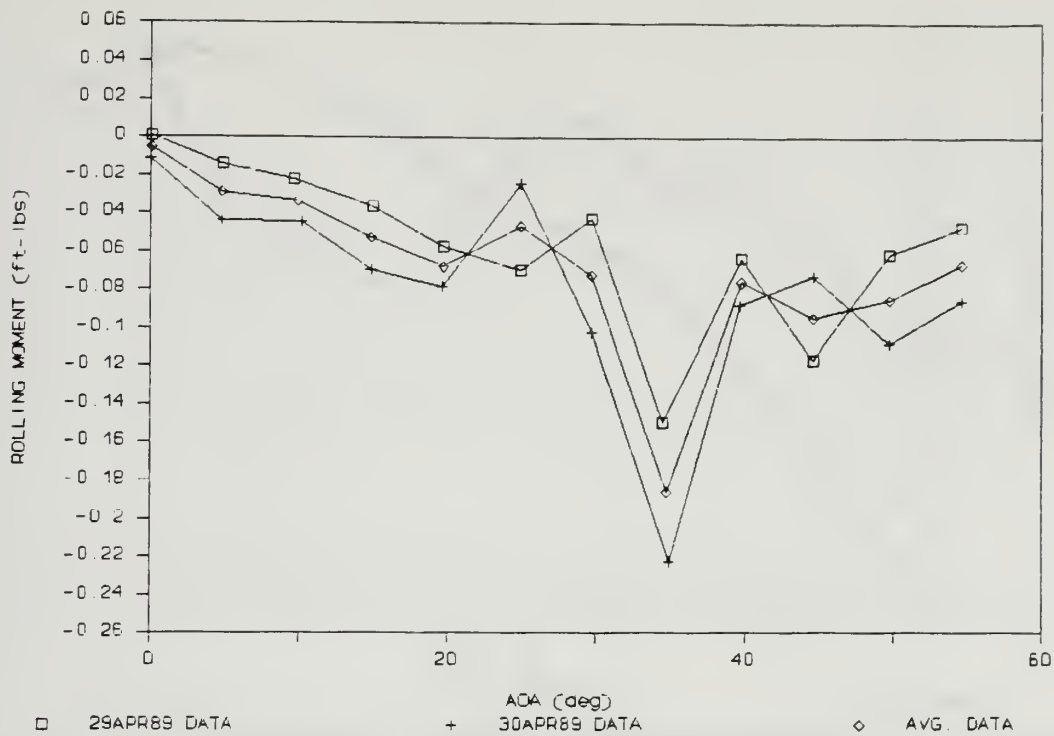
Figure 62. Rolling Moment (Fwd: Outboard/Long, Aft: Nozzle/Short)
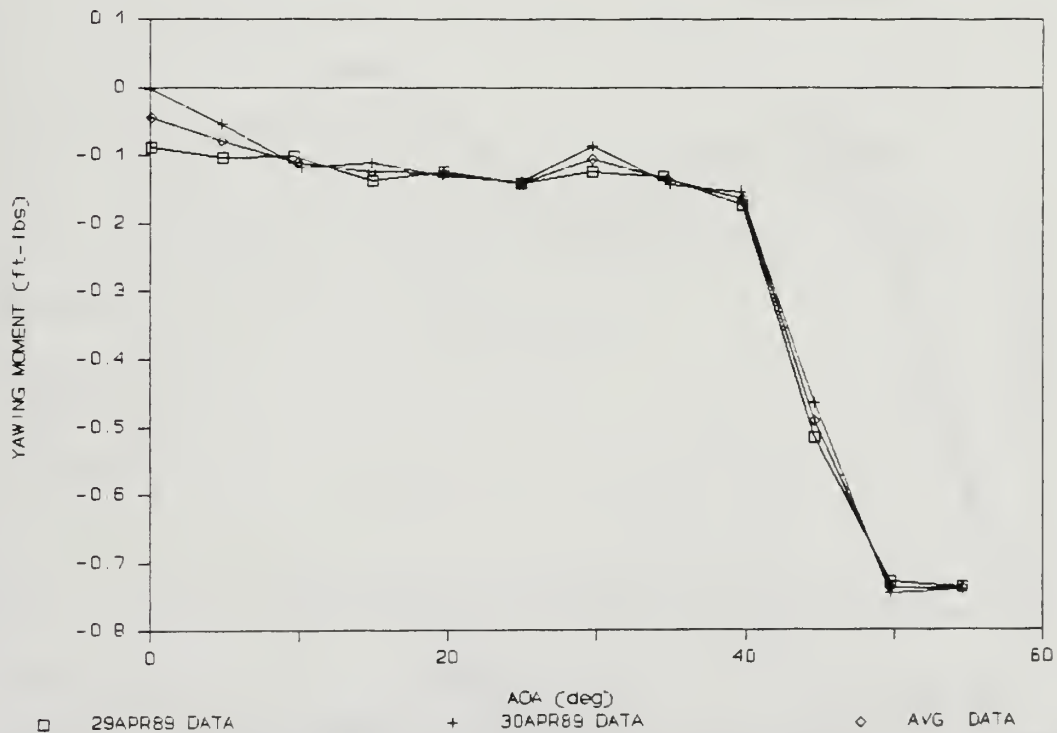
Figure 63. Yawing Moment (Fwd: Outboard/Long, Aft: Nozzle/Short)
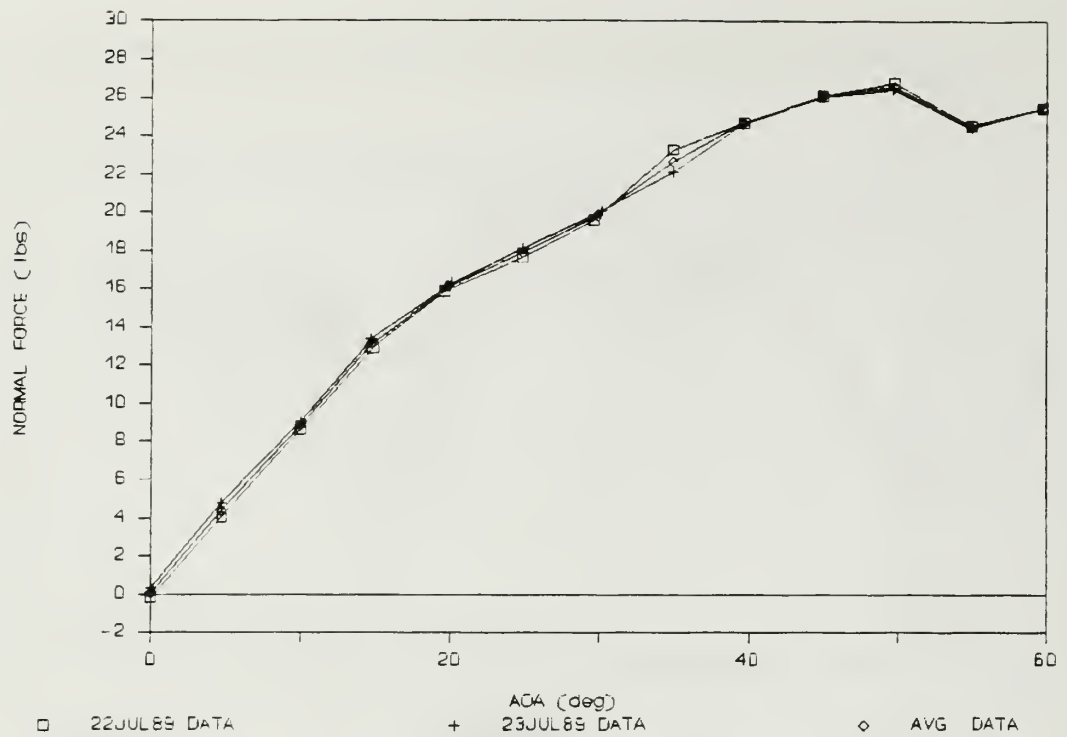
Figure 64. Normal Force (Fwd: Inboard/Medium, Aft: Hook/Long)
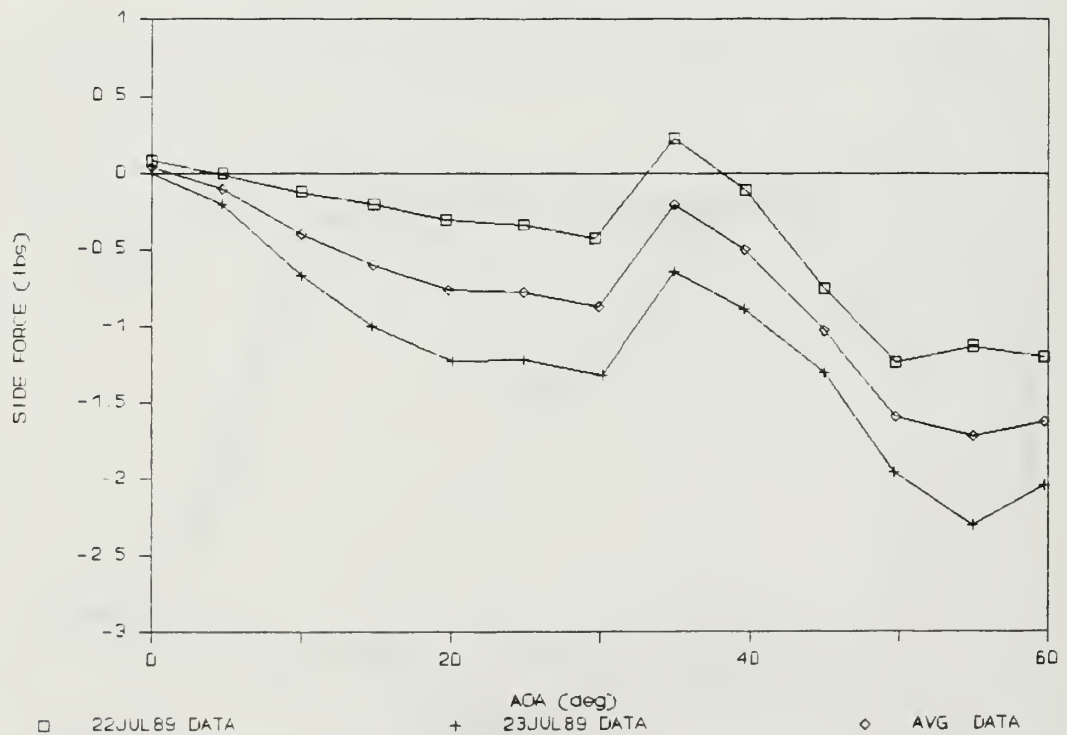
Figure 65. Side Force (Fwd: Inboard/Medium, Aft: Hook/Long)
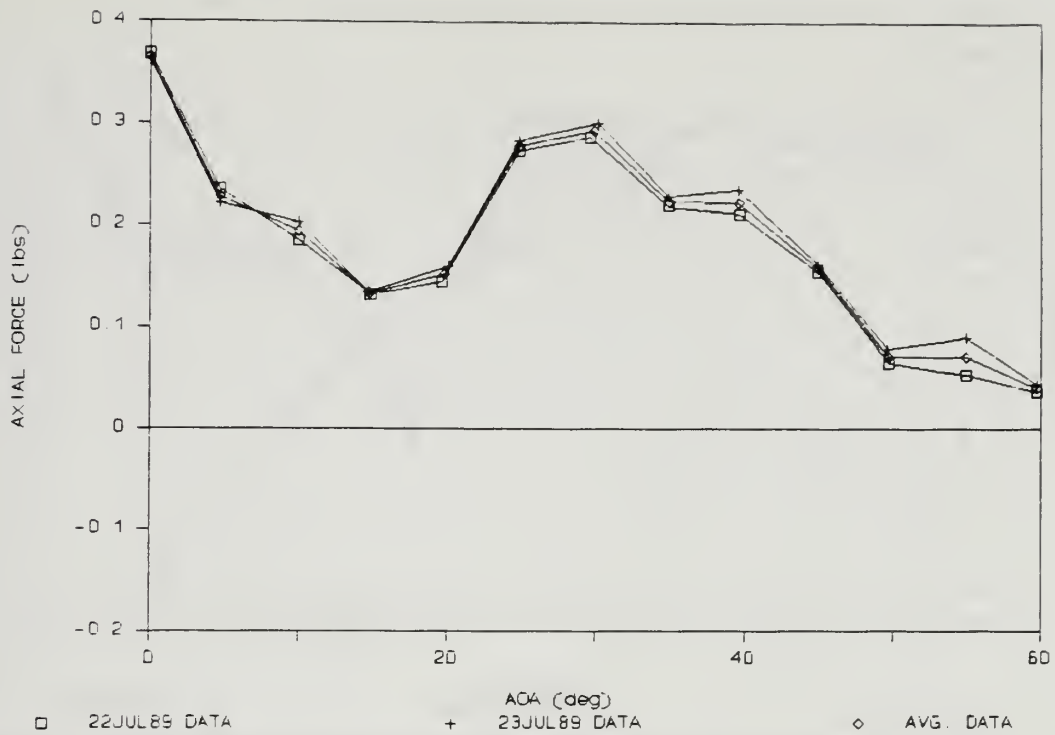
Figure 66. Axial Force (Fwd: Inboard/Medium, Aft: Hook/Long)
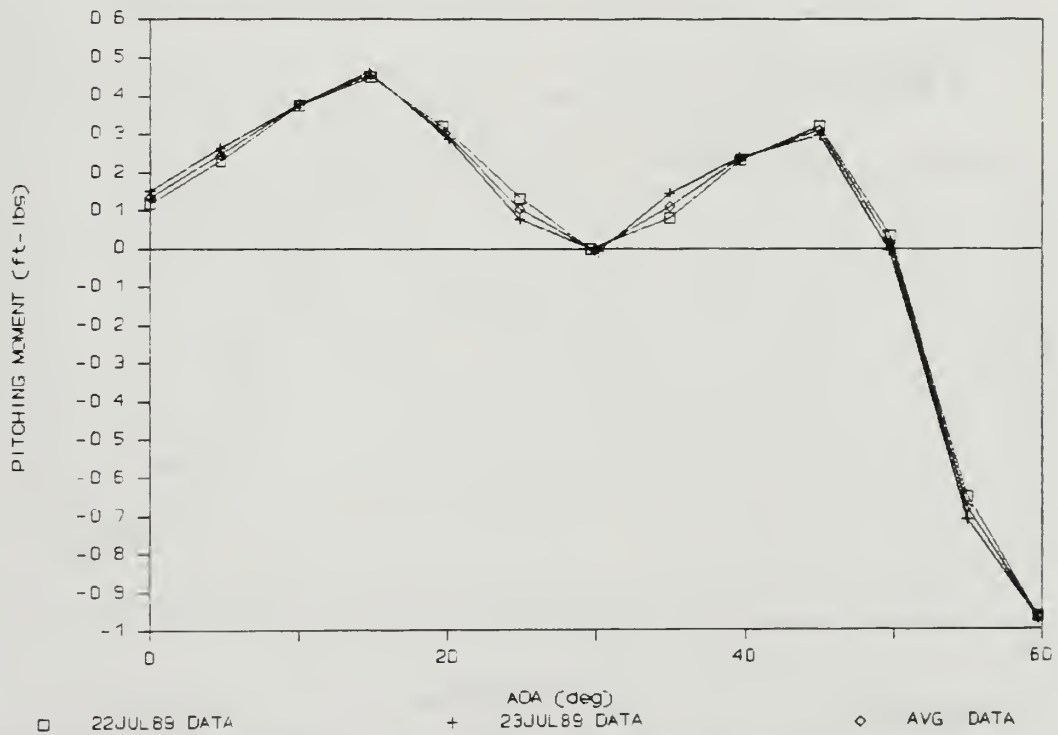
Figure 67. Pitching Moment (Fwd: Inboard/Medium, Aft: Hook/Long)
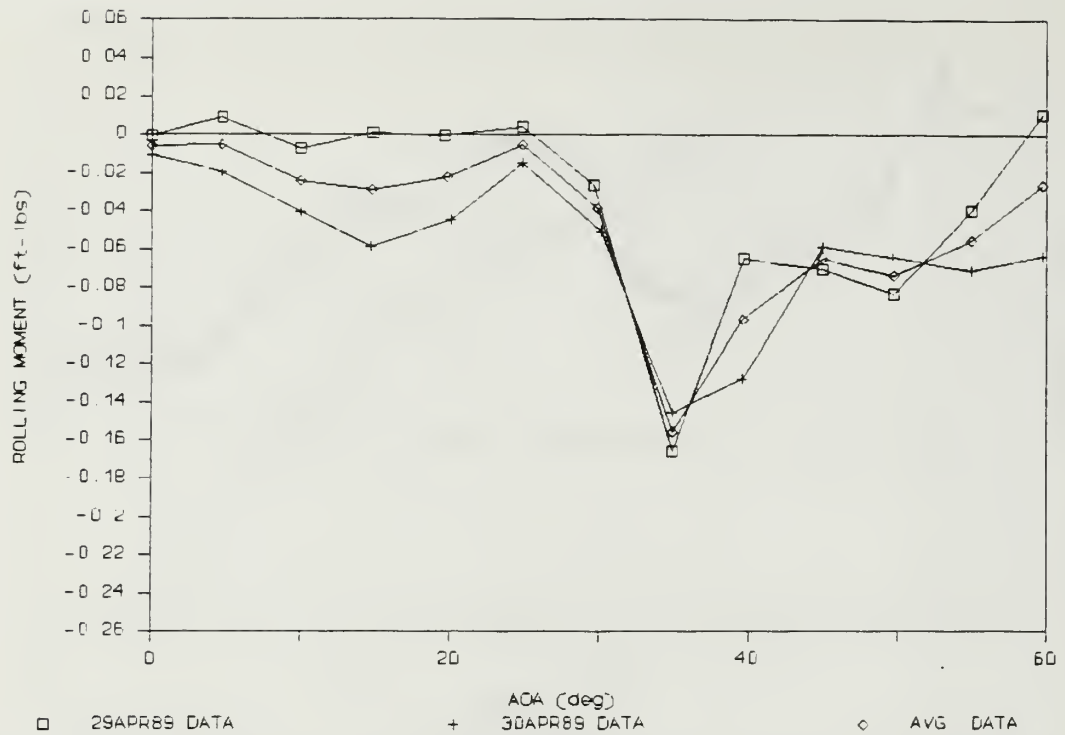
Figure 68. Rolling Moment (Fwd: Inboard/Medium, Aft: Hook/Long)
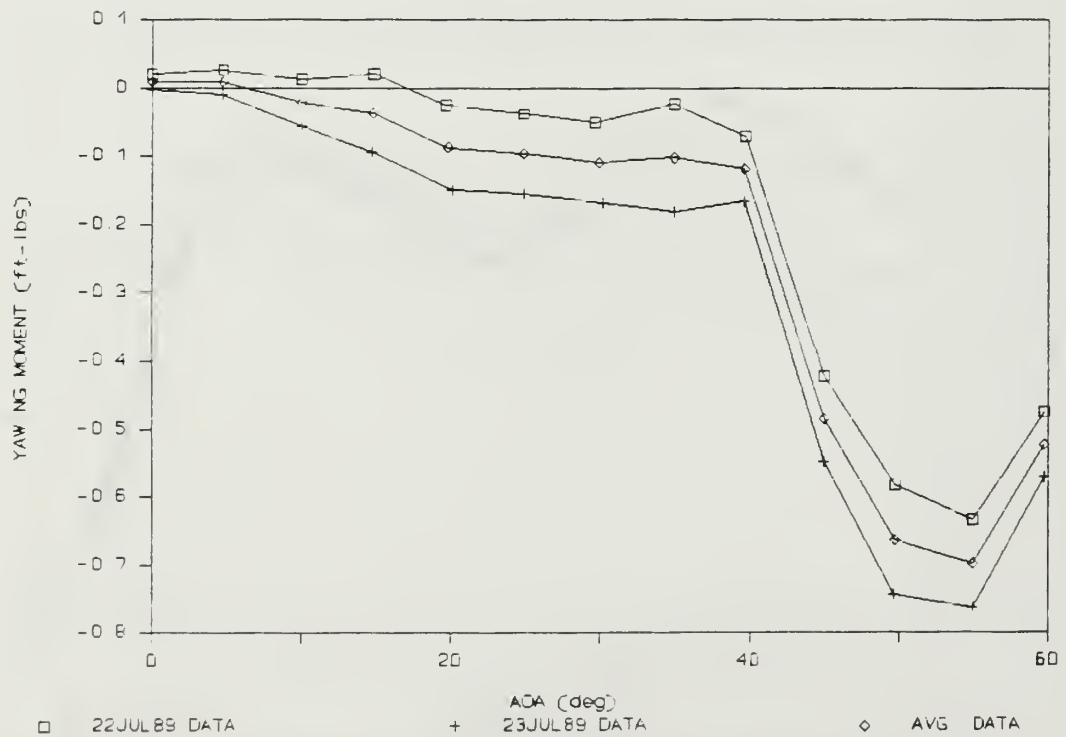
Figure 69. Yawing Moment (Fwd: Inboard/Medium, Aft: Hook/Long)
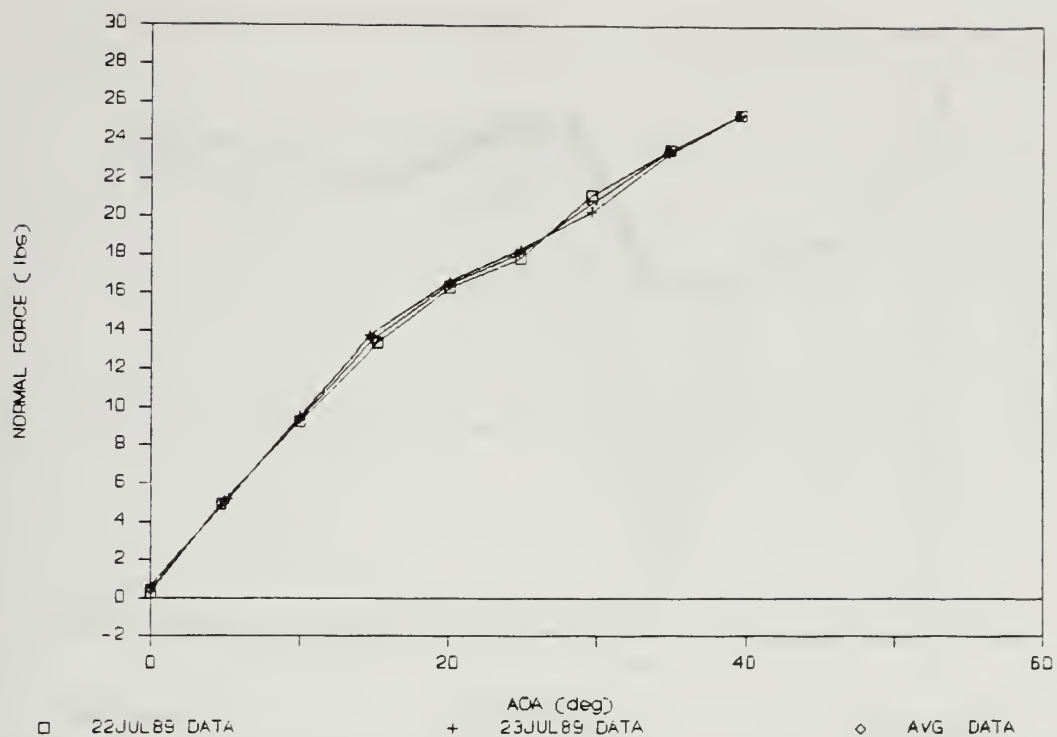
Figure 70. Normal Force (Fwd: Inboard/Medium, Aft: Nozzle/Long)
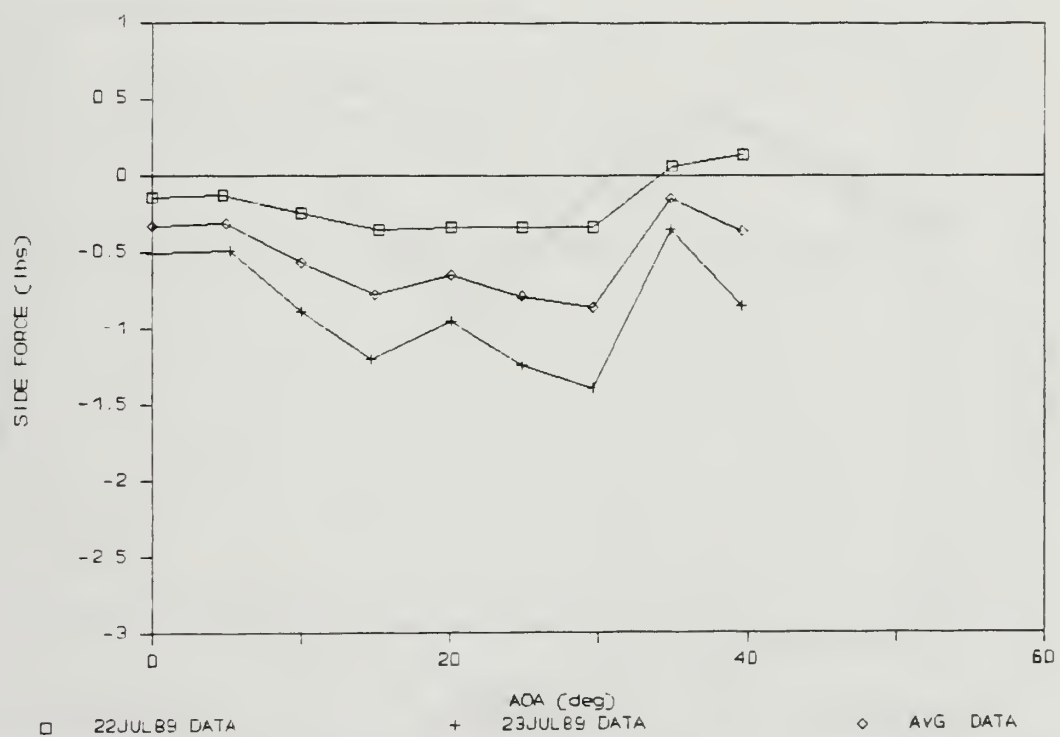
Figure 71. Side Force (Fwd: Inboard/Medium, Aft: Nozzle/Long)
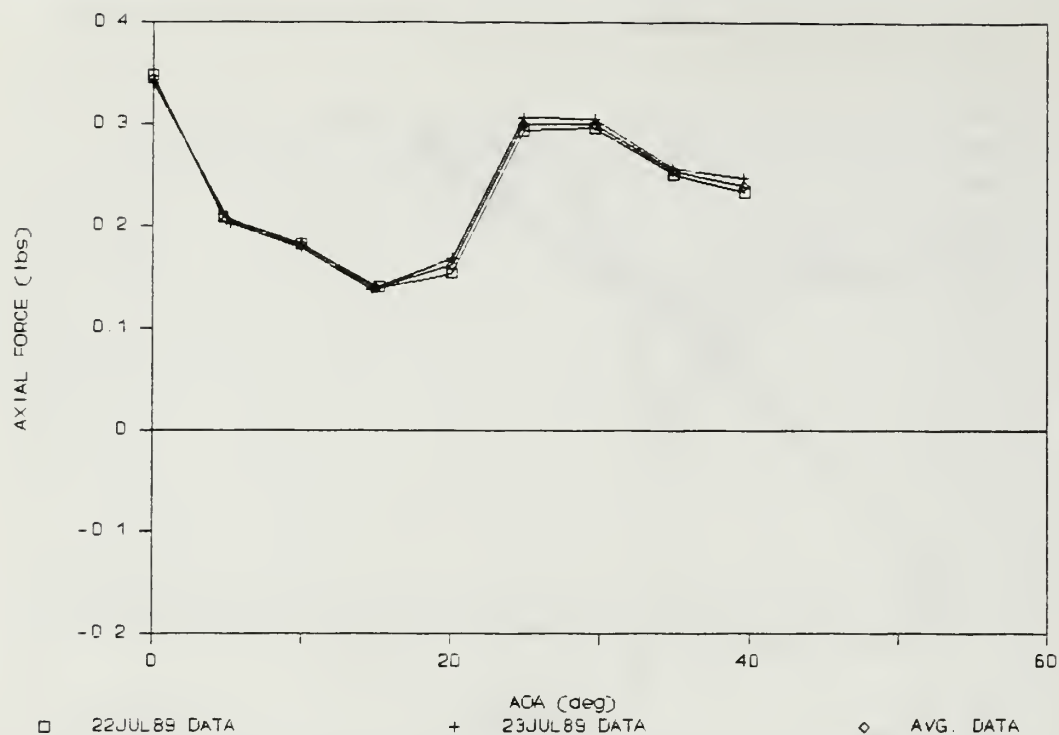
Figure 72. Axial Force (Fwd: Inboard/Medium, Aft: Nozzle/Long)
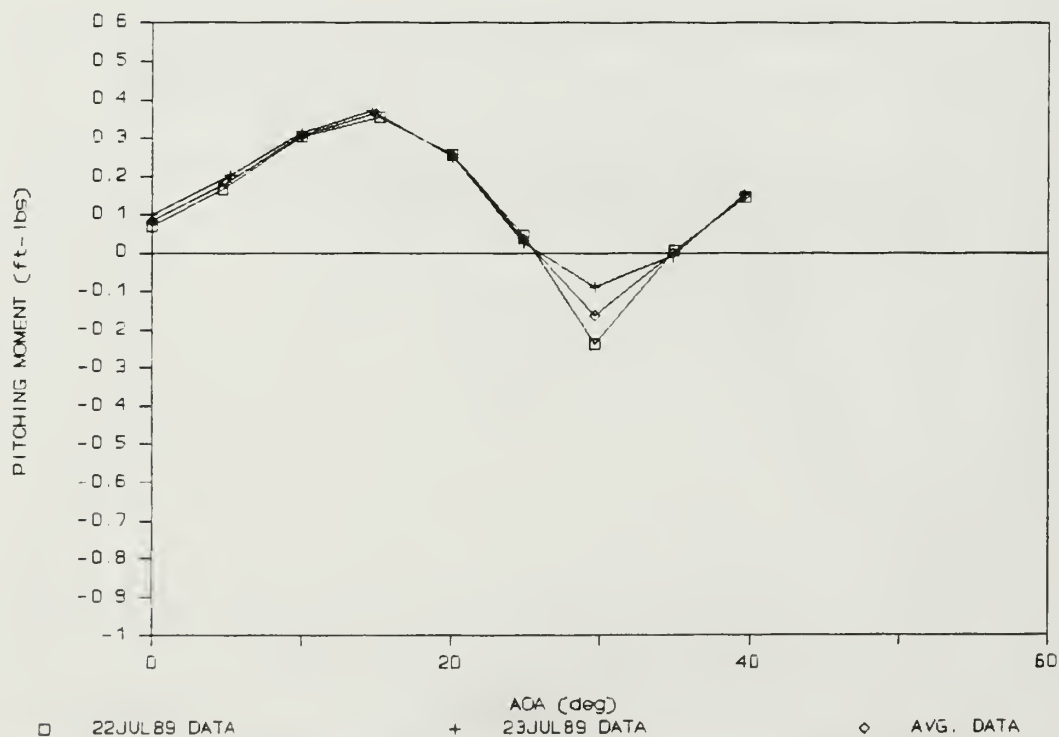
Figure 73. Pitching Moment (Fwd: Inboard/Medium, Aft: Nozzle/Long)
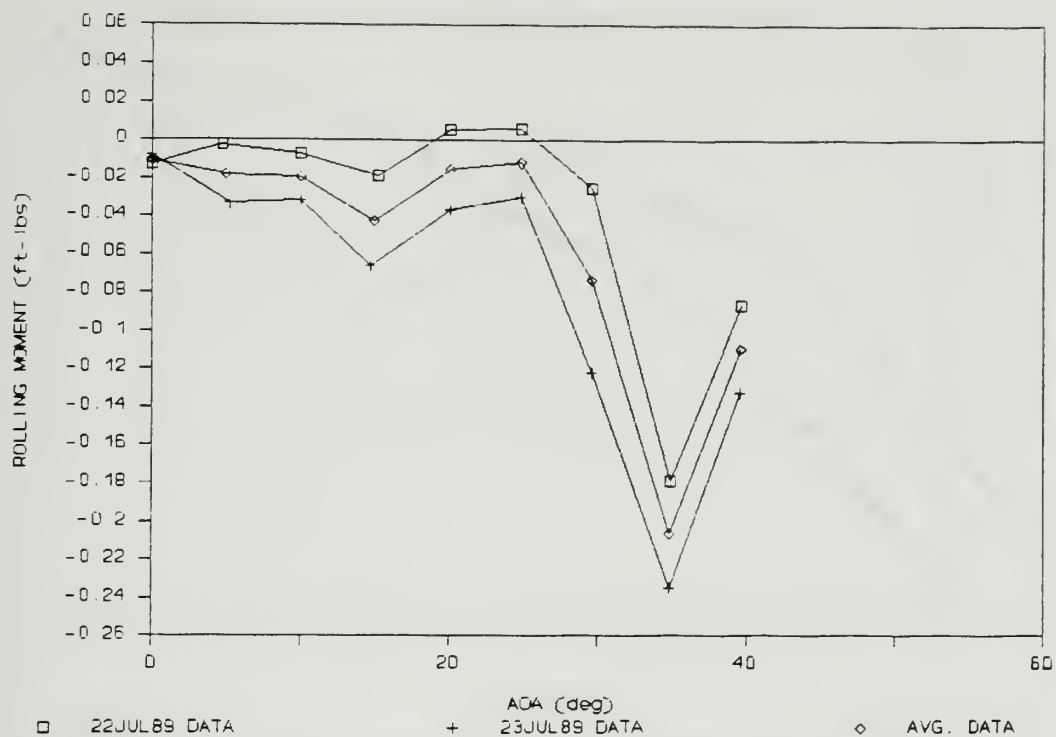
Figure 74. Rolling Moment (Fwd: Inboard/Medium, Aft: Nozzle/Long)
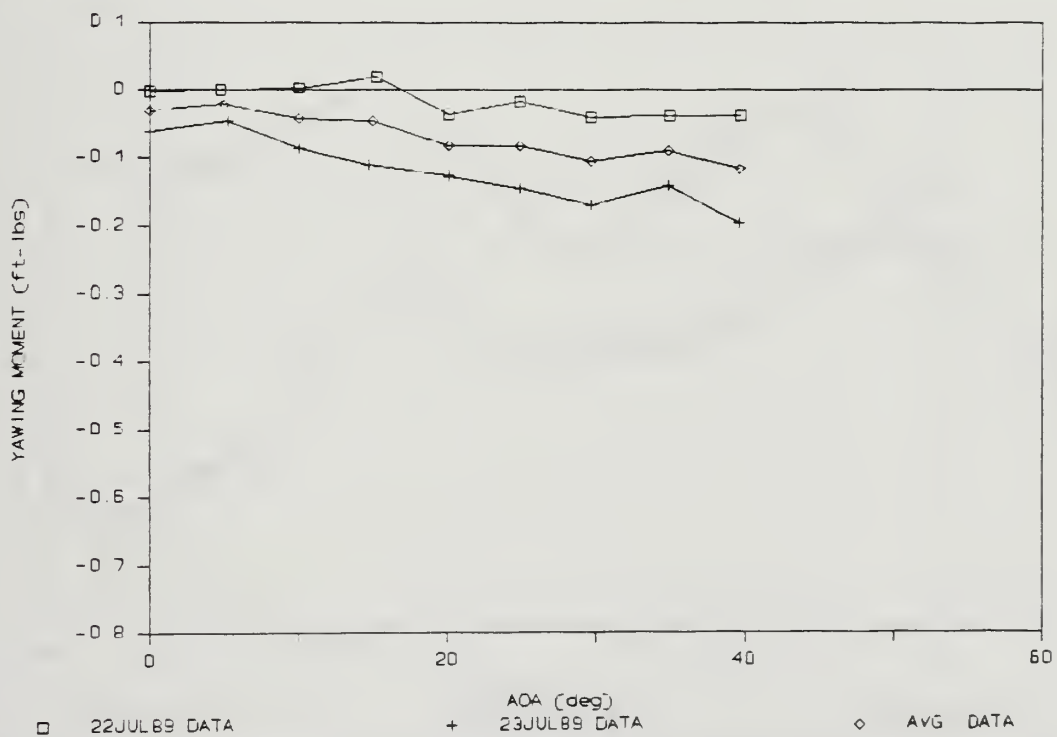
Figure 75. Yawing Moment (Fwd: Inboard/Medium, Aft: Nozzle/Long)
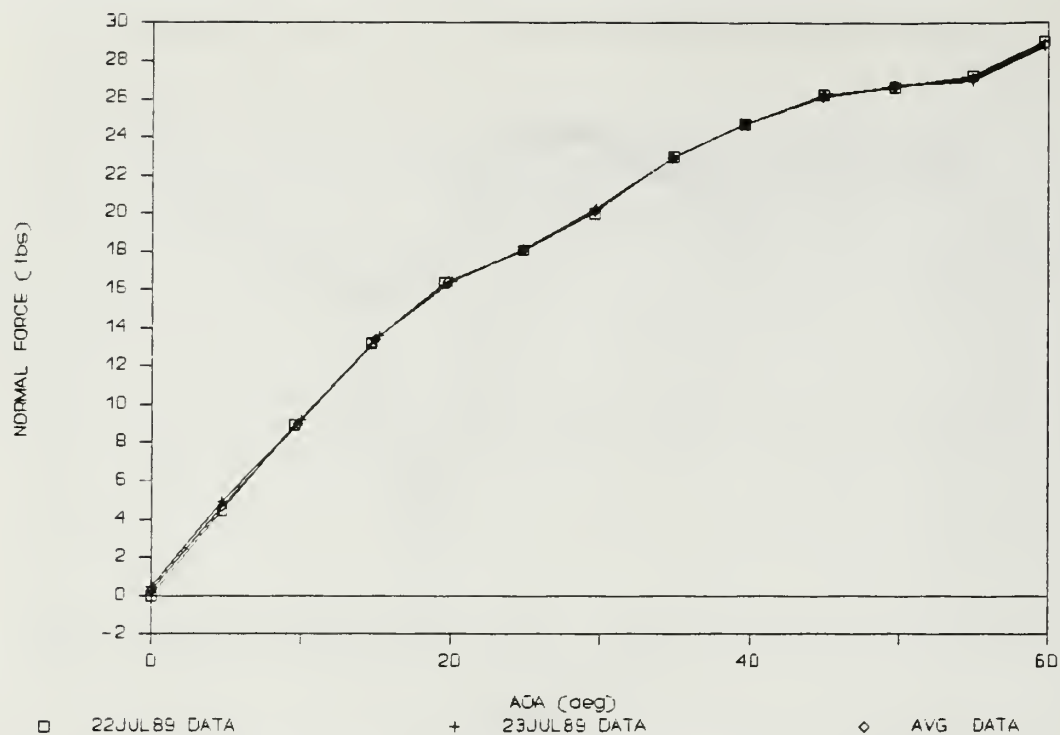
Figure 76. Normal Force (Fwd: Middle/Medium, Aft: Hook/Long)
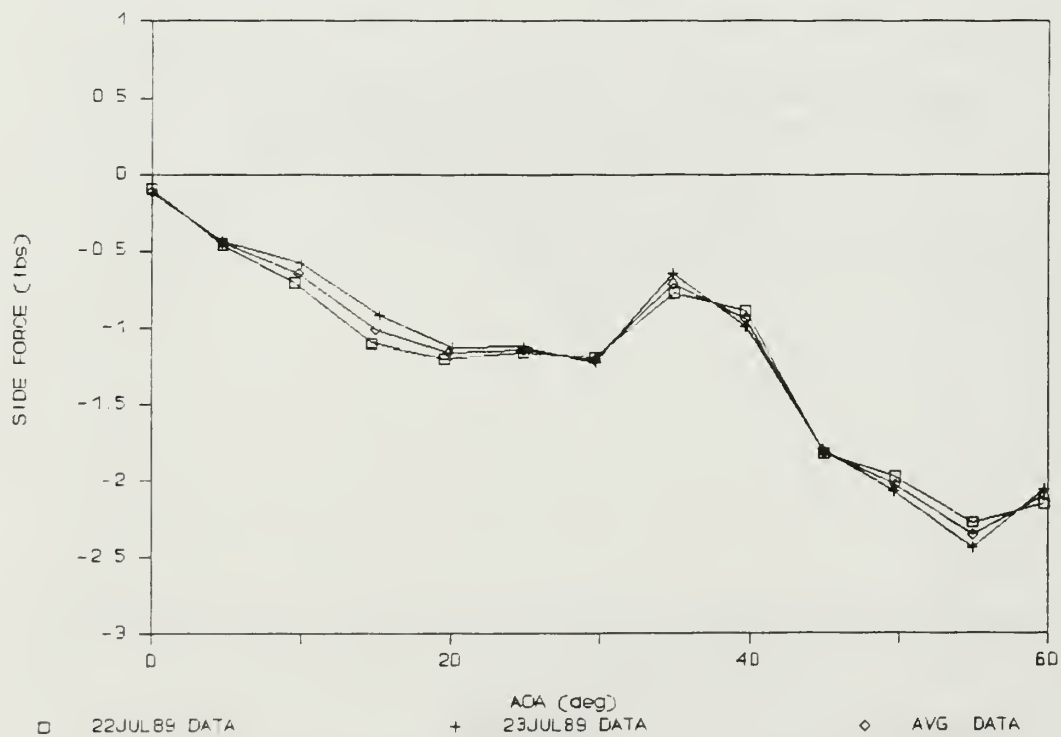
Figure 77. Side Force (Fwd: Middle/Medium, Aft: Hook/Long)
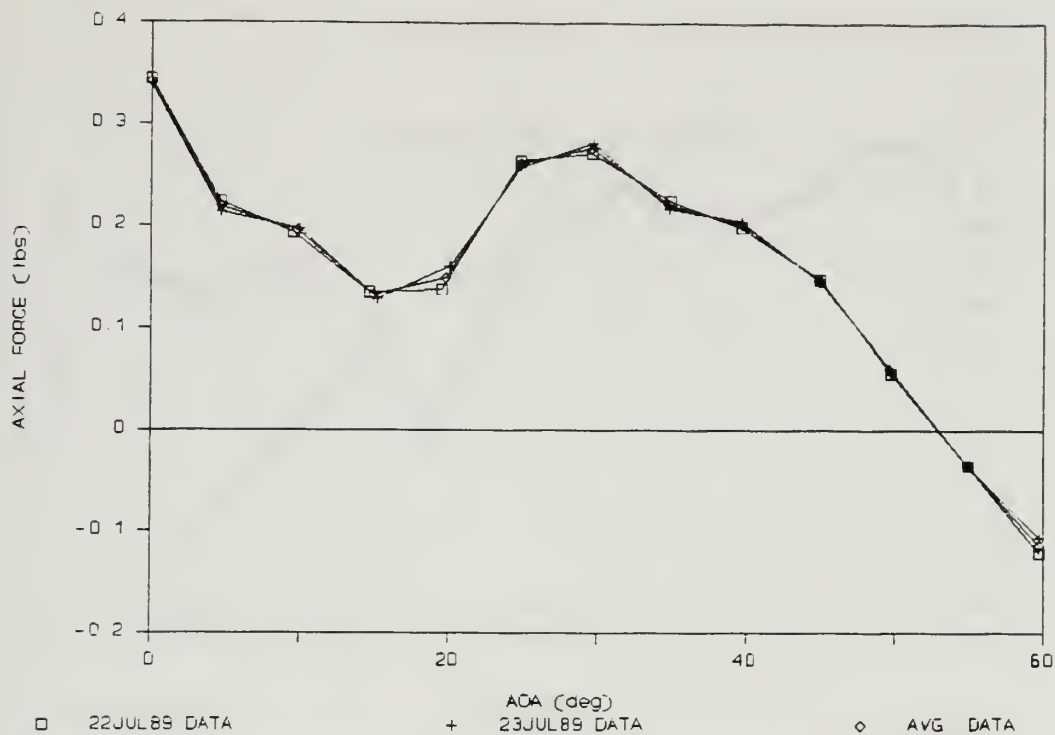
Figure 78. Axial Force (Fwd: Middle/Medium. Aft: Hook/Long)
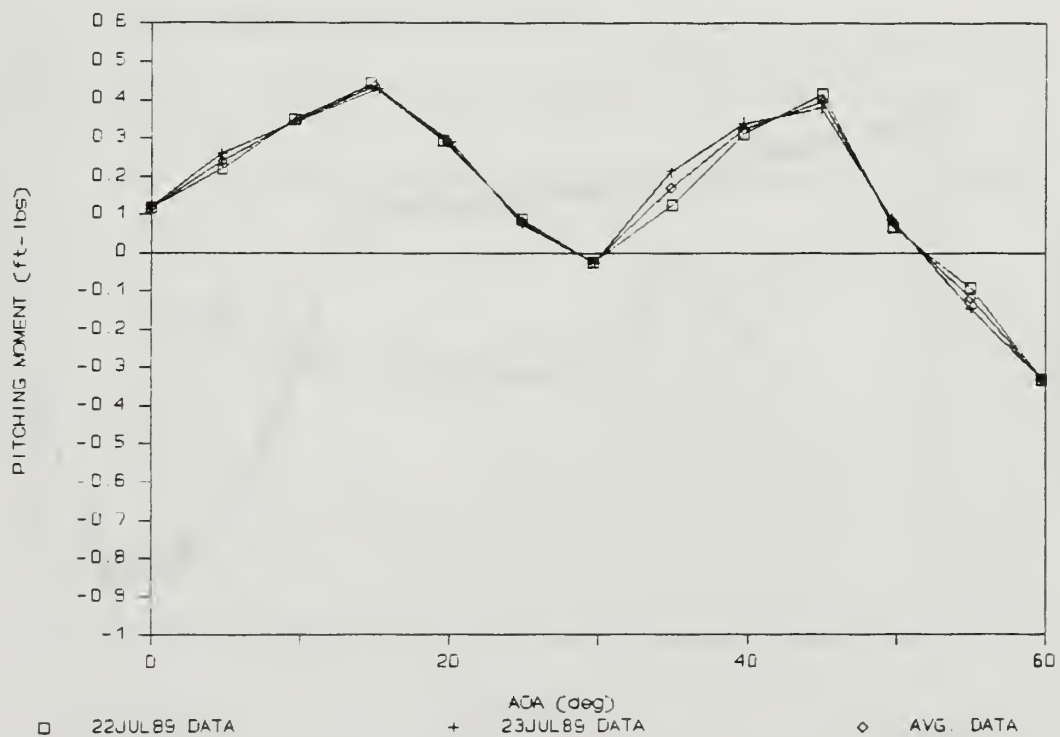
Figure 79. Pitching Moment (Fwd: Middle/Medium, Aft: Hook/Long)

95
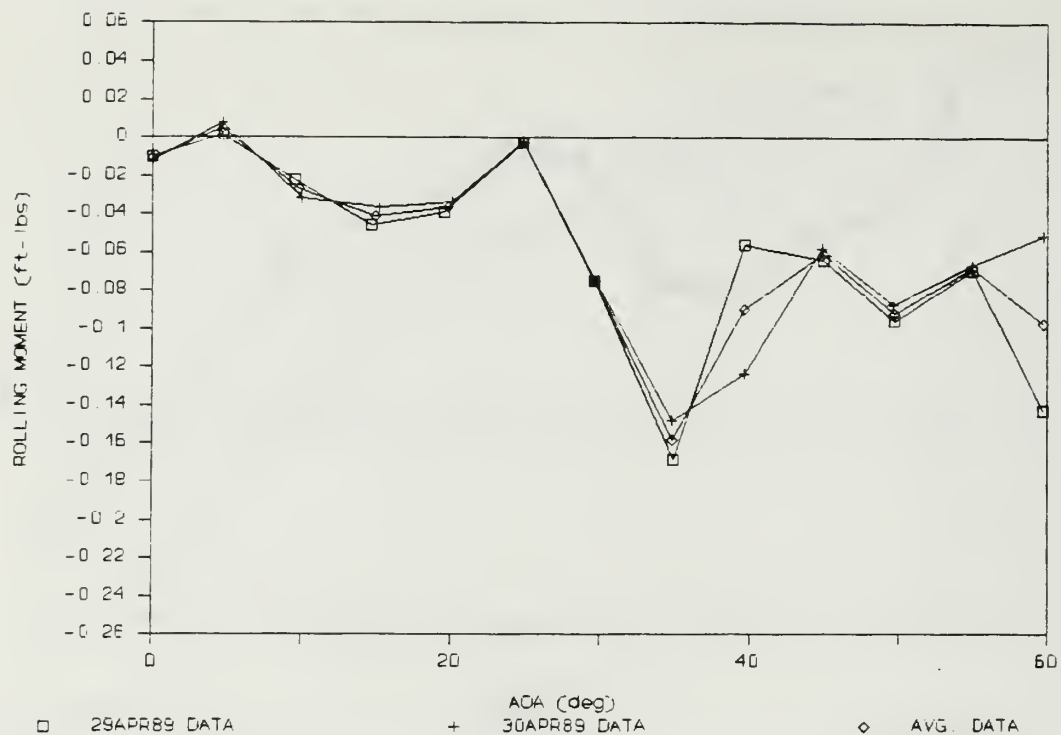
Figure 80. Rolling Moment (Fwd: Middle/Medium, Aft: Hook/Long)
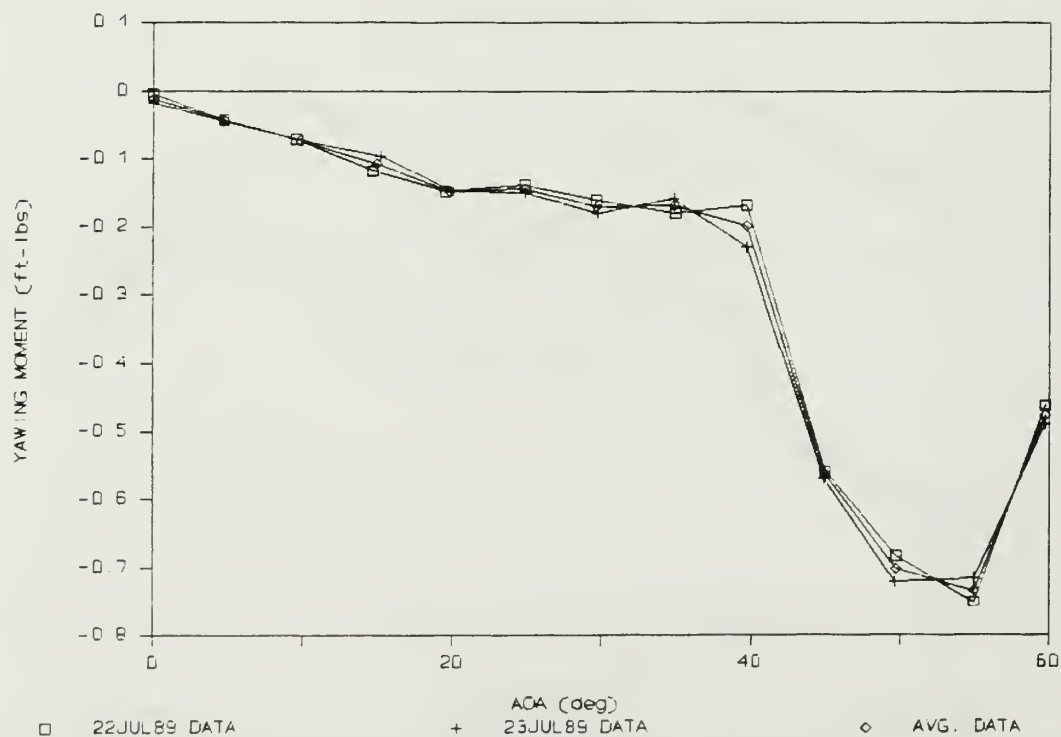
Figure 81. Yawing Moment (Fwd: Middle/Medium, Aft: Hook/Long)
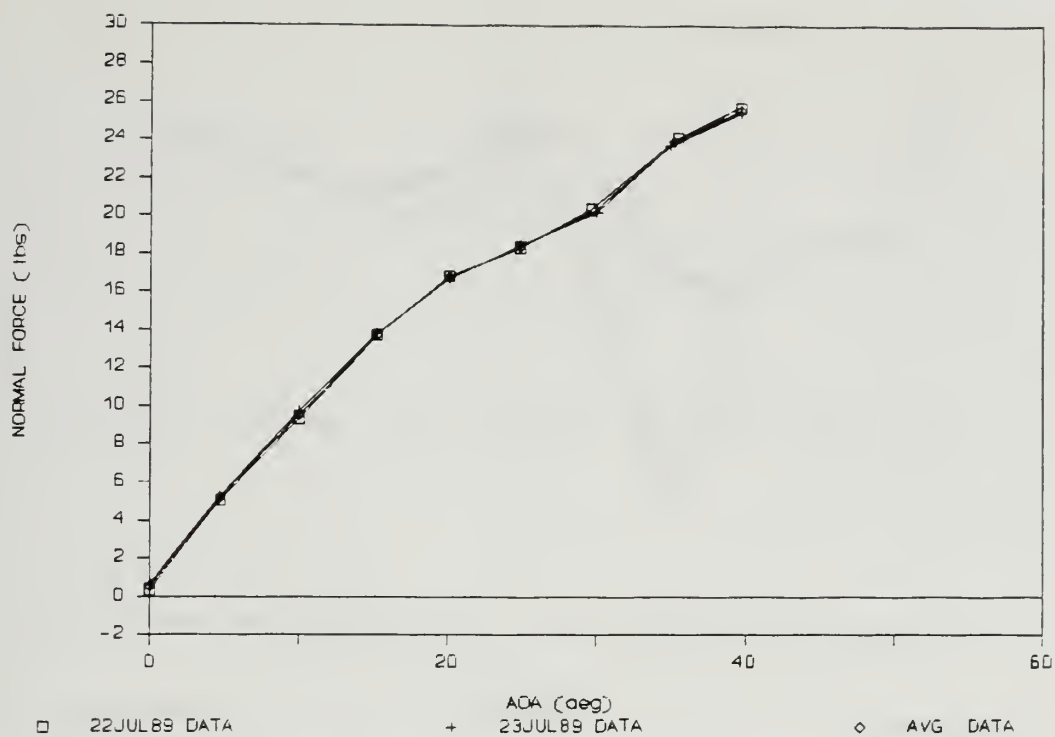
Figure 82. Normal Force (Fwd: Middle/Medium, Aft: Nozzle/Long)
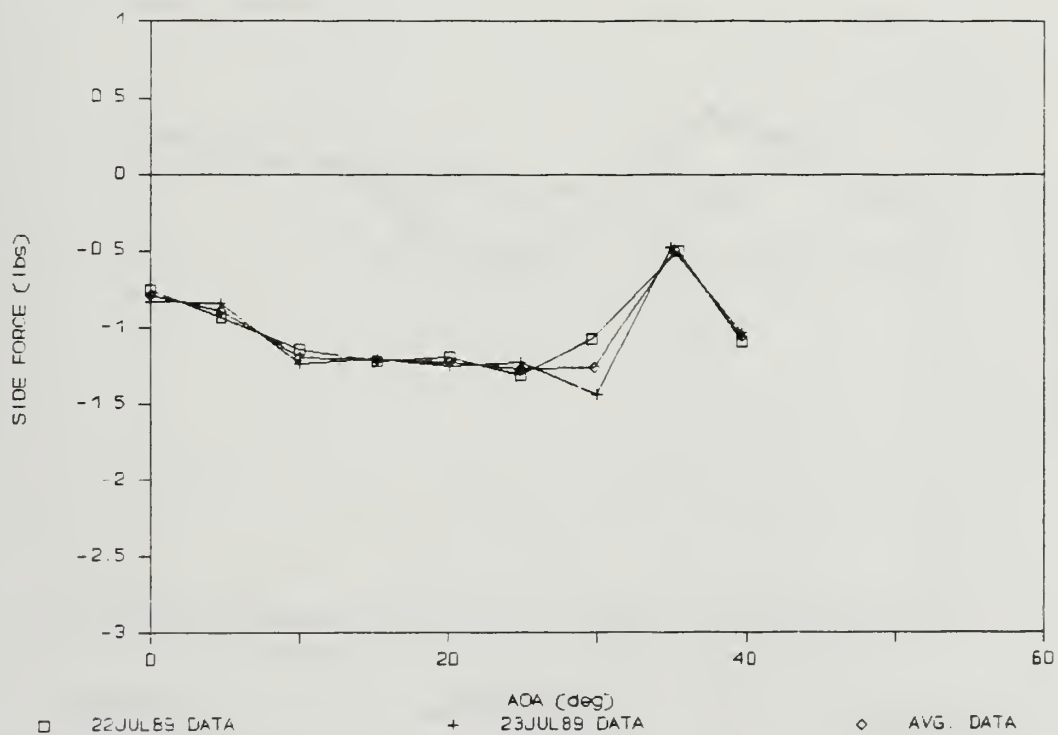
Figure 83. Side Force (Fwd: Middle/Medium, Aft: Nozzle/Long)
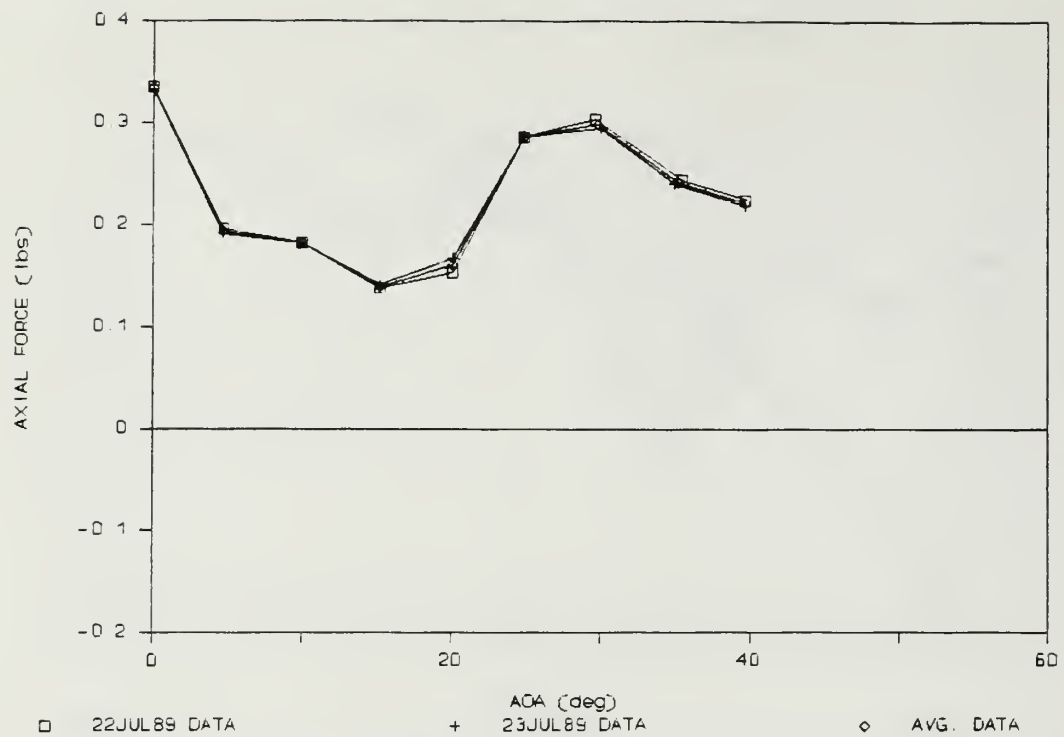
Figure 84. Axial Force (Fwd: Middle/Medium, Aft: Nozzle/Long)
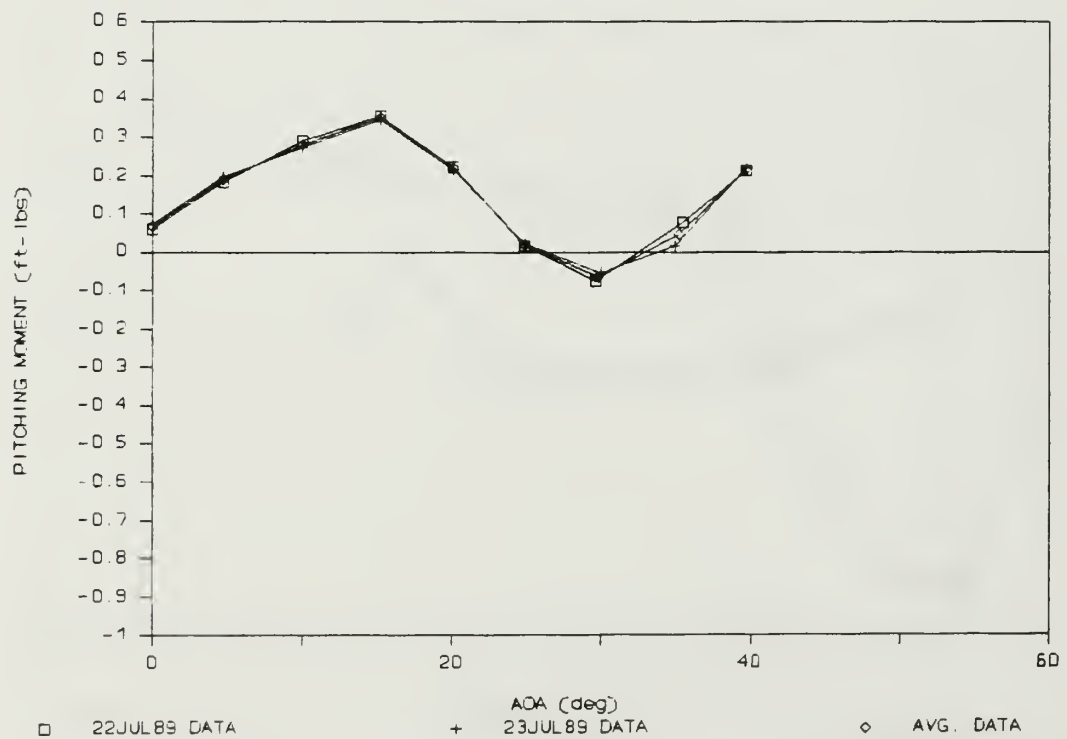
Figure 85. Pitching Moment (Fwd: Middle/Medium, Aft: Nozzle/Long)

98
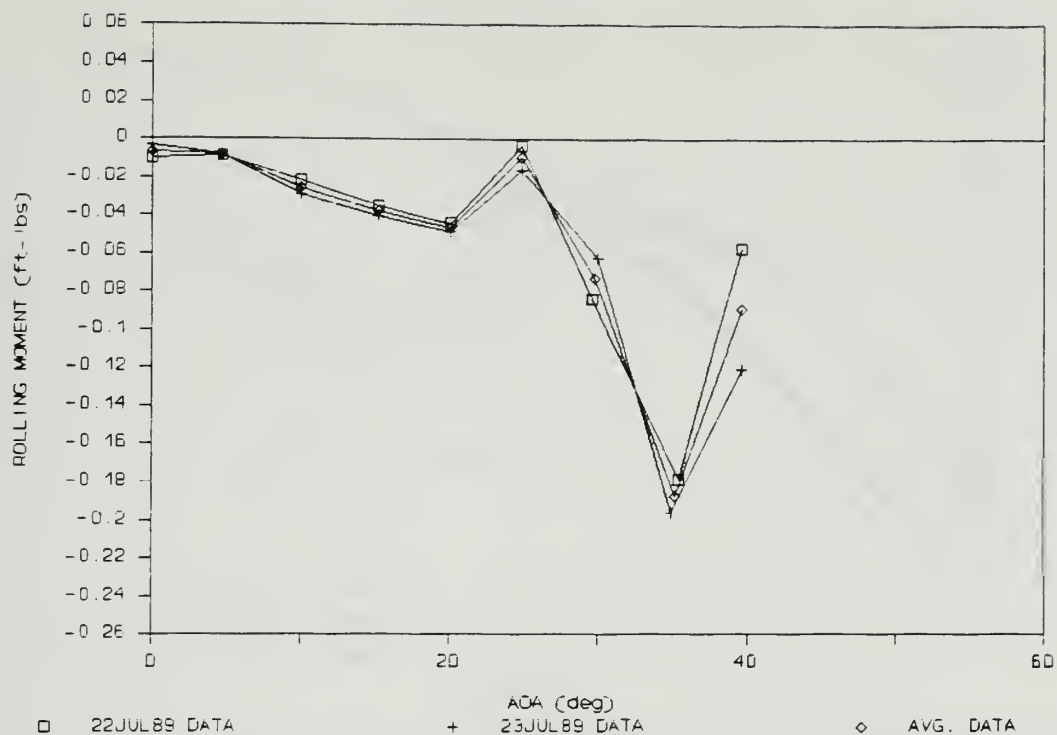
Figure 86. Rolling Moment (Fwd: Middle/Medium, Aft: Nozzle/Long)
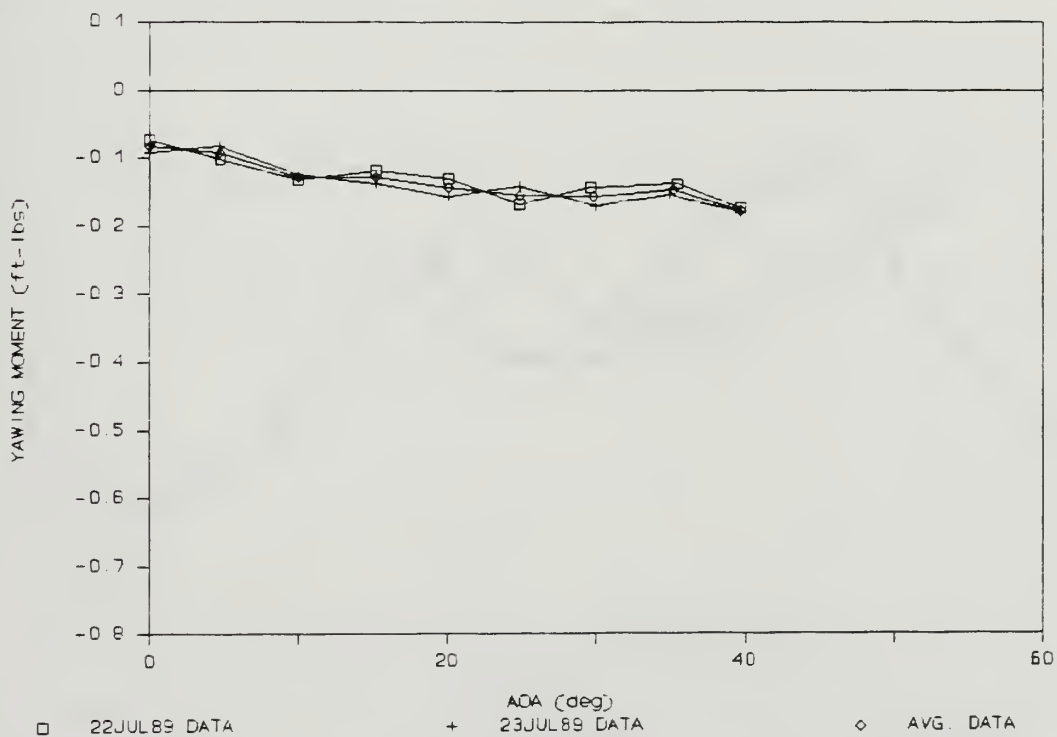
Figure 87. Yawing Moment (Fwd: Middle/Medium, Aft: Nozzle/Long)
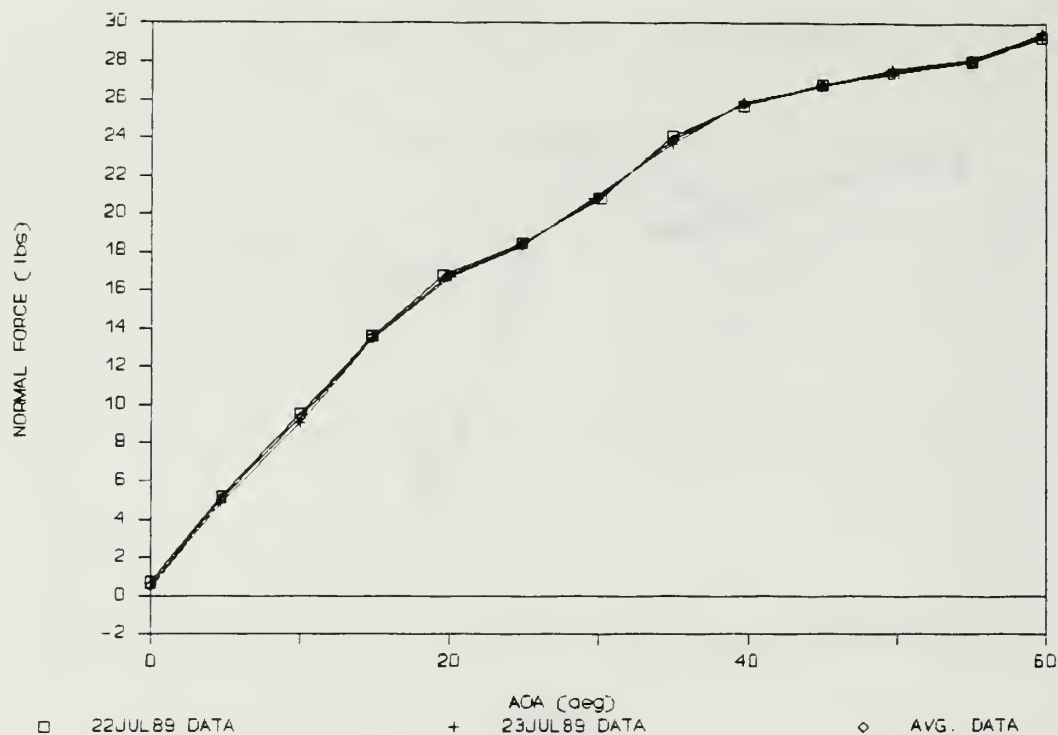
Figure 88. Normal Force (Fwd: Outboard/Medium, Aft: Hook/Long)
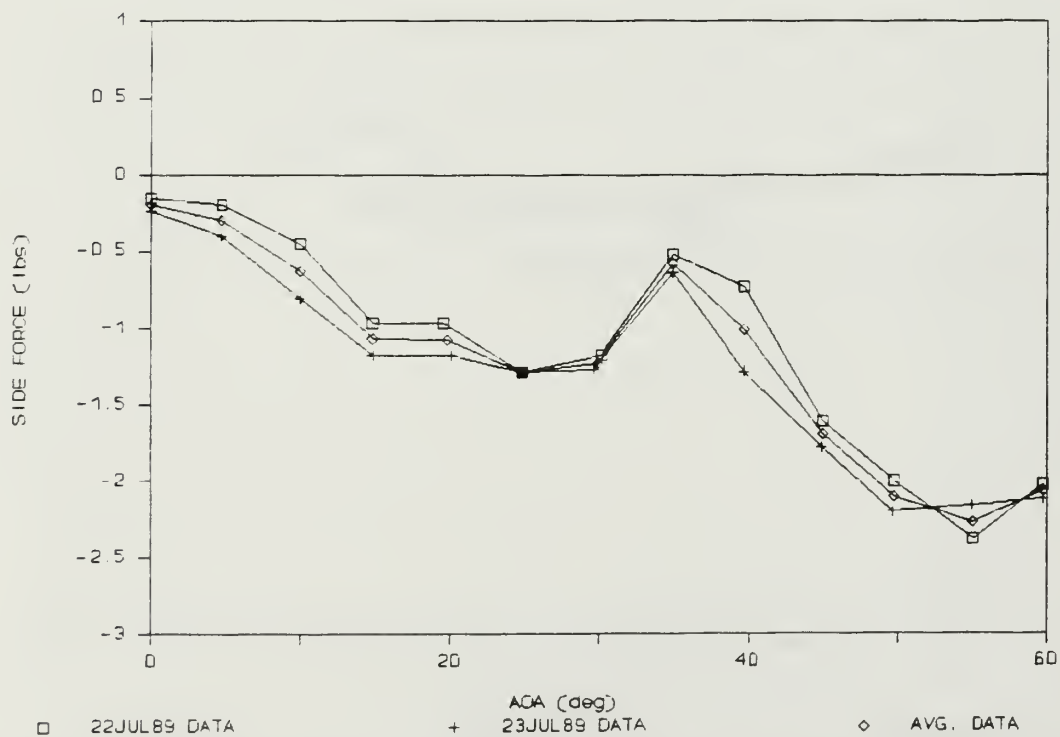
Figure 89. Side Force (Fwd: Outboard/Medium, Aft: Hook/Long)

100
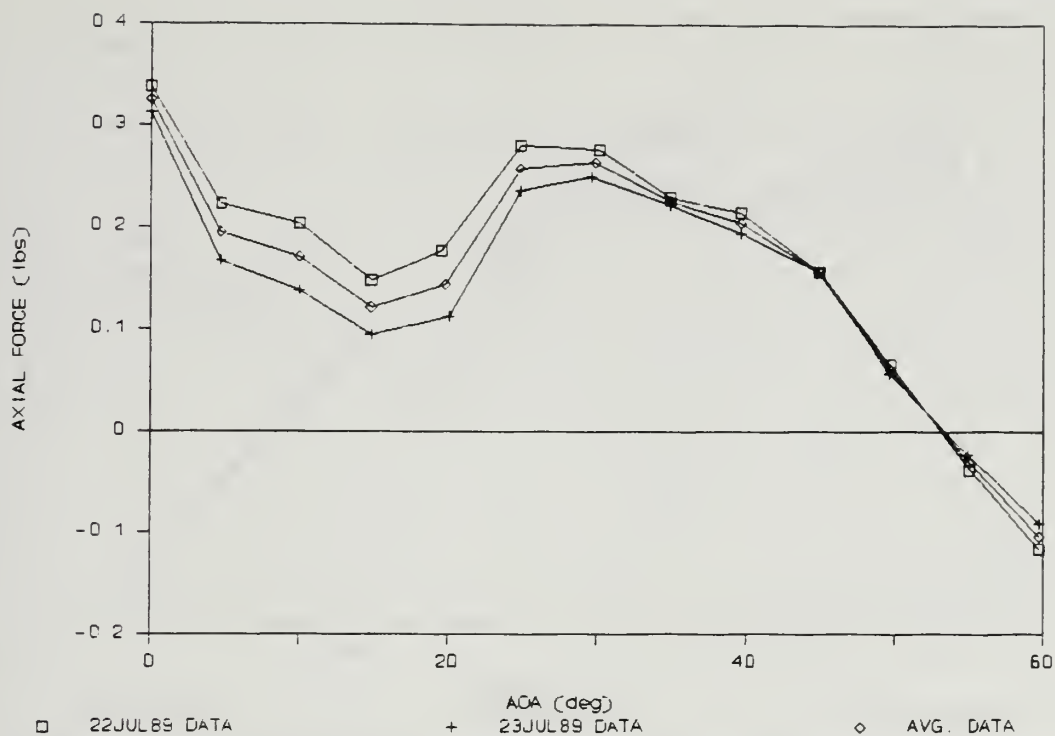
Figure 90. Axial Force (Fwd: Outboard/Medium, Aft: Hook/Long)
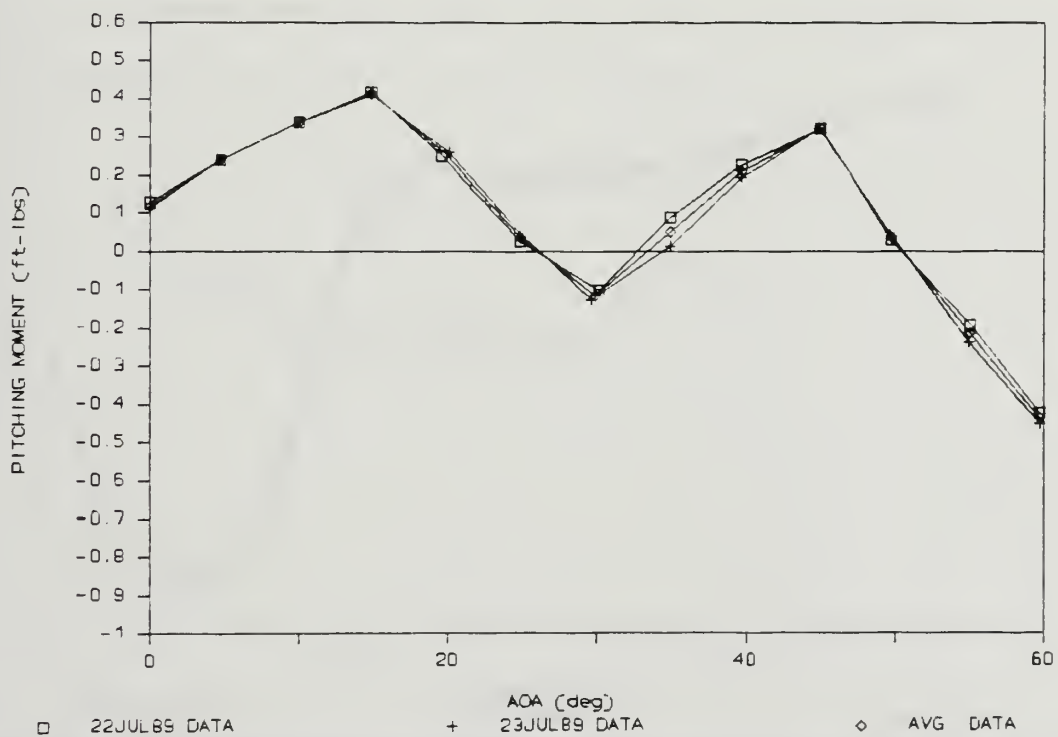
Figure 91. Pitching Moment (Fwd: Outboard/Medium, Aft: Hook/Long)

101
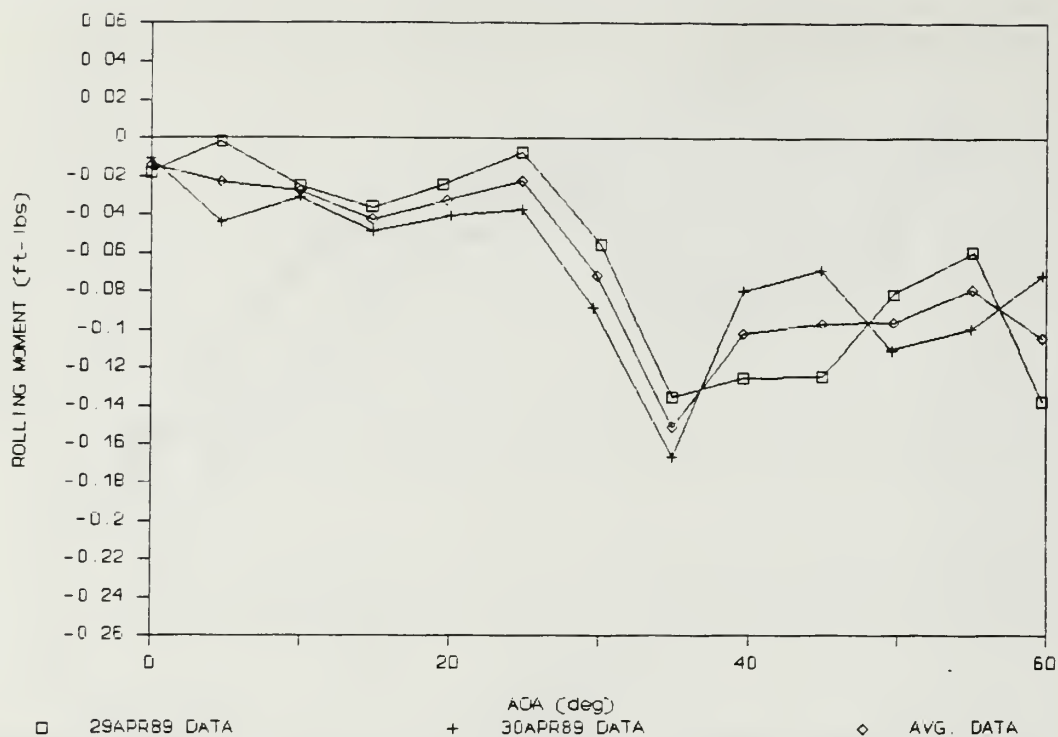
Figure 92. Rolling Moment (Fwd: Outboard/Medium, Aft: Hook/Long)
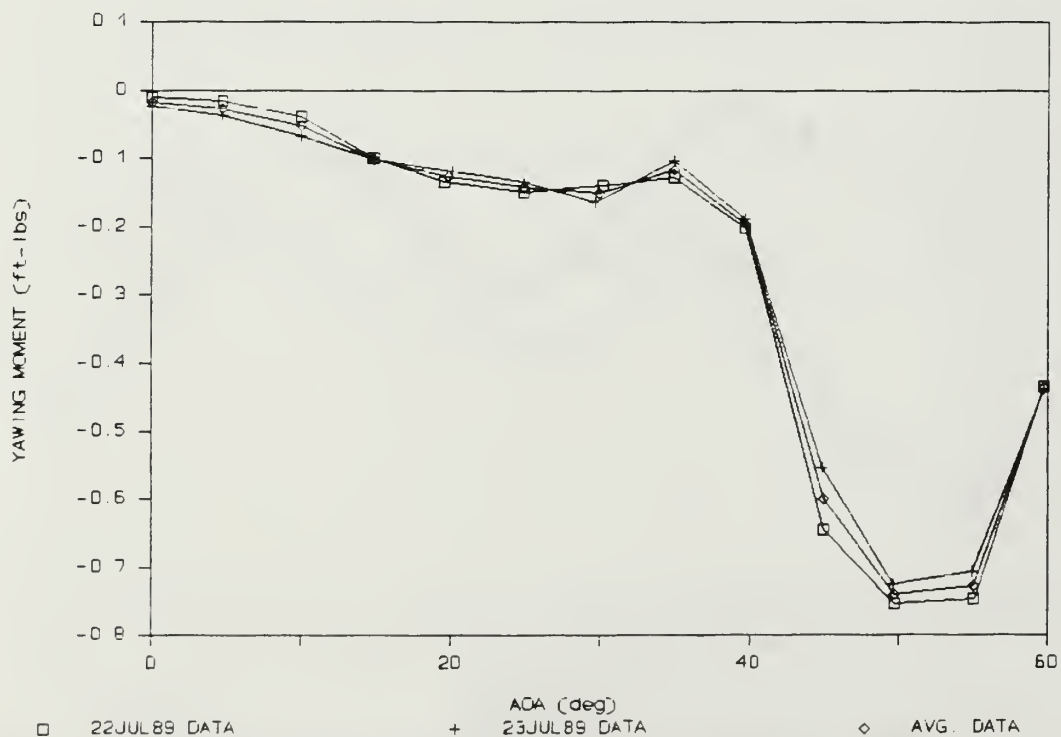
Figure 93. Yawing Moment (Fwd: Outboard/Medium, Aft: Hook/Long)
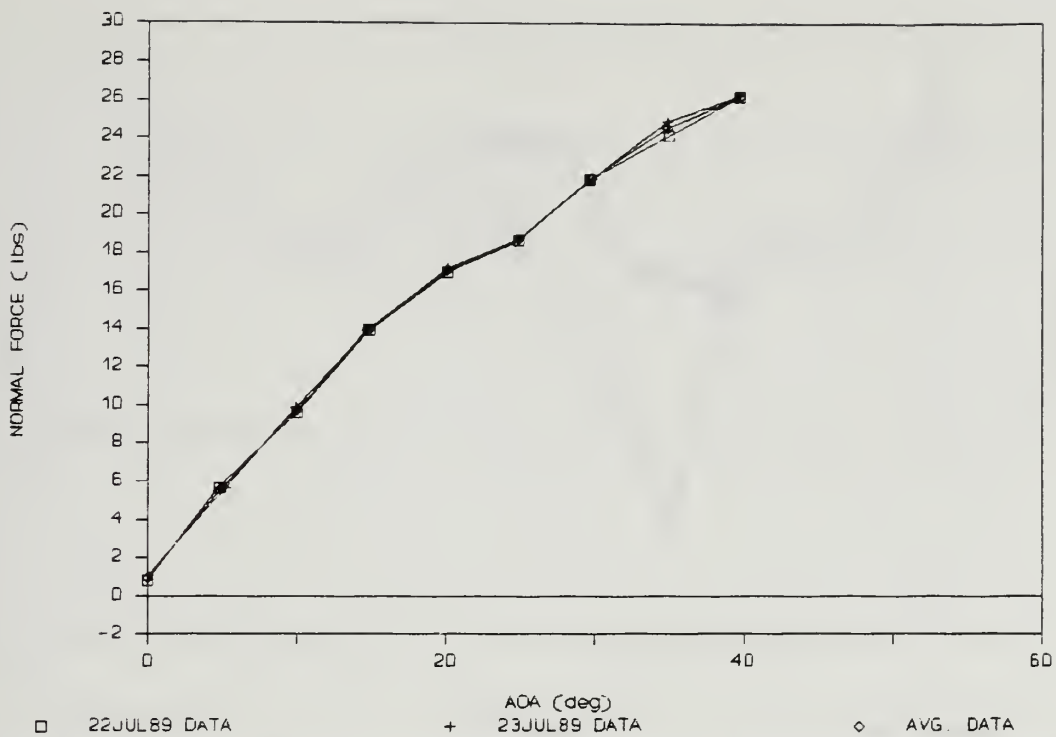
Figure 94. Normal Force (Fwd: Outboard/Medium, Aft: Nozzle/Long)
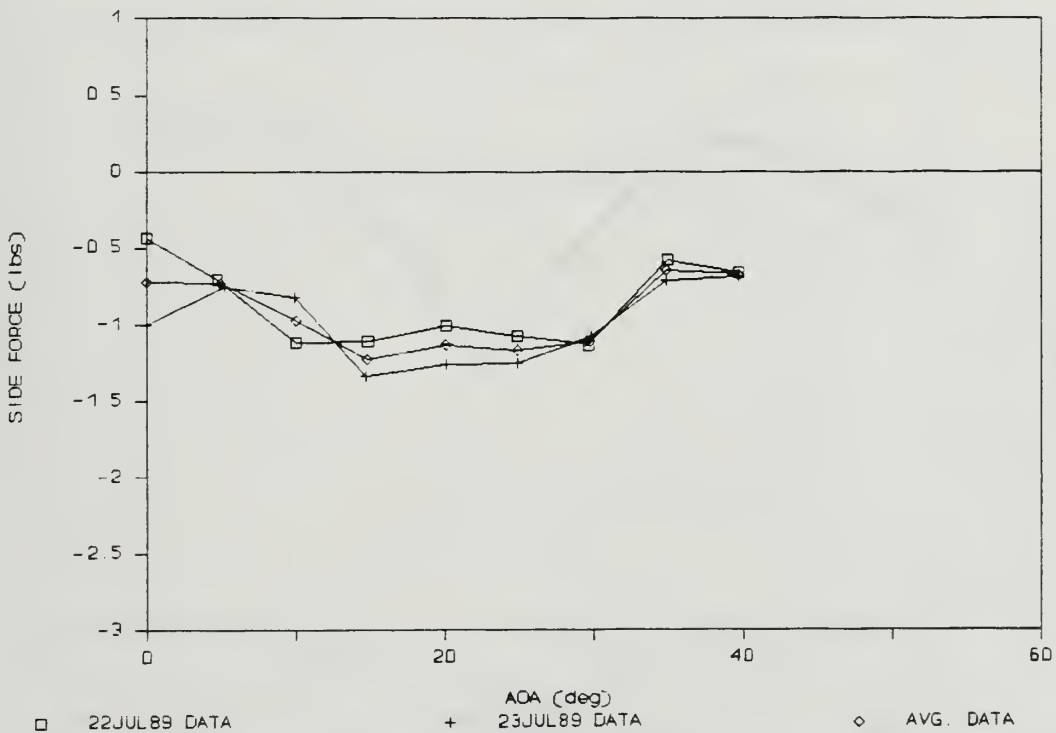
Figure 95. Side Force (Fwd: Outboard/Medium, Aft: Nozzle/Long)

103
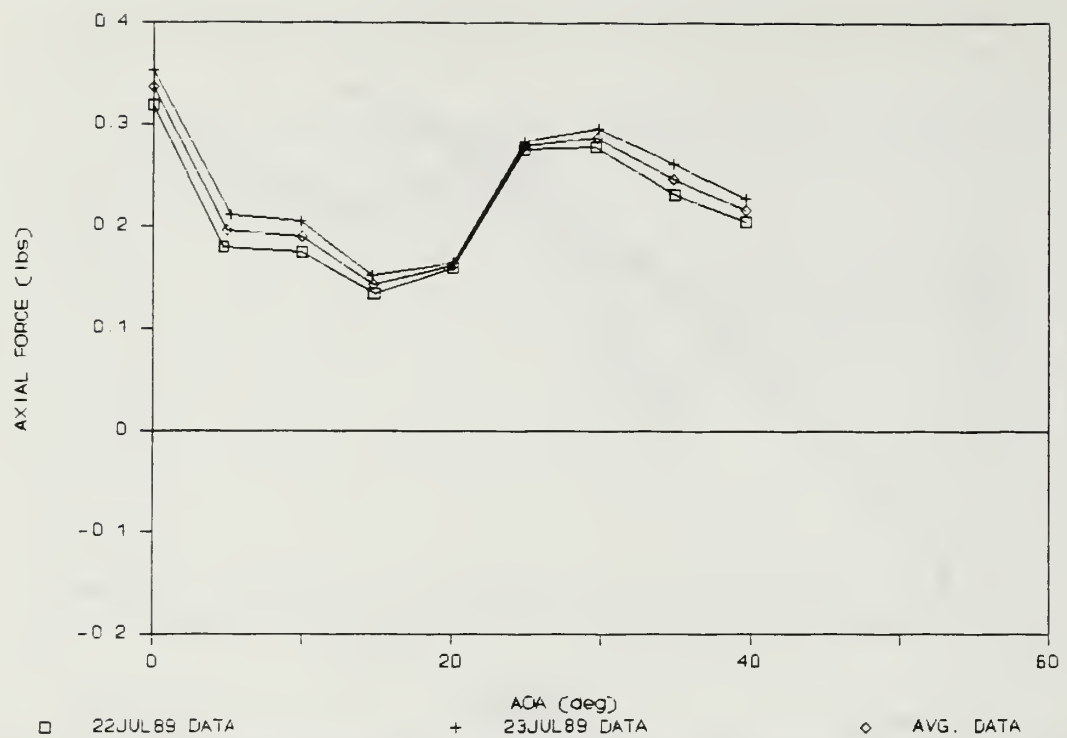
Figure 96. Axial Force (Fwd: Outboard/Medium, Aft: Nozzle/Long)
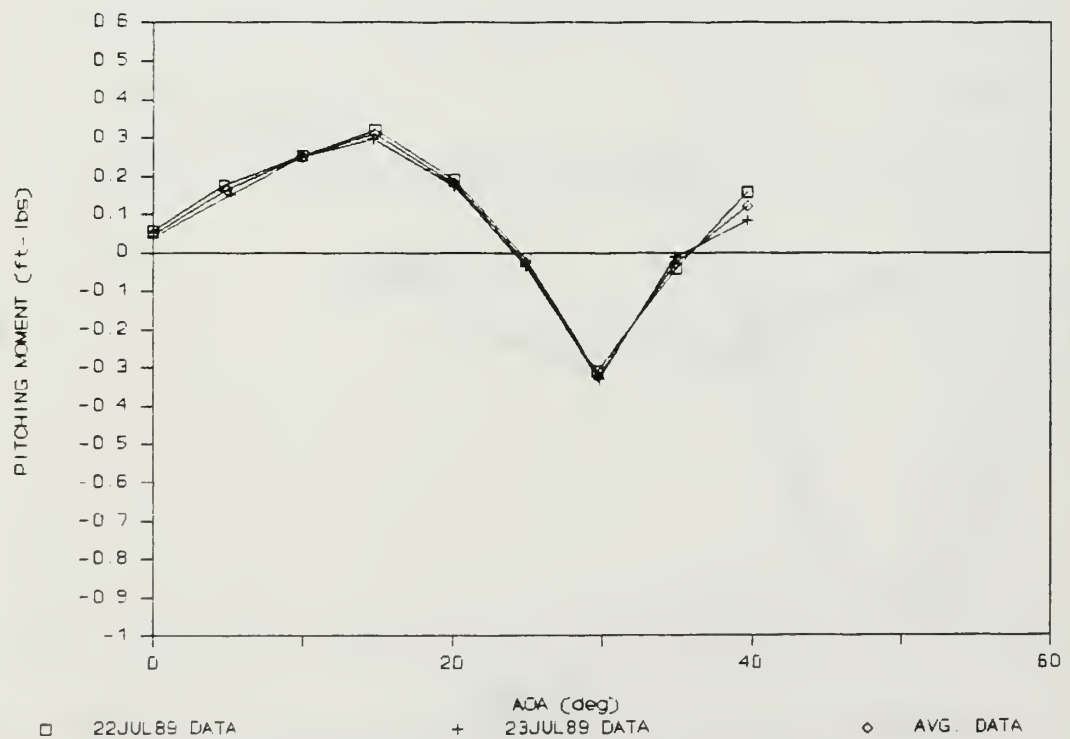
Figure 97. Pitching Moment (Fwd: Outboard/Medium, Aft: Nozzle/Long)

104
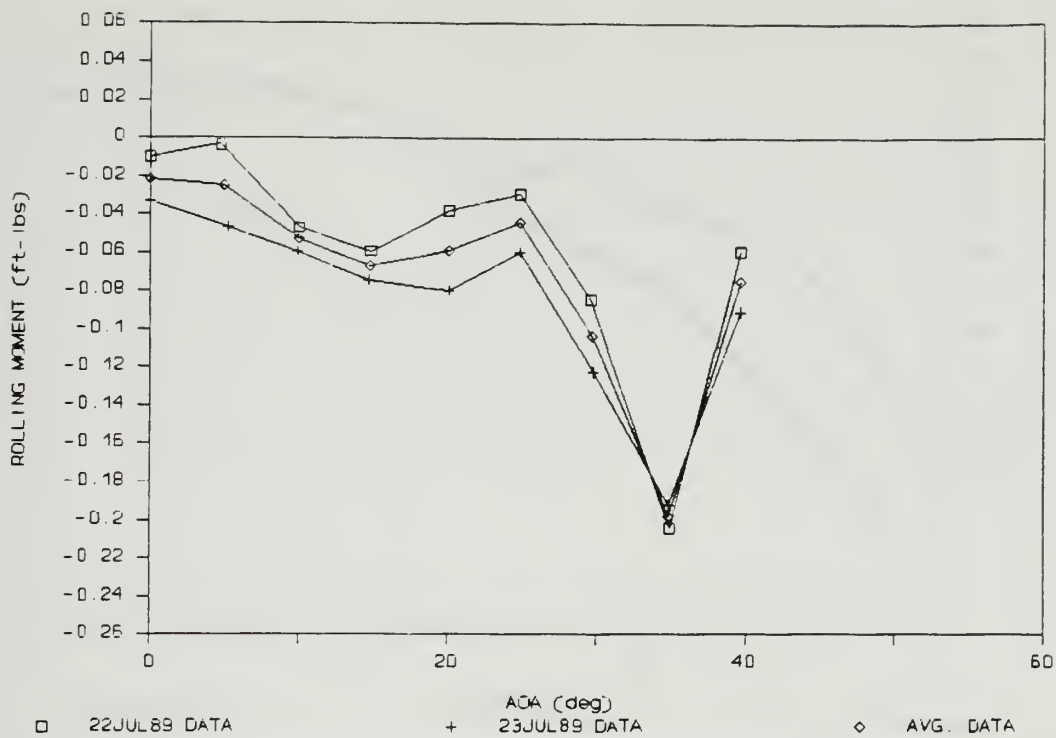
Figure 98. Rolling Moment (Fwd: Outboard/Medium, Aft: Nozzle/Long)
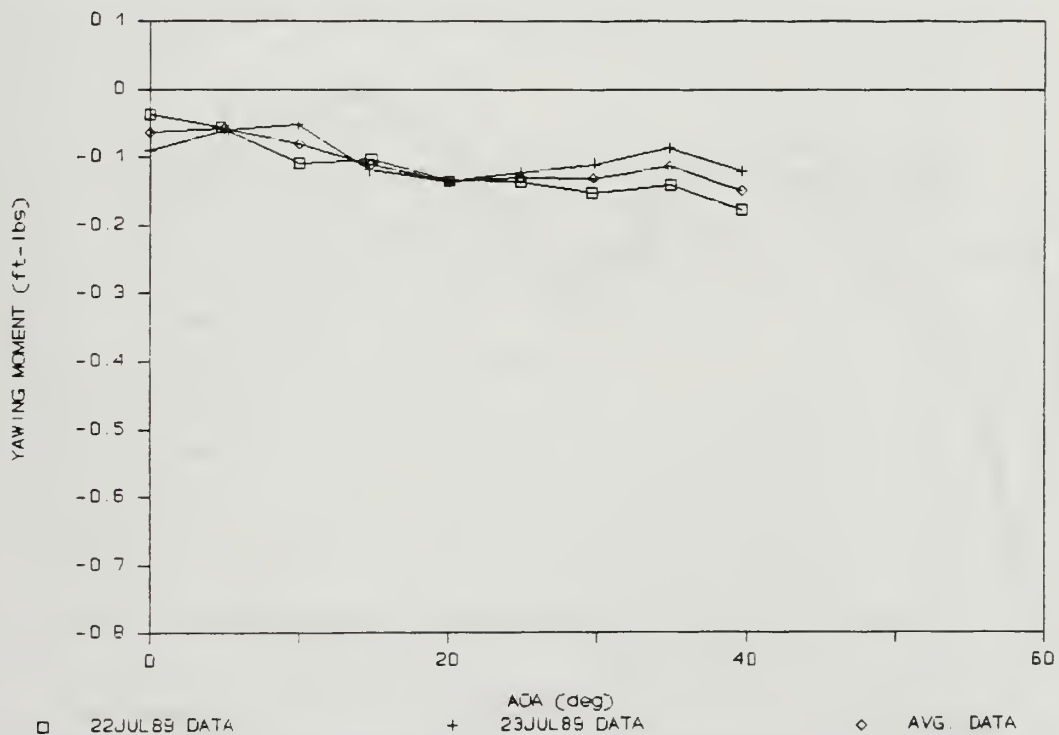
Figure 99. Yawing Moment (Fwd: Outboard/Medium, Aft: Nozzle/Long)

105
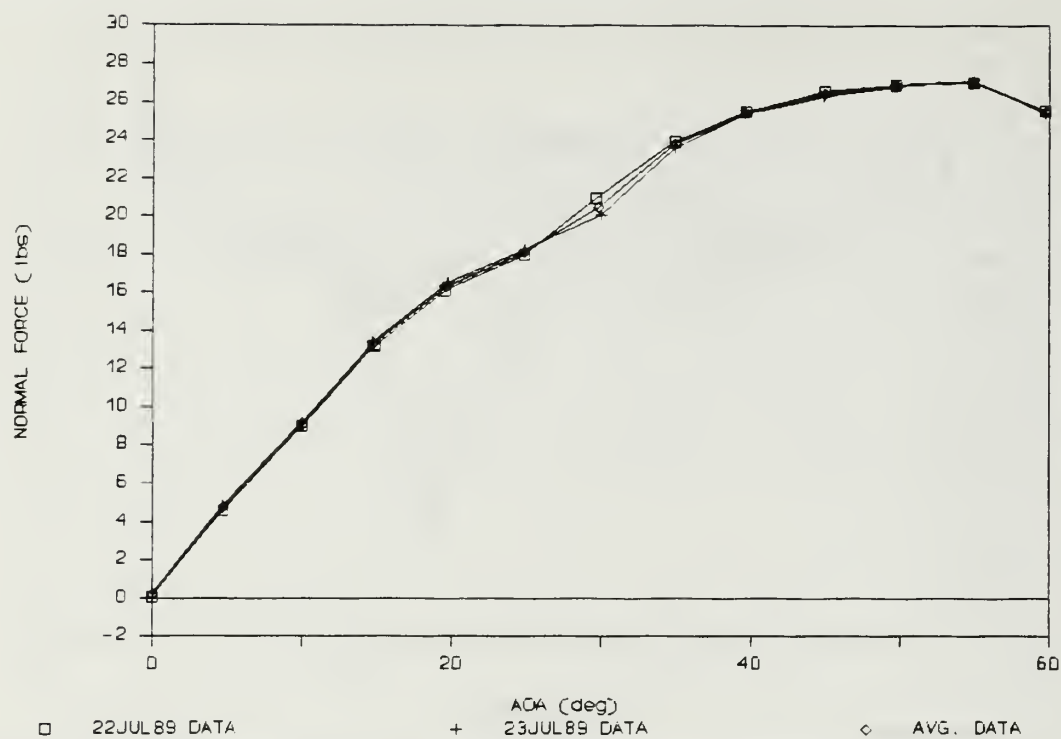
Figure 100. Normal Force (Fwd· Gear/Medium, Aft: Hook/Long)
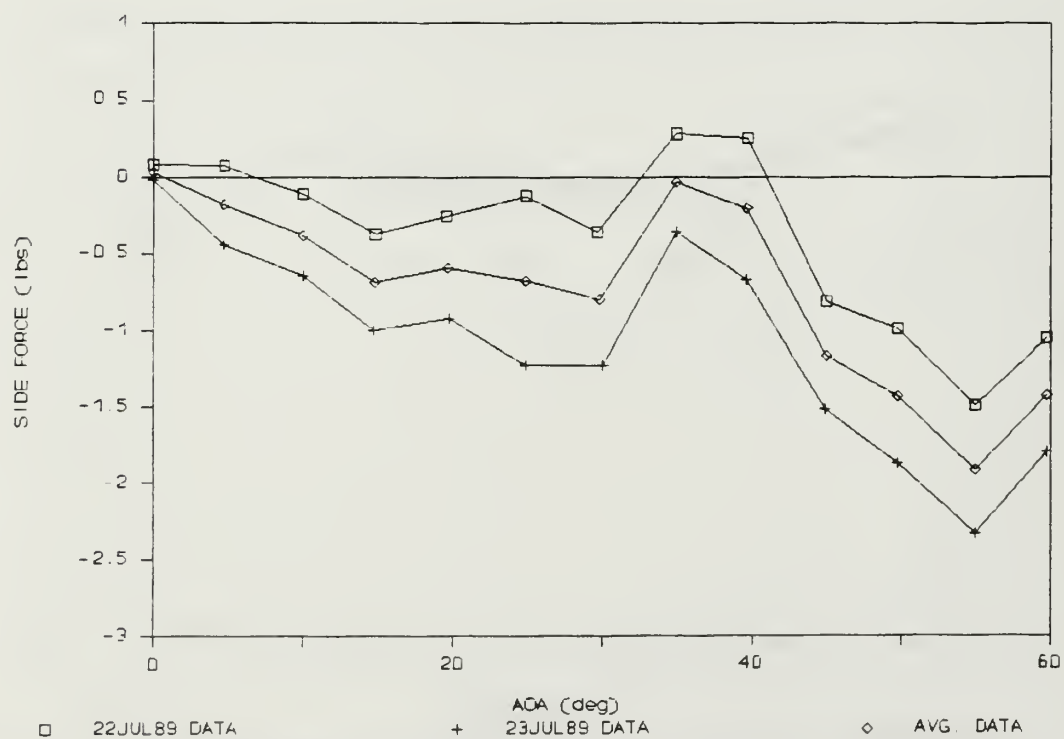
Figure 101. Side Force (Fwd: Gear/Medium, Aft: Hook/Long)
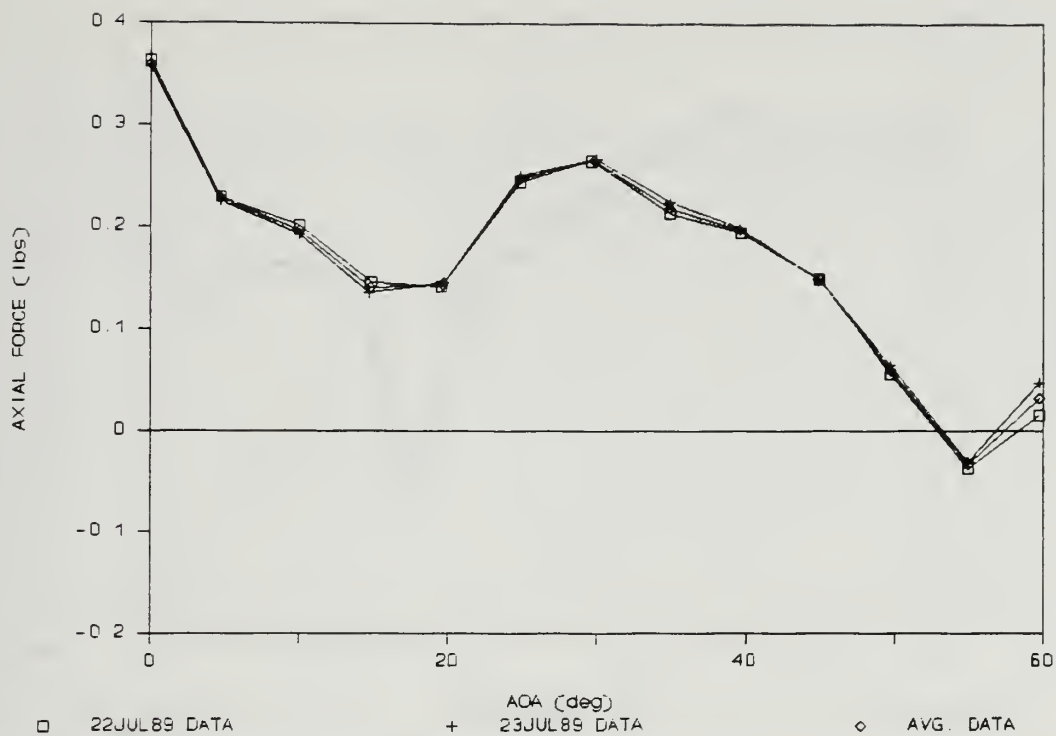
Figure 102. Axial Force (Fwd: Gear/Medium, Aft: Hook/Long)
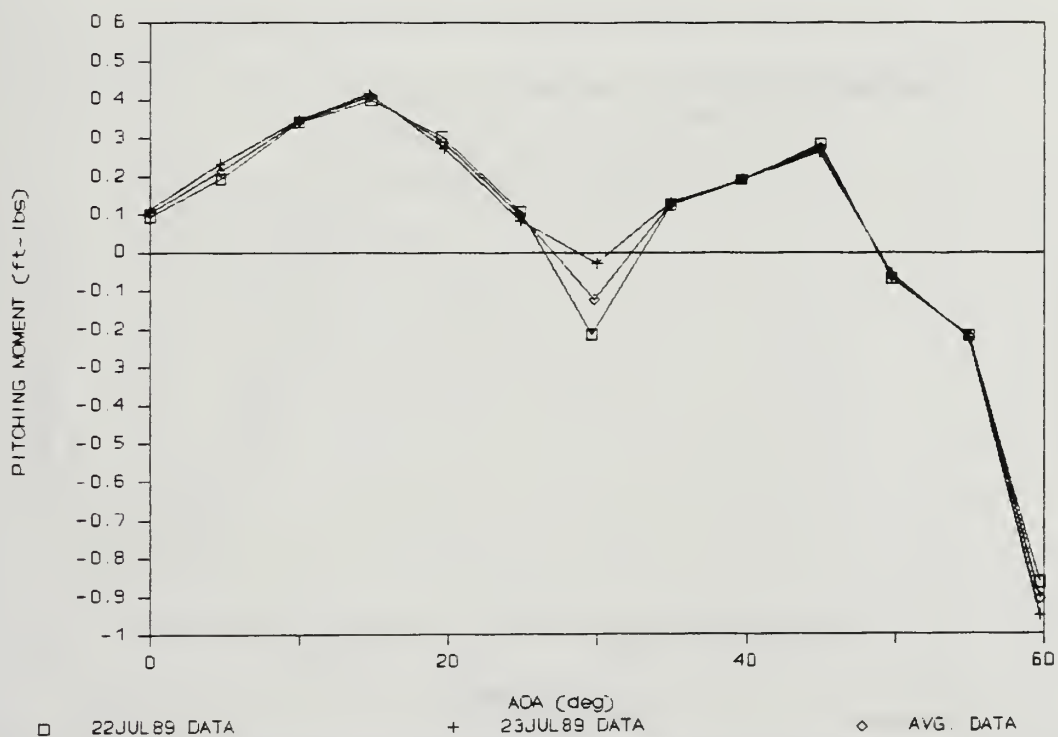
Figure 103. Pitching Moment (Fwd: Gear/Medium, Aft: Hook/Long)
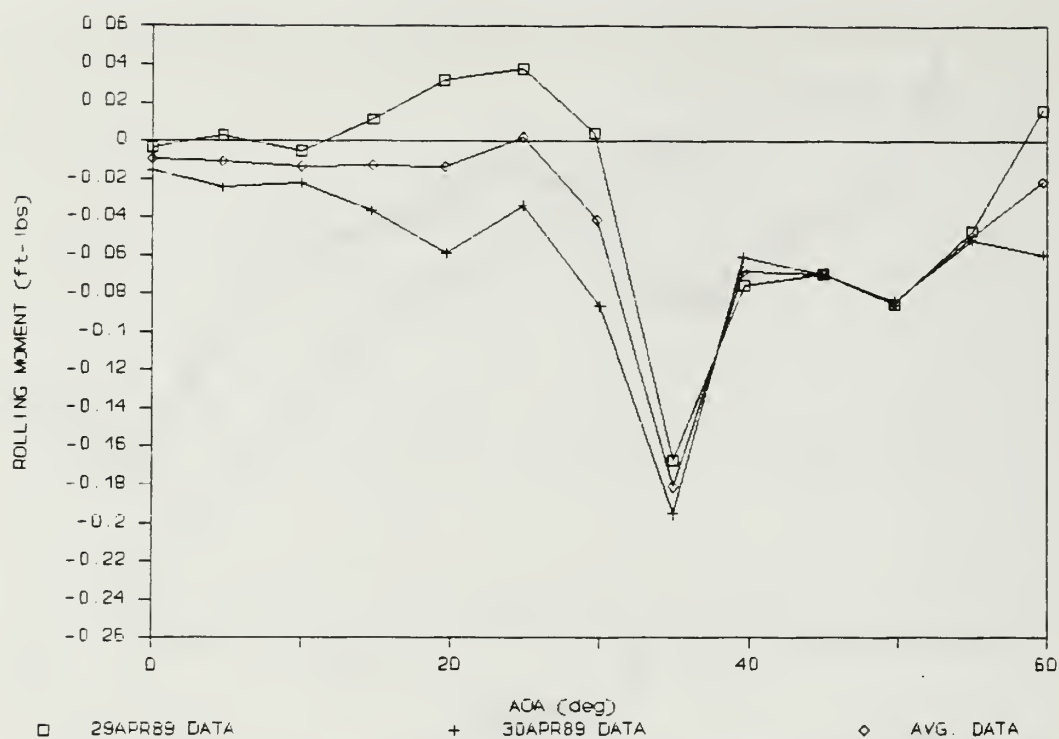
Figure 104. Rolling Moment (Fwd: Gear/Medium, Aft: Hook/Long)
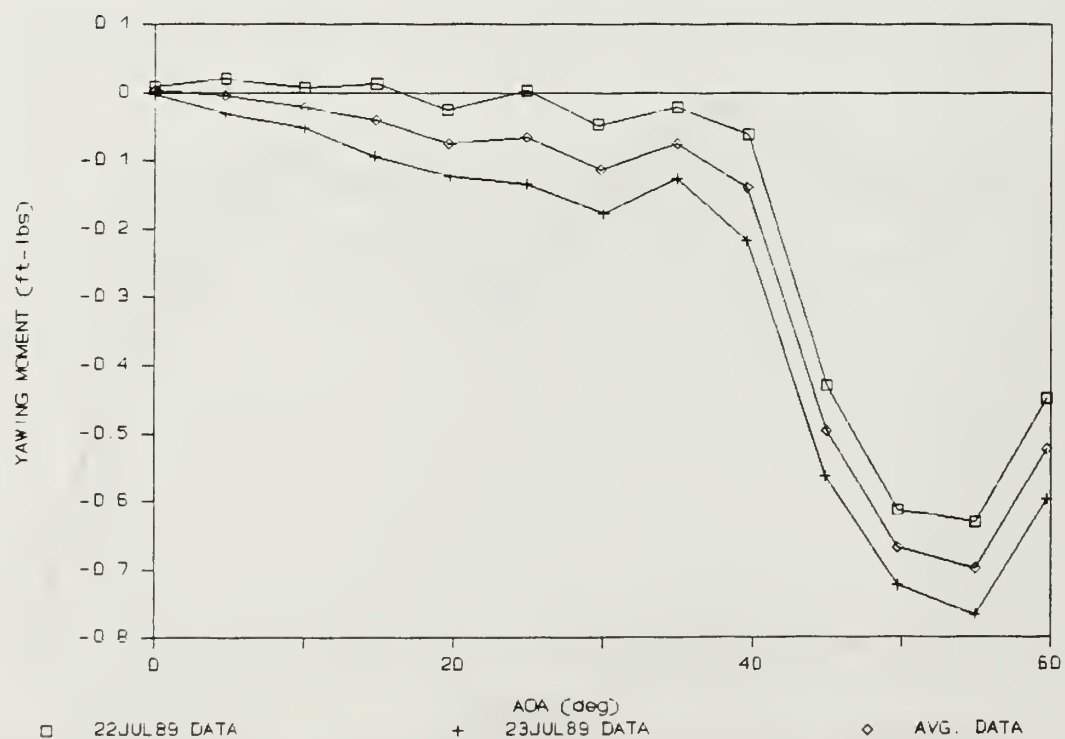
Figure 105. Yawing Moment (Fwd: Gear/Medium, Aft: Hook/Long)
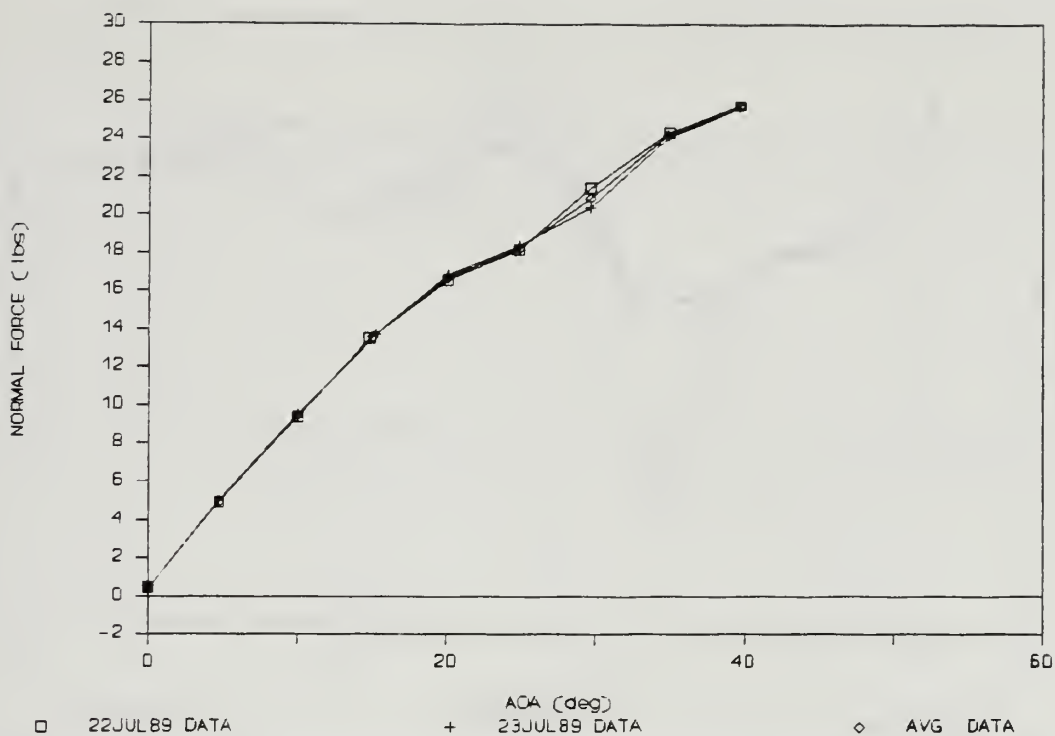
Figure 106. Normal Force (Fwd· Gear/Medium, Aft: Nozzle/Long)
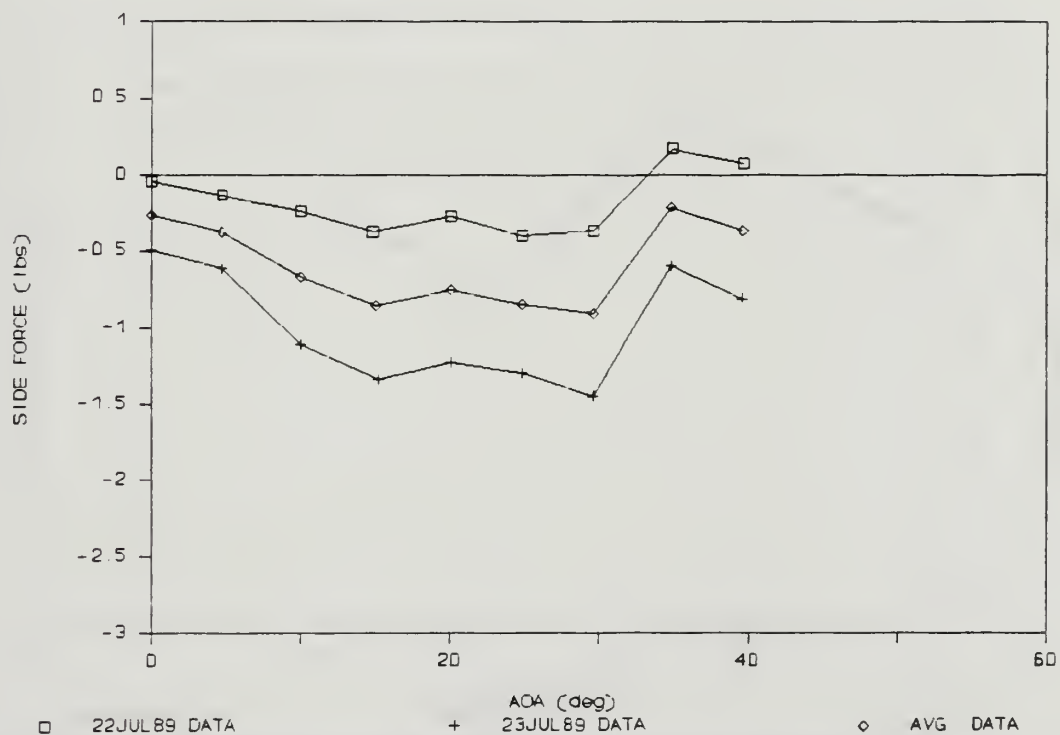
Figure 107. Side Force (Fwd: Gear/Medium. Aft: Nozzle/Long)

109
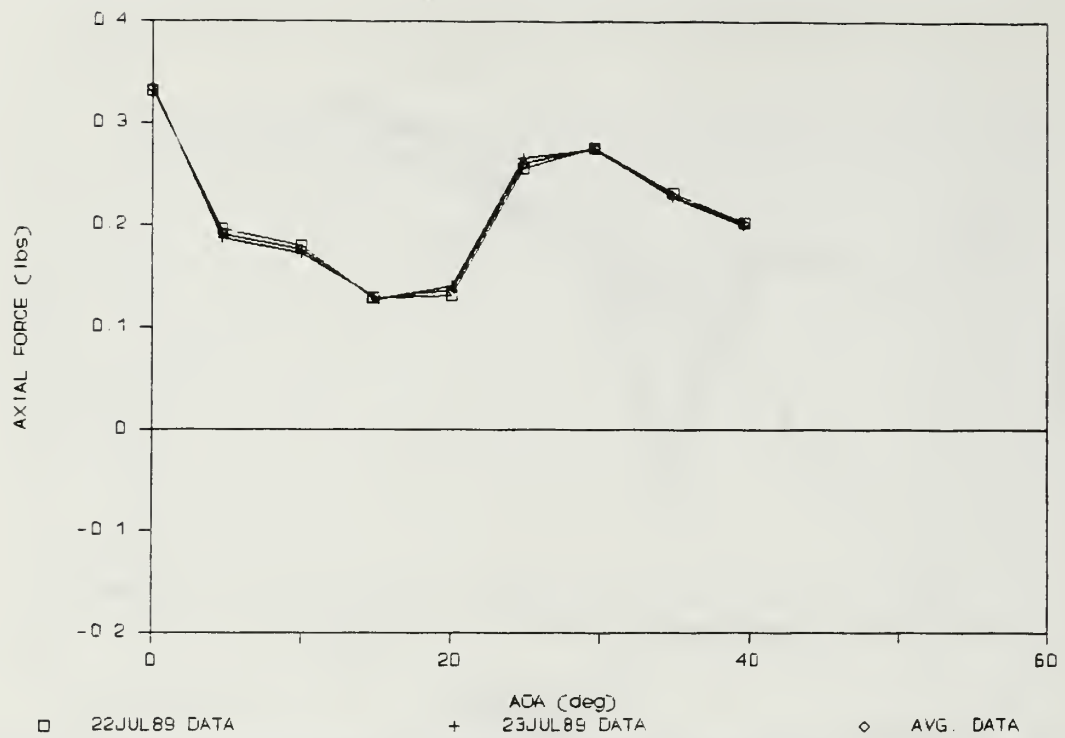
Figure 108. Axial Force (Fwd: Gear/Medium, Aft: Nozzle/Long)
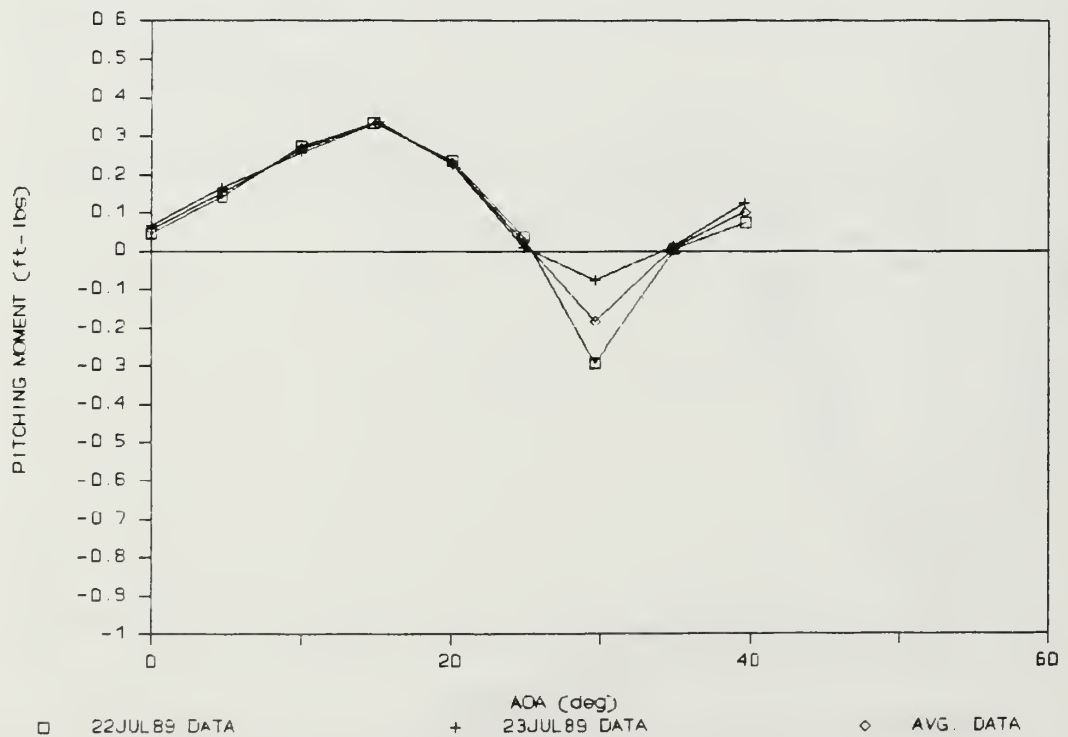
Figure 109. Pitching Moment (Fwd: Gear/Medium, Aft: Nozzle/Long)

110
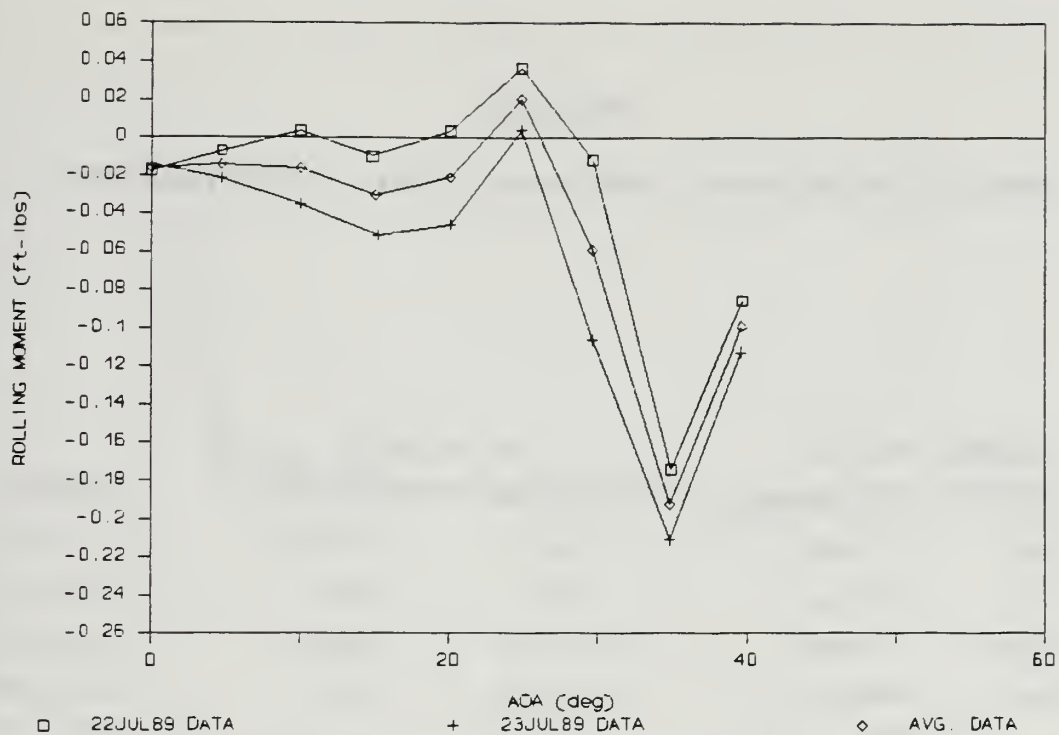
Figure 110. Rolling Moment (Fwd: Gear/Medium, Aft: Nozzle/Long)
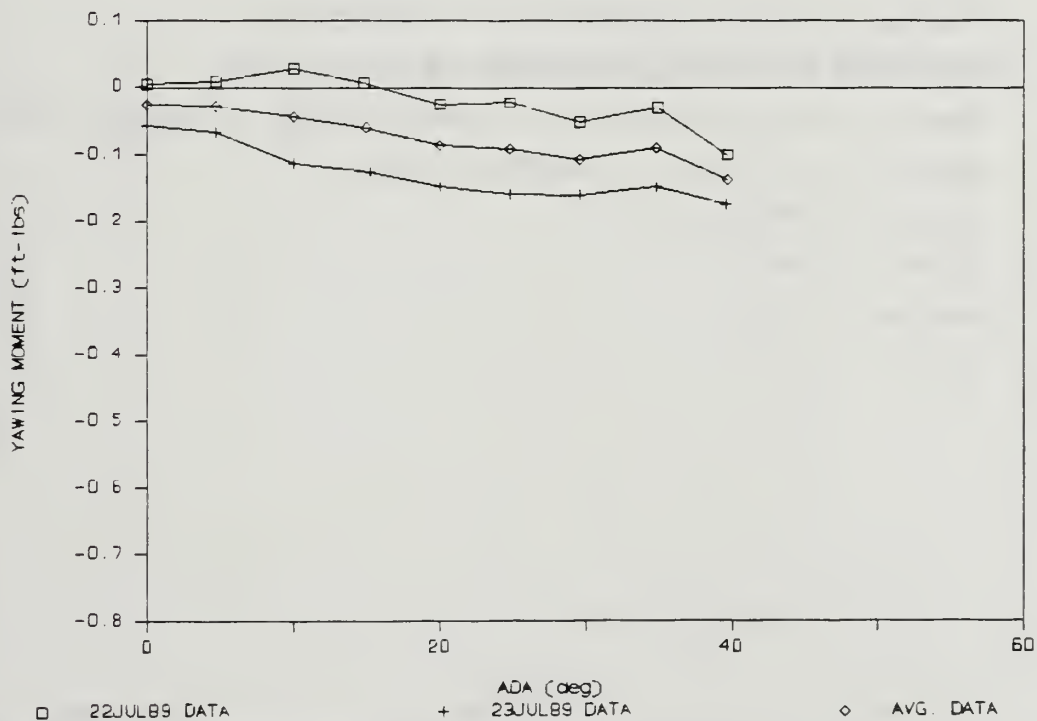
Figure 111. Yawing Moment (Fwd: Gear/Medium, Aft: Nozzle/Long)

111

APPENDIX F

PERCENT INTERFERENCE FOR VARIOUS STRUT CONFIGURATIONS

FOWARD STRUTS		AFT STRUTS		
LOCATION	EXTENSION	LOCATION	EXTENSION	FIGURES
Various	Long	Hook	Short	112-117
Various	Medium	Hook	Long	118-123
Various	Long	Nozzle	Short	124-129
Various	Medium	Nozzle	Long	130-135

Note: Inboard = 1.875" outboard of centerline
        Middle = 4.531" outboard of centerline
        Outboard = 6.188" outboard of centerline
        Gear = 1.875" outboard of centerline, 2" below wing
        Hook = 4.375" aft of moment center
        Nozzle = Nozzle lip
        Short = 0.4"
        Medium = 0.5"
   Long = 1.5"
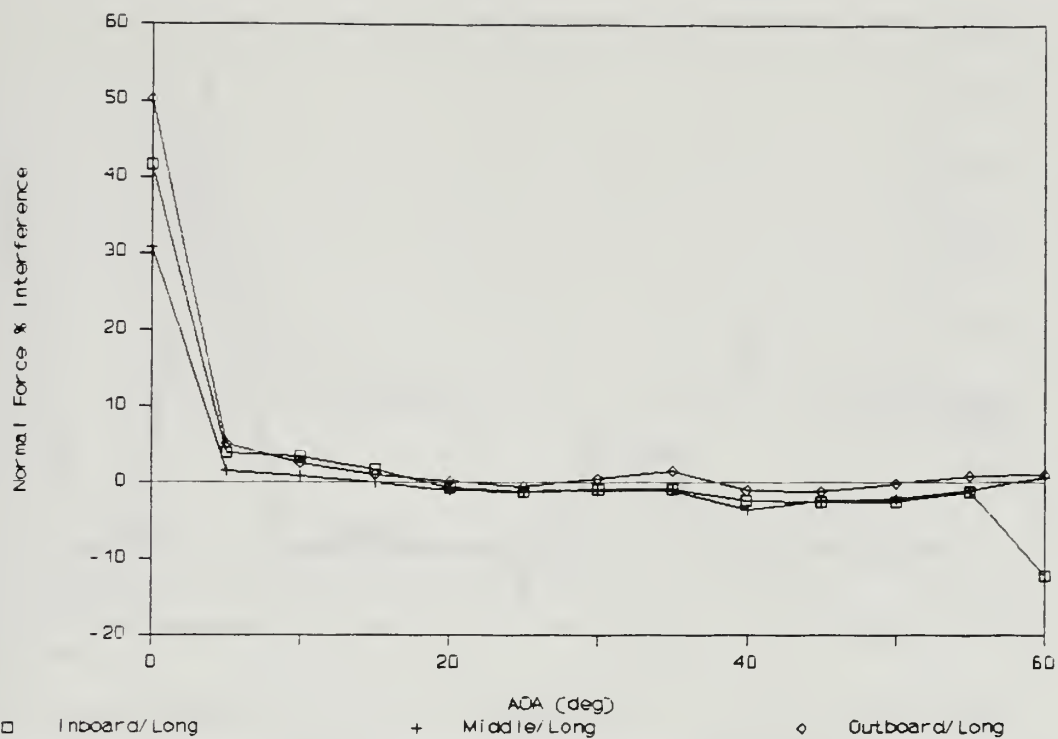
Figure 112. Normal Force % Interference (Aft: Hook/Short)
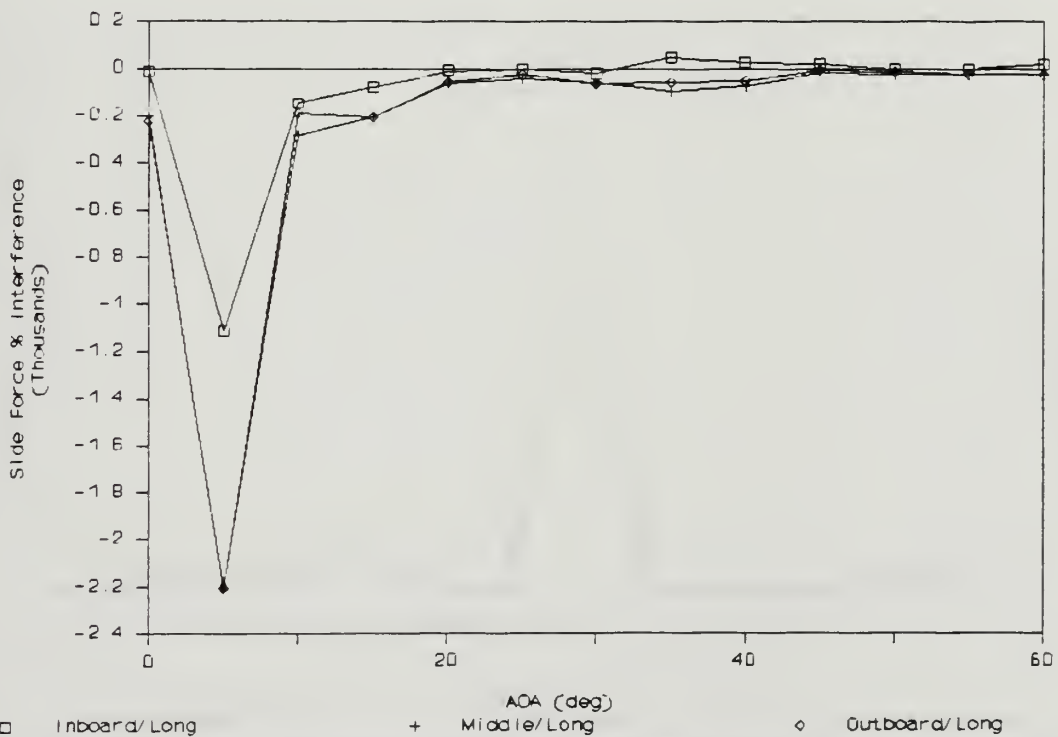
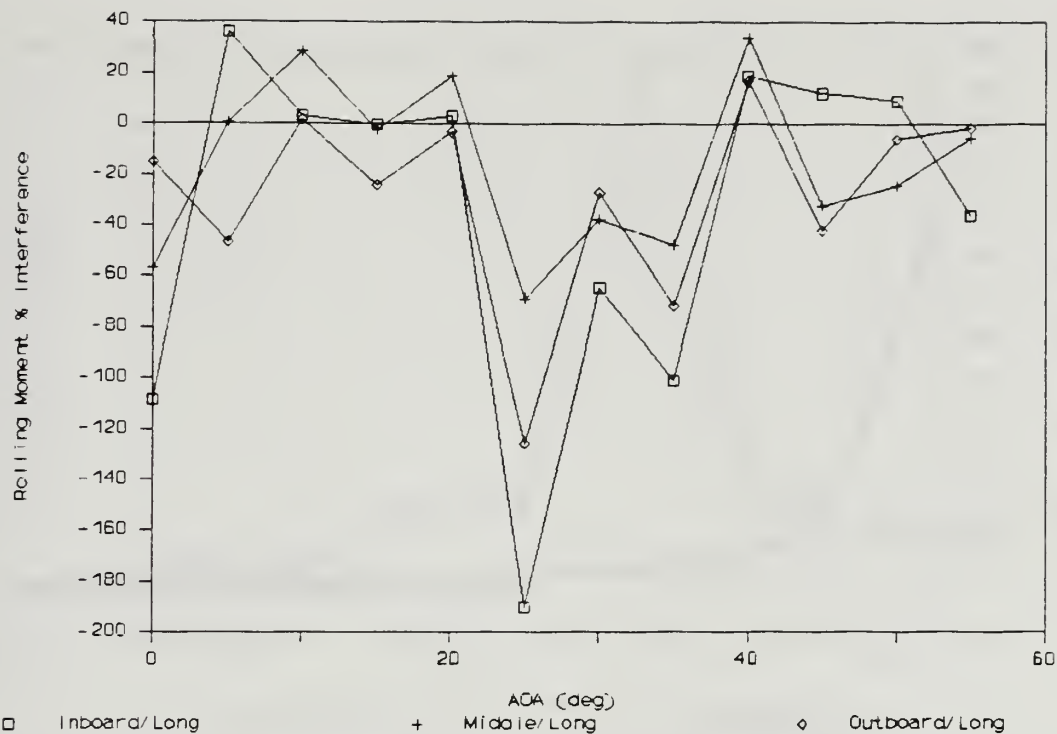**Figure 113.** Side Force % Interference (Aft: Hook/Short)

113
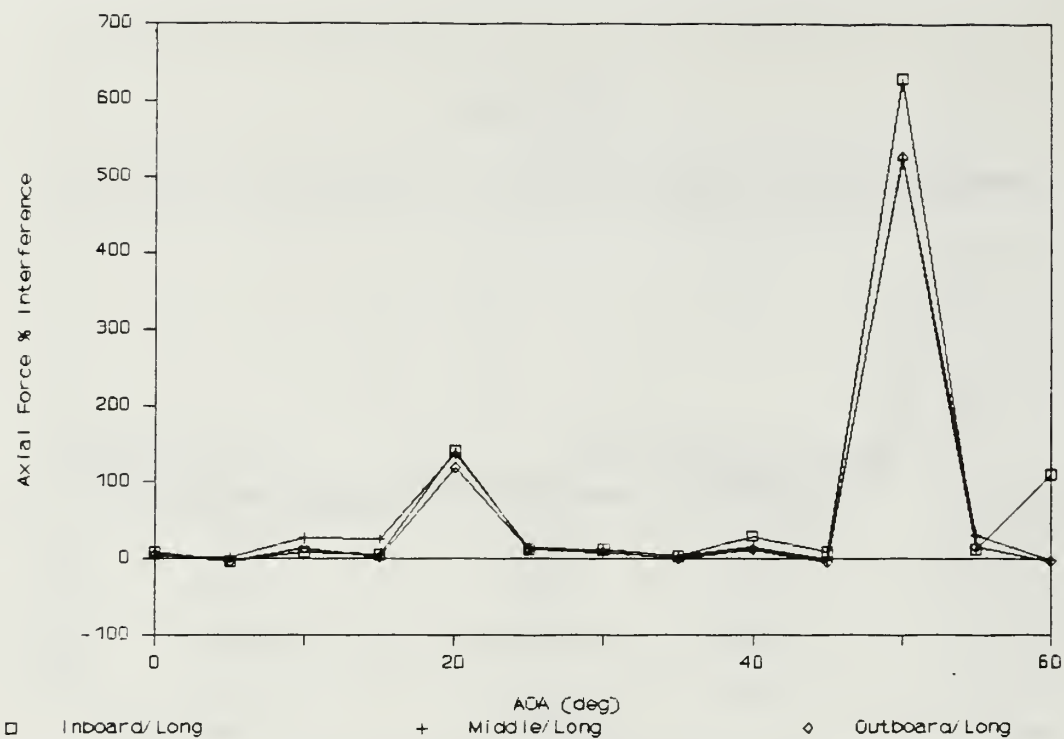
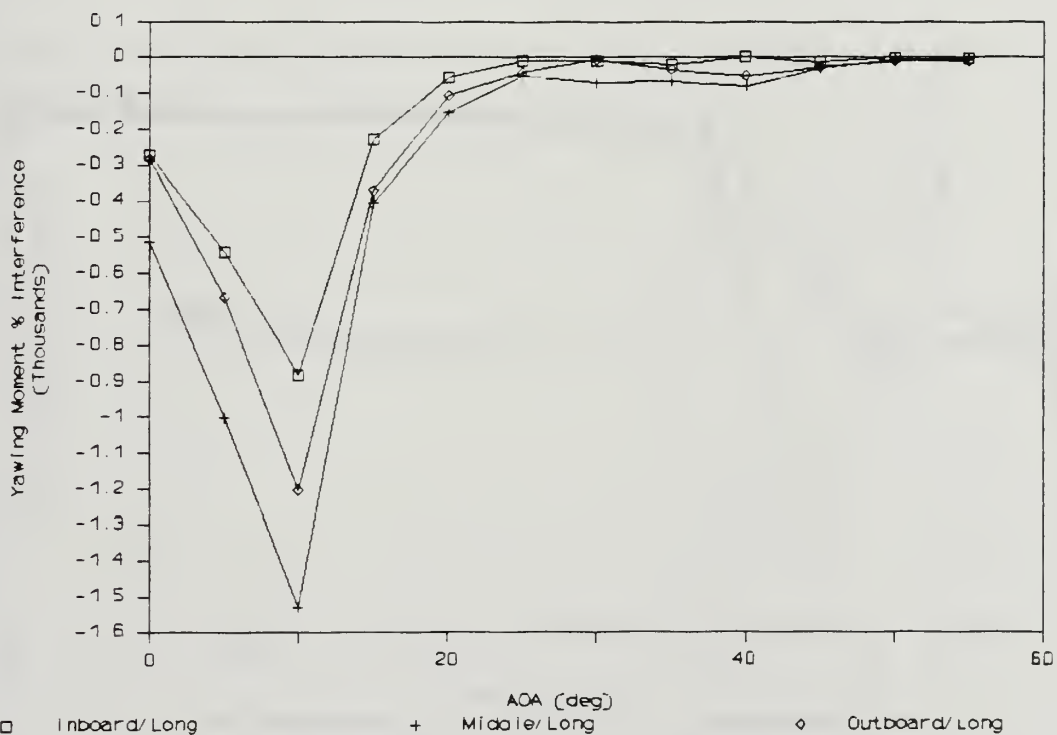**Figure 114.** Axial Force % Interference (Aft: Hook/Short)
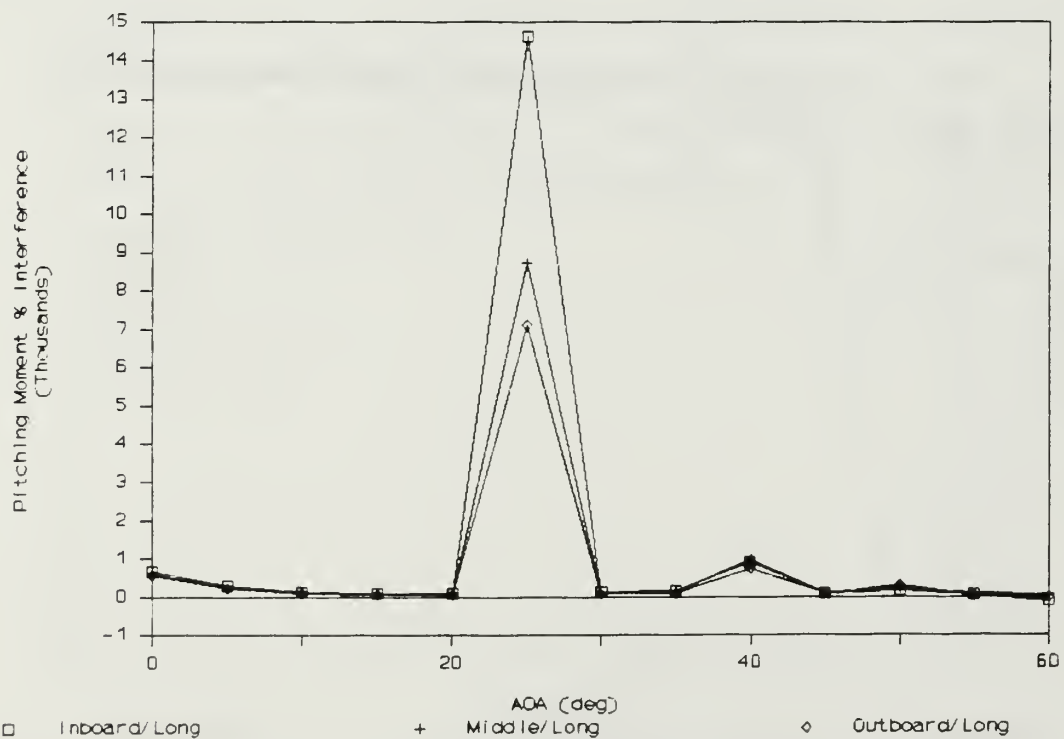
Figure 115. Pitching Moment % Interference (Aft: Hook/Short)

114
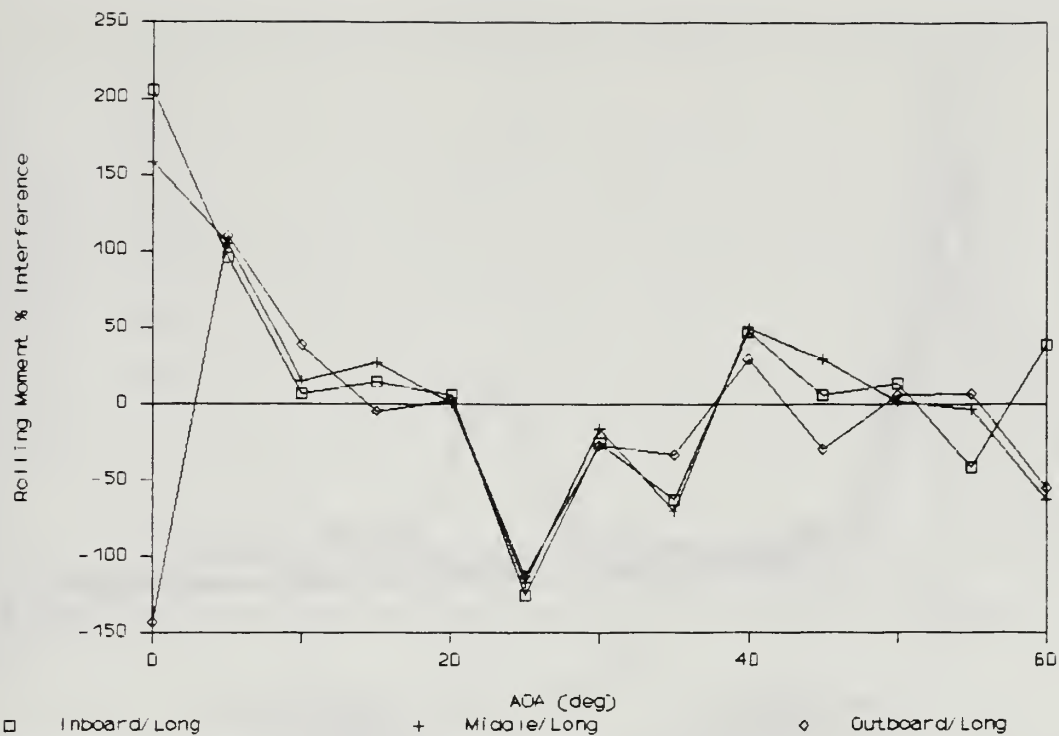
Figure 116. Rolling Moment % Interference (Aft: Hook/Short)
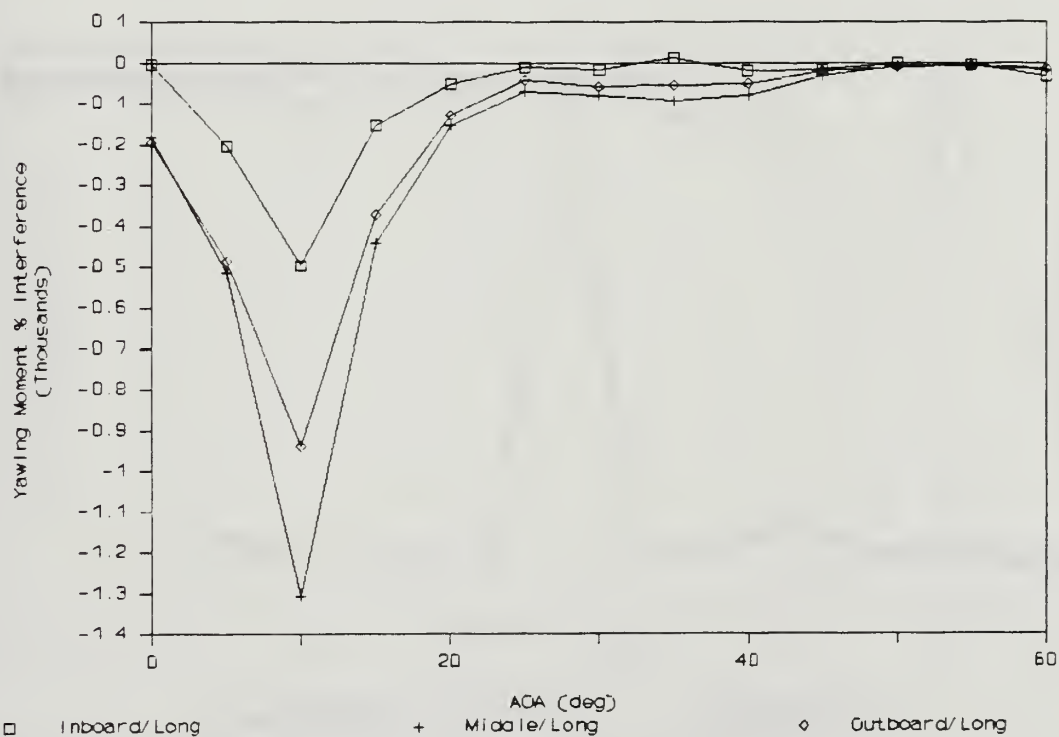
Figure 117. Yawing Moment % Interference (Aft: Hook/Short)

115
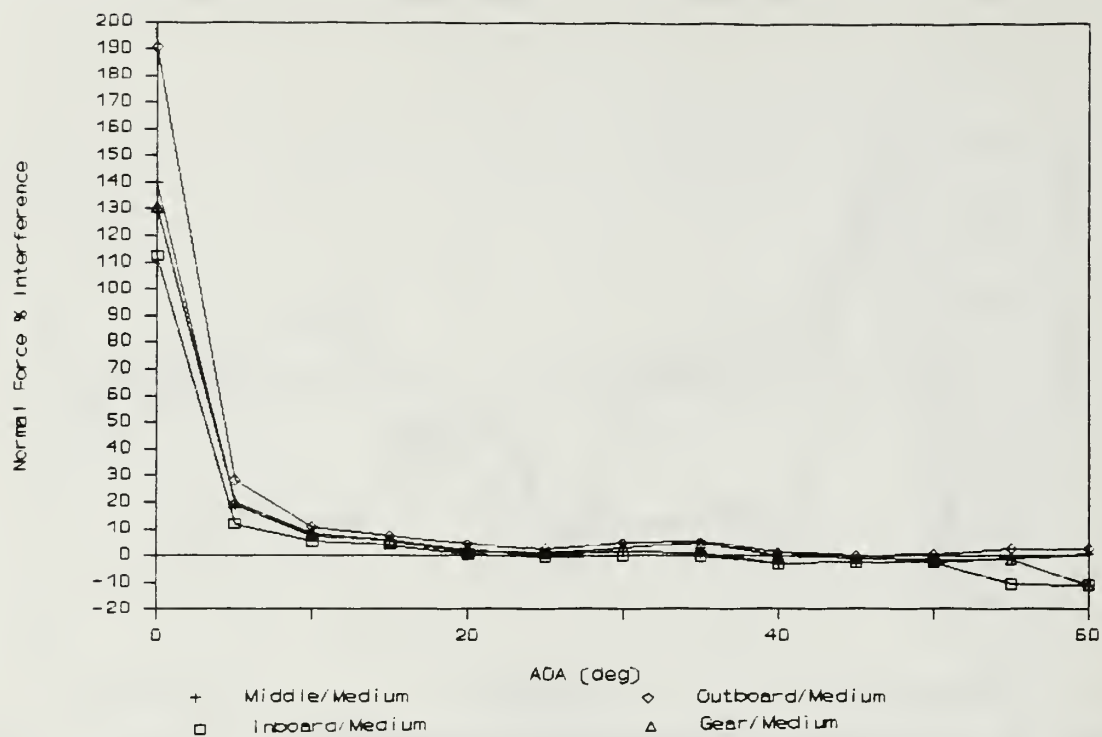
Figure 118. Normal Force % Interference (Aft: Hook/Long)
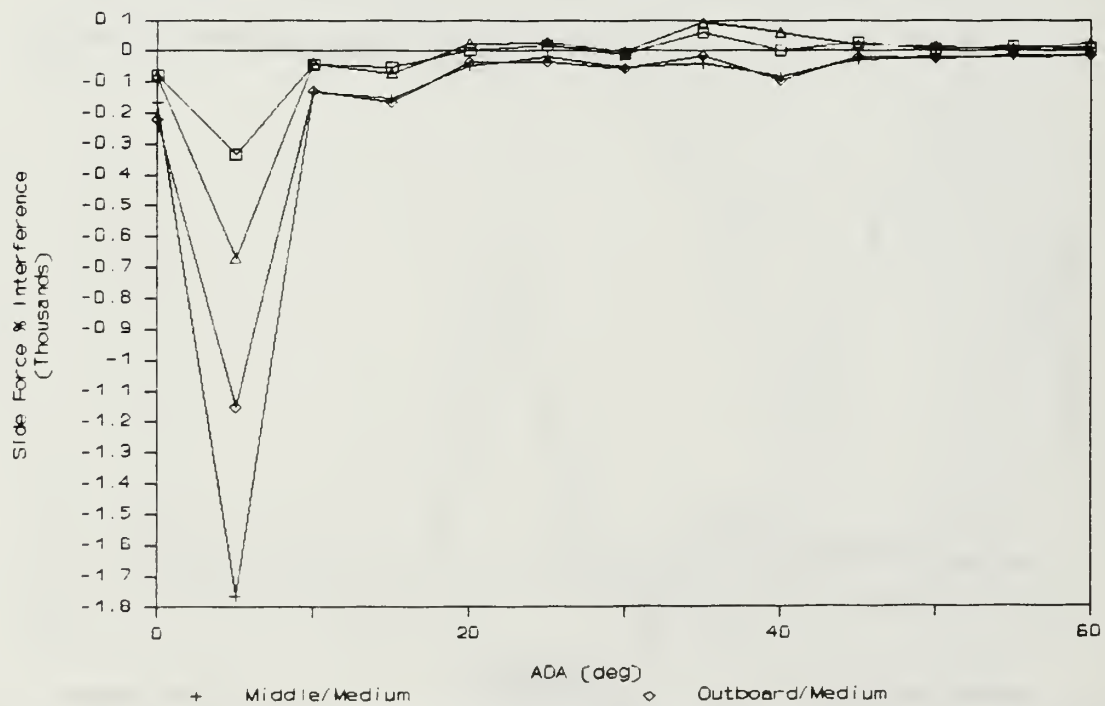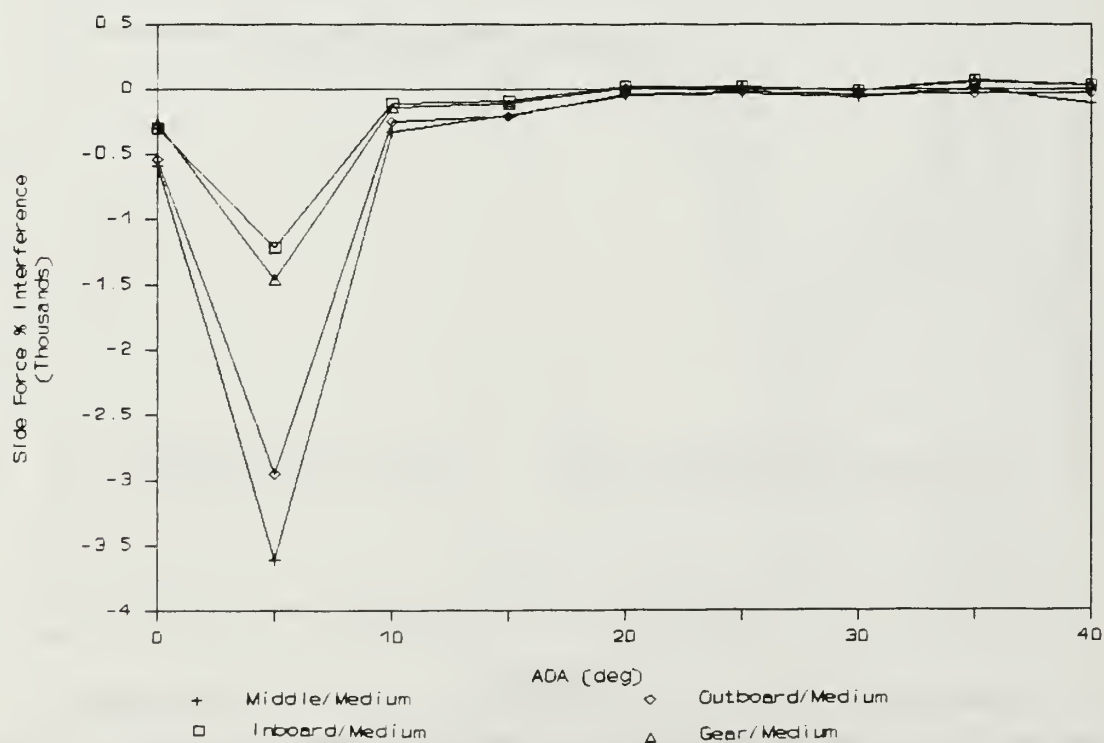

Figure 119. Side Force % Interference (Aft: Hook/Long)
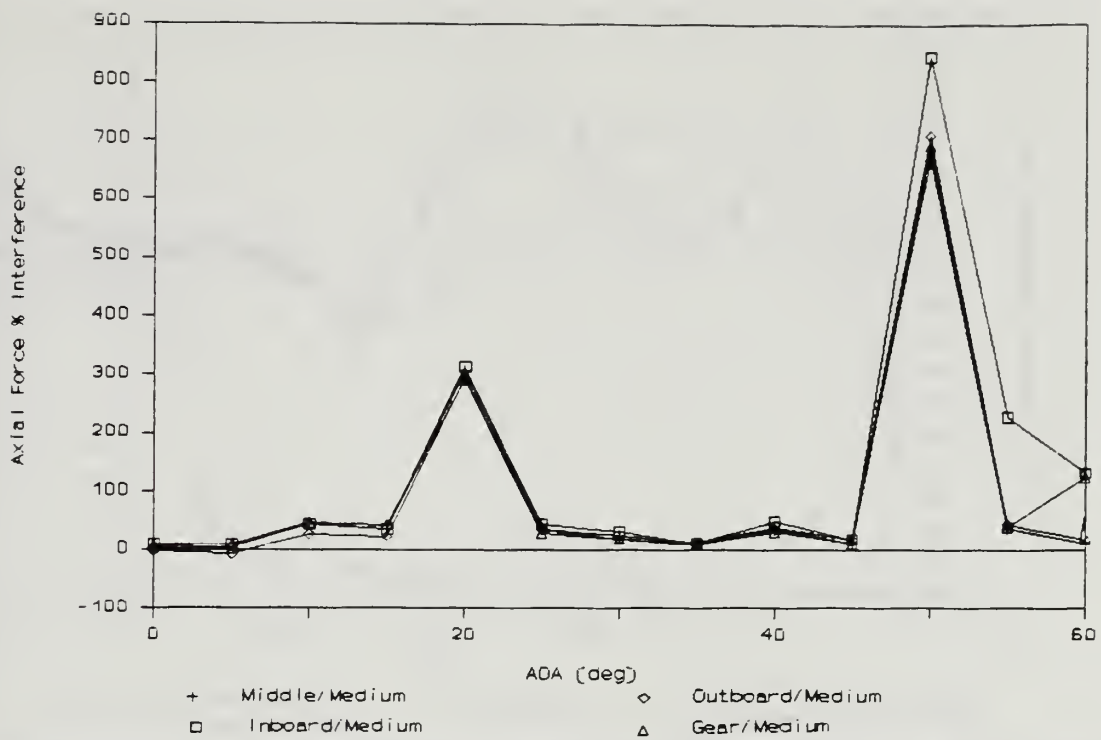
Figure 120. Axial Force % Interference (Aft: Hook/Long)
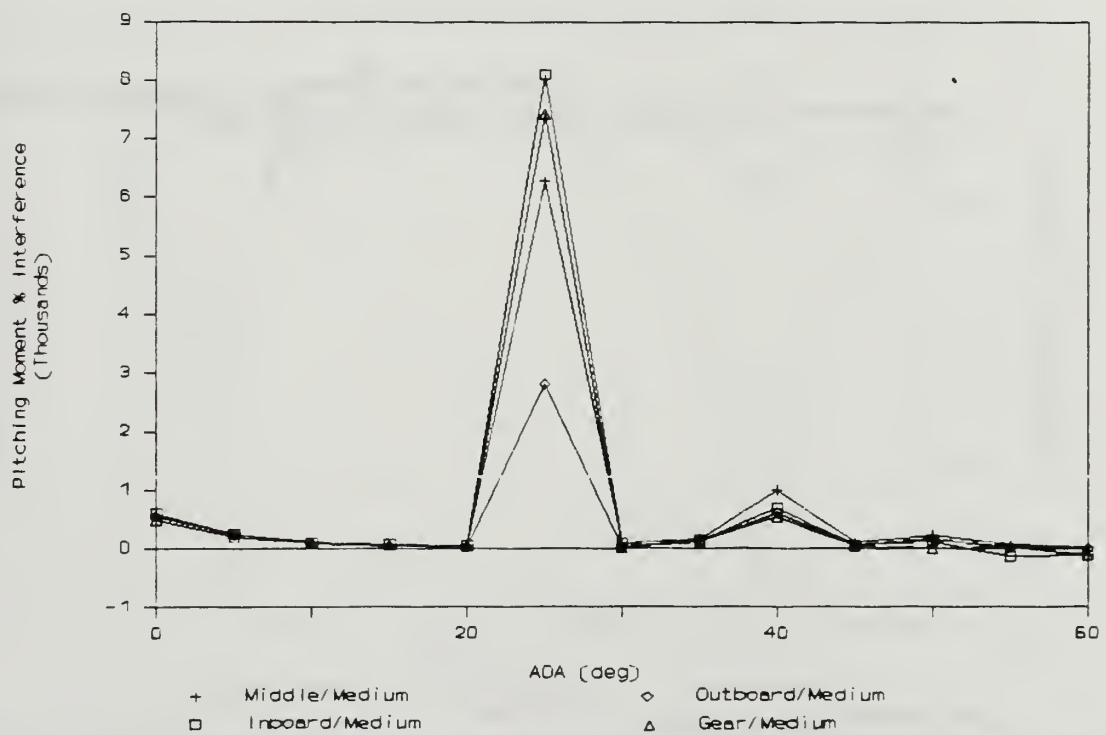
Figure 121. Pitching Moment % Interference (Aft: Hook/Long)

117
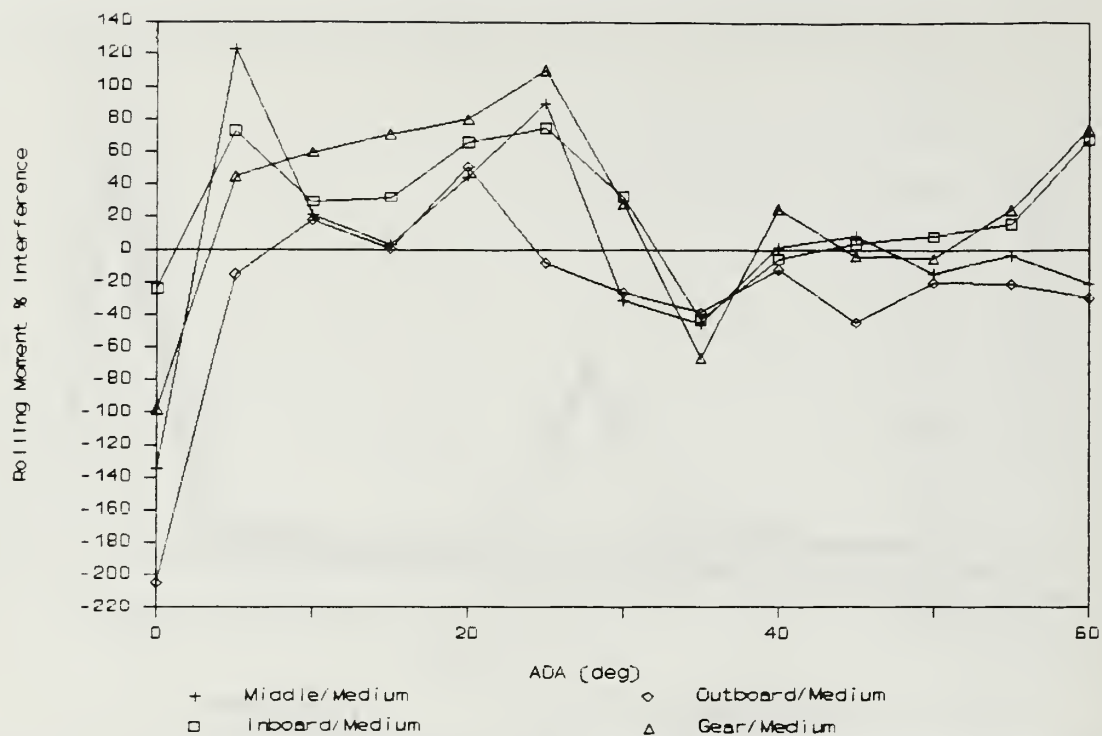
Figure 122. Rolling Moment % Interference (Aft: Hook/Long)
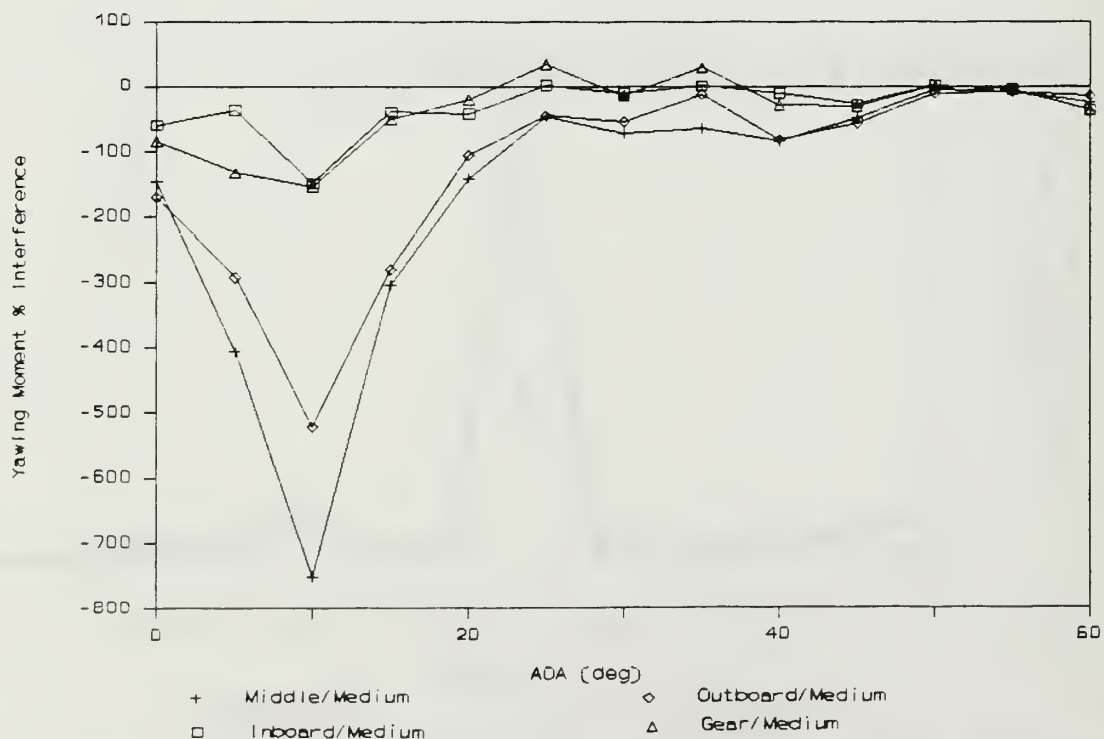
Figure 123. Yawing Moment % Interference (Aft: Hook/Long)

118
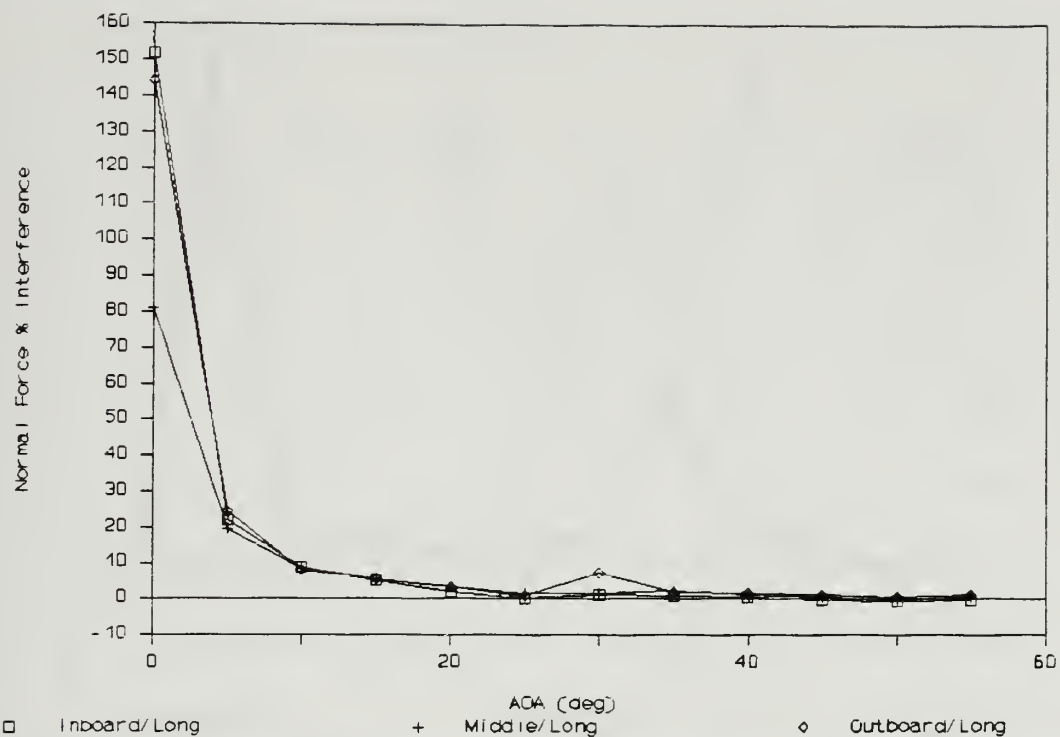
Figure 124. Normal Force % Interference (Aft: Nozzle/Short)
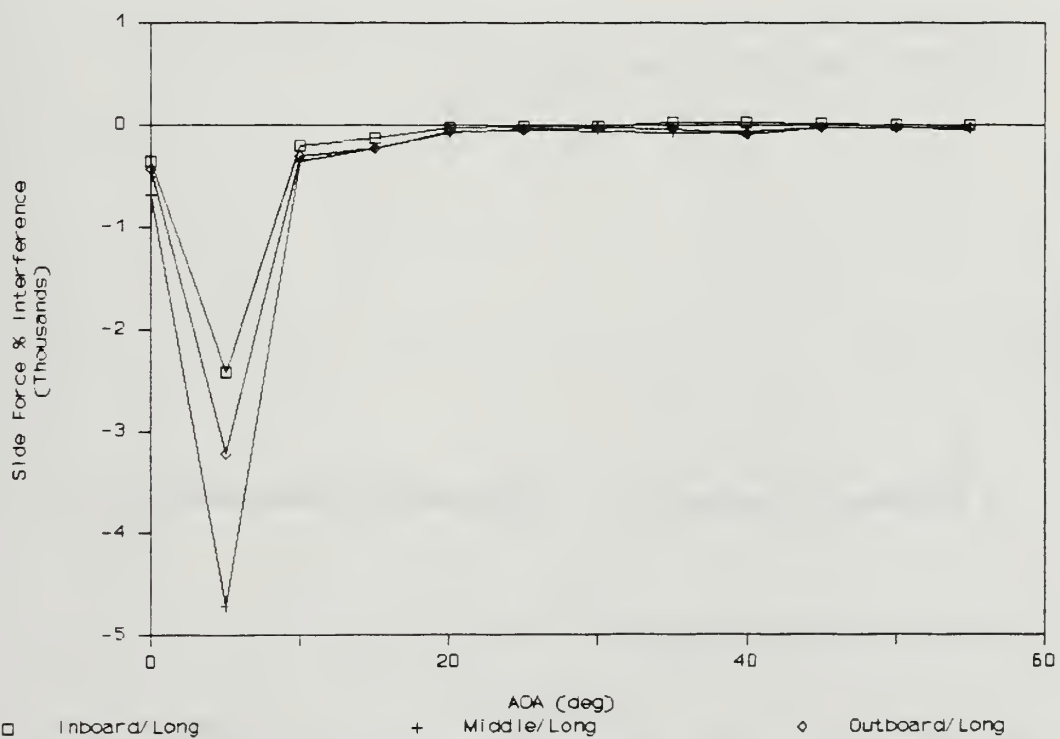
Figure 125. Side Force % Interference (Aft: Nozzle/Short)

119
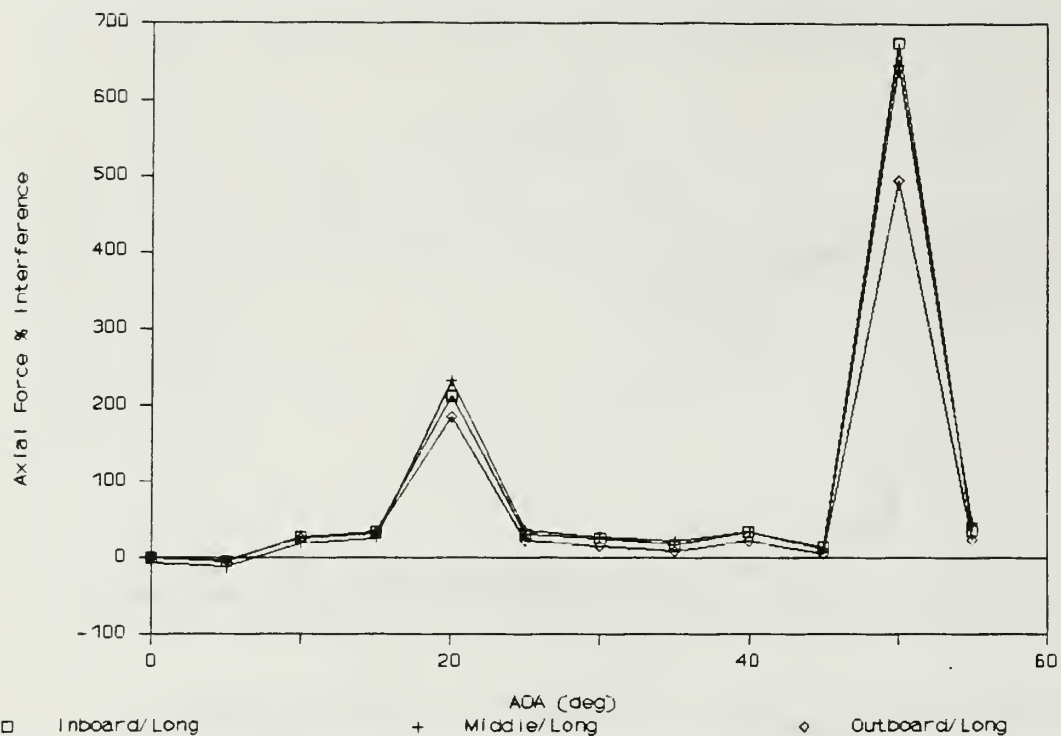
Figure 126. Axial Force % Interference (Aft: Nozzle/Short)
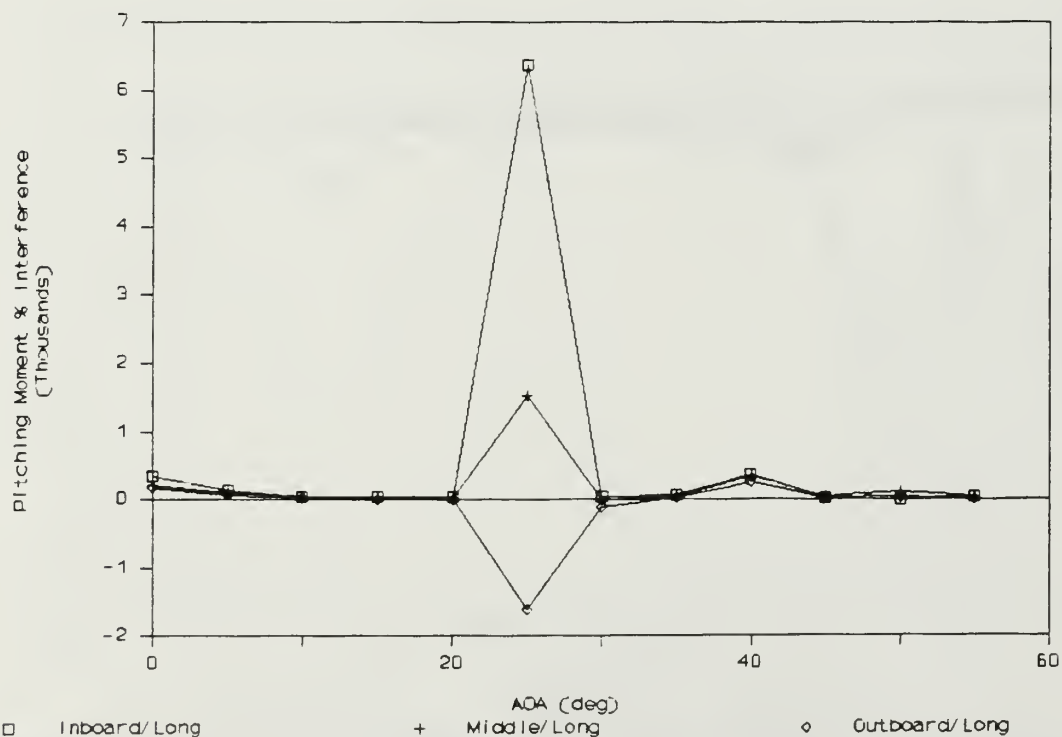
Figure 127. Pitching Moment % Interference (Aft: Nozzle/Short)

Figure 128. Rolling Moment % Interference (Aft: Nozzle/Short)

Figure 129. Yawing Moment % Interference (Aft: Nozzle/Short)

121
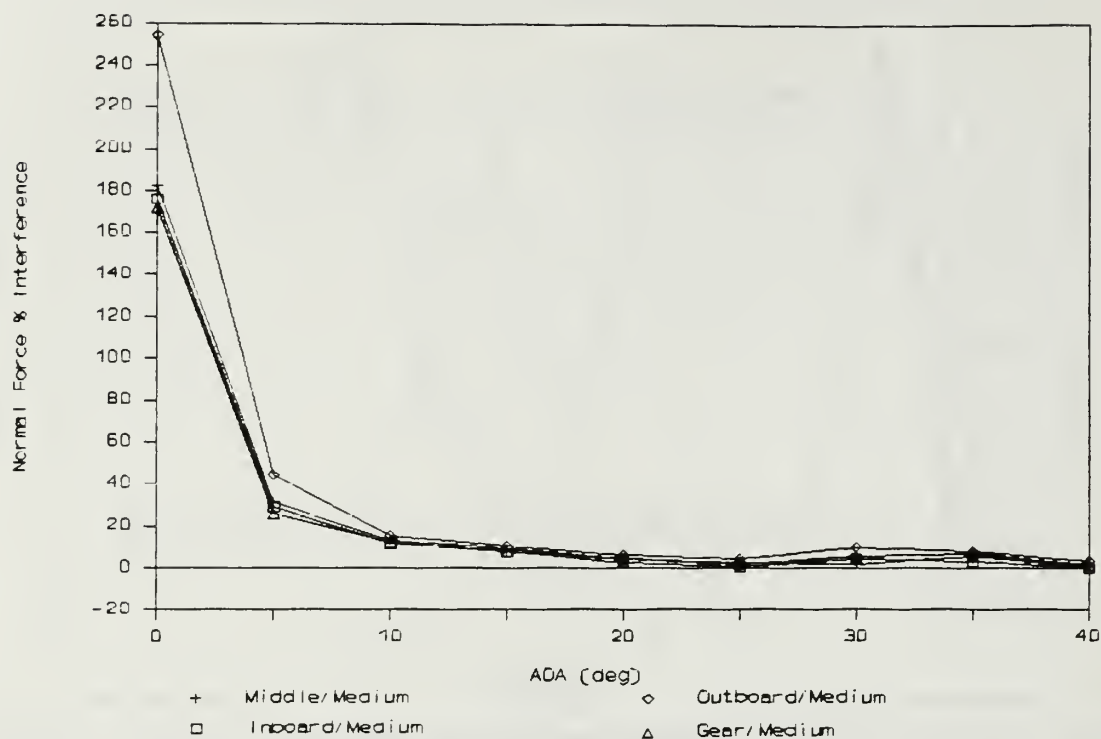
Figure 130. Normal Force % Interference (Aft: Nozzle/Long)

Figure 131. Side Force % Interference (Aft: Nozzle/Long)
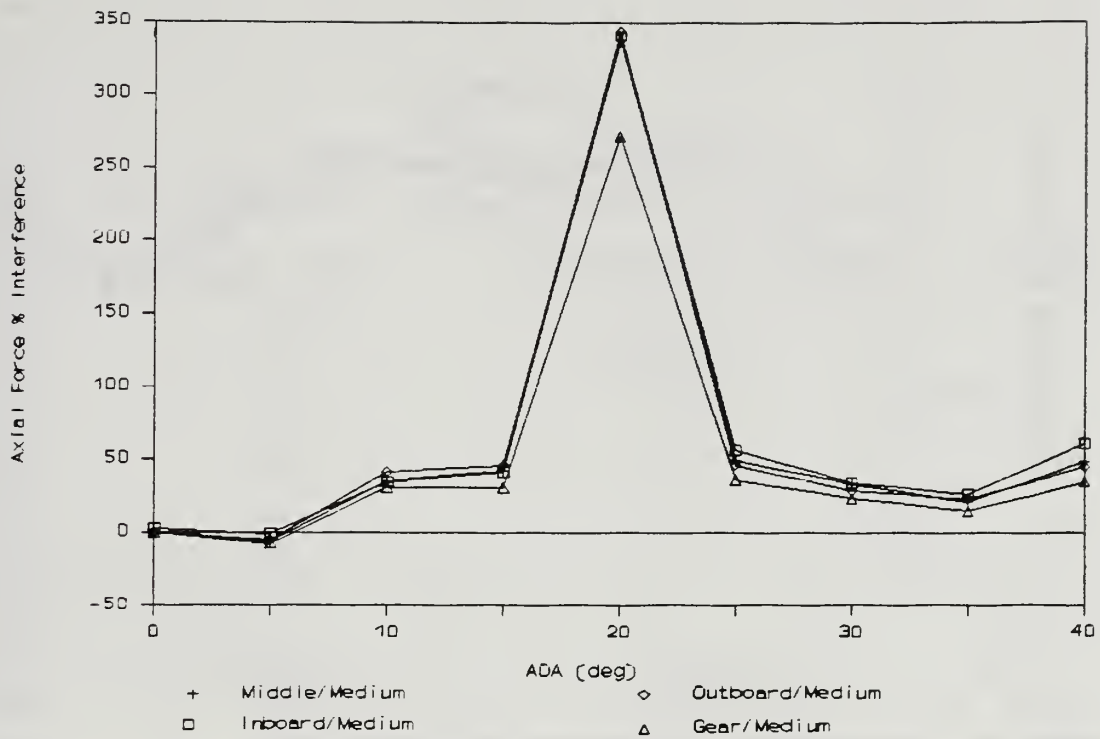
Figure 132. Axial Force % Interference (Aft: Nozzle/Long)
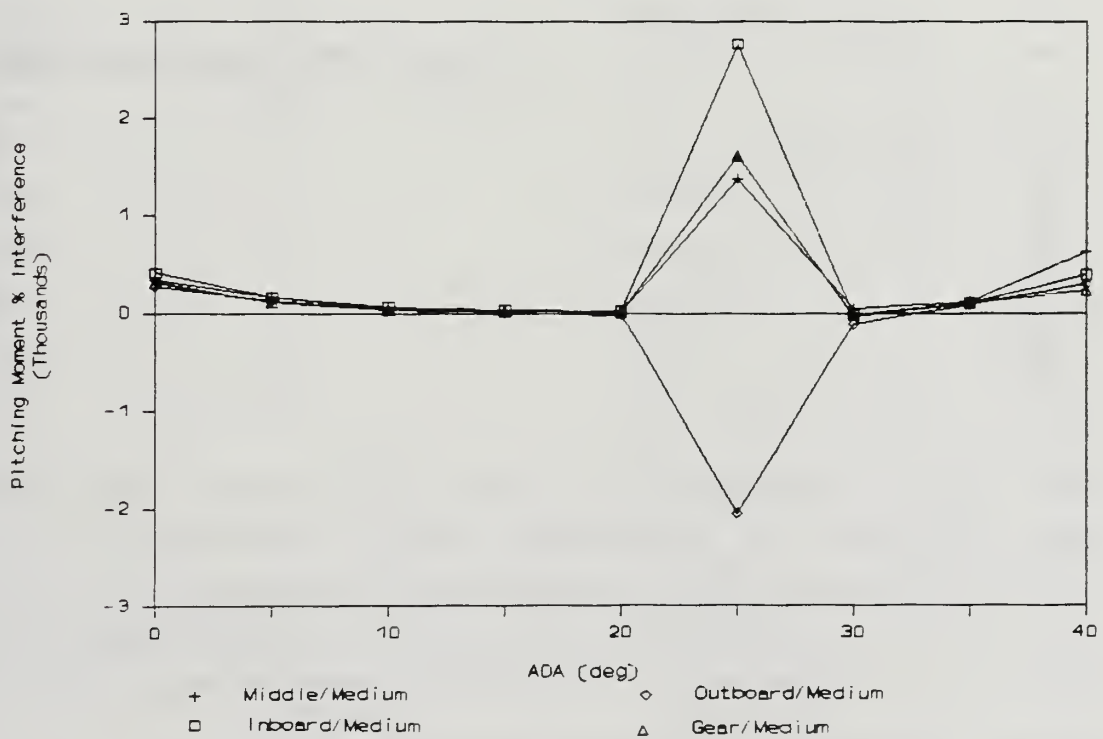
Figure 133. Pitching Moment % Interference (Aft: Nozzle/Long)
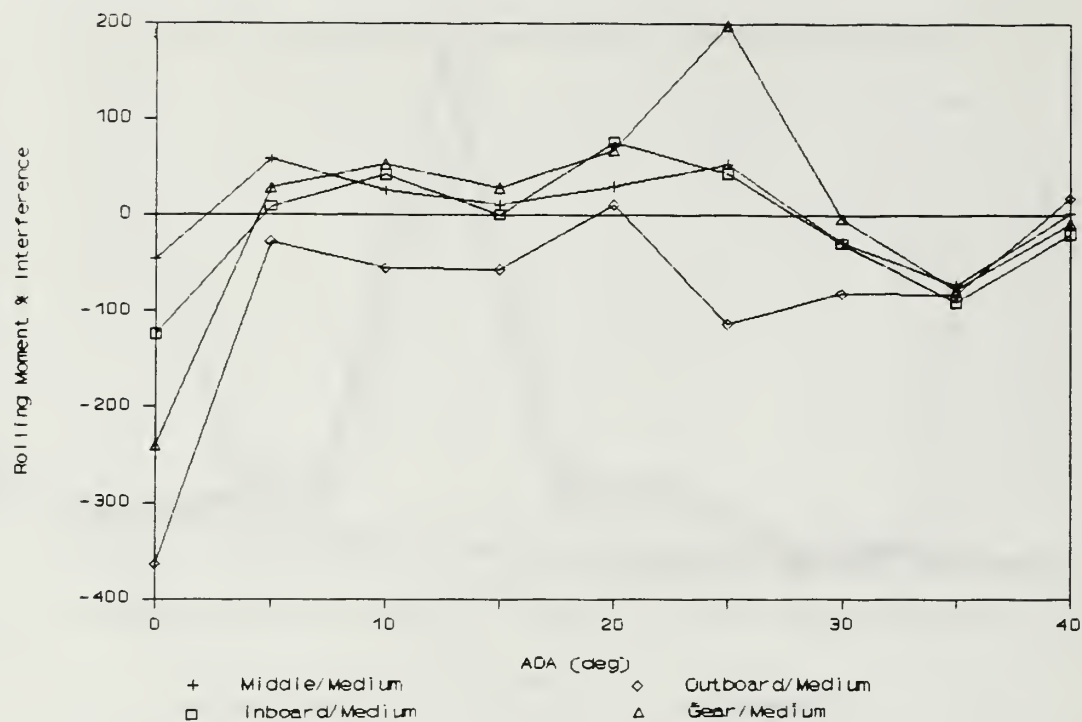
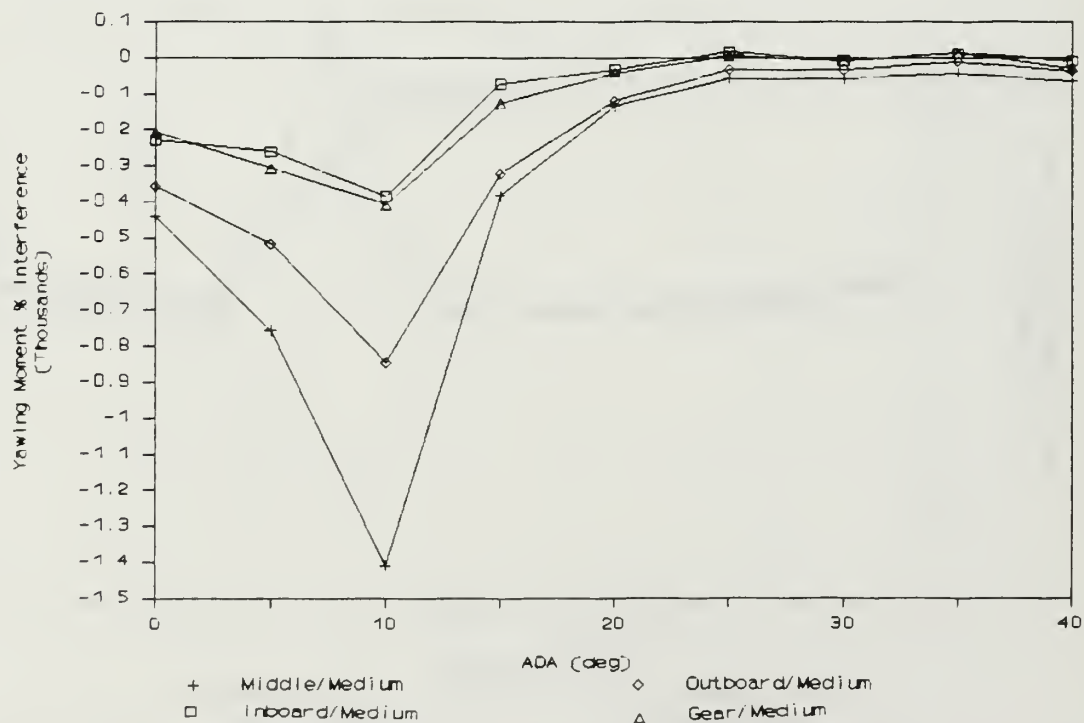**Figure 134.** Rolling Moment % Interference (Aft: Nozzle/Long)

Figure 135. Yawing Moment % Interference (Aft: Nozzle/Long)

124

APPENDIX G

FLOW VISUALIZATION IMAGES

STRUTS	AOA (deg)	LASER SHEET LOCATION	FIGURE
None	30	Forebody	136
Yes	30	Forebody	137
None	30	LEX	138
Yes	30	LEX	139
None	30	Wing	140
Yes	30	Wing	141
None	40	LEX	142
Yes	40	LEX	143
None	40	Wing	144
Yes	40	Wing	145
None	50	Forebody	146
Yes	50	Forebody	147
None	50	LEX	148
Yes	50	LEX	149
None	50	Wing	150
Yes	50	Wing	151
None	60	Forebody	152
Yes	60	Forebody	153
None	60	LEX	154
Yes	60	LEX	155

Note: When present, the strut configuration is with the foward struts 4.531" outboard of the centerline with 0.5" extensions, and the aft strut 4.375" aft of the moment center with a 1.5" extension.
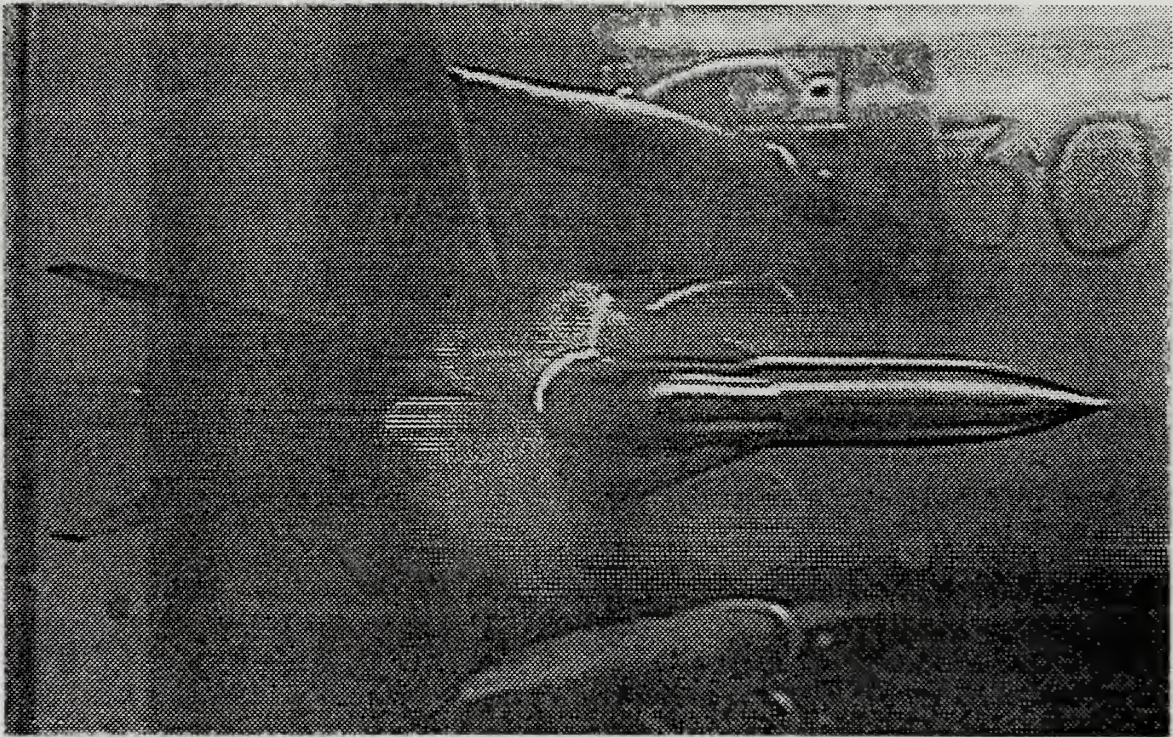
125

Figure 136. No Struts, 30° AOA, Forebody

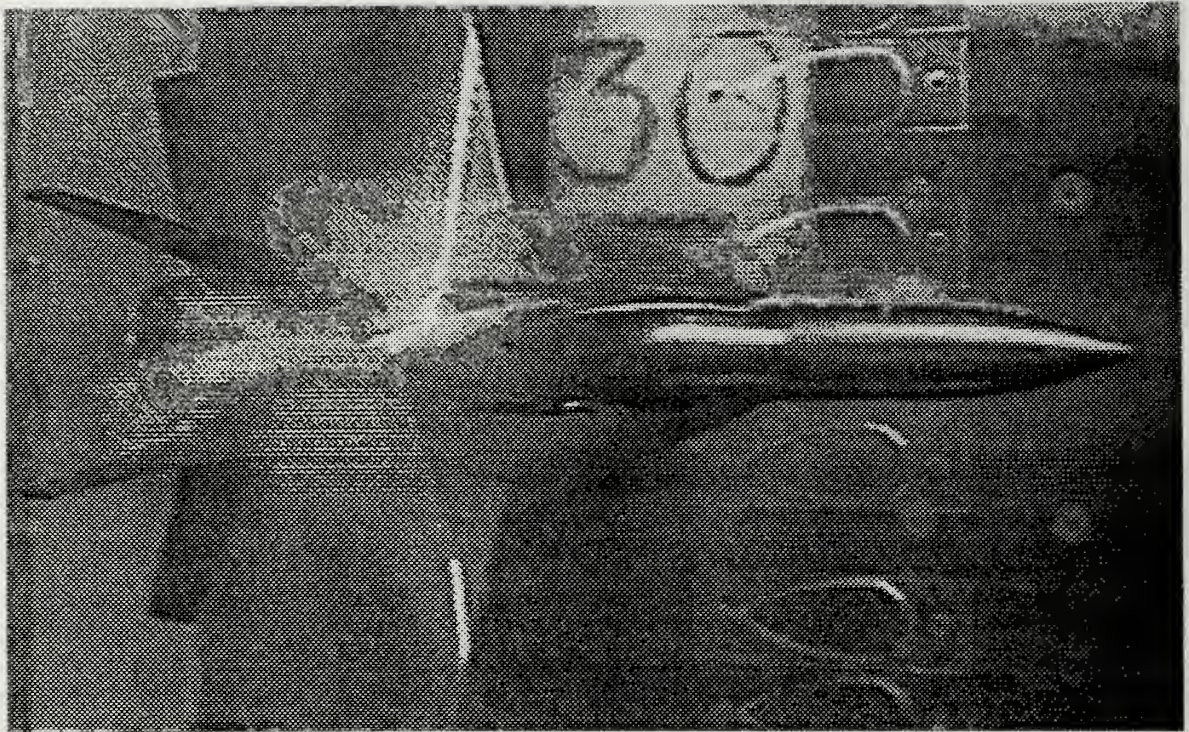**Figure 137.** Struts Present, 30° AOA, Forebody
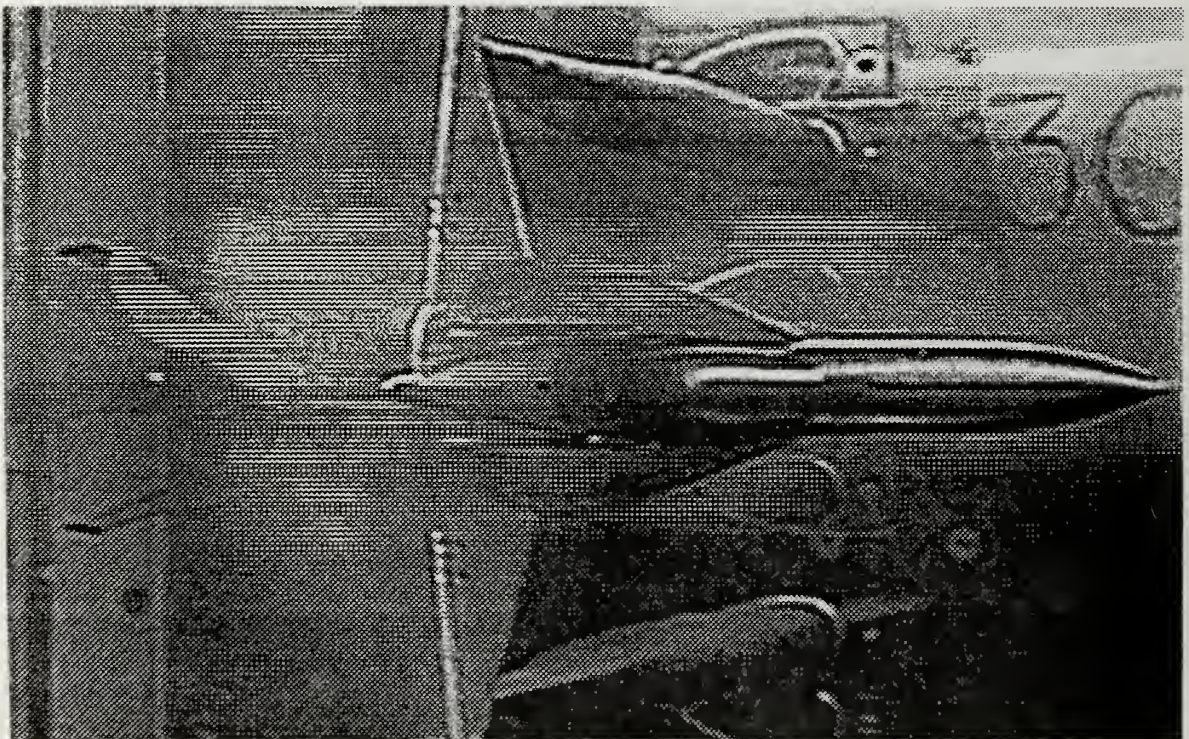
126

Figure 138. No Struts. 30° AOA, LEX

Figure 139. Struts Present. 30° AOA, LEX

Figure 140. No Struts, 30° AOA, Wing
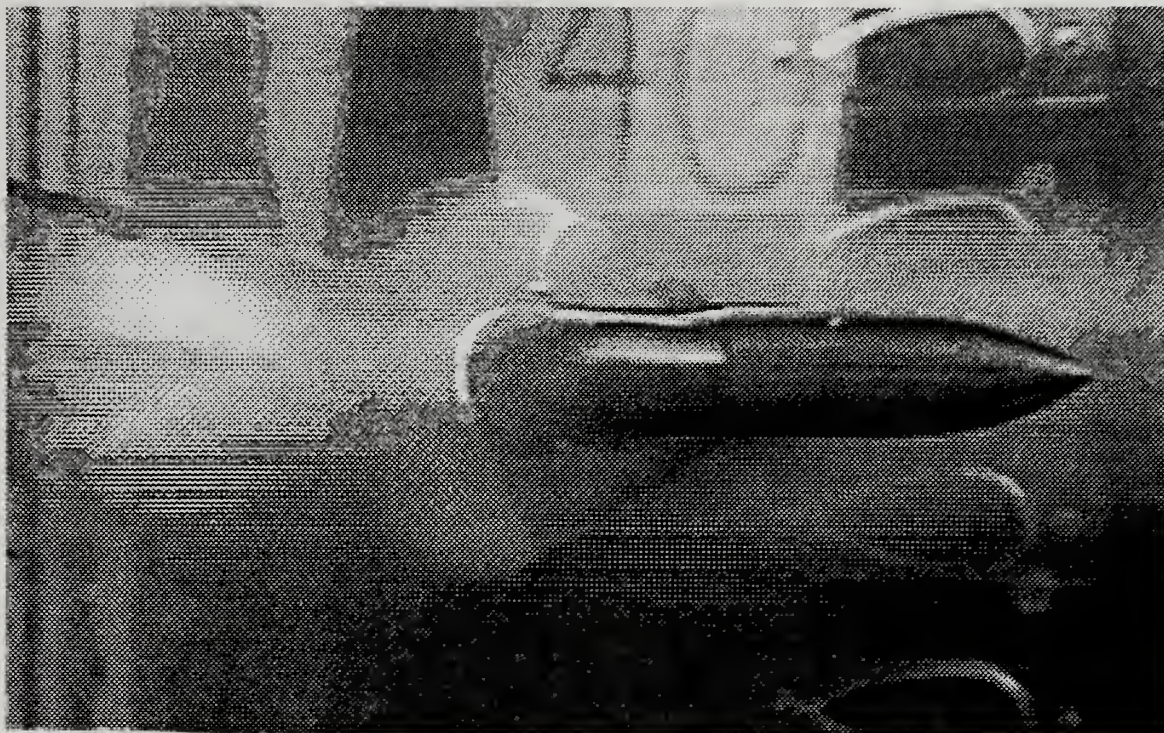

Figure 141. Struts Present, 30° AOA, Wing
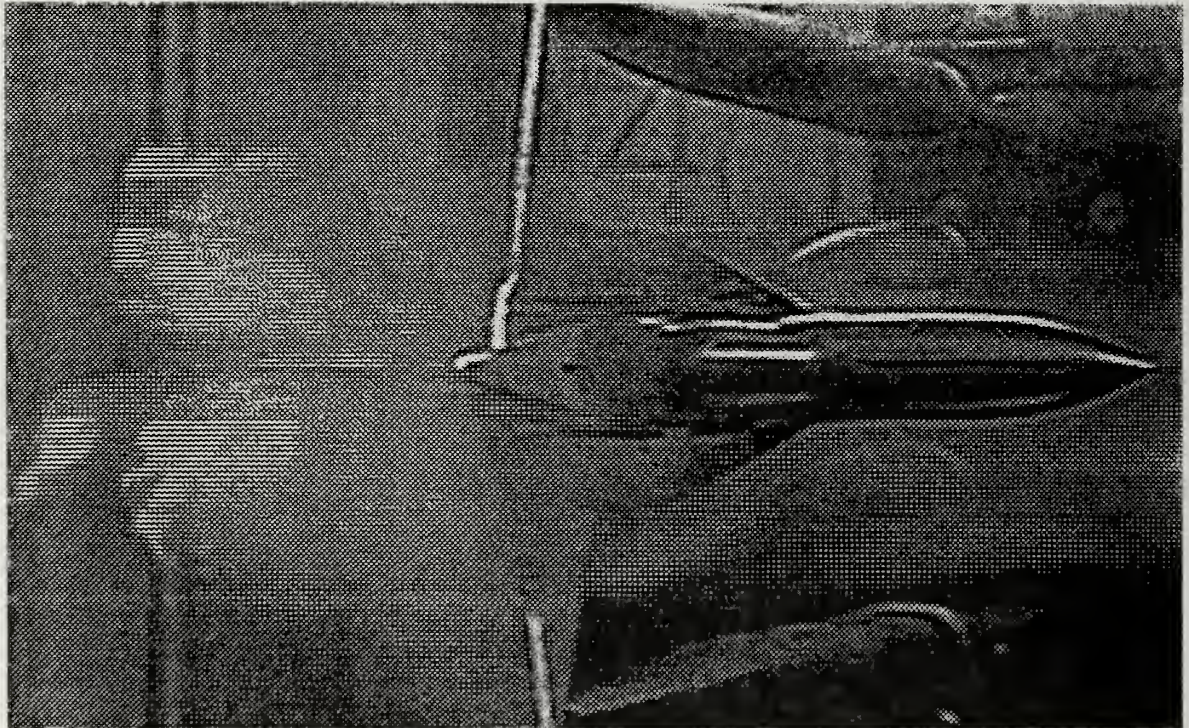
Figure 142. No Struts. 40° AOA. LEX

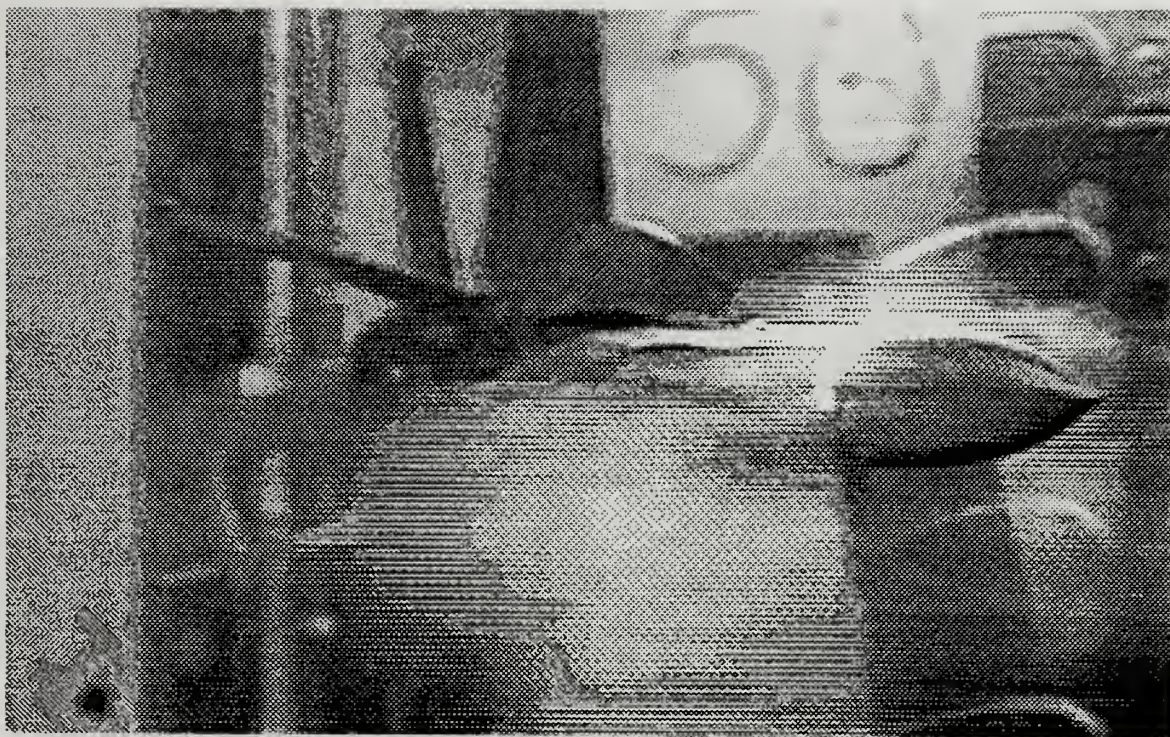**Figure 143.** Struts Present. 40° AOA. LEX
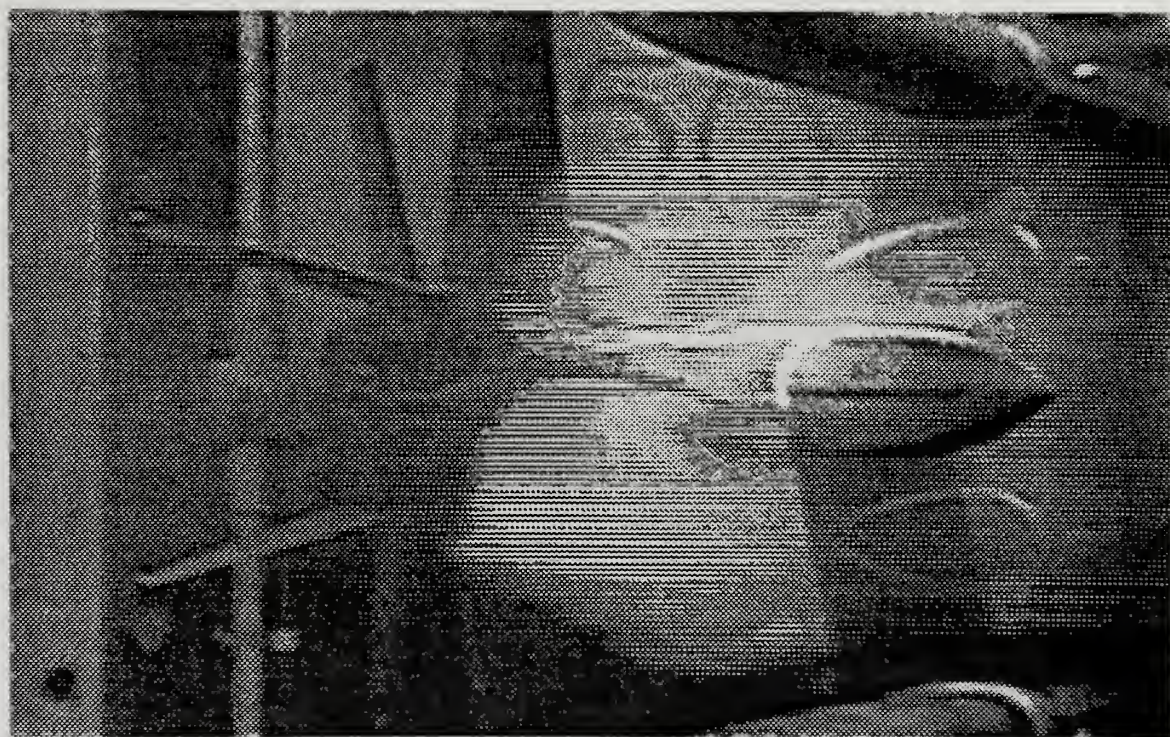
Figure 144. No Struts, 40° AOA, Wing

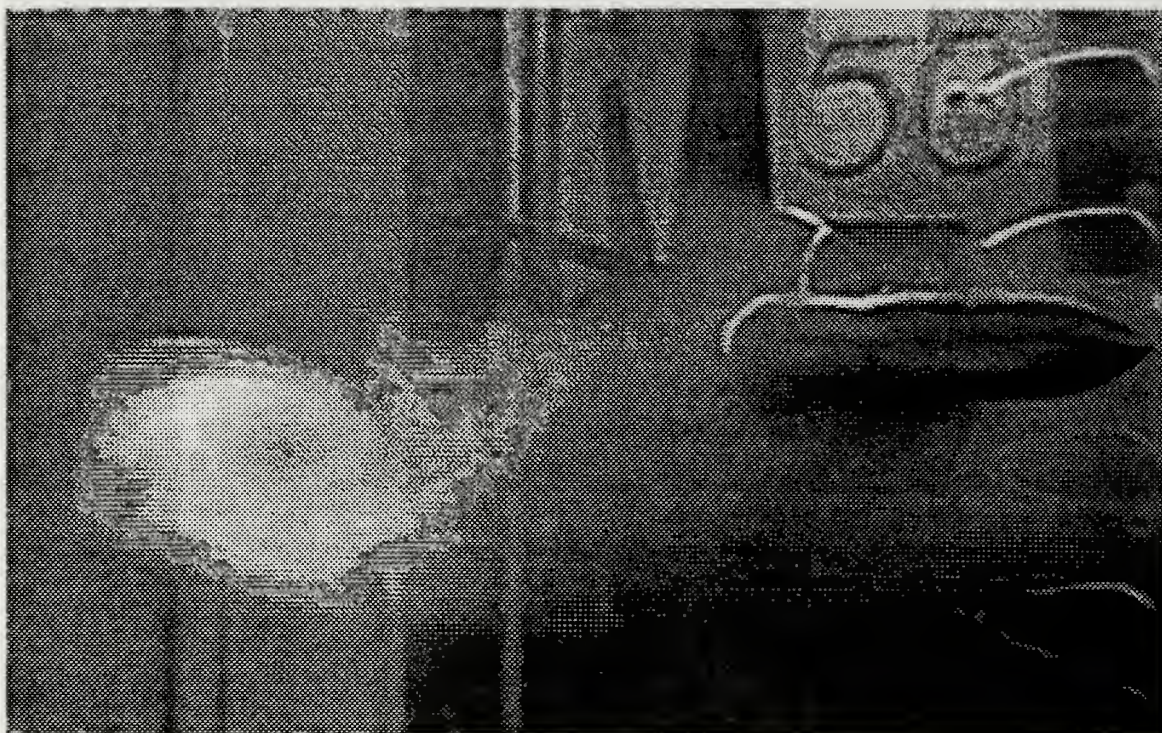**Figure 145.** Struts Present, 40° AOA, Wing

Figure 146. No Struts, 50° AOA, Forebody

Figure 147. Struts Present, 50° AOA, Forebody

131

Figure 148. No Struts. 50° AOA. LEX

Figure 149. Struts Present. 50° AOA. LEX

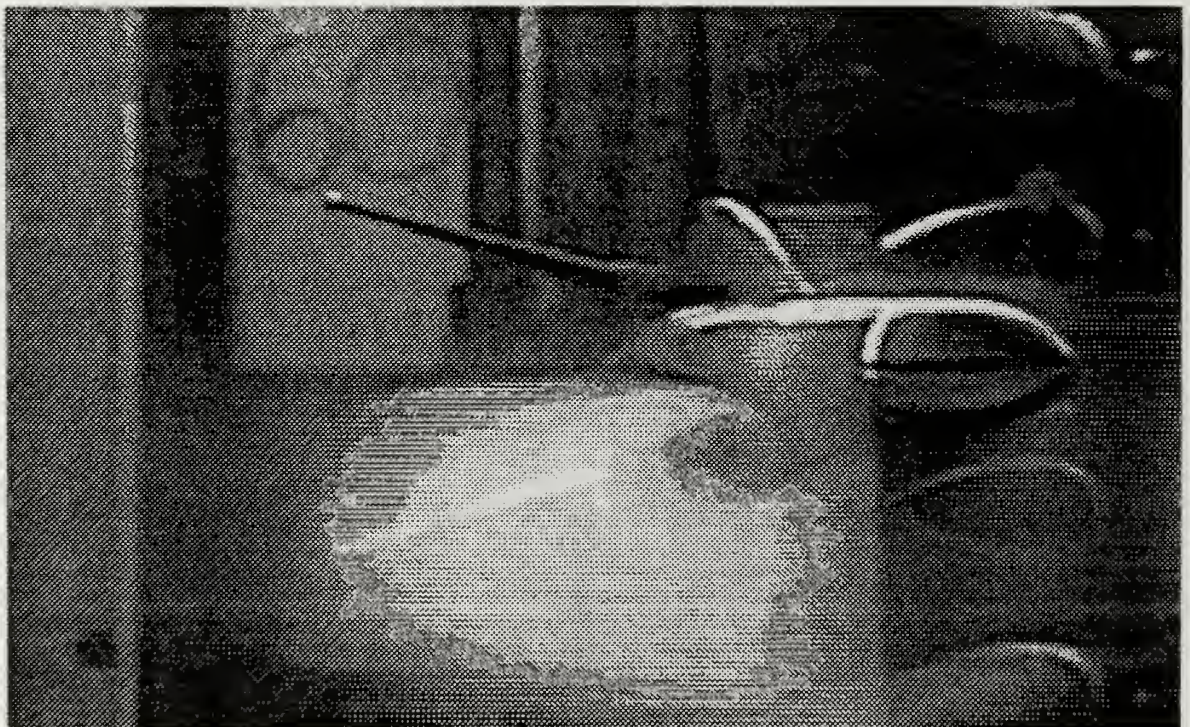**Figure 150.** No Struts, 50° AOA, Wing

Figure 151. Struts Present, 50° AOA, Wing

Figure 152. No Struts. 60° AOA. Forebody

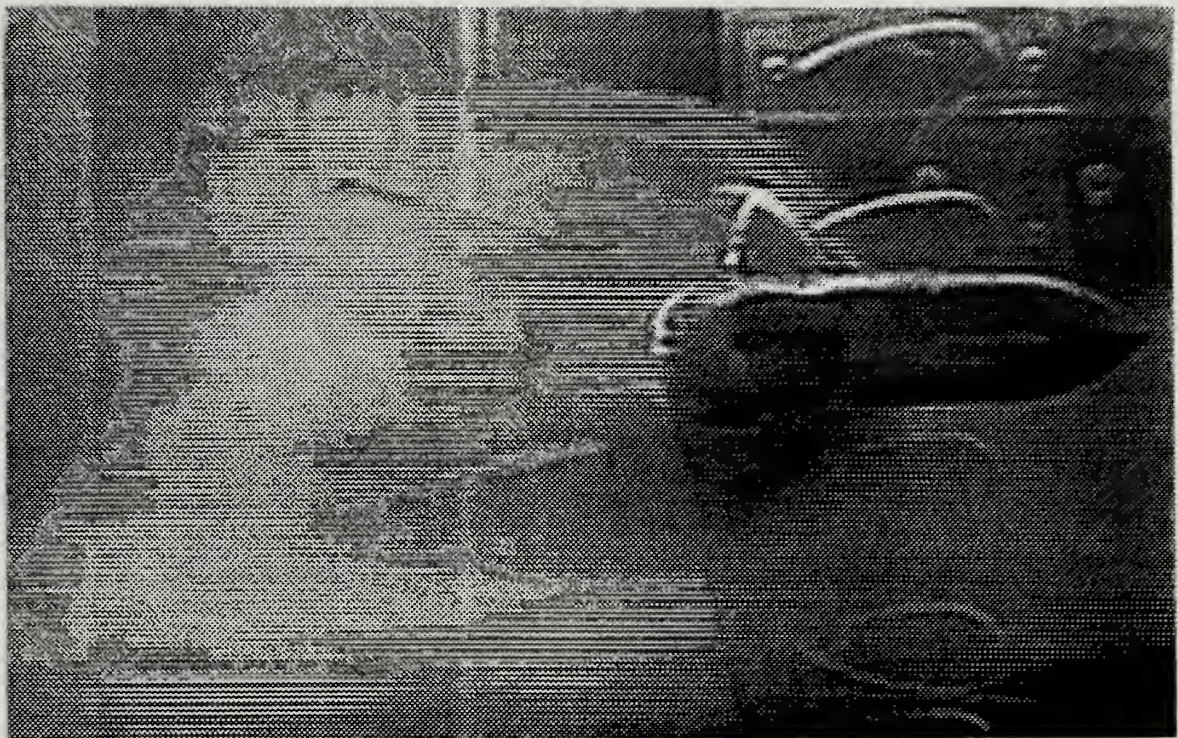**Figure 153.** Struts Present. 60° AOA. Forebody
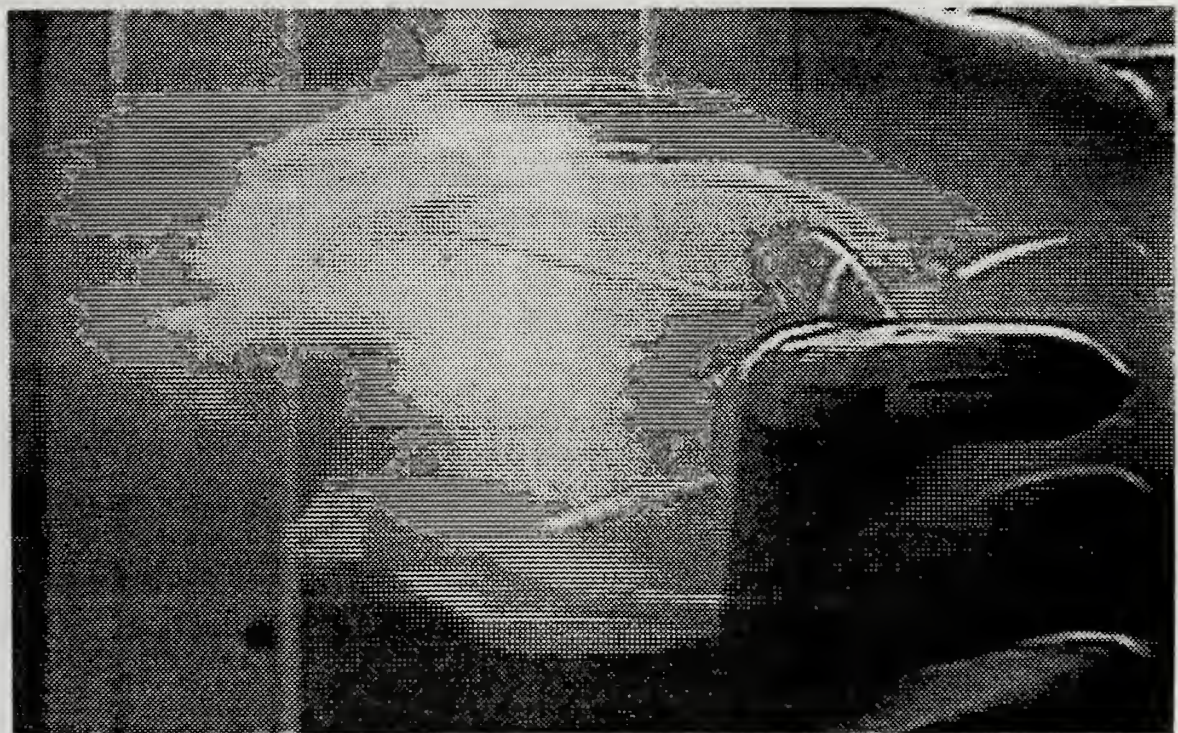
Figure 154. No Struts, 60° AOA, LEX

Figure 155. Struts Present, 60° AOA, LEX

LIST OF REFERENCES

1. Fink, D. E., and others, "Agile Sukhoi Su-27 Leads Strong Soviet Presentation", *Aviation Week and Space Technology*, v. 130, pp. 28-30, 19 June 1989.

2. Dornheim, M. A., "U.S. Firm Claims Modified F-16 Could Match Su-27 'Cobra' Maneuver", *Aviation Week and Space Technology*, v. 131, pp. 54-55, 14 August 1989.

3. Brief by Lewis B. Schiff, Fluid Dynamics Division NASA-Ames Research Center, to the Naval Postgraduate School, "The NASA High-Angle-of-Attack Technology Program", 10 May 1989.

4. Scott, W. B., "NASA Adds to Understanding of High Angle of Attack Regime", *Aviation Week and Space Technology*, v. 130, pp. 36-42, 22 May 1989.

5. Lawing, P. L., Kilgore, R. A., and Dress, D. A., "Magnets Promise Productivity", *Aerospace America*, v. 27, pp. 34-38, March 1989.

6. Pope, A., *Wind-Tunnel Testing*, pp. 97-99, John Wiley & Sons, Inc., 1954.

7. Chlebanowski, J. S. Jr., *Flow Visualization by Laser Sheet*, M. S. Thesis, Naval Postgraduate School, Monterey, California, March 1988.

8. *Laboratory Manual for Low Speed Wind Tunnel Testing*, Department of Aeronautics, Naval Postgraduate School, Monterey, California, October 1983.

9. Leedy, D. H., *An Experimental Investigation of a Fighter Aircraft Model at High Angles of Attack*, M. S. Thesis, Naval Postgraduate School, Monterey, California, September 1988.

10. *Calibration for TASK Mark 14-B Balance*, Balance Calibration Laboratory, NASA-Ames Research Facility, July 1987.

11. *Operation Manual for the Spectra-Physics Model 164 Laser and Model 265 Power Supply*, Laser Instruments Division, Spectra-Physics, Mountain View, California, February 1980.

INITIAL DISTRIBUTION LIST

		No Copies
1.	Defense Technical Information Center Cameron Station Alexandria, Virginia 22304-6145	2
2.	Library, Code 0142 Naval Postgraduate School Monterey, California 93943-5002	2
3.	S. K. Hebbar, Code 67Hb Department of Aeronautics and Astronautics Naval Postgraduate School Monterey, California 93943-5000	11
4.	E. R. Wood, Chairman Department of Aeronautics and Astronautics Naval Postgraduate School Monterey, California 93943-5000	1
5.	RADM R. W. West Jr., Superintendent Naval Postgraduate School Monterey, California 93943-5000	1
6.	M. F. Platzer, Code 67Pr Department of Aeronautics and Astronautics Naval Postgraduate School Monterey, California 93943-5000	1
7.	Lt. J. D. Sommers 8387 Abbots Hill Road San Diego, CA 92123	3
8.	Rich Howard, Code 67Ho Department of Aeronautics and Astronautics Naval Postgraduate School Monterey, California 93943-5000	1
9.	M. S. Chandrasekhara, Code 67Ch Department of Aeronautics and Astronautics Naval Postgraduate School Monterey, California 93943-5000	1

10. J. King, Code 67Jk   1
    Department of Aeronautics and Astronautics
    Naval Postgraduate School
    Monterey, California 93943-5000

11. Larry Meyn   1
    Fixed Wing Aerodynamics Branch
    NASA Ames Research Center (M.S. 247-2)
    Moffett Field, California 94035

12. Lewis Schiff   1
    Applied Computational Fluids Branch
    NASA Ames Research Center (M.S. 258-1)
    Moffett Field, California 94035

13. Heinz A. Gerhardt   1
    Northrop Corporation
    Aircraft Division, Department 3811/82
    One Northrop Avenue
    Hawthorne, California 90250

14. G. Ericson   1
    Mail Stop 294
    NASA Langley Research Center
    Hampton, Virginia 23665

15. Naval Air Systems Command   1
    Attn: Tom Momiyama, Director, Aircraft Division
    Code 931
    Washington, DC 20361-9320

16. Naval Air Development Center   1
    Attn: Lisa Cowles, Code 60C6
    Street Road
    Warminster, Pennsylvania 18974-5000